ENHANCED STRIATAL GLUTAMATERGIC FUNCTION UPON ANTIPSYCHOTIC ADMINISTRATION

by

Amanda Vernon
ScB Neuroscience
Brown University, 2012

SUBMITTED TO THE DEPARTMENT OF BRAIN AND COGNITIVE SCIENCES IN PARTIAL FULFILLMENT OF THE REQUIREMENTS FOR THE DEGREE OF DOCTOR OF PHILOSOPHY IN BRAIN AND COGNITIVE SCIENCES AT THE MASSACHUSETTS INSTITUTE OF TECHNOLOGY

JUNE 2019

Signature of Author: Signature redacted

Department of Brain and Cognitive Sciences

Certified by: Signature redacted

Myriam Heiman, Ph.D.

Associate Professor, Picower Institute, Department of Brain and Cognitive Sciences

Thesis Supervisor

Accepted by: Signature redacted

Matthew A. Wilson, Ph.D.

Sherman Fairchild Professor of Neuroscience and Picower Scholar

Director of Graduate Education for Brain and Cognitive Sciences

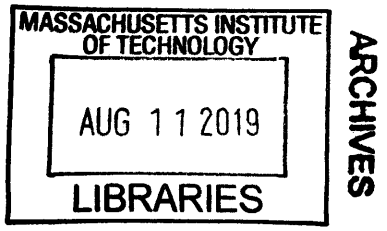

Enhanced Striatal Glutamatergic Function Upon Chronic Antipsychotic Action

By

Amanda Vernon

Submitted to the Department of Brain and Cognitive Sciences on May 3, 2019 in Partial Fulfillment of Requirements for the Degree of Doctor of Philosophy in Brain and Cognitive Sciences

ABSTRACT

Schizophrenia is a psychiatric disorder characterized by multiple clusters of symptoms including positive symptoms, such as hallucinations and delusions, negative symptoms, such as decreased motivation and flattened affect, and cognitive symptoms, such as memory impairment and impaired executive function. Currently available antipsychotics mitigate some symptoms of schizophrenia, particularly the positive symptoms, but there is no preventive treatment nor cure after schizophrenia develops. Efforts to generate more effective antipsychotics are made particularly challenging by the fact that the therapeutic effect of currently prescribed antipsychotics is not well understood and the cell type(s) and brain circuits crucial for beneficial effects have not been conclusively identified. Here we show that chronic antipsychotic administration enhances glutamatergic function in the ventral striatum through translational alterations and increased synaptic function. Cell type-specific mRNA profiling on spiny projection neurons (SPNs) of the direct (dSPNs) and indirect (iSPNs) pathways following chronic antipsychotic administration revealed cell type-specific molecular alterations indicating increases in components of the glutamatergic postsynaptic density. Subsequent functional experiments demonstrated the presence of calcium-permeable AMPARs and increased mEPSC frequency following chronic administration of one especially effective antipsychotic, clozapine. Furthermore, we find that striatal astrocytes also respond to chronic antipsychotic treatment with translational alterations promoting synaptogenesis. Together, these data have identified a core molecular signature of increased glutamatergic transmission in the striatum induced by chronic antipsychotic treatment. This work provides evidence that effective antipsychotics address a lack of glutamatergic drive into the striatum in cases of schizophrenia. Additionally, it suggests that drug development efforts seeking improved antipsychotics may benefit by finding compounds that feature an increased glutamatergic drive into the striatum as a core function.

Thesis Supervisor: Myriam Heiman
Title: Associate Professor of Neuroscience

Acknowledgements

I would first and foremost like to acknowledge and thank my advisor and mentor, Dr. Myriam Heiman. She has been a wonderful mentor for the past five years, providing scientific and professional support that made all of this work possible. Her brilliant mind and dedication to working at the highest standards possible provided unparalleled scientific training, while her encouragement and enthusiasm always kept me moving forward. I am forever grateful that she agreed to be my PhD mentor.

My committee, Drs. Troy Littleton, Weifeng Xu, and Matcheri Keshavan, has been an enriching source of scientific discussion and advice, and I deeply appreciate their time and wisdom over the course of our meetings. I am particularly grateful to Dr. Weifeng Xu for being interested in scientifically collaborating with us on this project and for her insights as this project developed.

Eduardo Elejalde, thank you for your financial support of this project for the past several years as we have launched our work to better understand antipsychotic mechanisms. Our Tripartite meetings were a consistent inspiration to work to improve the lives of people living with schizophrenia.

To the Heiman Lab Winners, thank you for your consistent help along the way – and also, perhaps more notably, thank you for your tolerance of my love of Photoshop and my odd sense of humor. I would like to particularly thank Dr. Robbie Fenster, Ruth Kulicke, and Dr. Lea Hachigian for their generosity in getting me started, both intellectually and technically, in my first months in the lab. Thanks also to the Xu Lab members who were so generous with their time and scientific aid, especially Dr. Dipanwita Ghose.

My family has been a consistent source of understanding and encouragement, perhaps most dramatically in their willingness to travel to Cambridge for multiple Thanksgivings in which I abandoned them to spend the morning in lab before coming home to a dinner they cooked me. I would like to especially thank my brothers Patrick and Jeffrey Vernon, who are younger than me and yet have provided me with a great deal of spiritual wisdom throughout my graduate work.

Thank you to my wonderful network of friends, from Best Group to Book Club to the Gurts and many, many others, especially Bridget McNamara, Anita Badejo, and Mariagrazia La Fauci. Your jokes, conversations, and kindness helped make these years a joy.

Finally, to my husband, James Hawrot, I am grateful for your steadfast love and support. You kept me optimistic and productive throughout these five years, no matter the basis of my anxiety du jour.

CONTENTS

Figure List
Chapter 2

Chapter 3

Chapter 4

Appendix 1

Table List

Chapter 2

Experimental Contributions

Chapter 2
Amanda Vernon performed all experiments and analyses, except for:
- cDNA amplification and sequencing, which was performed by **MIT BioMicro Center**.
- CUFFDIFF analysis to generate lists of DEGs, which was performed by **Dr. Fan Gao** in Picower Computational Core.

Chapter 3
Amanda Vernon performed all experiments and analyses, except for:
- Electrophysiological recordings, which were performed by **Dr. Dipanwita Ghose** in collaboration with **Dr. Weifeng Xu's lab**, and analysis of these recordings, which was performed by **Drs. Dipanwita Ghose and Weifeng Xu**.

Chapter 4
Amanda Vernon performed all experiments and analyses, except for:
- cDNA amplification and sequencing, which was performed by **UCSF Sequencing Core**
- CUFFDIFF and Deseq2 analysis to generate lists of DEGs, which was performed by **Dr. Fan Gao** in Picower Computational Core.

Appendix 1
Amanda Vernon performed all experiments and analyses, except for:
- Retro-TRAP viral injections and immuofluorescent imaging of injections, which was performed by **Dr. Cody Siciliano** in collaboration with **Dr. Kay Tye's lab**.

I. Schizophrenia

Clinical Symptoms

Schizophrenia is a neurodevelopmental disorder characterized by a cluster of psychiatric symptoms. The Positive and Negative Syndrome Scale (PANSS) was developed in 1987 to provide interview guidelines and introduce a positive-negative scale of schizophrenia-related syndromes which are related to each other and to the general severity of psychopathology (Kay et al, 1987). This scale is commonly used to this day to characterize severity of positive and negative symptoms in schizophrenia. Positive symptoms of schizophrenia include delusions, conceptual disorganization, hallucinatory behavior, excitement, grandiosity, suspiciousness, and hostility (Kay et al, 1987). Negative symptoms of schizophrenia include blunted affect, emotional withdrawal, poor rapport, social withdrawal, difficulty with abstract thinking, lack of flow of conversation, and stereotyped behavior (Kay et al, 1987). These negative symptoms can present as primary negative symptoms if they are core to the patient's disorder, or they can present as secondary negative symptoms if they arise as a result of drug side effects, changes in environment, or as a result of the disruptive effect of positive symptoms (Hasan et al, 2012). Cognitive symptoms of schizophrenia include numerous impairments, including deficits in verbal and nonverbal memory, motor performance, visual and auditory attention, intelligence, executive function, and language (Heinrichs & Zakzanis, 1998).

Like several other psychiatric disorders, schizophrenia has its peak onset during adolescence (Paus et al, 2008). The highest risk group is men younger than 40, although schizophrenia impacts both men and women and can occur later in life (Rossler et al, 2005). Schizophrenia onset typically proceeds through a series of phases. The first, the

premorbid phase, precedes any symptomology and in some cases is seen in childhood (Horton et al, 2015). It is characterized by cognitive impairments in areas including verbal memory and attention (Erlenmeyer-Kimling et al, 2000). These impairments have primarily been documented in studies of people known to be at high risk for developing schizophrenia due to genetic or environmental risk factors but who have not yet developed any behavioral symptoms (Keshavan et al, 2004). The premorbid phase is followed by the prodromal phase, which generally precedes the full manifestation of schizophrenia. The prodromal phase is characterized by early symptoms that are not sufficient for a definitive diagnosis of schizophrenia and are only formally recognized following an eventual diagnosis (Yung & McGorry, 1996). The prodromal phase can last from days to months and can be difficult to define clinically; its starting point may be defined as the time when the patient noticed a change or when others noticed a change in the patient (Yung & McGorry, 1996). It generally begins earlier in males than in females (approximately 18 vs. 20 years old), even though age of onset of psychosis is not different between the two sexes (Choi et al, 2009). There is a growing interest in successful diagnosis of schizophrenia during the prodromal phase because it is thought that early intervention, potentially before the onset of psychosis, can improve treatment outcomes. Much of this work has taken the form of seeking specific prodromal symptoms, such as depression, disorganization, and low-grade psychosis, that have predictive value in identifying people who will progress to a psychotic phase (Yung et al, 2003).

Approximately one-third of people with prodromal symptoms will progress to the psychotic phase of schizophrenia. In this phase, patients have an acute psychotic episode

that requires initial treatment with antipsychotics (Hasan et al, 2013). This psychotic episode can be comprised of a range of symptoms. It contains at least one clear symptom, including a paranoid delusion (typically persecutory delusion); a delusion that others can detect the patient's thoughts; passivity phenomena, or a patient's belief that they are being controlled by others; a patient hearing one's own thoughts aloud; or auditory hallucinations of voices speaking about the patient (Byrne, 2007). It also includes at least one less clear symptom, including vague hallucinations; auditory hallucinations of voices speaking to the patient; and general thought disorders, such as difficulty thinking abstractly (Byrne, 2007). The acute episode is generally followed by a stabilization period for 3-6 months after the acute phase as the patient is in transition to treatment stabilization (Hasan et al, 2013). This period is lengthy because it can take as long as six weeks to determine whether a given treatment is leading to symptom improvement; furthermore, symptoms can continue to improve following this initial stabilization period (Lehman et al, 2010).

If patients reach stabilization, the psychotic phase is followed by a stable phase, with a long period of treatment stretching for months or years. In this phase, symptoms are controlled, and the patient is seeking recovery and working to improve function aligned with their own individual goals (Rossler et al, 2005; Hasan et al, 2013). In this phase, social interventions including employment, skills training, and cognitive behavioral therapy can be beneficial (Hasan et al, 2013). Ultimately, the goal of this phase is to lower antipsychotic drug dosage to remove the patient from medication, but this goal depends dramatically on the individual patient situation. If the psychotic episode was a patient's first, length of treatment is recommended to be 1-2 years, but this window

may be extended as long as for the rest of life if the patient has had multiple episodes (Hasan et al, 2013). A minority of patients will be able to go off of medication without relapse (Lehman et al, 2010). However, within 1 year of treatment removal, 60-70% of patients will relapse, and within 2 years of removing treatment, 90% of patients will relapse (Lehman et al, 2010).

Schizophrenia is associated with a reduced life expectancy of approximately 10 years due to increased incidence of suicide (Rossler et al, 2005). Additionally, schizophrenia is responsible for 2.8% of the global years lived with disability (YLDs) (Rossler et al, 2005). There are significant indirect costs of schizophrenia that are difficult to quantify. These costs encompass areas such as loss of productivity from those with schizophrenia, their family members, and their caregivers (McEvoy et al, 2007). Total costs of schizophrenia in the United States in 2002 were estimated to be as high as $62.7 billion, with $22.7 billion due to direct costs of health care such as outpatient care, drugs, inpatient care, and long-term care, $7.6 billion due to living cost offsets, and $32.4 billion in indirect costs due to unemployment (Wu et al, 2005).

In sum, schizophrenia is a debilitating psychological disorder with a high societal burden. Its peak onset is in adolescence, with official diagnosis performed following a psychotic episode that includes symptoms such as hallucinations and delusions. A subset of patients sees meaningful improvement following antipsychotic treatment and is even able to top taking these drugs, but for many patients, current treatments are not efficacious and are accompanied by severe side effects.

Etiology

Schizophrenia affects approximately 1% of the global population, and its heritability has been estimated to be as high as 80% (International Schizophrenia Consortium, 2009). Genetic variation underlies schizophrenia risk in the form of many common alleles which each have a small effect on risk of development of schizophrenia. Genome wide association studies (GWAS) have been crucial for elucidating genes associated with schizophrenia as well as for identifying single nucleotide polymorphisms associated with increased risk for schizophrenia (Walsh et al, 2008; International Schizophrenia Consortium, 2009; Schizophrenia Working Group of the Psychiatric Genomics Consortium, 2014). These studies have implicated single nucleotide polymorphisms, *de novo* mutations in the form of small mutations or rare copy number variations, and chromosomal translocations in genetic risk for schizophrenia (Blackwood et al, 2001; Fromer et al, 2014; Marshall et al, 2017). Large GWAS have identified over 100 genetic associations with schizophrenia, including the dopamine D2 gene *DRD2* as well as genes important for glutamatergic neurotransmission (*GRIN2A, GRIA1, GRM3, SRR, SHANK1, SHANK3, DLG2*), calcium signaling (*CACNA1C, CACNB2, CACNA1I*) and targets of fragile-X mental retardation protein (FMRP) (Walsh et al, 2008; Lennertz et al, 2012; Schizophrenia Working Group of the Psychiatric Genomics Consortium, 2014; Huckins et al, 2019). These studies have also repeatedly implicated the major histocompatibility complex (MHC), pointing to the immune system as a potential area of particular risk (International Schizophrenia Consortium, 2009; Schizophrenia Working Group of the Psychiatric Genomics Consortium, 2014). Because these studies have implicated a diverse array of genes in schizophrenia risk, it has become increasingly

important to assess how these systems interact in an attempt to develop a cohesive model of schizophrenia progression (Lisman et al, 2008).

In addition to these genetic risks, meta-analyses of twin studies of schizophrenia have found evidence that environmental influence accounts for approximately 11% of the risk of development of schizophrenia (Sullivan et al, 2003). Complications during pregnancy, labor, and early infancy are linked with as much as a 2-fold higher risk for schizophrenia, and exposure to influenza infection while *in utero* is associated with higher risk for schizophrenia (Cannon et al, 2002, Brown & Derkits, 2010). Infection exposure may be particularly dangerous in the second trimester specifically, though evidence for this is currently limited (Mednick et al, 1988). Some of this risk appears to come from gene-environment interactions (International Schizophrenia Consortium, 2009). In these cases of early-life complications, polygenic risk scores are also higher. Interestingly, the loci associated with this risk are highly expressed in the placenta (Ursini et al, 2018). Furthermore, these placental genes are differentially expressed in male vs. female fetuses, which may partially explain higher risk for schizophrenia among males (Ursini et al, 2018). There is growing consensus that additional environmental factors, such as cannabis use, minority group status, and trauma during development can increase risk for schizophrenia (van Os et al, 2010). In line with this work, schizophrenia incidence is higher in urban populations and has been linked to higher stress levels (Lederbogen et al, 2011).

Genetic studies have improved our understanding of the heritable risk of schizophrenia and haveconsistently implicated signaling pathways that are important for synaptic function. In particular, they have pointed to abnormalities in excitatory

glutamatergic synapses. However, each individual risk gene only accounts for a small increase in risk for schizophrenia, and environmental components are an additional factor in schizophrenia development that is poorly understood.

Pathophysiology

The pathophysiology of schizophrenia remains largely unknown, despite consensus that identifying pathophysiology will likely be crucial for treatment improvement (Harrison & Weinberger, 2005; Schizophrenia Working Group of the Psychiatric Genomics Consortium, 2014; McCollum et al, 2015). At the same time, molecular and structural studies have made significant progress towards improving our understanding of the pathophysiology of schizophrenia and categorizing it as a developmental disorder (Weinberger, 1987).

Gray and White Matter Alterations

Imaging evidence suggests consistent loss of cortical thickness in superior frontal, middle frontal, and orbitofrontal regions and expansion of third ventricle size in progression of schizophrenia independent of antipsychotic administration (Cannon et al, 2015). Hippocampal tissue in the left hemisphere is also smaller in male patients at onset of schizophrenia (Bogerts et al, 1990). CA1 volume and subfield CA2/3 volumes negatively correlate with severity of PANNS positive symptom scores, with some evidence that CA1 volume is affected first, followed by loss of volume in other hippocampal subfields (Kuhn et al, 2012; Schobel et al, 2013; Ho et al, 2017). The CA1, preceding atrophy, displays hypermetabolism that appears to be due to increased levels of

extracellular glutamate in the hippocampus (Schobel et al, 2013). In line with this observation, GABAergic cells are reduced in number in the hippocampus of patients, but excitatory pyramidal cell numbers are not reduced (Benes et al, 1998; Zhang and Reynolds, 2000; Konradi et al, 2011a.).

Studies have also demonstrated major connectivity alterations across brain regions. Studies of white matter in schizophrenia patients have pointed to frontal-temporal connections and the corpus callosum as altered in schizophrenia, with myelination maturation processes diverging from that of controls (Bartzokis et al, 2003; Kubicki et al, 2005). Corticostriatal connections to both the dorsal and ventral striatum have been shown to be altered in schizophrenia, and patients with schizophrenia display both hypoconnectivity (in the case of the dorsal striatum) and hyperconnectivity (in the case of the ventral striatum) between the striatum and other brain regions (Fornito et al, 2013). Interestingly, some of these connectivity alterations are also seen in unaffected relatives of patients, suggesting that they are associated with risk for developing schizophrenia (Fornito et al, 2013).

Circuitry Abnormalities

Patients with schizophrenia frequently exhibit neural syncrony deficits. Oscillatory activity arises in the brain when large numbers of synapses function in synchrony. They are thought to link assemblies of neurons and promote synaptic plasticity to allow for long-term information consolidation and temporal representations (Buzsaki & Draguhn, 2004). Patients with schizophrenia display deficits in steady-state evoked potentials, including at the time of the first psychotic episode, and these deficits

correlate with hallucination severity (Kwon et al, 1999; Spencer et al, 2008; Spencer et al, 2009; Krishnan et al, 2009). Both the early appearance of these altered oscillatory patterns and their correlation with symptom severity suggest that the cortical circuitry is impaired prior to any antipsychotic administration and contributes to the disorder (Spellman & Gordon, 2015).

Oscillations in gamma-band synchrony have been specifically implicated in studies of patients with schizophrenia. In the case of working memory tasks, patients fail to increase gamma band power in the cortex with increased working memory load and exhibit overall excessive cortical gamma osccillatory activity instead, which may partially explain this cognitive deficit in schizophrenia (Basar-Eroglu et al, 2007; Barr et al, 2010). An additional cognitive symptom of schizophrenia is insufficient cognitive control for generating executive function. In this case, patients exhibit low cortical gamma oscillations, which may lead to insufficient activity driving into subcortical regions to generate impaired executive function (Cho et al, 2006).

Networks of GABAergic interneurons and cortical excitatory pyramidal cells have been implicated in this oscillatory dysfunction. Cortical pyramidal cells are common postsynaptic targets of inhibitory GABA neurons, and in normal conditions, these inhibitory neurons inhibit pyramidal cells with each GABA neuron spike, while pyramidal cells fire in synchronous fashion as the inhibition decays prior to the next GABA neuron spike (Gonzalez-Burgos et al, 2011). One proposed mechanism for oscillatory deficits in schizophrenia is dysfunction of GABA-mediated hyperpolarizing input into cortical pyramidal neurons failing to produce synchronized firing (Gonzalez-Burgos et al, 2011). In line with this model, cortical GABA itself is reduced in

postmortem brain tissue of schizophrenics (Perry et al, 1979). This deficit has been specifically narrowed down to basket and chandelier cells specifically, which are PV-positive interneurons key for network-wide function (Woo et al, 1998; Curley & Lewis, 2012). In addition to helping to explain the cognitive symptoms associated with altered gamma oscillations, this mechanism further proposes that hypoactivation of NMDAR in schizophrenia reduces the excitation of these fast-spiking interneurons, leading to disinhibition of pyramidal cells and a resulting subcortical hyperdopaminergic state that generates psychosis (Lisman et al, 2008).

Dendritic Spine Deficits

The site of input for connectivity between neurons is the dendritic spine. Spines are neuronal protrusions containing neurotransmitters and other proteins that provide a signaling mechanism for synaptic function (Nimchinsky, 2002). Loss of dendritic spines has been repeatedly implicated in schizophrenia pathophysiology (Glausier & Lewis, 2013). In particular, loss of spines in cortical layer III neurons has been consistently demonstrated in postmortem tissue of patients with schizophrenia (Glantz & Lewis, 2000; Glausier & Lewis, 2013). Induced pluripotent stem cell-derived forebrain neurons with mutant DISC1 (Disrupted In Schizophrenia 1) display deficits in synaptic vesicle release and dysregulated expression of synaptic genes, and DISC1 in rat cortical neurons is crucial for spine enlargement and stabilization (Hayashi-Takagi et al, 2010; Wen et al, 2014). Brain-derived neurotrophic factor (BDNF) is also reduced in the dorsolateral prefrontal cortex layers III, V, and VI in schizophrenia, which may be one mechanism by which synaptic density is reduced in the cortex in schizophrenia patients (Weickert et al,

2003; Ray et al, 2014). This altered spine formation during development is thought to lead to altered excitatory/inhibitory balance in the cortex which may underlie schizophrenia symptoms (Hensch, 2005). The striatum has also consistently been viewed as a potential site of abnormalities giving rise to schizophrenia, especially in light of the role of striatal dopamine release in associative learning and habit formation (Shen et al, 2008). Postmortem tissue shows reduced spine size in the caudate and putamen of patients (Roberts et al, 1996).

Altered Gene Expression

Gene expression studies of postmortem tissue have suggested that gene expression abnormalities in the cortex and striatum are a hallmark of schizophrenia pathophysiology. In the cortex, genes involved in metabolism are significantly decreased in the PFC of patients with schizophrenia, a pattern that is reversed in monkeys treated with haloperidol (Middleton et al, 2002). Furthermore, glutamic acid decarboxylase mRNA levels (specific for GABA synthesizing neurons) are decreased in schizophrenia patients (Heckers et al, 2002). Finally, microarray studies of schizophrenic patient PFC revealed decreased transcription of genes important for presynaptic function (Mirnics et al, 2000). In addition to these cortical findings, when human GWAS hits are mapped onto cell type specific gene expression studies, these schizophrenia risk genes are specifically enriched in striatal SPNs, cortical and striatal interneurons, and pyramidal cells (Skene et al, 2018). Each of these studies points to a pattern of gene expression alterations in patients with schizophrenia consistent with decreased activity of cortical GABAergic interneurons and dysfunctional cortical pyramidal cells.

Dopamine Hypothesis of Schizophrenia

Altogether, these studies provide evidence that schizophrenia is a disorder of the synapse that gives rise to a broad array of higher order, circuit-wide abnormalities. Two major hypotheses have arisen to explain these phenomena: the dopamine hypothesis of schizophrenia and the glutamate hypothesis of schizophrenia.

The dopamine hypothesis rose to prominence soon after the discovery of antipsychotics with the observation that all clinically effective drugs target the dopamine D2 receptor to reduce signaling (van Rossum et al, 1966). Furthermore, the gene *Drd2,* which encodes the dopamine D2 receptor, has been implicated itself as a risk gene for schizophrenia (Schizophrenia Working Group of the Psychiatric Genomics Consortium, 2014).

Dopamine receptors are expressed in several brain regions, including the striatum, cortex, pallidum, olfactory bulb, hypothalamus, midbrain, and pons (Lein et al, 2007). Furthermore, dopamine receptors are found both pre- and post-synaptically, with presynaptic receptors acting as autoreceptors that regulate dopamine release (Meador-Woodruff et al, 1989; Levey et al, 1993). This broad expression pattern, with dopamine receptors playing varied role and localized differentially in subcellular compartments, has made it challenging to identify the particular dopamine system abnormalities underlying schizophrenia pathophysiology.

There is some evidence that hyperdopaminergia in particular underlies positive symptoms of schizophrenia, and that this may partially explain why dopamine antagonists tend to be more successful in ameliorating positive symptoms than negative

symptoms (Crow et al, 1980). For example, amphetamine can induce psychotic symptoms and raise synaptic dopamine levels (Howes & Kapur, 2009). Furthermore, dopamine receptor binding is elevated in postmortem brains of schizophrenics (Snyder, 1981). However, additional studies complicated this picture. For example, patient cerebrospinal fluid does not contain higher levels of dopamine metabolites, which suggests that any abnormalities tied to alterations in dopamine levels themselves lead to psychosis vary in a cell type or region-specific manner (Maas et al, 1997). Furthermore, clozapine, which has comparatively lower dopamine receptor affinity than other effective antipsychotics, is a more effective antipsychotic drug, which should not be the case in a disorder of broad hyperdopaminergia (Jones et al, 2006). Higher resolution studies, including PET studies of cerebral blood flow, provided evidence for a region-specific model of dopamine's involvement in the development of schizophrenia. These studies pointed towards hypodopaminergia in the prefrontal cortex and hyperdopminergia in subcortical regions including the striatum (Howes & Kapur, 2009). In support of this model, dopamine D2/D3 receptor levels are modestly increased in the striatum of patients with schizophrenia (Kestler et al, 2001). To this day, blockade of the D2 receptor is thought to be the main therapeutic effect of antipsychotics. However, major questions remain about the site of dopamine signaling abnormalities in schizophrenia and potential loci of therapeutic benefit in the case of antipsychotics.

Glutamate Hypothesis of Schizophrenia

The glutamate hypothesis points to glutamatergic abnormalities as the original deficit leading to schizophrenia symptoms. It has its origins in experiments studying PCP

and ketamine, two N-methyl-D-aspartate receptor (NMDAR) antagonists, which lead to behaviors reminiscent of psychosis in mice, rats, and humans, including hallucinations, paranoia, and even, in some cases, negative symptoms like emotional withdrawal (Javitt & Zukin, 1991). Clinically, glycine site agonists, when used in conjunction with typical antipsychotics, can help to reduce negative symptoms of schizophrenia (Coyle et al, 2004). Furthermore, antipsychotic treatment has been shown to alter glutamatergic synaptic activity. This can occur through synaptic plasticity, the process by which excitatory neurons can re-wire synaptic connectivity by altering connection strength in response to a change in stimulus (Malenka & Bear, 2004; Ho et al, 2011; Bliss et al, 2014). LTP (long-term potentiation) and LTD (long-term depression) at synapses have both been shown to occur in response to antipsychotic administration. For example, at glutamatergic corticostriatal terminals in rats, normal conditions can normally induce LTD or LTP, but the presence of haloperidol, an antipsychotic, specifically induces NMDAR-dependent LTP via blockade of D2L (Centonze et al, 2004). Finally, glutamatergic signaling genes have been consistently associated with increased risks for schizophrenia, especially genes associated with NMDAR complexes and modulation of synaptic strength (Harrison & Weinberger, 2005; Fromer et al, 2014; Schizophrenia Working Group of the Psychiatric Genomics Consortium, 2014). Some of these risk genes have demonstrated effects in animal models; for example, mice with a schizophrenia-associated R1117X mutation in Shank3, a postsynaptic density scaffolding protein, display synaptic defects in the cortex and behavioral abnormalities consistent with schizophrenia pathophysiology (Zhou et al, 2016).

II Treatment of Schizophrenia

Antipsychotics

Antipsychotics generally fall into one of two categories: typical, or first-generation, and atypical, or second-generation. Typical antipsychotics were developed first and tend to be the most effective drugs for the psychotic symptoms of schizophrenia (Lieberman et al, 2005). They have a high affinity for dopamine D2 receptors and are associated with higher rates of extrapyramidal signs and tardive dyskinesia (Miyamoto et al, 2005; Lieberman et al, 2005). The clinical therapeutic doses of typical antipsychotics are positively correlated with dopamine D2 receptor occupancy, suggesting that blockade of this receptor is key to the therapeutic benefit of these drugs, and inversely correlated with 5-HT2c binding affinity, suggesting that 5-HT2c signaling may synergistically act with D2 receptor blockade to enhance antipsychotic benefits (Richtand et al, 2008).

Atypical antipsychotics were developed later, but they currently represent 90% of the market share of antipsychotics in the United States (Lieberman et al, 2005). This is largely due to the fact that atypical antipsychotics are associated with lower incidence of extrapyramidal symptoms, although they are also associated with significant side effects including weight gain and glucose metabolism abnormalities (Koro et al, 2002; Henderson et al, 2005). An additional potential benefit of atypical antipsychotics is their potential for reducing negative symptoms of schizophrenia (Lieberman et al, 2005). Atypical antipsychotics tend to display a lower affinity for dopamine D2 receptors and a higher affinity for serotonin (5-HT1a, 5-HT2a, 5-HT2c, 5-HT3, 5-HT6, 5-HT7) and norepinephrine (α1, α2) receptors, though action at serotonin receptors and 5-HT1a receptors in particular vary widely by drug (Bardin et al, 2005; Miyamoto et al, 2005).

They also display a correlation between clinically effective dosage and D3 dopamine receptor binding, suggesting that action through the D3 receptor may be important for their therapeutic benefits (Richtand et al, 2008).

In general, it is not always possible to cleanly sort a given drug into the categories of typical or atypical (Hasan et al, 2013). There is even some evidence that atypical antipsychotics are no better than typical antipsychotics in terms of clinical outcome (Jones et al, 2006). The major exception to this rule is the drug clozapine, which demonstrates greater efficacy with positive symptoms and also reduces negative and cognitive symptoms in some patients (Bardin et al, 2005; Smith et al, 2019). Perhaps most dramatically, clozapine alone stands as an option in the case of schizophrenia that has proven treatment-resistant (Jones et al, 2006; Lehman et al, 2010; Hasan et al, 2012). Approximately 60% of patients who have failed to respond to other medications will respond to clozapine treatment (Meltzer et al, 1992). Unfortunately, clozapine is associated with a potentially fatal side effect in 1-2% of patients, agranulocytosis (lowered white blood cell count), which restricts it from being used as a first-line antipsychotic (Alvir et al, 1993).

This side effect is particularly unfortunate in a context in which antipsychotics display low efficacy for many patients (Lieberman et al, 2005). Patients in their first episode of schizophrenia are the most likely to respond well to antipsychotics, and 70% of these patients will reach remission of psychotic symptoms within 3-4 months of their first episode (Lehman et al, 2010). However, 10-30% of patients do not respond to antipsychotics, and an additional 30% display only a partial response even after multiple antipsychotic trials of at least 6 weeks each (Lehman et al, 2010).

In addition to low efficacy, adherence to drug regimen is a particular issue with antipsychotic treatment. In one study, 74% of patients discontinued their assigned study medication before 18 months (Lieberman et al, 2005). Even for patients who do remain on their regimen, there are major side effects that can interfere with quality of life. These include blunted affect, cardiovascular issues, sedation, sexual dysfunction, metabolic disorders, and endocrine disorders (Hasan et al, 2013). In all, it is estimated that as many as half of all patients take less than 70% of their prescribed dose (Hasan et al, 2012).

For patients who do respond to antipsychotics, the largest improvement occurs within the first week of treatment, but there continues to be a reduction in scores on the PANSS as late as week 4 of treatment, suggesting both an early- and delayed-onset effect of antipsychotics (Agid et al, 2003).

Mechanisms of Antipsychotics

All effective antipsychotics block activity at the dopamine D2 receptor, but pure dopamine D2 antagonism is not sufficient to explain antipsychotic treatment. In efforts to explain the mechanism by which these drugs work, several groups have worked to elucidate their molecular effects.

Antipsychotics are known to alter transcription in multiple brain regions with D2-receptor expressing cells. For example, acute haloperidol administration induces immediate early gene c-fos and zif268 transcription in the caudate putamen and c-fos transcription in the nucleus accumbens; acute clozapine administration induces zif268 transcription in the caudate-putamen and c-fos transcription in the nucleus accumbens (Nguyen et al, 1992). These transcriptional alterations are thought to lead to protein

product alterations, such as AP-1 binding, which subsequently lead to longer-term gene expression regulations (Nguyen et al, 1992). There are several examples of chronic effects following antipsychotic treatment; for example, 14- or 21-day administration of haloperidol leads to increased D2 receptor mRNA in rat striatum (Moine et al, 1990). Chronic haloperidol administration changes gene expression in the striatum, hippocampus, and cortex of the rat, and striatal changes center around alterations in transcription factor and neurotransmitter signaling pathways (Fatemi et al, 2011; Girgenti et al, 2010). Chronic administration appears to have distinct effects from acute administration; for example, chronic haloperidol treatment induces structural changes in glutamatergic synapses in the striatum that suggest excitatory transmission potentiation, but acute treatment does not (Meshul & Casey, 1989). Furthermore, gene expression profiles appear to differ between typical and atypical antipsychotics (Girgenti et al, 2010; Fatemi et al, 2011; Park et al, 2013). In culture, atypical antipsychotics such as aripiprazole and olanzapine increase BDNF and PSD-95 levels in rat hippocampal cultures, while typical antipsychotic haloperidol decreases PSD-95 levels; in line with these changes in scaffolding proteins, atypical antipsychotics increased dendritic growth while haloperidol did not (Park et al, 2013). This effect may be specific to hippocampal neurons or *in vitro* conditions, however, because other work has shown that 24 day treatment with haloperidol leads to increased dendritic spines and synaptic boutons in the rat striatum (Kerns et al, 1992). Additionally, 2-week haloperidol treatment of rats increased dopamine-binding sites and perforated synapse number in the caudate (Meshul & Casey, 1989). Perforated synapses are thought to be intermediate synapses in the process of becoming more mature synapses (Nieto-Sampredo et a, 1982). Atypical

antipsychotics clozapine and risperidone have been shown to decrease mGlu2 transcription via decreased mGlu2 promoter histone acetylation and increased binding of HDAC2; interestingly, haloperidol did not have this effect (Kurita et al, 2012).

Altogether, these studies are limited to study of a small number of genes, and many are performed in culture and/or with antipsychotic doses significantly higher than those typically used in the clinic. Many of them are not approached in a cell type-specific way, a real caveat given the evidence that pathophysiology of schizophrenia reveals specific cell types are particularly vulnerable.

Locus of action of antipsychotics

The genes that have been identified as risk genes for schizophrenia are associated as molecular markers of specific neuronal cell types: spiny projection neurons; pyramidal cells; and striatal and cortical interneurons (Skene et al, 2018). One of the most striking features of spiny projection neurons (SPNs) of the striatum is that they are a site of high dopamine receptor expression (Boyson et al, 1986; Meador-Woodruff et al, 1989). This, combined with the knowledge that all effective antipsychotics bind to the dopamine D2 receptor, pinpoints the striatum as a key site for understanding antipsychotic action.

The majority of neurons in the striatum are SPNs, a population of cells generally equal in size and morphology but further subdivided into dSPNs and iSPNs based on their expression of either the dopamine D1 or dopamine D2 receptors (Shen et al, 2008). SPNs display high resting membrane potentials and are therefore reliant on excitatory inputs from several brain regions to generate output (Thomas et al, 2001). To receive this excitatory input, SPNs express α-amino-3-hydroxy-5-methyl-4-isoxazolepropionic acid

receptors (AMPA) and NMDA receptors in the postsynaptic density of glutamatergic synapses. These synapses are part of ongoing synaptic adaptation during development and neuronal activity. For example, blocking neuronal activity increases GluR1 dendritic synthesis, a potential mechanism for AMPAR synaptic accumulation and synaptic strengthening following blockade (Ju et al, 2004). Furthermore, striatal glutamate release generates new dendritic spine growth, and glutamate binding to NMDA receptors depletes GluR1 and GluR2 mRNAs, allowing for synaptic adaptation (Grooms et al, 2006, Kozorovitskiy et al, 2012).

A subset of SPNs express both D1 and D2 receptors, and coexpression of D1 and D2 receptors along with other dopamine receptors D3, D4, and D5 in the same cell means that half of SPNs express both D1 and D2 class mRNAs (Surmeier et al, 1996). The identity of dopamine receptor expressed informs the overall function of the cells in broader brain circuitry. D1 class receptors, comprising D1 and D5 receptors, and D2 class receptors, comprising D2, D3, and D4 receptors have distinct and opposing GPCR signaling pathways.

D1 class receptors are coupled to adenylyl cyclase through G_{olf}. Signaling through these receptors leads to an increase in cAMP followed by activation of PKA and phosphorylation of many proteins including DARPP-32 (Surmeier et al, 2007). Signaling through the D1 receptor, and specifically through this PKA cascade, has been linked to increased surface expression of AMPA and NMDA receptors (Synder et al, 2000; Hallett et al, 2006). D1 signaling is important for promoting up states in SPNs, when the SPN is at -60mV instead of -80mV, and thus likelier to generate action potentials. This is thought to occur via PKDA phosphorylation which leads to the opening of L-type calcium

channels anchored near glutamatergic synapses by SHANK proteins (Surmeier et al, 2007). In sum, signaling through D1 class receptors will tend to make dSPNs more responsive to glutamatergic input.

D2 class receptors, in contrast, are coupled to $G_{i/o}$ subunits, which inhibit adenylyl cyclase and thus lead to the opposite cascade of that found in D1 receptor expressing neurons (Surmeier et al, 2007). D2 receptor signaling cascades lead to an overall decrease in iSPN responsivity through a variety of mechanisms. First, activation of D2 receptors will generally decrease AMPA currents (Cepeda et al, 1993). This is thought to happen through dephosphorylation of GluR1 at S845 and subsequent trafficking of GluR1 out of the synaptic membrane (Hakansson et al, 2006). D2 signaling also reduces presynaptic glutamatergic release either through pre- or postsynaptic dopamine D2 signaling, and reduces Na+ voltage dependent channel opening through PKC signaling (Surmeier et al, 2007). Finally, D2 signaling can lead to increases potassium channel opening (Greif et al, 1995). In sum, signaling through D2 class receptors will tend to make iSPNs less responsive.

Both populations of SPNs receive excitatory inputs from the cortex and thalamus, as well as neuromodulatory, predominantly dopaminergic, inputs from the substantia nigra pars compacta (Calabresi et al, 2014). However, because of their divergent projections, SPNs are functionally divided into dSPNs and iSPNs.

dSPNs are part of the direct, or striatonigral, pathway. This pathway is classically associated with motor behavior, and excitation of this pathway increases locomotion and reduces freezing (Kravitz et al, 2010). dSPNs project directly to inhibit neurons in the substantia nigra pars reticula, which then disinhibits activity in thalamic glutamatergic

neurons, which drives activity back from the thalamus to the cortex (Calabresi et al, 2014).

iSPNs are part of the indirect, or striatopallidal, pathway. This pathway serves as a break on the motor effects of dSPNs, and excitation of these SPNs leads to a Parkinsoninan state of increased freezing and decreased locomotion (Kravitz et al, 2010). iSPNs project to and inhibit neurons in the external globus pallidus, which disinhibits activity in glutamatergic neurons of the subthalamic nucleus, which activates GABAergic substantia nigra pars reticula neurons that subsequently inhibit the thalamic glutamatergic neurons (Surmeier et al, 1996; Calabresi et al, 2014). In this way, iSPNs and the indirect pathway have opposing effects to dSPNs and the direct pathway in the context of broader basal ganglia circuitry.

The mesolimbic dopamine system, also called the reward pathway, projects from the ventral tegmental area to the ventral striatum, which contains the nucleus accumbens (Thomas et al, 2001). This pathway is generally important for associative learning, reward, and decision-making and has been implicated in schizophrenia, particularly the negative and cognitive symptoms (Fornito et al, 2013). The striatal release of dopamine is involved in habit formation, with signaling through D1 receptors promoting LTP and signaling through D2 receptors promoting LTD (Shen et al, 2008). The ventral striatum responds to prediction errors, and this response is altered in patients with schizophrenia and leads to reward prediction dysfunction (Morris et al, 2012). Furthermore, studies of postmortem brains have shown an increase in asymmetric (excitatory) synapses but smaller postsynaptic densities of these synapses in the nucleus accumbens core, suggestive of impaired signaling through the ventral striatum (McCollum et al, 2015).

In addition to dopaminoceptive SPNs, it is possible that striatal astrocytes may be another important locus of action of antipsychotics. Striatal astrocytes, but not cerebellar astrocytes, have been shown to express D2 receptor mRNA and D1 receptors *in vitro* (Bal et al, 1994; Zanassi et al, 1999). Furthermore, astrocytes have been shown to express D2 receptors on their processes (Cervetto et al, 2017). Astrocytes are integral to synapse formation, first shown in retinal ganglion cell cultures, in which neurons formed few synapses unless astrocytes were included in the culture (Ullian et al, 2001). Astrocytes accomplish this by secreting many different kinds of molecules, including thrombospondins and TGF-beta1, which bind to neuronal receptors on a variety of synaptic subtypes to have a variety of effects depending on the molecule released (Baldwin & Eroglu, 2017). For example, thrombospondins bind to $\alpha 2\delta 1$ receptors at excitatory synapses to induce silent synapse formation (Baldwin & Eroglu, 2017). Following injury or disease, astrocytes can promote either neurodegeneration or neuroprotection; A1 astrocytes, which are a subtype of reactive astrocytes, are less able to promote synaptogenesis and can even induce neuronal cell death (Liddelow et al, 2017). A2 astrocytes, on the other hand, are a type with high expression of protective neurotrophic factors (Liddelow et al, 2017). Given their key role in maintenance of glutamatergic synapses and their potential to repond to alterations in dopamine signaling, striatal astrocytes may be one additional cell type targeted by antipsychotics.

Summary

Schizophrenia is a devastating psychiatric disorder, and there is a great public need for improved therapeutics. Unfortunately, although several risk genes for schizophrenia have been discovered and numerous cell types and brain regions have been associated with schizophrenia, the cause of this disorder remains poorly defined. At the same time, these studies have consistently pointed to the dopamine D2 receptor in particular and glutamatergic functioning in general as being crucially affected in schizophrenia. Further hampering our efforts to improve treatment for schizophrenia, the mechanism of action of antipsychotic drugs, which provide limited but crucial improvements, is not well understood. The main feature of this class of drugs is that they all modulate signaling at the dopamine D2 receptor, but this mechanism alone cannot explain their efficacy. These drugs have been shown to affect numerous receptor and cell types, but our understanding of the cellular effects of these drugs remains incomplete.

Studies of schizophrenia pathophysiology have consistently pointed towards structural and genetic alterations that implicate altered striatal glutamatergic function. Furthermore, the striatum, specifically due to cells of the indirect pathway, is one of the sites with the highest dopamine D2 receptor expression in the brain. We therefore hypothesize that antipsychotics address abnormalities in striatal function in schizophrenia by increasing glutamatergic drive in this brain region. We predict that chronic administration of antipsychotics increases expression of genes related to synaptic function and structure, and that these alterations lead to increased glutamatergic function in the striatum. Finally, because astrocytes express dopamine receptors, we predict that astrocytes may also respond to antipsychotic treatment by increasing translation of genes

important for enhanced glutamatergic function in the striatum. In sum, we predict that antipsychotic administration will generate a core signature of increased glutamatergic function in the striatum.

Chapter 2: Antipsychotics Alter Translation in dSPNs and iSPNs in a Pattern of Decreased Metabolism and Increased Glutamatergic Function

Background

Antipsychotics are effective for some patients, but even in cases where antipsychotics show some efficacy, their major side effects have frequently led to low adherence. An improved understanding of the therapeutic mechanisms of antipsychotics could lead to improved outcomes for patients by providing a means of developing more targeted therapeutics with potentially lower rates of side effects. Additionally, understanding the mechanisms of antipsychotics and seeking convergence with existing studies on schizophrenia pathophysiology helps us to better understand the disorder itself (Thomas, 2006).

It is already known that antipsychotic administration alters neuronal gene expression, and this effect has been linked to their therapeutic benefit (Fatemi et al, 2012; Girgenti et al, 2010). However, the data generated thus far are generally limited to specific genes of interest, are performed *in vitro*, and frequently use approaches that are not cell type-specific (Middleton et al, 2002; Kontkanen et al, 2002; Thomas, 2006; Park et al 2013; Sakuma et al, 2015).

We sought to address these caveats by using the cell type-specific translating ribosome affinity purification (TRAP) technology to profile genome-wide gene expression and mRNA translation in mouse SPNs after treatment with clinically relevant doses of clozapine, risperidone, aripiprazole, or haloperidol. We pursued this study in wild-type, previously untreated mice (aside from the TRAP transgene) because, although

there are several mouse models of schizophrenia, none of these models represents face, predictive, and construct validity (Belzung & Lemoine, 2001). Use of these models for drug discovery has frequently resulted in compound development that fails to fundamentally advance treatment for schizophrenia (Pratt et al, 2012). Furthermore, antipsychotic drugs have a similar effect on schizophrenia endophenotypes including prepulse inhibition in both wild-type and schizophrenia model mice (Duncan et al, 2006).

Following chronic administration and analyses of differentially translated genes, our study revealed a set of genes and pathways that constitute core, shared SPN responses to a range of antipsychotics as well as sets of genes and pathways unique to individual drugs.

Results

1. Treatment paradigm produces behaviors that mimic therapeutic benefit

Before studying the molecular and cellular effects of antipsychotics on SPNs, we sought a treatment paradigm reminiscent of treatment of schizophrenia in patients. We pursued this goal along three main axes: antipsychotics that represented a range of classes of drugs available; duration of treatment; and dosage.

1.1: Antipsychotic drug choice

Generally, antipsychotics fall into one of two categories: first-generation, or typical, antipsychotics, and second-generation, or atypical, antipsychotics. Second-generation antipsychotics were later in development and are associated with lower levels of extrapyramidal symptoms, but first-generation antipsychotics are still commonly used because a subset of patients sees greater symptomatic relief from these drugs (Lieberman et al, 2005; Jones et al, 2006). Further complicating matters, clozapine, a second-generation antipsychotic, is the most effective antipsychotic and capable of addressing positive, negative, and cognitive symptoms of schizophrenia, but its accompanying risk of agranulocytosis keeps it from acting as a first-order drug (Meltzer et al, 1992; Bardin et al, 2005; Jones et al, 2006; Lieberman et al, 2010; Hasan et al, 2012). With all of this in mind, we chose to administer a panel of four antipsychotic drugs alongside a vehicle control: haloperidol (first-generation), aripiprazole and risperidone (second-generation), and clozapine (second-generation, improved therapeutic benefit) (Table 2.1). This panel allowed us to directly compare a variety of treatments to address questions such as: all antipsychotics share dopamine D2 receptor antagonism; do they display a core molecular

signature? Are there meaningful differences between haloperidol and aripiprazole, risperidone, and clozapine that might explain the basis of extrapyramidal symptoms? Is there a meaningful difference at the molecular level between clozapine and other antipsychotics that may explain its dramatically improved therapeutic effects and allow us to recapitulate these effects in novel drug development?

1.2 Antipsychotic dosage choice

Studies of the effects of antipsychotics have used a wide range of doses, and effective patient doses range significantly as well (Lehman et al, 2010; Hasan et al, 2013). We selected an initial panel of drug doses that are commonly used in studies in mice and also within the range used for patient treatment (Bardin et al, 2006; PDR Network LLC, 2016). We then turned to behavioral analyses previously established in the field to confirm that we were using antipsychotic doses that were high enough to mimic therapeutic benefit but were not so high that they would produce unrealistic cellular effects.

A major phenotype of antipsychotic administration in the mouse is reduced locomotion due to antagonism of the dopamine D2 receptor, and this effect is pronounced in first-generation antipsychotics (Sanberg 1980; Bardin et al, 2006). As expected, an initial full-dose treatment showed that second-generation antipsychotics clozapine, aripiprazole, and risperidone induced less catalepsy than first-generation antipsychotic haloperidol (Figure 2.1 A). None of our lower, first day of chronic administraion doses of antipsychotic drugs reduced motor activity (Figure 2.1 B), and at the first day in which all drugs were given at their maximum dose, only haloperidol reduced motor activity (Figure

2.1 C). It is interesting that over time, clozapine did reduce motor activity (Figure 2.1 D); this may be due to the long-term alterations to dopamine receptor expression level, which is important for locomotion, following clozapine treatment. Because antipsychotics are increasingly considered for treatment of generalized anxiety, we were interested to assess whether these drug doses altered anxiety-associated behavior in mice (Hershenberg et al, 2014). To do so, we calculated thigmotaxis following open field recordings. Thigmotaxis is a ratio of time animals spend in the edges of the open field compared to the center of the open field, with more time spent along the edge of the open field being associated with higher anxiety-like states (Simon et al, 1994). Our experiments did not show any effect of antipsychotic administration on thigmotaxis following a single administration of the antipsychotic full dose (Figure 2.1 E) or following 6 weeks of administration (Figure 2.1 F).

Because of its improved therapeutic benefit, we were particularly interested in additional experiments examining the molecular and cellular effects of clozapine. We therefore performed additional experiments to confirm our dose range was within a therapeutic dose and reaching the mouse brain. To this end, we performed mass spectrometry to measure levels of clozapine in the brain, and we performed prepulse inhibition behavioral testing to measure prepulse inhibition following acute dosage with clozapine. This behavioral test is a measure of sensorimotor gating and records the change in startle response when a prepulse precedes a startle pulse. The presence of a prepulse typically lowers the startle response to a loud pulse. Acute treatment readout of prepulse inhibition is used as a screening tool for development of novel therapeutics (Rigdon & Viik, 1991; Ouagazzal et al, 2001). It is thought to be particularly relevant for

schizophrenia treatment because prepulse inhibition is also impaired in schizophrenic patients and prepulse inhibition restoration in rats is correlated with antipsychotic clinical potency (Swerdlow & Geyer, 1993).

We expected to find that clozapine IP injection permitted clozapine to enter the mouse brain and that acute dosage with 2.0 mg/kg clozapine would increase prepulse inhibition. Indeed, we confirmed that clozapine was present in the mouse brain following IP injection, increasing to an average of 46.31 ng clozapine / g mouse brain (Figure 2.2 A). Furthermore, acute administration of 2.0 mg/kg clozapine increased prepulse inhibition as has been shown at other doses previously (Figure 2.2 B, Swerdlow & Geyer, 1993). Because of clozapine's improved therapeutic benefit for activities associated with the reward pathway and the ventral striatum, we were also interested in assessing whether there was any effect of clozapine on a test of motivation, the forced swim test (Porsolt et al, 1978; Cryan et al, 2004; Yankelevitch-Yahav et al, 2015). Acute clozapine treatment increased immobility time in the forced swim test, which may have been due to motor side effects of clozapine too small to be detected in the open field test (Figure 2.2 C). We did not see any increase in immobility time 24H following a first dose of clozapine, a time window in which we would expect motor effects to be absent (Figure 2.2 D). Together, these data suggest that our study's dose of clozapine mimics the effects seen in therapeutic doses and is reaching the brain but does not affect anxiety-like behavior or, when given acutely, improve motivation in the forced swim test.

In addition to confirming the therapeutic relevance of our doses, we were further interested in the chronic behavioral readout of clozapine treatment. Because symptoms can take weeks to improve following beginning of antipsychotic treatment, we

hypothesized that chronic behavioral models of antipsychotic efficacy may provide a method to predict whether drugs will have a long-term, lasting improvement of schizophrenia symptoms. To examine this chronic effect, we studied prepulse inhibition and startle habituation following 6 weeks of clozapine administration. We did not observe differences in prepulse inhibition following chronic treatment with clozapine, which may be due to increased baseline prepulse inhibition in chronically injected vehicle control animals (Figure 2.2 E). Clozapine administration also did not alter startle habituation after 6 weeks of treatment (Figure 2.2 F).

1.3 Antipsychotic treatment duration

Treatment duration was an important variable in our study because patients with schizophrenia generally take antipsychotics for a period of weeks to months, with some patients remaining on antipsychotics for the remainder of their lives. Chronic models have commonly used a period of time around 3 weeks (Moreno et al, 2012; de la Fuente Revenga et al, 2018). Because we were increasing our doses gradually, we chose a period of time of 3 weeks beginning at full dose, which would mimic chronic administration in line with that used in the field (Figure 2.3).

2. TRAP-Seq allows for molecular profiling of SPNs

Because dopamine D2 receptors are thought to be a primary target of antipsychotics, we sought a profiling of iSPNs, a site of especially high expression of the D2 receptor (Meador-Woodruff et al, 1989; Surmeier et al, 1996; Heiman et al, 2008). iSPNs make up approximately half of the striatal SPN population, with the other half comprised of

dopamine receptor D1 expressing SPNs; a minority population of SPNs express both D1 and D2 receptors (Surmeier et al, 1996). Because these dSPNs are also crucially involved in broader basal ganglia circuitry, and because antipsychotics may be blocking presynaptic dopamine receptors and therefore affecting overall dopamine levels in the striatum, we hypothesized that dSPNs could also be affected by chronic treatment (Shen et al, 2008). These two neuronal populations make up the majority of the striatal neuronal population (Gokce et al, 2016), and so targeting these two neuronal populations represents a nearly comprehensive assessment of the striatal projection population following antipsychotic treatment.

To target these cellular populations, we took advantage of two transgenic mouse lines: Drd1::EGFP-L10a, targeting dSPNs, and Drd2::EGFP-L10a, targeting iSPNs (Figure 2.4 A). We administered antipsychotics to these transgenic mice and subsequently purified mRNAs from them in a cell type-specific manner following the TRAP (Translating Ribosome Affinity Purification) protocol, which uses a GFP "tag" on actively translating ribosomes in a BAC transgenic model to allow for specific purification of mRNAs from a cell population of interest (Heiman et al, 2008). Following mRNA purification, we sequenced these mRNAs and identified differentially translated genes and altered pathways (Figure 2.4 B) For these analyses, we used the mm9 reference genome and the STAR 2.4.0 RNA-Seq aligner followed by Cuffquant processing in Cufflinks 2.0.0 for gene expression quantification follwoed by the Cuffdiff moedule for library normalization (Trapnell et al, 2012; Dobin et al, 2013). Genes with false discovery rate adjusted p-value <0.05 were categorized as differentially expressed genes. We identified enriched gene expression pathways and gene ontologies using Enrichr (Chen et

al, 2013; Kuleshov et al, 2016). We generated heat maps of gene and pathway changes using Morpheus software (The Broad Institute, https://software.broadinstitute.org/morpheus).

Yields for iSPN samples did not vary across treatments, but yields for dSPN samples treated with clozapine, risperidone, and haloperidol were lower than that for vehicle and aripiprazole treatments (Figure 2.5 A). This could not be explained by changes in Drd1a or Drd2 expression (Figure 2.5 B). Our study was well powered, with power ranging from 0.31-0.62 for 2-fold changes and 0.64-0.95 for 3-fold changes (Figure 2.5 C). These values indicate to us that we can detect many small fold changes, allowing us to have a more full picture of the broad translational changes occurring following antipsychotic administration.

3. Necab1 is primarily expressed in iSPNs in the striatum

An ongoing challenge in studies of striatal biology is the task of visually differentiating d- and iSPNs without cell type-specific transgenic insertions, as many of the differentially expressed genes in the wild-type mouse have low expression, are expressed in dendrites and therefore difficult to pinpoint as belonging to one individual cell, or are different at the population level but are still expressed to some degree in both cell types and therefore result in a positive immunofluorescence result in both cell types. Future studies would benefit from the identification of proteins that are differentially expressed in d- and iSPNs, expressed in the cell body, and have high-quality antibodies available.

Previous work had completed a highly-powered study of differential translation between dSPNs and iSPNs, and these findings pointed to the gene Necab1 as one of the most differentially translated genes between the two cell types that was expressed in the cytoplasm (Sudmant et al, 2018). Necab1 also appeared in our TRAP dataset to be predominantly expressed in iSPNs, not dSPNs, in our vehicle comparison of the two cell types (Figure 2.6 A). By immunofluorescence, we found that nearly 80% of cells in D2-TRAP tissue which positive for Necab1, GFP, or both were double-labeled, while approximately 10% of cells were positive for only Necab1 or GFP (Figure 2.6 B). Conversely, almost no cells in D1-TRAP tissue were double positive for Necab1 and GFP (Figure 2.6 C). These data indicate that Necab1 labels almost no dSPNs and most iSPNs, allowing it great utility as a marker of SPNs.

4. Antipsychotic administration alters gene expression

Each antipsychotic treatment led to increased and decreased transcript levels in both cell types. Interestingly, although antipsychotics primarily target the D2 receptor and not the D1 receptor, hundreds of translational alterations were observed in both dSPNs (Figure 2.7 A, Tables 2.2-2.9) and iSPNs (Figure 2.7 B, Tables 2.10-2.17). In fact, aripiprazole, risperidone, and haloperidol administration resulted in more genes changing in dSPNs than in iSPNs, a surprise given that the Drd2 receptor, which is more highly expressed in iSPNs than dSPNs, is the primary target of antipsychotics. We were particularly intrigued by a dramatic cell type-specific effect of clozapine: dSPNs showed very few altered transcripts altered following clozapine treatment (Figure 2.7 A), while iSPNs showed hundreds of altered transcripts (Figure 2.7 B). Hundreds of genes were

commonly changed in both cell types following aripiprazole (Figure 2.7 C), risperidone (Figure 2.7 E), and haloperidol (Figure 2.7 F); in the case of clozapine, where few genes changed in the iSPN population, half of the genes which were changing in the dSPNs were in common with the iSPN changes (Figure 2.7 D). There were 29 genes changing in common across all dSPNs treated with antipsychotics (Figure 2.8 A) and 126 genes changing in common across all iSPNs (Figure 2.8 B). These genes represent a "core signature" of chronic antipsychotic treatment in these two cell types.

5. Gene expression alterations found in TRAP studies overlap with genes identified in human studies of schizophrenia

Several of the genes that we saw changing following antipsychotic administration, including Drd2, have been previously implicated in elevated risk for development of schizophrenia (Lennertz et al, 2012; Schizophrenia Working Group of the Psychiatric Genomics Consortium, 2014). We were interested to understand the gene alterations that were in common with implicated genes in other studies. To characterize this, we looked specifically at genes increasing across all treatments in the iSPN population and their overlap with the DisGeNET database (Pinero et al, 2015), which aggregates genes that have been implicated in risk for schizophrenia (Figure 2.9 A). This analysis showed that 18 genes were in common between these two groups; pathway analysis of this gene list using the Kyoto Encyclopedia of Genes and Genomes (Kanehisa et al, 2000; Kuleshov et al, 2016) revealed that the only significantly associated pathway is "Glutamatergic Signaling" (Figure 2.9 B).

5. Antipsychotic administration reduces translation of gene associated with metabolic function

To better understand the cellular effects of chronic antipsychotic treatment in each cell type, we performed KEGG pathway analysis on each condition for both increased and decreased transcripts. When we looked at transcript levels decreased following antipsychotic treatment, we identified broad downregulation of genes involved in mitochondrial function in the iSPN cell type. These genes, most notably in the pathway "oxidative phosphorylation," emerged as the most significantly altered clusters of genes in iSPNs following aripiprazole (Figure 2.10 A, Table 2.18) and clozapine treatment (Figure 2.10 B, Table 2.19), the second-most altered cluster following risperidone treatment (Figure 2.10 C, Table 2.20), and the third-most altered cluster following haloperidol treatment (Figure 2.10 D, Table 2.21). Interestingly, these changes appear to have some specificity to the iSPN cell type. KEGG pathway analysis of the genes decreasing in dSPNs following antipsychotic treatment revealed different pathways, including calcium reabsorption following aripiprazole treatment (Figure 2.11 A, Table 2.22) and phenylalanine metabolism following clozapine treatment (Figure 2.11 B, Table 2.23). Following risperidone (Figure 2.11 C, Table 2.24) and haloperidol treatment (Figure 2.11 D, Table 2.25), components of the GABAergic synapse emerged as the most differentially translated pathway in dSPNs. In iSPNs, the genes implicated in oxidative phosphorylation alterations particularly pointed to decreased translation of genes important in Complex 1 and Complex 4 function (Figure 2.12). Many of these individual genes are also changing in dSPNs, but to a lesser degree or in an opposing direction compared to the iSPN cell population (Figure 2.13). RT-PCR of total striatal RNA

samples confirmed a subset of oxidative phosphorylation transcript decreases following antipsychotic administration (Figure 2.14).

6. Antipsychotic administration promotes translation of genes associated with glutamatergic signaling

When we performed pathway analysis for upregulated transcripts following antipsychotic administration, we saw increases in transcripts associated broadly with synaptic function. In iSPNs, we found that the pathway "glutamatergic synapse" was changing across all four treatments, emerging as the most significantly altered pathway following aripiprazole (Figure 2.15 A, Table 2.26), clozapine (Figure 2.15 B, Table 2.27), and haloperidol (Figure 2.15 C, Table 2.28), and the third most significantly altered pathway following risperidone administration (Figure 2.15 D., Table 2.29). In dSPNs, pathways associated with the "synaptic vesicle cycle" were altered following both aripiprazole (Figure 2.16 A, Table 2.30) and clozapine administration (Figure 2.16 B, Table 2.31). The pathway "glutamatergic synapse" was altered following both risperidone (Figure 2.16 C, Table 2.32) and haloperidol administration (Figure 2.16 D, Table 2.33).

Because many of these individual treatment and cell type analyses revealed alterations in the glutamatergic synapse, we were curious to better understand which pathways were the most commonly altered across treatments and both SPN populations. We found that "glutamatergic synapse" was in fact the most commonly altered pathway, significantly altered in every cell type and treatment except for the D1 aripiprazole and clozapine conditions (Figure 2.17). When we looked more closely at the molecular

changes underlying this pathway, we identified scaffolding proteins, such as *Shank3, Dlg4,* and *Shank1* were among those most commonly altered following antipsychotic administration, along with presynaptic release factors including Stxbp1 and Syp, and AMPA/NMDAR receptor subunits such as Grin2b and Gria1 (Figure 2.18).

We found that genes associated with glutamatergic signalling were typically increased in both dSPNs and iSPNs, but to a greater degree and/or number in the iSPNs, leading to the glutamatergic pathway emerging as a more consistent and significantly altered pathway in this cell type following antipsychotic administration (Figure 2.19). RT-PCR from dSPN and iSPN cDNA samples confirmed increased transcript levels of *Shank3* in following all antipsychotic treatments in both cell types, except for no significant change in dSPN samples from mice treated with clozapine (Figure 2.20). Psd95 protein levels were also confirmed to increase in total striatum protein following chronic clozapine administration (Figure 2.21). These molecular changes point towards an increase in translation of synaptic components associated with increase glutamatergic function following chronic antipsychotic treatment.

Chapter 2 Summary & Discussion

Summary

We have undertaken a whole-genome, unbiased, *in vivo* study of the translational alterations in SPNs induced by chronic antipsychotic administration across a panel of antipsychotics (aripiprazole, clozapine, risperidone, and haloperidol). This drug selection represents typical (haloperidol) and atypical (aripiprazole, clozapine, and risperidone) antipsychotics; D2 antagonists (clozapine, risperidone, and haloperidol) and a D2 partial agonist (aripiprazole); and the most efficacious antipsychotic on the market (clozapine). By studying both SPN cell types of the striatum, we were able to uncover the translational alterations occurring in 95% of the neurons of the striatum, a brain region consistently implicated in schizophrenia and antipsychotic administration.

In addition to revealing a cell type-specific marker, Necab1, that will be useful in subsequent cell type-specific studies of SPNs, this study allowed us to interrogate similarities and differences across first- and second-generation antipsychotics and two neuronal cell types crucial for basal ganglia function. We have demonstrated broad translational alterations following chronic antipsychotic administration that shows chronic administration of aripiprazole, risperidone, or haloperidol change gene expression of more genes in dSPNs than in iSPNs.

Increased Components of the Glutamatergic Synapse following Antipsychotic Administration

We have uncovered a common core signature of increased glutamatergic function common to all antipsychotics, a key discovery given that these four antipsychotics

represent a diversity of neuroleptic drugs. The specific genes with increased translation implicate increased glutamatergic postsynaptic number or strength as a key to understanding what efficacious antipsychotics have in common. Increases in the postsynaptic scaffolding molecule PSD95 are one example, as PSD95-dependent increases in glutamatergic function have been functionally demonstrated (Phillips et al, 2011). An additional postsynaptic scaffolding molecule that increases in iSPNs across all four antipsychotics, SHANK3, has been implicated as a risk gene for schizophrenia (de Sena et al, 2017).

Furthermore, we identified a cell type-specific effect of clozapine treatment that could partially explain its increased efficacy in the clinic. Clozapine altered translation of hundreds of genes in iSPNs, but very few genes in dSPNs. At the same time, the pathways altered in iSPNs were very similar to those altered in iSPNs by aripiprazole, risperidone, and haloperidol, but with more pathway members altered and to a greater degree.

Better Understanding Causes of Antipsychotic Side Effects: Metabolic and Tardive Dyskinesia

One interesting finding from our mRNA profiling data is that metabolic components of complex I and complex IV are significantly decreased, especially in iSPNs, following antipsychotic treatment. Metabolic genes have been implicated as risk genes for schizophrenia in GWAS, and so it is possible that these changes are a therapeutic benefit of antipsychotics. On the other hand, metabolic changes have been implicated in side effects of antipsychotics. It would be interesting to specifically alter

complex I and/or complex IV function in SPNs *in vivo* and perform behavioral analyses to study whether this change impacts measures of antipsychotic efficacy, such as prepulse inhibition.

Tardive Dyskinesia (TD) is a motor disorder common with typical antipsychotics such as haloperidol, and it is generally irreversible. It is not well understood how chronic antipsychotic administration leads to TD, nor why only a subset of patients develops this motor disorder, although variants in the dopamine D3 receptor have been implicated as leading to increased risk for developing TD (Burke et al, 1982; Lerer et al, 2002; Cornett et al, 2017). Our transcriptional database would also make it possible to perform analysis and mechanistic studies of genes that change only after haloperidol treatment and not after treatment with atypical antipsychotics. Some of these genes may be involved in long-term development of TD, especially given that dSPNs and iSPNs are crucial for motor behavior. Identifying the transcriptional profile associated with motor side effects could lead to development of therapeutics that could prevent these motor side effects or potentially reverse them.

Validation of TRAP Profiling

Although we did independently confirm reductions in some transcripts associated with oxidative phosphorylation and increases in some PSD gene transcripts or proteins, additional experiments could be performed to more fully validate our TRAP findings. These fall into two main categories. The first is to validate changing transcript or protein levels of individual genes changing in the TRAP dataset, especially those related to oxidative phosphorylation or glutamatergic synapses. To validate individual genes, there

are several approaches we could take. At the level of RNA, we could perform RT-qPCR on RNA samples purified from an additional cohort of TRAP mice. At the level of protein, we could perform cell type-specific analyses of protein levels using costains of Necab1. There are several challenges that exist for validation of RNA sequencing datasets. First, studies of RNA sequencing use a different statistical approach than RT-qPCR approaches. For example, Cuffdiff models and accounts for technical variability of cDNA library preparation and biological variability across samples; sequencing at relatively high depth, which we performed, allows for higher power to detect smaller fold changes (Trapnell et al, 2012). These approaches are not available in RT-PCR or immunofluorescent staining protocols. As a result, these methods are valuable for claiming positive findings, but a relatively higher false negative rate of these validation approaches would prevent us from discarding targets based on negative findings.

A second form of validation would be to study functional alterations that would be predicted to directly follow from the alterations in our TRAP dataset. For example, our TRAP profiling data show increased GABAergic release transcripts, which suggests the potential for increased release probability in iSPNs following chronic clozapine administration. The nucleus accumbens has two primary outputs: the substantia nigra, for dSPNs, and the globus pallidus, for iSPNs. These outputs produce opposing effects on cortical excitation and drive back into the striatum; clozapine increasing GABAergic output in iSPNs but not dSPNs could lead to a change in direct:indirect pathway strength ratio. To test the functional effects of increased GABAergic release transcripts following chronic clozapine administration, one initial test would be to perform paired pulse ratio recordings in the substantia nigra and the globus pallidus following stimulation of

presynaptic SPNs. We would predict that we would not see changes to paired pulse ratio when recording from neurons of the substantia nigra, the output of dSPNs, but would see a decrease in paired pulse ratio when recording from neurons of the globus pallidus external, the output of iSPNs, reflective of increased GABAergic output from the iSPN population specifically.

Drug	Class	Receptor Affinities	Dose
Haloperidol (Haldol)	Typical / First Generation	D2, 5-HT2, α1, D1	0.221 mg/kg
Clozapine (Clozaril)	Atypical / Second Generation	5-HT2A, 5-HT2C, D2, D4, H1, M1-5, α1, α2	2.000 mg/kg
Risperidone (Risperdal)	Atypical / Second Generation	5-HT2, D2, H1, 5-HT1A, 5-HT1C, 5-HT1D, D1	0.074 mg/kg
Aripiprazole (Abilify)	Atypical / Second Generation	D2, 5-HT1A, 5-HT2A, α1, α2, H1	0.294 mg/kg

Table 2.1: Category and receptor affinities of antipsychotics. The 4 drugs used in subsequent antipsychotic administration experiments categorized by drug class, receptor affinity, and dosage used in subsequent experiments.

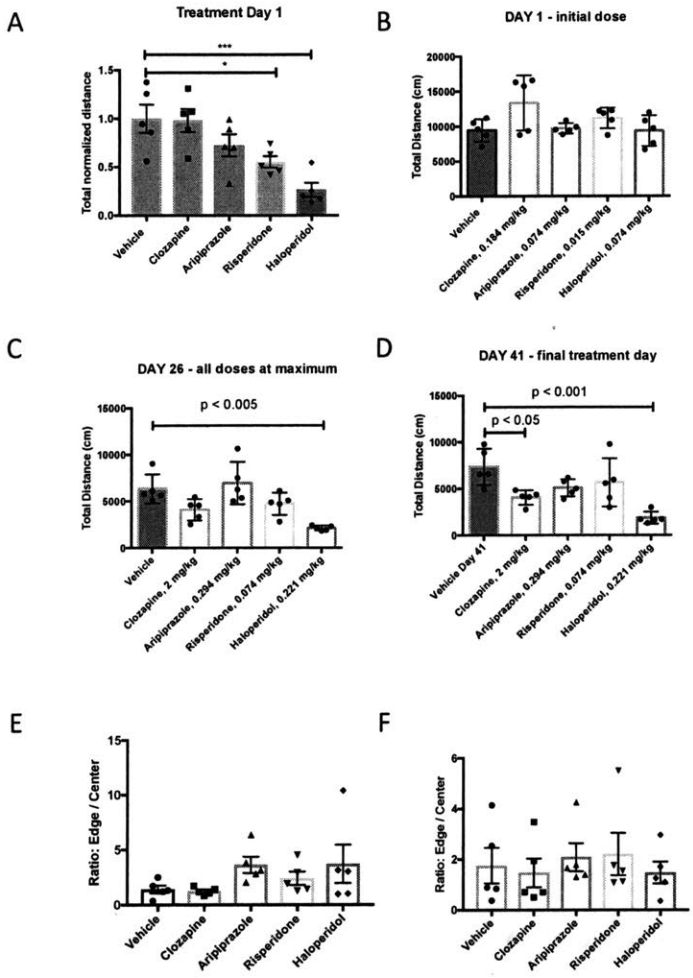

Figure 2.1: Locomotor behavior is differentially affected by individual antipsychotics and varies by dose. Open field overall activity immediately following dosage with a single full dose of each antipsychotic (A), one initial, lower dose of each antipsychotic (B), the first full dose in the chronic treatment paradigm (C), and on the final day of 6 weeks of treatment (D). Thigmotaxis measurements following 1 full dose (E) and 6 weeks of dosage (F). N=5 animals in each condition. All error bars: mean +/- SEM. * $p<0.05$, ** $p<0.01$, *** $p<0.001$

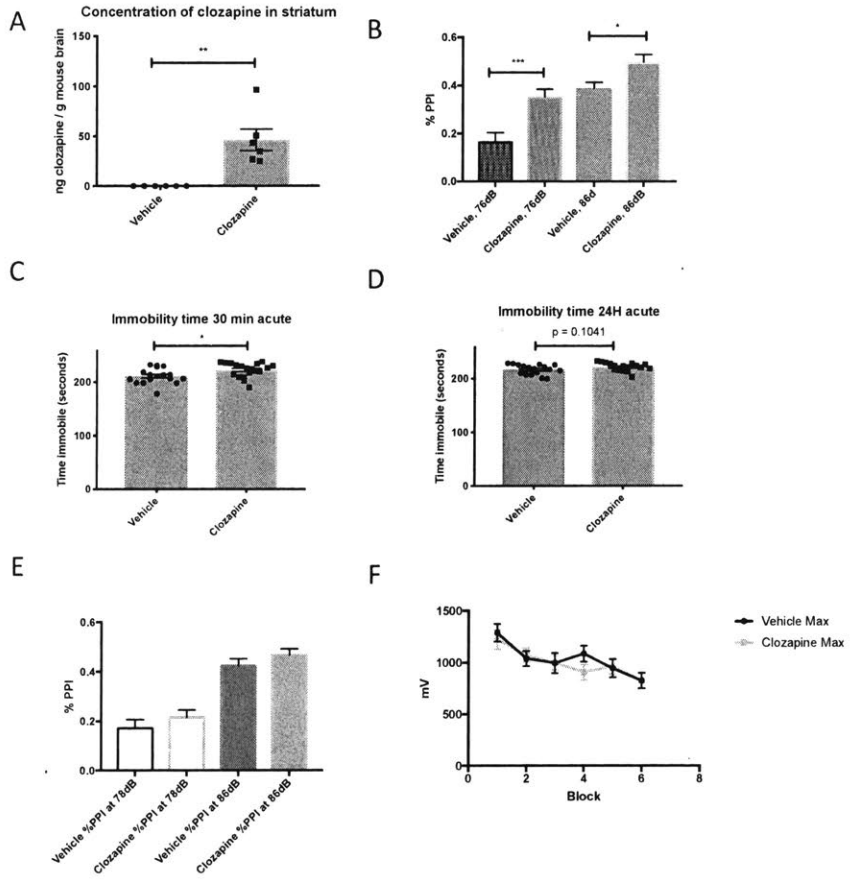

Figure 2.2: Clozapine reaches the striatum and acute dosage increases prepulse inhibition and immobility during the forced swim test.
Concentration of clozapine in striatum following administration as measured by mass spectrometry (A). Percent of prepulse inhibition following one full dose of clozapine (B). Immobility time in the forced swim test 30 minutes after one full dose of clozapine (C) and 24H after one full dose of clozapine (D). Percent of prepulse inhibition following 6 weeks of clozapine administration (E). Startle habituation following 6 weeks of clozapine administration (F). N=6 per condition for clozapine level measurements; N=20 for prepulse inhibition experiments, startle habituation experiment, and forced swim experiments. All error bars: mean +/- SEM. * $p<0.05$, ** $p<0.01$, *** $p<0.001$

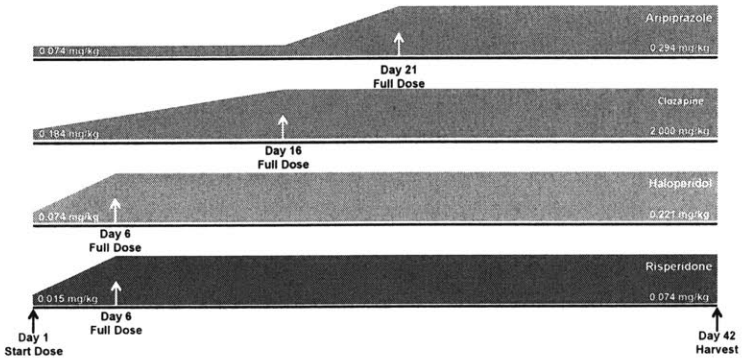

Figure 2.3: Chronic antipsychotic dosage. Dosage amounts and time to ramp up for aripiprazole, clozapine, risperidone, and haloperidol.

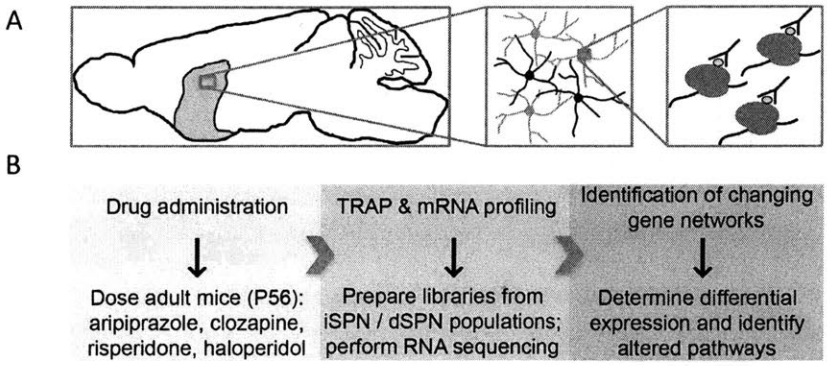

Figure 2.4: Experimental design of cell type-specific mRNA profiling following chronic antipsychotic treatment. Schematic demonstrating TRAP as a method to target a subpopulation of genetically defined actively translating ribosome-associated mRNAs (A). Experimental design of TRAP harvest and analysis, including drug administration, mRNA profiling, and gene network analysis (B).

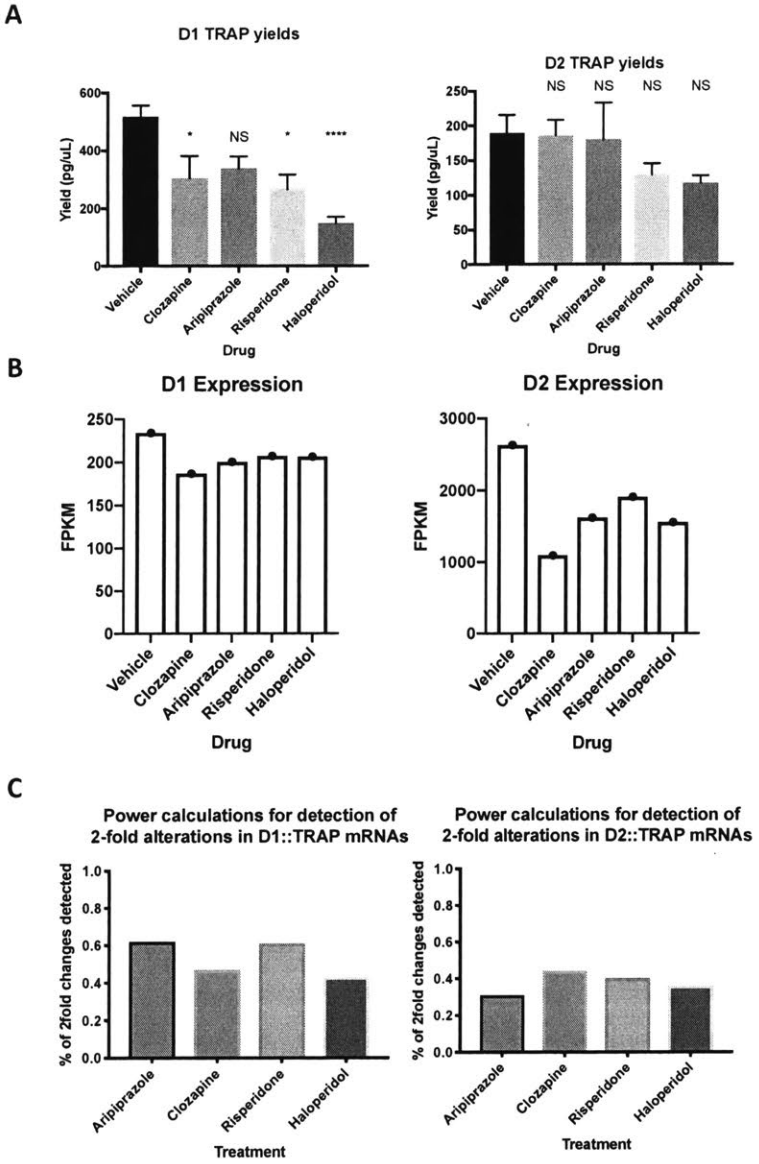

Figure 2.5: mRNA yields following immunopurification and power analysis of RNA-Seq experiments. mRNA yields in dSPNs and iSPNs by drug treatment (A). Relative levels of Drd1a and Drd2 expression in RNA-seq samples by drug treatment (B). Power calculations for 2-fold gene expression changes in dSPNs (C) and iSPNs (D). N=6 per condition. For yields, error bars = mean +/- SEM. * $p<0.05$ **** $p<0.0001$

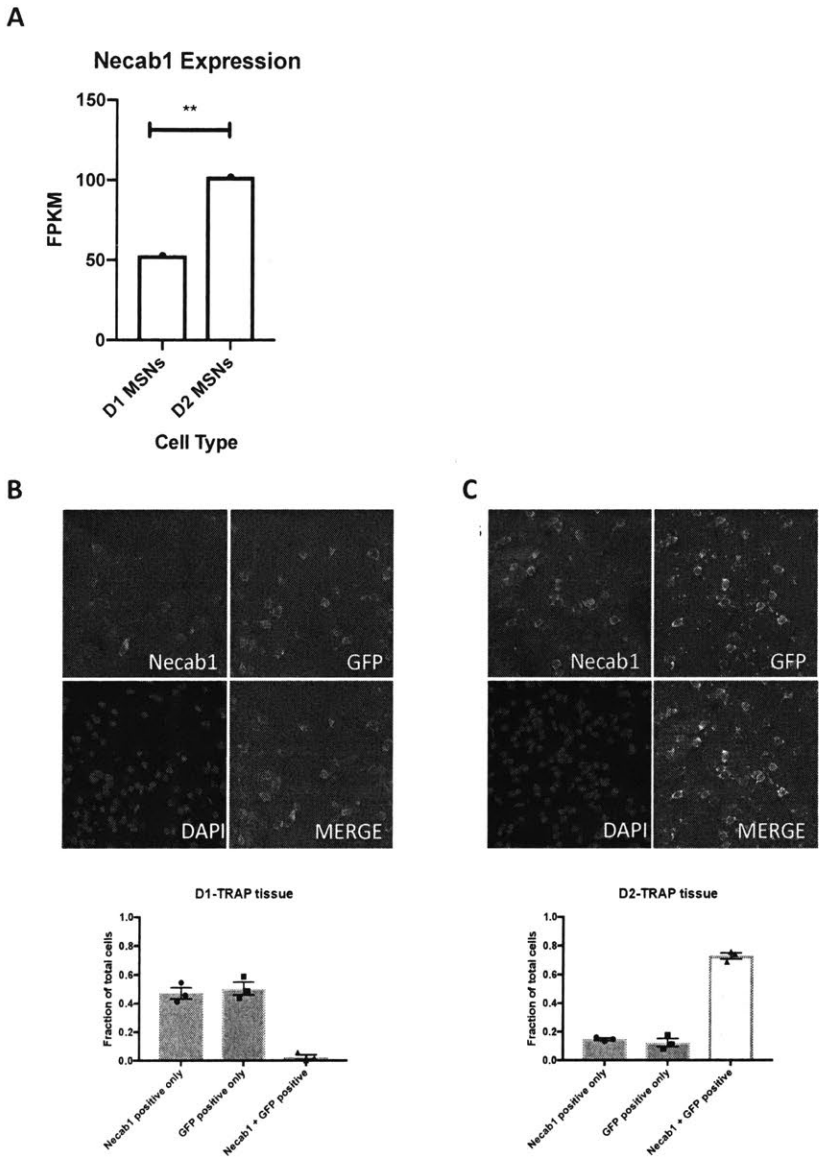

Figure 2.6: *Necab1* is primarily expressed in iSPNs. RNA-Seq reads of Necab1 in dSPNs and iSPNs (A). Immunofluorescence of D1-GFP tissue costained for GFP and Necab1 and quantification (B). Immunofluorescence of D2-GFP tissue costained for GFP and Necab1 and quantification (C). N=6 per condition for RNA-Seq reads and N=3 per condition for indirect immunofluorescence. Error bars are means +/- SEM. ** $p<0.01$

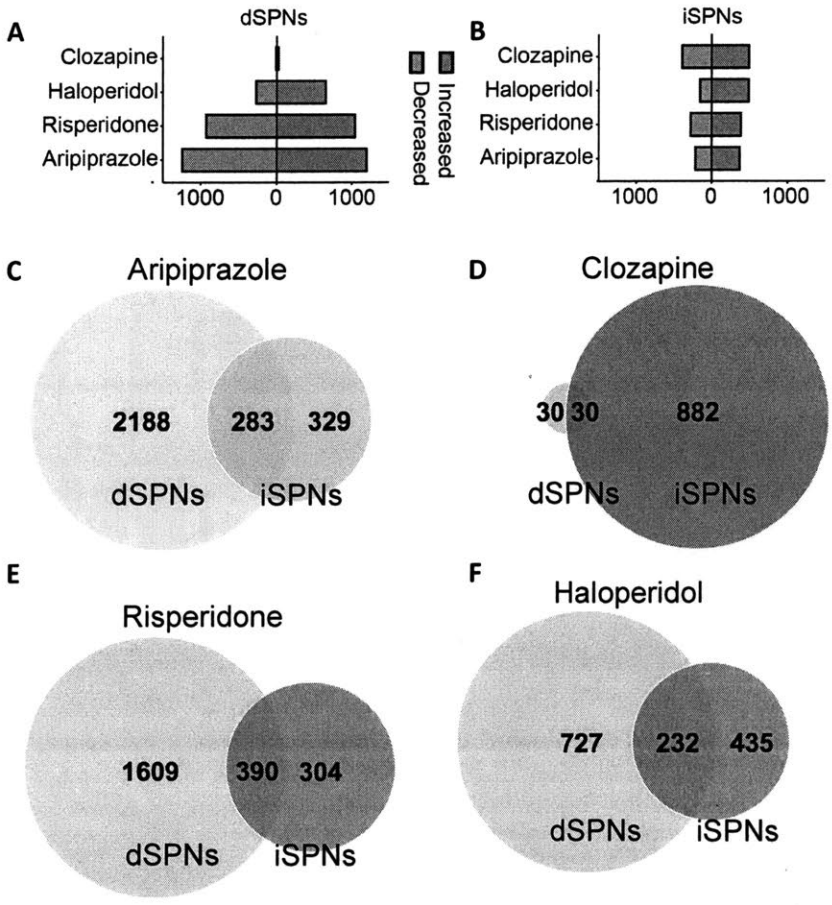

Figure 2.7: Antipsychotic administration leads to altered translation in both dSPNs and iSPNs. Differentially translated genes in dSPNs (A) and iSPNs (B) following treatment with clozapine, haloperidol, risperidone, and aripiprazole. Significant genes (adjusted p-value <0.05) are highlighted in red (upregulated) or blue (downregulated). Overlaps of genes changing in both dSPNs and iSPNs following each of four treatments (C-F).

gene	sample_1	sample_2	value_1 (dSPN aripiprazole)	value_2 (dSPN vehicle)	log2 (fold_change) dSPN Aripiprazole vs. Vehicle	q_value
Dgkg	Arip_D1	Veh_D1	31.0232	46.0459	-0.569727	0.000814699
Akap9	Arip_D1	Veh_D1	54.6315	81.0301	-0.568724	0.000814699
Usp45	Arip_D1	Veh_D1	16.7193	24.7934	-0.568436	0.000814699
Tgfa	Arip_D1	Veh_D1	64.9453	96.2918	-0.568188	0.000814699
Erbb2ip	Arip_D1	Veh_D1	14.7804	21.8855	-0.566288	0.000814699
Rims2	Arip_D1	Veh_D1	24.8297	36.7464	-0.565536	0.000814699
Coch	Arip_D1	Veh_D1	45.1238	66.6789	-0.56334	0.000814699
Cipc	Arip_D1	Veh_D1	35.1538	51.876	-0.561387	0.000814699
Slc2a13	Arip_D1	Veh_D1	23.6047	34.7432	-0.557654	0.000814699
Plcb1	Arip_D1	Veh_D1	81.3251	119.606	-0.556516	0.000814699
Mff	Arip_D1	Veh_D1	88.1566	129.521	-0.555049	0.000814699
Wsb2	Arip_D1	Veh_D1	80.4187	117.579	-0.548027	0.000814699
Rps4x	Arip_D1	Veh_D1	123.991	181.065	-0.54627	0.000814699
Kif5a	Arip_D1	Veh_D1	65.2851	95.0301	-0.541631	0.000814699
Pbx3	Arip_D1	Veh_D1	69.579	101.25	-0.5412	0.000814699
Usp32	Arip_D1	Veh_D1	27.6071	40.0662	-0.537344	0.000814699
Wnk1	Arip_D1	Veh_D1	38.9927	56.5673	-0.536765	0.000814699
Tmed9	Arip_D1	Veh_D1	107.04	155.211	-0.536078	0.000814699
Cnksr2	Arip_D1	Veh_D1	105.956	153.607	-0.535784	0.000814699
Tac1	Arip_D1	Veh_D1	293.908	425.203	-0.532786	0.000814699
R3hdm1	Arip_D1	Veh_D1	83.4542	120.655	-0.531837	0.000814699
Nefm	Arip_D1	Veh_D1	175.805	253.709	-0.529198	0.000814699
Kif5c	Arip_D1	Veh_D1	63.0765	90.9496	-0.527964	0.000814699
Ank2	Arip_D1	Veh_D1	35.3998	50.9713	-0.525943	0.000814699
Fat3	Arip_D1	Veh_D1	13.8874	19.9203	-0.520462	0.000814699
Eif5	Arip_D1	Veh_D1	68.352	97.7997	-0.516846	0.000814699
Synj1	Arip_D1	Veh_D1	97.4149	139.364	-0.516644	0.000814699
Kif5b	Arip_D1	Veh_D1	24.8753	35.3336	-0.506328	0.000814699
Canx	Arip_D1	Veh_D1	38.1911	54.1473	-0.50365	0.000814699
Cox6c	Arip_D1	Veh_D1	430.265	609.507	-0.502415	0.000814699
Cnr1	Arip_D1	Veh_D1	40.306	57.0225	-0.500536	0.000814699
Sipa1l1	Arip_D1	Veh_D1	77.0281	108.94	-0.500074	0.000814699
Ube2d3	Arip_D1	Veh_D1	164.449	232.506	-0.499625	0.000814699
Rab14	Arip_D1	Veh_D1	81.2714	114.63	-0.496162	0.000814699
Kcna2	Arip_D1	Veh_D1	34.0185	47.876	-0.49298	0.000814699
Cnbp	Arip_D1	Veh_D1	210.753	296.152	-0.490781	0.000814699
Lrrc7	Arip_D1	Veh_D1	66.5447	92.9999	-0.482906	0.000814699
Tubb4b	Arip_D1	Veh_D1	193.15	268.755	-0.476569	0.000814699
9930021J03Rik	Arip_D1	Veh_D1	34.9497	48.561	-0.474518	0.000814699
Rasgef1a	Arip_D1	Veh_D1	139.144	191.755	-0.462682	0.000814699

Table 2.2: Top 40 downregulated genes in dSPNs following aripiprazole administration. Genes are sorted by q-value and then $\log_2$fold change.

gene	sample_1	sample_2	value_1 (dSPN aripiprazole)	value_2 (dSPN vehicle)	log2 (fold_change) dSPN Aripiprazole vs. Vehicle	q_value
Mir6236	Arip_D1	Veh_D1	9154.87	2125.72	2.10659	0.000814699
Syp	Arip_D1	Veh_D1	374.825	97.7603	1.9389	0.000814699
Hist2h4	Arip_D1	Veh_D1	87.7142	23.3897	1.90694	0.000814699
Bahcc1	Arip_D1	Veh_D1	31.6804	8.60347	1.8806	0.000814699
Psd	Arip_D1	Veh_D1	103.16	28.8783	1.83683	0.000814699
Tnrc18	Arip_D1	Veh_D1	48.2525	13.5778	1.82936	0.000814699
Sepw1	Arip_D1	Veh_D1	318.89	93.3541	1.77227	0.000814699
Dand5	Arip_D1	Veh_D1	41.4864	12.296	1.75446	0.000814699
Ptp4a3	Arip_D1	Veh_D1	19.416	5.8043	1.74205	0.000814699
2610306M01Rik	Arip_D1	Veh_D1	12.2804	3.68563	1.73637	0.000814699
Polr2f	Arip_D1	Veh_D1	67.3091	20.2086	1.73583	0.000814699
Crabp1	Arip_D1	Veh_D1	40.9579	12.3314	1.7318	0.000814699
Dact2	Arip_D1	Veh_D1	12.5079	3.77711	1.72749	0.000814699
Psmd9	Arip_D1	Veh_D1	22.4775	7.0451	1.67379	0.000814699
Tomm6	Arip_D1	Veh_D1	171.454	53.8807	1.66998	0.000814699
Junb	Arip_D1	Veh_D1	24.0251	7.56024	1.66804	0.000814699
Asic4	Arip_D1	Veh_D1	15.8237	4.9985	1.66252	0.000814699
Samd1	Arip_D1	Veh_D1	8.31154	2.73262	1.60483	0.000814699
Cabp1	Arip_D1	Veh_D1	16.6685	5.55474	1.58534	0.000814699
Prdx5	Arip_D1	Veh_D1	124.582	43.208	1.52773	0.000814699
Slc25a22	Arip_D1	Veh_D1	53.8909	18.7113	1.52613	0.000814699
Wdr83os	Arip_D1	Veh_D1	251.418	87.6	1.52109	0.000814699
Rnf187	Arip_D1	Veh_D1	497.79	174.443	1.51278	0.000814699
Ptms	Arip_D1	Veh_D1	646.848	227.15	1.50979	0.000814699
6030419C18Rik	Arip_D1	Veh_D1	30.7243	10.8616	1.50014	0.000814699
Fam57b	Arip_D1	Veh_D1	9.53626	3.37862	1.49699	0.000814699
Rad23a	Arip_D1	Veh_D1	27.3237	9.86344	1.46999	0.000814699
Foxo6	Arip_D1	Veh_D1	13.8824	5.06104	1.45575	0.000814699
Prr12	Arip_D1	Veh_D1	131.286	47.9938	1.45179	0.000814699
Dtx3	Arip_D1	Veh_D1	68.0703	24.9271	1.44931	0.000814699
Ring1	Arip_D1	Veh_D1	23.0437	8.49345	1.43995	0.000814699
Map3k11	Arip_D1	Veh_D1	10.9283	4.06496	1.42676	0.000814699
Psenen	Arip_D1	Veh_D1	46.6295	17.3843	1.42346	0.000814699
Ube2v1	Arip_D1	Veh_D1	36.6182	13.6755	1.42097	0.000814699
Cpne6	Arip_D1	Veh_D1	30.9797	11.5935	1.41801	0.000814699
Rab1b	Arip_D1	Veh_D1	43.0642	16.1878	1.41158	0.000814699
2810428I15Rik	Arip_D1	Veh_D1	50.4293	19.1191	1.39925	0.000814699
Pard6b	Arip_D1	Veh_D1	9.73216	3.69738	1.39626	0.000814699
Khdrbs2	Arip_D1	Veh_D1	17.5897	6.72492	1.38715	0.000814699
Snrpa	Arip_D1	Veh_D1	55.9932	21.4274	1.38579	0.000814699

Table 2.3: Top 40 upregulated genes in dSPNs following aripiprazole administration. Genes are sorted by q-value and then $\log_2$fold change.

gene	sample_1	sample_2	value_1 (dSPN clozapine)	value_2 (dSPN vehicle)	log2 (fold_change) dSPN Clozapine vs. Vehicle	q_value
Gpr155	Cloz_Chron_D1	Veh_Chron_D1	35.2645	57.2307	-0.698571	0.0475167
Uqcrb	Cloz_Chron_D1	Veh_Chron_D1	211.573	354.95	-0.746465	0.0403443
Tmem230	Cloz_Chron_D1	Veh_Chron_D1	25.3427	53.5748	-1.07999	0.0245776
Trpm3	Cloz_Chron_D1	Veh_Chron_D1	2.72248	8.31645	-1.61105	0.0245776
Enpp2	Cloz_Chron_D1	Veh_Chron_D1	27.2629	99.9384	-1.8741	0.0245776
Igf2	Cloz_Chron_D1	Veh_Chron_D1	3.01724	12.9007	-2.09615	0.0245776
Col8a1	Cloz_Chron_D1	Veh_Chron_D1	0.332592	2.41601	-2.8608	0.0245776
Ttr	Cloz_Chron_D1	Veh_Chron_D1	40.8436	448.068	-3.45554	0.0245776
Prlr	Cloz_Chron_D1	Veh_Chron_D1	0.206758	4.40634	-4.41356	0.0245776
Serpinb9b	Cloz_Chron_D1	Veh_Chron_D1	0	0.171133	#VALUE!	0.0475167
S100a5	Cloz_Chron_D1	Veh_Chron_D1	0	0.291812	#VALUE!	0.0403443
Pde6h	Cloz_Chron_D1	Veh_Chron_D1	0	0.248124	#VALUE!	0.0245776
Olfr461	Cloz_Chron_D1	Veh_Chron_D1	0	0.267225	#VALUE!	0.0339405
Olfr1417	Cloz_Chron_D1	Veh_Chron_D1	0	0.264152	#VALUE!	0.0403443
Hpd	Cloz_Chron_D1	Veh_Chron_D1	0	0.232096	#VALUE!	0.0475167
Defb22	Cloz_Chron_D1	Veh_Chron_D1	0	0.252024	#VALUE!	0.0245776
Ccl4	Cloz_Chron_D1	Veh_Chron_D1	0	0.228361	#VALUE!	0.0475167
9230104L09Rik	Cloz_Chron_D1	Veh_Chron_D1	0	0.59303	#VALUE!	0.0475167
2410137M14Rik	Cloz_Chron_D1	Veh_Chron_D1	0	0.2328	#VALUE!	0.0403443
1700109G15Rik	Cloz_Chron_D1	Veh_Chron_D1	0	0.577847	#VALUE!	0.0339405
1700064M15Rik	Cloz_Chron_D1	Veh_Chron_D1	0	0.194221	#VALUE!	0.0339405

Table 2.4: All 21 downregulated genes in dSPNs following clozapine administration. Genes are sorted by q-value and then $\log_2$fold change.

gene	sample_1	sample_2	value_1 (dSPN clozapine)	value_2 (dSPN vehicle)	log2 (fold_change) dSPN Clozapine vs. Vehicle	q_value
Wbp2nl	Cloz_Chron_D1	Veh_Chron_D1	0.209564	0	#NAME?	0.0245776
Vaultrc5	Cloz_Chron_D1	Veh_Chron_D1	0.859988	0	#NAME?	0.0245776
Hrct1	Cloz_Chron_D1	Veh_Chron_D1	0.362245	0	#NAME?	0.0245776
Efnb1	Cloz_Chron_D1	Veh_Chron_D1	4.05049	0.603352	2.74702	0.0245776
Foxo6	Cloz_Chron_D1	Veh_Chron_D1	19.9561	5.01283	1.99314	0.0245776
Ccdc3	Cloz_Chron_D1	Veh_Chron_D1	11.278	3.44731	1.70997	0.0245776
Gm10336	Cloz_Chron_D1	Veh_Chron_D1	6.32501	1.93641	1.70769	0.0245776
Syp	Cloz_Chron_D1	Veh_Chron_D1	240.73	96.9358	1.31231	0.0245776
Shank1	Cloz_Chron_D1	Veh_Chron_D1	38.2098	16.0507	1.25131	0.0245776
Arhgap23	Cloz_Chron_D1	Veh_Chron_D1	19.7448	9.51926	1.05255	0.0245776
Satb1	Cloz_Chron_D1	Veh_Chron_D1	15.4021	7.62751	1.01384	0.0245776
Psd	Cloz_Chron_D1	Veh_Chron_D1	53.0857	28.6235	0.891124	0.0245776
Prr12	Cloz_Chron_D1	Veh_Chron_D1	87.3588	47.5411	0.877778	0.0245776
Celsr2	Cloz_Chron_D1	Veh_Chron_D1	24.2462	13.4895	0.84592	0.0245776
Ncdn	Cloz_Chron_D1	Veh_Chron_D1	230.546	134.154	0.781167	0.0245776
Atp6v1a	Cloz_Chron_D1	Veh_Chron_D1	185.298	108.757	0.768747	0.0245776
Glul	Cloz_Chron_D1	Veh_Chron_D1	120.281	71.157	0.757331	0.0245776
Diras1	Cloz_Chron_D1	Veh_Chron_D1	58.2533	34.5046	0.755554	0.0245776
Dpysl2	Cloz_Chron_D1	Veh_Chron_D1	92.392	55.0778	0.746296	0.0245776
Spock2	Cloz_Chron_D1	Veh_Chron_D1	75.3395	47.9175	0.652855	0.0245776
Defb1	Cloz_Chron_D1	Veh_Chron_D1	0.306678	0	#NAME?	0.0339405
Kctd15	Cloz_Chron_D1	Veh_Chron_D1	3.74517	0.605683	2.6284	0.0339405
Stk17b	Cloz_Chron_D1	Veh_Chron_D1	6.82108	1.65762	2.04089	0.0339405
Slc6a7	Cloz_Chron_D1	Veh_Chron_D1	6.72267	2.23699	1.58747	0.0339405
Bhlhe40	Cloz_Chron_D1	Veh_Chron_D1	22.5401	10.5729	1.09212	0.0339405
Kat5	Cloz_Chron_D1	Veh_Chron_D1	41.0068	20.0148	1.0348	0.0339405
Ptms	Cloz_Chron_D1	Veh_Chron_D1	377.552	225.19	0.745537	0.0339405
Eef1a2	Cloz_Chron_D1	Veh_Chron_D1	119.008	72.5007	0.714987	0.0339405
Rnf187	Cloz_Chron_D1	Veh_Chron_D1	282.984	172.89	0.710862	0.0339405
Eno2	Cloz_Chron_D1	Veh_Chron_D1	390.558	251.933	0.632496	0.0339405
Gm9159	Cloz_Chron_D1	Veh_Chron_D1	0.199785	0	#NAME?	0.0403443
Zfp114	Cloz_Chron_D1	Veh_Chron_D1	3.79929	0.701714	2.43677	0.0403443
Mir6236	Cloz_Chron_D1	Veh_Chron_D1	4397.94	2108.05	1.06092	0.0403443
Mical2	Cloz_Chron_D1	Veh_Chron_D1	36.9311	20.6433	0.839164	0.0403443
Slc8a2	Cloz_Chron_D1	Veh_Chron_D1	28.7193	16.2447	0.82205	0.0403443
Mpp2	Cloz_Chron_D1	Veh_Chron_D1	55.8081	32.9014	0.762325	0.0403443
Unc13a	Cloz_Chron_D1	Veh_Chron_D1	19.66	11.8284	0.733015	0.0403443
Car8	Cloz_Chron_D1	Veh_Chron_D1	1.94899	0.361723	2.42977	0.0475167
Efhd2	Cloz_Chron_D1	Veh_Chron_D1	25.429	10.1557	1.32418	0.0475167

Table 2.5: Top 40 upregulated genes in dSPNs following clozapine administration. Genes are sorted by q-value and then $\log_2$fold change.

gene	sample_1	sample_2	value_1 (dSPN risperidone)	value_2 (dSPN vehicle)	log2 (fold_change) dSPN Risperidone vs. Vehicle	q_value
Ywhaq	Risp_D1	Veh_D1	75.4621	122.982	-0.704628	0.00106657
Hook3	Risp_D1	Veh_D1	6.33995	10.3218	-0.703153	0.00106657
Efcab14	Risp_D1	Veh_D1	16.8274	27.3548	-0.700985	0.00106657
Macf1	Risp_D1	Veh_D1	4.88091	7.91897	-0.698163	0.00106657
Slc4a10	Risp_D1	Veh_D1	16.536	26.7527	-0.694072	0.00106657
Galnt13	Risp_D1	Veh_D1	26.2407	42.3938	-0.692049	0.00106657
Hsp90aa1	Risp_D1	Veh_D1	135.494	218.892	-0.691992	0.00106657
Gucy1a2	Risp_D1	Veh_D1	18.4367	29.7118	-0.688452	0.00106657
Gucy1a3	Risp_D1	Veh_D1	57.9426	93.3697	-0.688329	0.00106657
Mff	Risp_D1	Veh_D1	79.7508	127.907	-0.681523	0.00106657
Tac1	Risp_D1	Veh_D1	262.233	419.856	-0.679044	0.00106657
Gatc	Risp_D1	Veh_D1	95.9039	153.534	-0.678895	0.00106657
Rtn4	Risp_D1	Veh_D1	195.832	311.89	-0.671425	0.00106657
Fam163b	Risp_D1	Veh_D1	37.3404	59.2377	-0.66578	0.00106657
Btbd3	Risp_D1	Veh_D1	18.91	29.9405	-0.662947	0.00106657
2900056M20Rik	Risp_D1	Veh_D1	28.6753	45.396	-0.662757	0.00106657
Eps15	Risp_D1	Veh_D1	26.6796	42.2083	-0.661791	0.00106657
H3f3b	Risp_D1	Veh_D1	65.3194	103.223	-0.660185	0.00106657
Mmd	Risp_D1	Veh_D1	80.3341	126.537	-0.655473	0.00106657
Slc25a46	Risp_D1	Veh_D1	49.1242	77.3372	-0.654731	0.00106657
Scd2	Risp_D1	Veh_D1	28.8859	45.3659	-0.651246	0.00106657
Bmpr2	Risp_D1	Veh_D1	41.8137	65.6628	-0.651101	0.00106657
Sh3gl2	Risp_D1	Veh_D1	107.602	168.718	-0.648904	0.00106657
Ccdc88a	Risp_D1	Veh_D1	14.4715	22.6139	-0.643998	0.00106657
Mfsd6	Risp_D1	Veh_D1	31.846	49.176	-0.626845	0.00106657
Ankrd12	Risp_D1	Veh_D1	29.0792	44.749	-0.62187	0.00106657
Kif5a	Risp_D1	Veh_D1	60.9883	93.8434	-0.621722	0.00106657
Gls	Risp_D1	Veh_D1	82.1321	126.337	-0.621257	0.00106657
Rab14	Risp_D1	Veh_D1	73.7348	113.188	-0.618305	0.00106657
Neto2	Risp_D1	Veh_D1	39.4574	60.5523	-0.617885	0.00106657
Thsd7a	Risp_D1	Veh_D1	22.9202	35.1323	-0.616176	0.00106657
Xpr1	Risp_D1	Veh_D1	32.3796	49.3569	-0.608167	0.00106657
Snap91	Risp_D1	Veh_D1	92.4706	140.447	-0.602963	0.00106657
Akap9	Risp_D1	Veh_D1	52.8268	80.0181	-0.599056	0.00106657
Tubb4b	Risp_D1	Veh_D1	176.049	265.41	-0.59225	0.00106657
Ank2	Risp_D1	Veh_D1	34.1342	50.3369	-0.560398	0.00106657
Fam160b2	Risp_D1	Veh_D1	101.511	149.635	-0.559809	0.00106657
Eif4g2	Risp_D1	Veh_D1	84.122	123.315	-0.551791	0.00106657
Apc	Risp_D1	Veh_D1	27.2043	39.8315	-0.550073	0.00106657
Zfp706	Risp_D1	Veh_D1	65.372	95.182	-0.542016	0.00106657

Table 2.6: Top 40 downregulated genes in dSPNs following risperidone administration. Genes are sorted by q-value and then $\log_2$fold change.

gene	sample_1	sample_2	value_1 (dSPN risperidone)	value_2 (dSPN vehicle)	log2 (fold_change) dSPN Risperidone vs. Vehicle	q_value
Mir6236	Risp_D1	Veh_D1	11304.6	2098.94	2.42918	0.00106657
Hist2h4	Risp_D1	Veh_D1	119.878	23.0923	2.37608	0.00106657
Tnrc18	Risp_D1	Veh_D1	64.564	13.4051	2.26795	0.00106657
Bahcc1	Risp_D1	Veh_D1	36.4637	8.49336	2.10205	0.00106657
Sepw1	Risp_D1	Veh_D1	389.475	92.1729	2.07912	0.00106657
Samd1	Risp_D1	Veh_D1	10.7584	2.69761	1.9957	0.00106657
Prr12	Risp_D1	Veh_D1	176.548	47.3811	1.89768	0.00106657
Asic4	Risp_D1	Veh_D1	18.2206	4.93529	1.88436	0.00106657
Syp	Risp_D1	Veh_D1	354.557	96.5317	1.87694	0.00106657
Tmem143	Risp_D1	Veh_D1	20.099	5.76267	1.80231	0.00106657
Psd	Risp_D1	Veh_D1	98.8078	28.514	1.79296	0.00106657
Ptp4a3	Risp_D1	Veh_D1	18.8408	5.73238	1.71666	0.00106657
Lrrc47	Risp_D1	Veh_D1	27.6588	8.57454	1.68961	0.00106657
Ptms	Risp_D1	Veh_D1	721.28	224.289	1.6852	0.00106657
Tomm6	Risp_D1	Veh_D1	170.436	53.2046	1.67961	0.00106657
Pard6b	Risp_D1	Veh_D1	11.5526	3.65087	1.66191	0.00106657
Dtx1	Risp_D1	Veh_D1	13.8689	4.39226	1.65882	0.00106657
Snrpa	Risp_D1	Veh_D1	66.6038	21.155	1.6546	0.00106657
Dact2	Risp_D1	Veh_D1	11.4259	3.7287	1.61556	0.00106657
Mn1	Risp_D1	Veh_D1	58.5664	19.9517	1.55356	0.00106657
Creld1	Risp_D1	Veh_D1	23.0143	7.90599	1.54151	0.00106657
Lrrc20	Risp_D1	Veh_D1	21.199	7.35409	1.52737	0.00106657
Ccdc106	Risp_D1	Veh_D1	24.7903	8.6046	1.5266	0.00106657
6030419C18Rik	Risp_D1	Veh_D1	30.7417	10.7242	1.51933	0.00106657
Ints5	Risp_D1	Veh_D1	10.597	3.72067	1.51002	0.00106657
Ube2v1	Risp_D1	Veh_D1	38.3044	13.5027	1.50426	0.00106657
Gpx4	Risp_D1	Veh_D1	33.4613	11.8144	1.50195	0.00106657
Scaf1	Risp_D1	Veh_D1	23.856	8.50491	1.48798	0.00106657
Pwwp2b	Risp_D1	Veh_D1	21.3889	7.68967	1.47587	0.00106657
Wdr83os	Risp_D1	Veh_D1	240.391	86.4846	1.47487	0.00106657
Tada3	Risp_D1	Veh_D1	21.8062	7.86737	1.47078	0.00106657
Rnf187	Risp_D1	Veh_D1	477.312	172.238	1.47053	0.00106657
Khdrbs2	Risp_D1	Veh_D1	18.3819	6.64144	1.46872	0.00106657
Agfg2	Risp_D1	Veh_D1	47.7592	17.4166	1.45532	0.00106657
Dtx3	Risp_D1	Veh_D1	67.4894	24.614	1.45518	0.00106657
Arpc4	Risp_D1	Veh_D1	124.413	45.4892	1.45154	0.00106657
2810428I15Rik	Risp_D1	Veh_D1	51.559	18.8757	1.4497	0.00106657
Map3k10	Risp_D1	Veh_D1	7.71899	2.85162	1.43663	0.00106657
Rcc2	Risp_D1	Veh_D1	19.1202	7.10518	1.42815	0.00106657
Bcl9l	Risp_D1	Veh_D1	15.0966	5.63019	1.42297	0.00106657

Table 2.7: Top 40 upregulated genes in dSPNs following risperidone administration. Genes are sorted by q-value and then $\log_2$fold change.

gene	sample_1	sample_2	value_1 (dSPN haloperidol)	value_2 (dSPN vehicle)	log2 (fold_change) dSPN Haloperidol vs. Vehicle	q_value
Igf2	Hal_D1	Veh_D1	1.50616	12.7589	-3.08256	0.00239579
Enpp2	Hal_D1	Veh_D1	15.3651	98.8428	-2.68548	0.00239579
Car10	Hal_D1	Veh_D1	9.29089	28.0741	-1.59535	0.00239579
Cntn3	Hal_D1	Veh_D1	3.00982	7.9881	-1.40818	0.00239579
Sema5a	Hal_D1	Veh_D1	1.81803	4.70599	-1.37212	0.00239579
Lrtm2	Hal_D1	Veh_D1	38.4785	87.8675	-1.19128	0.00239579
Vsnl1	Hal_D1	Veh_D1	412.917	931.939	-1.17438	0.00239579
Ipo7	Hal_D1	Veh_D1	14.9469	31.294	-1.06604	0.00239579
Mcl1	Hal_D1	Veh_D1	28.5234	59.3371	-1.05679	0.00239579
Vti1a	Hal_D1	Veh_D1	33.133	67.9231	-1.03563	0.00239579
AA987161	Hal_D1	Veh_D1	7.04168	14.3277	-1.02482	0.00239579
Cat	Hal_D1	Veh_D1	14.8972	30.0482	-1.01224	0.00239579
Prdx1	Hal_D1	Veh_D1	35.3889	70.7554	-0.999542	0.00239579
Uqcrb	Hal_D1	Veh_D1	177.04	351.081	-0.987731	0.00239579
Fbxo9	Hal_D1	Veh_D1	49.6124	97.799	-0.97912	0.00239579
Smap1	Hal_D1	Veh_D1	40.7558	80.2561	-0.977606	0.00239579
9530082P21Rik	Hal_D1	Veh_D1	20.1109	39.4163	-0.970812	0.00239579
Basp1	Hal_D1	Veh_D1	67.4793	127.567	-0.918742	0.00239579
Sh3gl2	Hal_D1	Veh_D1	89.9106	167.662	-0.898996	0.00239579
Fut9	Hal_D1	Veh_D1	11.3723	21.078	-0.890211	0.00239579
Rpl12	Hal_D1	Veh_D1	117.394	216.113	-0.880427	0.00239579
Hnrnpa0	Hal_D1	Veh_D1	33.8088	61.6038	-0.865622	0.00239579
Cul4b	Hal_D1	Veh_D1	14.1107	25.4067	-0.848414	0.00239579
Hsp90aa1	Hal_D1	Veh_D1	124.363	217.45	-0.80612	0.00239579
Chchd2	Hal_D1	Veh_D1	312.109	542.819	-0.798423	0.00239579
Smc6	Hal_D1	Veh_D1	11.8956	20.5063	-0.785635	0.00239579
Dbpht2	Hal_D1	Veh_D1	139.955	241.217	-0.785371	0.00239579
Tmed9	Hal_D1	Veh_D1	89.1939	152.241	-0.771341	0.00239579
Tmem30a	Hal_D1	Veh_D1	50.0336	85.2687	-0.769119	0.00239579
Atp5g3	Hal_D1	Veh_D1	352.177	598.55	-0.765172	0.00239579
Snap91	Hal_D1	Veh_D1	83.1707	139.522	-0.746348	0.00239579
Nrxn1	Hal_D1	Veh_D1	44.307	74.1987	-0.74386	0.00239579
Tspan13	Hal_D1	Veh_D1	51.7447	86.4084	-0.739762	0.00239579
Casc4	Hal_D1	Veh_D1	41.9217	68.6979	-0.712568	0.00239579
Tmem47	Hal_D1	Veh_D1	43.4243	70.9017	-0.707316	0.00239579
Ap1s2	Hal_D1	Veh_D1	132.495	213.581	-0.688845	0.00239579
Pgm2l1	Hal_D1	Veh_D1	51.171	80.6184	-0.655783	0.00239579
Arhgap5	Hal_D1	Veh_D1	43.2667	66.7814	-0.626189	0.00239579
Reps2	Hal_D1	Veh_D1	108.431	166.865	-0.621901	0.00239579
Gucy1a2	Hal_D1	Veh_D1	19.4064	29.5199	-0.605153	0.00239579

Table 2.8: Top 40 downregulated genes in dSPNs following haloperidol administration. Genes are sorted by q-value and then $\log_2$fold change.

gene	sample_1	sample_2	value_1 (dSPN haloperidol)	value_2 (dSPN vehicle)	log2 (fold_change) dSPN Haloperidol vs. Vehicle	q_value
Ext2	Hal_D1	Veh_D1	84.3372	9.39739	3.16584	0.00239579
Gjb1	Hal_D1	Veh_D1	9.71795	1.32826	2.87112	0.00239579
Nid1	Hal_D1	Veh_D1	2.48506	0.357894	2.79568	0.00239579
Tnrc18	Hal_D1	Veh_D1	71.3258	13.3168	2.42118	0.00239579
Bahcc1	Hal_D1	Veh_D1	40.7551	8.43494	2.27253	0.00239579
Prr12	Hal_D1	Veh_D1	197.684	47.0572	2.07071	0.00239579
Scd1	Hal_D1	Veh_D1	25.429	6.1859	2.03942	0.00239579
Mir6236	Hal_D1	Veh_D1	8279.87	2086.01	1.98886	0.00239579
Syp	Hal_D1	Veh_D1	374.806	95.9403	1.96594	0.00239579
Dact2	Hal_D1	Veh_D1	13.8697	3.70336	1.90503	0.00239579
Asic4	Hal_D1	Veh_D1	17.4798	4.9031	1.83393	0.00239579
Psd	Hal_D1	Veh_D1	98.7949	28.3299	1.80211	0.00239579
Zcchc3	Hal_D1	Veh_D1	16.468	4.74883	1.79402	0.00239579
Sepw1	Hal_D1	Veh_D1	308.456	91.586	1.75186	0.00239579
Wnt7a	Hal_D1	Veh_D1	7.92048	2.35557	1.74951	0.00239579
Fam195b	Hal_D1	Veh_D1	38.6314	11.5986	1.73582	0.00239579
Prdx5	Hal_D1	Veh_D1	138.531	42.388	1.70848	0.00239579
Zfp324	Hal_D1	Veh_D1	7.97796	2.48667	1.6818	0.00239579
Unk	Hal_D1	Veh_D1	12.0726	3.78461	1.67351	0.00239579
Adi1	Hal_D1	Veh_D1	107.098	33.7895	1.66429	0.00239579
Agk	Hal_D1	Veh_D1	11.7969	3.76298	1.64846	0.00239579
Ivd	Hal_D1	Veh_D1	24.1081	7.77714	1.6322	0.00239579
6030419C18Rik	Hal_D1	Veh_D1	32.8979	10.6549	1.62648	0.00239579
Rai1	Hal_D1	Veh_D1	87.3684	29.5862	1.56219	0.00239579
Mn1	Hal_D1	Veh_D1	58.1592	19.8168	1.55328	0.00239579
Pip4k2b	Hal_D1	Veh_D1	60.9253	20.7742	1.55225	0.00239579
Ptms	Hal_D1	Veh_D1	652.951	222.83	1.55103	0.00239579
Shank3	Hal_D1	Veh_D1	32.9899	11.2759	1.54878	0.00239579
Lrrc20	Hal_D1	Veh_D1	21.2422	7.3068	1.53962	0.00239579
Dtx1	Hal_D1	Veh_D1	12.6547	4.36391	1.53598	0.00239579
Banf1	Hal_D1	Veh_D1	118.652	41.1128	1.52907	0.00239579
Rian	Hal_D1	Veh_D1	48.6235	16.9349	1.52166	0.00239579
Kdm6b	Hal_D1	Veh_D1	13.7163	4.82618	1.50694	0.00239579
Wbp11	Hal_D1	Veh_D1	15.3056	5.39464	1.50447	0.00239579
Pick1	Hal_D1	Veh_D1	27.7012	9.97024	1.47425	0.00239579
Mnt	Hal_D1	Veh_D1	13.5126	4.87551	1.47068	0.00239579
Tomm6	Hal_D1	Veh_D1	146.374	52.8501	1.46968	0.00239579
Slc25a22	Hal_D1	Veh_D1	50.6744	18.359	1.46477	0.00239579
Arhgap23	Hal_D1	Veh_D1	25.9332	9.42113	1.46082	0.00239579
Dtx3	Hal_D1	Veh_D1	67.1802	24.4509	1.45815	0.00239579

Table 2.9: Top 40 upregulated genes in dSPNs following haloperidol administration. Genes are sorted by q-value and then $\log_2$fold change.

gene	sample_1	sample_2	value_1 (iSPN aripiprazole)	value_2 (iSPN vehicle)	log2 (fold_change) iSPN Aripiprazole vs. Vehicle	q_value
Fladl	Arip_Chron_D2	Veh_Chron_D2	5.00233	495.776	-6.63094	0.00368672
Ttr	Arip_Chron_D2	Veh_Chron_D2	33.8107	573.536	-4.08433	0.00368672
Gm561	Arip_Chron_D2	Veh_Chron_D2	11.6188	70.5602	-2.60239	0.00368672
Coq7	Arip_Chron_D2	Veh_Chron_D2	12.1087	54.9008	-2.18079	0.00368672
Spag7	Arip_Chron_D2	Veh_Chron_D2	37.0523	119.447	-1.68873	0.00368672
Ap2a1	Arip_Chron_D2	Veh_Chron_D2	24.01	75.4191	-1.6513	0.00368672
Ndufa6	Arip_Chron_D2	Veh_Chron_D2	52.8879	162.647	-1.62073	0.00368672
Enpp2	Arip_Chron_D2	Veh_Chron_D2	34.9553	95.3292	-1.4474	0.00368672
Syngr3	Arip_Chron_D2	Veh_Chron_D2	23.4096	61.6023	-1.39588	0.00368672
Cox7b	Arip_Chron_D2	Veh_Chron_D2	115.647	301.043	-1.38024	0.00368672
Atp5g3	Arip_Chron_D2	Veh_Chron_D2	218.578	518.641	-1.24659	0.00368672
Tspan13	Arip_Chron_D2	Veh_Chron_D2	36.7387	87.158	-1.24633	0.00368672
Slmo1	Arip_Chron_D2	Veh_Chron_D2	30.2042	69.6008	-1.20436	0.00368672
Cox5a	Arip_Chron_D2	Veh_Chron_D2	96.455	203.681	-1.07838	0.00368672
Cox6c	Arip_Chron_D2	Veh_Chron_D2	309.262	651.876	-1.07577	0.00368672
Uqcrh	Arip_Chron_D2	Veh_Chron_D2	258.621	543.859	-1.07239	0.00368672
Cep19	Arip_Chron_D2	Veh_Chron_D2	50.2683	104.681	-1.05827	0.00368672
Gpr88	Arip_Chron_D2	Veh_Chron_D2	285.245	580.177	-1.02429	0.00368672
Chchd2	Arip_Chron_D2	Veh_Chron_D2	234.282	468.996	-1.00133	0.00368672
Pfn2	Arip_Chron_D2	Veh_Chron_D2	73.0604	144.405	-0.982956	0.00368672
Higd1a	Arip_Chron_D2	Veh_Chron_D2	53.194	102.014	-0.939431	0.00368672
Rpl41	Arip_Chron_D2	Veh_Chron_D2	512.126	971.683	-0.923986	0.00368672
Napb	Arip_Chron_D2	Veh_Chron_D2	103.588	184.688	-0.834238	0.00368672
Ppp2ca	Arip_Chron_D2	Veh_Chron_D2	112.516	195.281	-0.795422	0.00368672
Arf4	Arip_Chron_D2	Veh_Chron_D2	118.369	204.325	-0.787577	0.00368672
Fam160b2	Arip_Chron_D2	Veh_Chron_D2	90.6021	153.083	-0.7567	0.00368672
0610012G03Rik	Arip_Chron_D2	Veh_Chron_D2	6.02638	21.3304	-1.82354	0.00605
Tmem230	Arip_Chron_D2	Veh_Chron_D2	21.9224	62.9419	-1.52162	0.00605
Uqcrb	Arip_Chron_D2	Veh_Chron_D2	153.032	382.129	-1.32023	0.00605
Ndufa5	Arip_Chron_D2	Veh_Chron_D2	115.856	268.968	-1.2151	0.00605
Atp5h	Arip_Chron_D2	Veh_Chron_D2	222.972	427.733	-0.939847	0.00605
Cox6a1	Arip_Chron_D2	Veh_Chron_D2	384.751	735.443	-0.934687	0.00605
Ndufb6	Arip_Chron_D2	Veh_Chron_D2	106.552	239.991	-1.17142	0.00804375
Rpl12	Arip_Chron_D2	Veh_Chron_D2	92.4126	204.067	-1.14289	0.00804375
Necab2	Arip_Chron_D2	Veh_Chron_D2	78.5649	144.841	-0.882513	0.00804375
Atpif1	Arip_Chron_D2	Veh_Chron_D2	606.354	1091.3	-0.847816	0.00804375
Ube2b	Arip_Chron_D2	Veh_Chron_D2	98.5816	167.398	-0.763896	0.00804375
Rps29	Arip_Chron_D2	Veh_Chron_D2	201.703	438.796	-1.12132	0.00956554
Gatc	Arip_Chron_D2	Veh_Chron_D2	85.8034	149.719	-0.803148	0.00956554
Tspan7	Arip_Chron_D2	Veh_Chron_D2	117.835	196.721	-0.739384	0.00956554

Table 2.10: Top 40 downregulated genes in iSPNs following aripiprazole administration. Genes are sorted by q-value and then $\log_2$fold change.

gene	sample_1	sample_2	value_1 (iSPN aripiprazole)	value_2 (iSPN vehicle)	log2 (fold_change) iSPN Aripiprazole vs. Vehicle	q_value
Mapk8ip2	Arip_Chron_D2	Veh_Chron_D2	23.0839	4.38051	2.39772	0.00368672
Daam2	Arip_Chron_D2	Veh_Chron_D2	8.20336	1.56754	2.38772	0.00368672
Sox10	Arip_Chron_D2	Veh_Chron_D2	25.301	6.31169	2.0031	0.00368672
Megf8	Arip_Chron_D2	Veh_Chron_D2	7.03992	1.83931	1.9364	0.00368672
Dync1h1	Arip_Chron_D2	Veh_Chron_D2	58.7148	15.6297	1.90943	0.00368672
Gab1	Arip_Chron_D2	Veh_Chron_D2	22.6186	6.11861	1.88623	0.00368672
Trf	Arip_Chron_D2	Veh_Chron_D2	37.8916	10.3788	1.86824	0.00368672
Acin1	Arip_Chron_D2	Veh_Chron_D2	60.1577	16.4915	1.86702	0.00368672
Fam214b	Arip_Chron_D2	Veh_Chron_D2	29.4901	8.22714	1.84177	0.00368672
Pla2g16	Arip_Chron_D2	Veh_Chron_D2	16.3667	4.63415	1.82038	0.00368672
Fbxl20	Arip_Chron_D2	Veh_Chron_D2	17.3335	4.98072	1.79914	0.00368672
4933426M11Rik	Arip_Chron_D2	Veh_Chron_D2	11.0037	3.25274	1.75826	0.00368672
Sema6a	Arip_Chron_D2	Veh_Chron_D2	9.05	2.72729	1.73045	0.00368672
6030419C18Rik	Arip_Chron_D2	Veh_Chron_D2	36.9523	11.1486	1.7288	0.00368672
Cnp	Arip_Chron_D2	Veh_Chron_D2	166.772	50.4242	1.72569	0.00368672
Pde1c	Arip_Chron_D2	Veh_Chron_D2	26.4316	8.1113	1.70426	0.00368672
Myrf	Arip_Chron_D2	Veh_Chron_D2	18.1121	5.56964	1.70129	0.00368672
Nfix	Arip_Chron_D2	Veh_Chron_D2	22.6633	6.98021	1.69902	0.00368672
Mpp2	Arip_Chron_D2	Veh_Chron_D2	96.203	30.9833	1.63459	0.00368672
Glul	Arip_Chron_D2	Veh_Chron_D2	221.532	71.4648	1.63221	0.00368672
Bcl9l	Arip_Chron_D2	Veh_Chron_D2	25.9742	8.4441	1.62107	0.00368672
Asrgl1	Arip_Chron_D2	Veh_Chron_D2	30.0084	9.78674	1.61646	0.00368672
Cntn2	Arip_Chron_D2	Veh_Chron_D2	7.17173	2.35609	1.60593	0.00368672
Nacc2	Arip_Chron_D2	Veh_Chron_D2	18.4748	6.07316	1.60504	0.00368672
Arhgap23	Arip_Chron_D2	Veh_Chron_D2	40.8097	13.5411	1.59157	0.00368672
Kmt2d	Arip_Chron_D2	Veh_Chron_D2	16.5139	5.55484	1.57186	0.00368672
Cln5	Arip_Chron_D2	Veh_Chron_D2	27.204	9.21353	1.56199	0.00368672
Slc1a2	Arip_Chron_D2	Veh_Chron_D2	102.856	35.0488	1.55319	0.00368672
Vps52	Arip_Chron_D2	Veh_Chron_D2	45.3632	15.9096	1.51162	0.00368672
Bahcc1	Arip_Chron_D2	Veh_Chron_D2	93.2589	32.7307	1.5106	0.00368672
Rasl10b	Arip_Chron_D2	Veh_Chron_D2	55.834	19.9966	1.48139	0.00368672
Ermn	Arip_Chron_D2	Veh_Chron_D2	52.3646	18.7769	1.47964	0.00368672
Plp1	Arip_Chron_D2	Veh_Chron_D2	192.283	70.9623	1.43811	0.00368672
Ptprz1	Arip_Chron_D2	Veh_Chron_D2	9.48301	3.53285	1.42451	0.00368672
Car2	Arip_Chron_D2	Veh_Chron_D2	75.0573	27.9862	1.42328	0.00368672
Bcl9	Arip_Chron_D2	Veh_Chron_D2	52.1661	19.4759	1.42142	0.00368672
Setd1b	Arip_Chron_D2	Veh_Chron_D2	14.662	5.49101	1.41694	0.00368672
Lrp1	Arip_Chron_D2	Veh_Chron_D2	13.7487	5.15081	1.41643	0.00368672
Bach2	Arip_Chron_D2	Veh_Chron_D2	15.5161	5.83233	1.41162	0.00368672
Atp1a2	Arip_Chron_D2	Veh_Chron_D2	20.1759	7.74366	1.38155	0.00368672

Table 2.11: Top 40 upregulated genes in iSPNs following aripiprazole administration. Genes are sorted by q-value and then $\log_2$fold change.

gene	sample_1	sample_2	value_1 (iSPN clozapine)	value_2 (iSPN vehicle)	log2 (fold_change) iSPN Clozapine vs. Vehicle	q_value
Nhp2l1	Cloz_Chron_D2	Veh_Chron_D2	56.5991	110.188	-0.961118	0.00274962
Cox6a1	Cloz_Chron_D2	Veh_Chron_D2	388.742	755.769	-0.959132	0.00274962
Rpl41	Cloz_Chron_D2	Veh_Chron_D2	515.652	998.446	-0.953286	0.00274962
Rps3a1	Cloz_Chron_D2	Veh_Chron_D2	62.6201	120.049	-0.93893	0.00274962
Uqcr10	Cloz_Chron_D2	Veh_Chron_D2	188.475	359.824	-0.932919	0.00274962
Cdr1	Cloz_Chron_D2	Veh_Chron_D2	439.656	835.981	-0.927095	0.00274962
Atp5g3	Cloz_Chron_D2	Veh_Chron_D2	280.622	532.971	-0.925427	0.00274962
Rtn4	Cloz_Chron_D2	Veh_Chron_D2	207.173	392.302	-0.921127	0.00274962
Dynlt3	Cloz_Chron_D2	Veh_Chron_D2	142.94	269.7	-0.915952	0.00274962
Bod1	Cloz_Chron_D2	Veh_Chron_D2	116.384	214.168	-0.879842	0.00274962
Gal3st3	Cloz_Chron_D2	Veh_Chron_D2	29.6291	54.3112	-0.874234	0.00274962
Rpl23	Cloz_Chron_D2	Veh_Chron_D2	83.9179	153.282	-0.869139	0.00274962
Atp5o	Cloz_Chron_D2	Veh_Chron_D2	124.24	226.48	-0.866258	0.00274962
Gpm6a	Cloz_Chron_D2	Veh_Chron_D2	152.34	277.242	-0.863849	0.00274962
Brk1	Cloz_Chron_D2	Veh_Chron_D2	115.739	207.338	-0.841114	0.00274962
Hmgn1	Cloz_Chron_D2	Veh_Chron_D2	174.087	311.84	-0.840998	0.00274962
Zcrb1	Cloz_Chron_D2	Veh_Chron_D2	118.289	211.637	-0.839267	0.00274962
Penk	Cloz_Chron_D2	Veh_Chron_D2	2049.79	3666.65	-0.838987	0.00274962
Ndufa13	Cloz_Chron_D2	Veh_Chron_D2	111.597	199.155	-0.835591	0.00274962
Nptn	Cloz_Chron_D2	Veh_Chron_D2	212.469	377.455	-0.829055	0.00274962
Serinc3	Cloz_Chron_D2	Veh_Chron_D2	51.4139	91.2991	-0.828442	0.00274962
Chmp3	Cloz_Chron_D2	Veh_Chron_D2	49.9565	88.1823	-0.819817	0.00274962
Ap1s2	Cloz_Chron_D2	Veh_Chron_D2	97.5593	171.503	-0.813879	0.00274962
Tmsb4x	Cloz_Chron_D2	Veh_Chron_D2	340.033	594.236	-0.805363	0.00274962
Mxd1	Cloz_Chron_D2	Veh_Chron_D2	29.4591	51.4013	-0.803092	0.00274962
Dynll1	Cloz_Chron_D2	Veh_Chron_D2	94.7931	164.221	-0.792787	0.00274962
Aff3	Cloz_Chron_D2	Veh_Chron_D2	32.1589	55.3645	-0.783744	0.00274962
Ube2b	Cloz_Chron_D2	Veh_Chron_D2	100.071	171.97	-0.781131	0.00274962
Galnt13	Cloz_Chron_D2	Veh_Chron_D2	31.1905	53.4725	-0.777689	0.00274962
Adnp	Cloz_Chron_D2	Veh_Chron_D2	43.0385	73.6649	-0.77535	0.00274962
Micu3	Cloz_Chron_D2	Veh_Chron_D2	51.7403	88.3867	-0.772541	0.00274962
Atpif1	Cloz_Chron_D2	Veh_Chron_D2	659.99	1121.68	-0.765143	0.00274962
Fam160b2	Cloz_Chron_D2	Veh_Chron_D2	92.7408	157.425	-0.763388	0.00274962
Slc25a3	Cloz_Chron_D2	Veh_Chron_D2	235.271	397.128	-0.755282	0.00274962
Nrsn2	Cloz_Chron_D2	Veh_Chron_D2	353.859	587.761	-0.732055	0.00274962
Rfx7	Cloz_Chron_D2	Veh_Chron_D2	21.6769	35.749	-0.721744	0.00274962
Spock3	Cloz_Chron_D2	Veh_Chron_D2	60.6766	99.6223	-0.715328	0.00274962
Pbx3	Cloz_Chron_D2	Veh_Chron_D2	61.6941	100.855	-0.709071	0.00274962
Nrgn	Cloz_Chron_D2	Veh_Chron_D2	295.707	472.976	-0.677602	0.00274962
Gucy1a3	Cloz_Chron_D2	Veh_Chron_D2	129.203	202.362	-0.647297	0.00274962

Table 2.12: Top 40 downregulated genes in iSPNs following clozapine administration. Genes are sorted by q-value and then $\log_2$fold change.

gene	sample_1	sample_2	value_1 (iSPN clozapine)	value_2 (iSPN vehicle)	log2 (fold_change) iSPN Clozapine vs. Vehicle	q_value
Rpph1	Cloz_Chron_D2	Veh_Chron_D2	260.778	42.3978	2.62076	0.00274962
Tprn	Cloz_Chron_D2	Veh_Chron_D2	5.34547	0.957091	2.48159	0.00274962
Litaf	Cloz_Chron_D2	Veh_Chron_D2	6.11031	1.17836	2.37447	0.00274962
Efhd2	Cloz_Chron_D2	Veh_Chron_D2	24.527	4.81344	2.34923	0.00274962
Slc2a1	Cloz_Chron_D2	Veh_Chron_D2	20.7267	4.89712	2.08149	0.00274962
Asrgl1	Cloz_Chron_D2	Veh_Chron_D2	40.0573	10.0506	1.99478	0.00274962
Slc17a7	Cloz_Chron_D2	Veh_Chron_D2	28.4279	7.71112	1.8823	0.00274962
Tmem88b	Cloz_Chron_D2	Veh_Chron_D2	44.8795	12.6104	1.83144	0.00274962
Ccdc184	Cloz_Chron_D2	Veh_Chron_D2	19.3498	5.43701	1.83144	0.00274962
Gab1	Cloz_Chron_D2	Veh_Chron_D2	21.8763	6.2817	1.80014	0.00274962
Mapk8ip2	Cloz_Chron_D2	Veh_Chron_D2	15.5557	4.49687	1.79045	0.00274962
Glul	Cloz_Chron_D2	Veh_Chron_D2	252.059	73.414	1.77963	0.00274962
Map3k10	Cloz_Chron_D2	Veh_Chron_D2	9.31488	2.77623	1.74641	0.00274962
Clic4	Cloz_Chron_D2	Veh_Chron_D2	10.4773	3.12397	1.74582	0.00274962
Trf	Cloz_Chron_D2	Veh_Chron_D2	35.2263	10.6556	1.72505	0.00274962
Nfix	Cloz_Chron_D2	Veh_Chron_D2	23.1585	7.17362	1.69077	0.00274962
Csrp1	Cloz_Chron_D2	Veh_Chron_D2	142.97	45.4105	1.65461	0.00274962
Cryab	Cloz_Chron_D2	Veh_Chron_D2	105.195	34.3449	1.6149	0.00274962
Car2	Cloz_Chron_D2	Veh_Chron_D2	87.1905	28.7715	1.59953	0.00274962
Tbr1	Cloz_Chron_D2	Veh_Chron_D2	10.4675	3.47229	1.59196	0.00274962
Apod	Cloz_Chron_D2	Veh_Chron_D2	35.7592	11.9357	1.58303	0.00274962
Baalc	Cloz_Chron_D2	Veh_Chron_D2	22.0988	7.391	1.58013	0.00274962
Trim3	Cloz_Chron_D2	Veh_Chron_D2	17.5608	5.9099	1.57115	0.00274962
Pdyn	Cloz_Chron_D2	Veh_Chron_D2	18.8255	6.38806	1.55924	0.00274962
Rasl10b	Cloz_Chron_D2	Veh_Chron_D2	60.1189	20.5397	1.5494	0.00274962
Shank1	Cloz_Chron_D2	Veh_Chron_D2	45.0037	15.671	1.52195	0.00274962
Nptx1	Cloz_Chron_D2	Veh_Chron_D2	14.7845	5.15014	1.5214	0.00274962
Klf12	Cloz_Chron_D2	Veh_Chron_D2	36.2219	12.7539	1.50592	0.00274962
Cnp	Cloz_Chron_D2	Veh_Chron_D2	146.525	51.7986	1.50016	0.00274962
Slc1a2	Cloz_Chron_D2	Veh_Chron_D2	101.348	36.0037	1.49309	0.00274962
Ermn	Cloz_Chron_D2	Veh_Chron_D2	53.7836	19.3026	1.47837	0.00274962
Syp	Cloz_Chron_D2	Veh_Chron_D2	322.771	118.222	1.44901	0.00274962
Plekhb1	Cloz_Chron_D2	Veh_Chron_D2	70.1765	26.1094	1.42642	0.00274962
Plp1	Cloz_Chron_D2	Veh_Chron_D2	194.303	72.9094	1.41413	0.00274962
Kcnj10	Cloz_Chron_D2	Veh_Chron_D2	14.2431	5.37477	1.40599	0.00274962
Mtss1l	Cloz_Chron_D2	Veh_Chron_D2	14.5529	5.55159	1.39034	0.00274962
Cck	Cloz_Chron_D2	Veh_Chron_D2	234.255	89.7548	1.38402	0.00274962
Paqr8	Cloz_Chron_D2	Veh_Chron_D2	12.0971	4.6983	1.36445	0.00274962
Sbk1	Cloz_Chron_D2	Veh_Chron_D2	27.3164	10.7378	1.34707	0.00274962
Gca	Cloz_Chron_D2	Veh_Chron_D2	18.8422	7.45119	1.33842	0.00274962

Table 2.13: Top 40 upregulated genes in iSPNs following clozapine administration. Genes are sorted by q-value and then $\log_2$fold change.

gene	sample_1	sample_2	value_1 (iSPN risperidone)	value_2 (iSPN vehicle)	log2 (fold_change) iSPN Risperidone vs. Vehicle	q_value
Ttr	Risp_Chron_D2	Veh_Chron_D2	3.91058	582.341	-7.21834	0.00301064
Fladl	Risp_Chron_D2	Veh_Chron_D2	3.94529	502.713	-6.99346	0.00301064
Nrp2	Risp_Chron_D2	Veh_Chron_D2	0.0649239	1.74054	-4.74464	0.00301064
Cpne9	Risp_Chron_D2	Veh_Chron_D2	1.15502	11.2261	-3.28087	0.00301064
Enpp2	Risp_Chron_D2	Veh_Chron_D2	13.6842	96.8548	-2.82331	0.00301064
Trpm3	Risp_Chron_D2	Veh_Chron_D2	1.44572	8.64863	-2.58068	0.00301064
BC068157	Risp_Chron_D2	Veh_Chron_D2	1.75424	8.55646	-2.28617	0.00301064
Spag7	Risp_Chron_D2	Veh_Chron_D2	40.8477	121.38	-1.57121	0.00301064
Cntn3	Risp_Chron_D2	Veh_Chron_D2	4.72748	13.3971	-1.50278	0.00301064
Tmed9	Risp_Chron_D2	Veh_Chron_D2	54.0091	141.333	-1.38782	0.00301064
Fundc1	Risp_Chron_D2	Veh_Chron_D2	18.8421	47.104	-1.32189	0.00301064
Tspan13	Risp_Chron_D2	Veh_Chron_D2	35.8023	88.5233	-1.30601	0.00301064
Uqcrb	Risp_Chron_D2	Veh_Chron_D2	157.297	388.219	-1.30338	0.00301064
Fbxo9	Risp_Chron_D2	Veh_Chron_D2	34.0326	82.0663	-1.26987	0.00301064
Vsnl1	Risp_Chron_D2	Veh_Chron_D2	137.936	321.56	-1.22109	0.00301064
Gatc	Risp_Chron_D2	Veh_Chron_D2	70.3773	152.167	-1.11247	0.00301064
Chchd2	Risp_Chron_D2	Veh_Chron_D2	220.873	476.443	-1.10909	0.00301064
Zcchc9	Risp_Chron_D2	Veh_Chron_D2	47.4002	101.658	-1.10076	0.00301064
Hsp90aa1	Risp_Chron_D2	Veh_Chron_D2	89.7799	192.181	-1.098	0.00301064
Rfk	Risp_Chron_D2	Veh_Chron_D2	24.6375	50.8349	-1.04496	0.00301064
Tmem30a	Risp_Chron_D2	Veh_Chron_D2	41.9299	84.0799	-1.00378	0.00301064
Atp5g3	Risp_Chron_D2	Veh_Chron_D2	273.404	526.834	-0.946316	0.00301064
Malat1	Risp_Chron_D2	Veh_Chron_D2	361.026	689.587	-0.933631	0.00301064
Ttc7b	Risp_Chron_D2	Veh_Chron_D2	50.5409	96.3048	-0.930156	0.00301064
Cox7b	Risp_Chron_D2	Veh_Chron_D2	160.664	305.769	-0.928396	0.00301064
Mff	Risp_Chron_D2	Veh_Chron_D2	59.6247	111.537	-0.90354	0.00301064
Fam160b2	Risp_Chron_D2	Veh_Chron_D2	83.7893	155.579	-0.892809	0.00301064
Rab14	Risp_Chron_D2	Veh_Chron_D2	51.8582	93.7146	-0.853701	0.00301064
Gpm6a	Risp_Chron_D2	Veh_Chron_D2	152.42	274.037	-0.846317	0.00301064
Cox6c	Risp_Chron_D2	Veh_Chron_D2	372.742	662.068	-0.828801	0.00301064
Galnt13	Risp_Chron_D2	Veh_Chron_D2	29.7955	52.8371	-0.826454	0.00301064
Ap1s2	Risp_Chron_D2	Veh_Chron_D2	96.1358	169.493	-0.818077	0.00301064
Flrt1	Risp_Chron_D2	Veh_Chron_D2	8.63352	18.4228	-1.09347	0.00518315
Ildr2	Risp_Chron_D2	Veh_Chron_D2	6.92511	14.6012	-1.07618	0.00518315
Lrtm2	Risp_Chron_D2	Veh_Chron_D2	36.4574	68.8168	-0.91655	0.00518315
Ndufv2	Risp_Chron_D2	Veh_Chron_D2	76.3197	142.254	-0.89834	0.00518315
Fkbp3	Risp_Chron_D2	Veh_Chron_D2	161.101	296.931	-0.882159	0.00518315
Rtn4	Risp_Chron_D2	Veh_Chron_D2	210.399	387.776	-0.882094	0.00518315
Uqcrh	Risp_Chron_D2	Veh_Chron_D2	307.814	552.333	-0.843478	0.00518315
Dnajb4	Risp_Chron_D2	Veh_Chron_D2	88.5562	152.244	-0.78172	0.00518315

Table 2.14: Top 40 downregulated genes in iSPNs following risperidone administration. Genes are sorted by q-value and then $\log_2$fold change.

gene	sample_1	sample_2	value_1 (iSPN risperidone)	value_2 (iSPN vehicle)	log2 (fold_change) iSPN Risperidone vs. Vehicle	q_value
Mir6236	Risp_Chron_D2	Veh_Chron_D2	18322.5	2887	2.66598	0.00301064
Tpcn1	Risp_Chron_D2	Veh_Chron_D2	13.9746	3.08369	2.18008	0.00301064
Gltscr1	Risp_Chron_D2	Veh_Chron_D2	35.0534	8.13392	2.10753	0.00301064
Rcc2	Risp_Chron_D2	Veh_Chron_D2	32.677	7.6066	2.10295	0.00301064
Adam19	Risp_Chron_D2	Veh_Chron_D2	11.7646	2.77981	2.08139	0.00301064
Megf8	Risp_Chron_D2	Veh_Chron_D2	7.22707	1.86743	1.95235	0.00301064
Fam222a	Risp_Chron_D2	Veh_Chron_D2	30.3747	7.93551	1.93648	0.00301064
Sepw1	Risp_Chron_D2	Veh_Chron_D2	664.157	176.639	1.91072	0.00301064
Kcnj10	Risp_Chron_D2	Veh_Chron_D2	18.2061	5.31228	1.77702	0.00301064
Erf	Risp_Chron_D2	Veh_Chron_D2	40.5619	11.9143	1.76743	0.00301064
Lrrc47	Risp_Chron_D2	Veh_Chron_D2	38.3401	11.4313	1.74586	0.00301064
Bahcc1	Risp_Chron_D2	Veh_Chron_D2	110.88	33.2497	1.73758	0.00301064
Rasl10b	Risp_Chron_D2	Veh_Chron_D2	63.9589	20.3117	1.65483	0.00301064
Tomm6	Risp_Chron_D2	Veh_Chron_D2	237.908	75.9388	1.64749	0.00301064
Tmem88b	Risp_Chron_D2	Veh_Chron_D2	38.8664	12.4671	1.64039	0.00301064
6030419C18Rik	Risp_Chron_D2	Veh_Chron_D2	35.0446	11.3227	1.62998	0.00301064
Bag6	Risp_Chron_D2	Veh_Chron_D2	39.3282	12.7617	1.62374	0.00301064
Prr12	Risp_Chron_D2	Veh_Chron_D2	458.061	149.214	1.61816	0.00301064
Mn1	Risp_Chron_D2	Veh_Chron_D2	139.379	45.777	1.60632	0.00301064
Ptms	Risp_Chron_D2	Veh_Chron_D2	897.698	298.715	1.58746	0.00301064
Mpp2	Risp_Chron_D2	Veh_Chron_D2	94.464	31.4865	1.58503	0.00301064
Syp	Risp_Chron_D2	Veh_Chron_D2	349.269	116.894	1.57914	0.00301064
Acin1	Risp_Chron_D2	Veh_Chron_D2	49.773	16.7486	1.57132	0.00301064
Tnrc18	Risp_Chron_D2	Veh_Chron_D2	153.512	52.5691	1.54606	0.00301064
Asrgl1	Risp_Chron_D2	Veh_Chron_D2	28.7966	9.93702	1.53501	0.00301064
Shank3	Risp_Chron_D2	Veh_Chron_D2	39.8272	14.2686	1.48091	0.00301064
Dach1	Risp_Chron_D2	Veh_Chron_D2	46.2319	16.625	1.47554	0.00301064
Tbc1d16	Risp_Chron_D2	Veh_Chron_D2	13.5884	4.92347	1.46463	0.00301064
Psd	Risp_Chron_D2	Veh_Chron_D2	112.936	41.1005	1.45827	0.00301064
Kdm6b	Risp_Chron_D2	Veh_Chron_D2	38.4609	14.3003	1.42735	0.00301064
Setd1b	Risp_Chron_D2	Veh_Chron_D2	14.8433	5.57778	1.41205	0.00301064
March6	Risp_Chron_D2	Veh_Chron_D2	82.673	31.1003	1.41049	0.00301064
Arhgap23	Risp_Chron_D2	Veh_Chron_D2	36.5158	13.7504	1.40905	0.00301064
Bsdc1	Risp_Chron_D2	Veh_Chron_D2	39.4994	14.9379	1.40285	0.00301064
Fam53c	Risp_Chron_D2	Veh_Chron_D2	30.5713	11.626	1.39482	0.00301064
Pcbp3	Risp_Chron_D2	Veh_Chron_D2	39.2953	15.1034	1.37949	0.00301064
Ankrd13b	Risp_Chron_D2	Veh_Chron_D2	24.354	9.39591	1.37406	0.00301064
Vps52	Risp_Chron_D2	Veh_Chron_D2	41.8878	16.17	1.37321	0.00301064
Hdac5	Risp_Chron_D2	Veh_Chron_D2	28.4736	11.013	1.37042	0.00301064
Bcl9l	Risp_Chron_D2	Veh_Chron_D2	22.1276	8.57779	1.36717	0.00301064

Table 2.15: Top 40 upregulated genes in iSPNs following risperidone administration. Genes are sorted by q-value and then $\log_2$fold change.

gene	sample_1	sample_2	value_1 (iSPN haloperidol)	value_2 (iSPN vehicle)	log2 (fold_change) iSPN Haloperidol vs. Vehicle	q_value
Flad1	Hal_Chron_D2	Veh_Chron_D2	6.36477	489.42	-6.26482	0.00245749
Ttr	Hal_Chron_D2	Veh_Chron_D2	11.6523	567.516	-5.60597	0.00245749
Ap2a1	Hal_Chron_D2	Veh_Chron_D2	13.2074	74.5734	-2.49731	0.00245749
Enpp2	Hal_Chron_D2	Veh_Chron_D2	23.0483	94.3885	-2.03395	0.00245749
Spag7	Hal_Chron_D2	Veh_Chron_D2	38.3226	118.198	-1.62493	0.00245749
Syngr3	Hal_Chron_D2	Veh_Chron_D2	19.9461	60.9356	-1.61118	0.00245749
Polr2e	Hal_Chron_D2	Veh_Chron_D2	45.0252	118.022	-1.39025	0.00245749
Vti1a	Hal_Chron_D2	Veh_Chron_D2	24.2282	52.1266	-1.10533	0.00245749
Fgf11	Hal_Chron_D2	Veh_Chron_D2	48.1998	100.378	-1.05834	0.00245749
Npas2	Hal_Chron_D2	Veh_Chron_D2	23.8314	48.1795	-1.01555	0.00245749
Hsp90aa1	Hal_Chron_D2	Veh_Chron_D2	95.6746	187.172	-0.968159	0.00245749
Cox7b	Hal_Chron_D2	Veh_Chron_D2	162.274	297.901	-0.876403	0.00245749
Rgs2	Hal_Chron_D2	Veh_Chron_D2	156.125	285.598	-0.871286	0.00245749
Tmem30a	Hal_Chron_D2	Veh_Chron_D2	45.2077	81.9224	-0.857688	0.00245749
Gpr88	Hal_Chron_D2	Veh_Chron_D2	321.539	574.252	-0.836689	0.00245749
Fam160b2	Hal_Chron_D2	Veh_Chron_D2	86.123	151.502	-0.81487	0.00245749
Drd2	Hal_Chron_D2	Veh_Chron_D2	1555.44	2603.8	-0.743298	0.00245749
Slc13a4	Hal_Chron_D2	Veh_Chron_D2	0.028933	2.73515	-6.56276	0.00431376
Chchd2	Hal_Chron_D2	Veh_Chron_D2	253.78	464.172	-0.87108	0.00431376
Ndufa6	Hal_Chron_D2	Veh_Chron_D2	64.621	160.956	-1.31659	0.00602821
Slc25a3	Hal_Chron_D2	Veh_Chron_D2	233.982	382.404	-0.708701	0.00602821
Ptpn14	Hal_Chron_D2	Veh_Chron_D2	0.0165621	0.748262	-5.49758	0.0074438
Gpm6a	Hal_Chron_D2	Veh_Chron_D2	169.946	267.008	-0.651807	0.0074438
Zdhhc14	Hal_Chron_D2	Veh_Chron_D2	12.7071	31.1879	-1.29535	0.0101239
Nhp2l1	Hal_Chron_D2	Veh_Chron_D2	50.4988	106.141	-1.07167	0.0101239
Slc25a5	Hal_Chron_D2	Veh_Chron_D2	107.803	195.086	-0.855716	0.0101239
Galnt13	Hal_Chron_D2	Veh_Chron_D2	29.5617	51.4708	-0.800025	0.0101239
Rtn4	Hal_Chron_D2	Veh_Chron_D2	233.903	377.819	-0.691789	0.0101239
Nptn	Hal_Chron_D2	Veh_Chron_D2	230.463	363.397	-0.657014	0.0101239
Ndufv2	Hal_Chron_D2	Veh_Chron_D2	77.776	138.568	-0.833194	0.011455
Htr2c	Hal_Chron_D2	Veh_Chron_D2	10.3159	22.551	-1.12832	0.0127946
Aldh5a1	Hal_Chron_D2	Veh_Chron_D2	13.6829	27.3528	-0.99932	0.0127946
Cox7a2	Hal_Chron_D2	Veh_Chron_D2	81.6975	186.769	-1.19289	0.014106
Dstyk	Hal_Chron_D2	Veh_Chron_D2	7.37175	15.5541	-1.07722	0.014106
Marcks	Hal_Chron_D2	Veh_Chron_D2	33.2439	58.3563	-0.811798	0.0166845
Atp5g3	Hal_Chron_D2	Veh_Chron_D2	294.168	513.262	-0.803052	0.0166845
Ap1s2	Hal_Chron_D2	Veh_Chron_D2	100.249	165.143	-0.720126	0.0166845
Serinc3	Hal_Chron_D2	Veh_Chron_D2	53.397	87.9125	-0.71931	0.0166845
Phf19	Hal_Chron_D2	Veh_Chron_D2	0.0384173	1.72769	-5.49094	0.0179694
Rpl7	Hal_Chron_D2	Veh_Chron_D2	47.2137	104.023	-1.13962	0.0201104

Table 2.16: Top 40 downregulated genes in iSPNs following haloperidol administration. Genes are sorted by q-value and then $\log_2$fold change.

gene	sample_1	sample_2	value_1 (iSPN haloperidol)	value_2 (iSPN vehicle)	log2 (fold_change) iSPN Haloperidol vs. Vehicle	q_value
Kif18b	Hal_Chron_D2	Veh_Chron_D2	8.03367	0.0581064	7.11122	0.00245749
Rmi2	Hal_Chron_D2	Veh_Chron_D2	3.04669	0.0525579	5.85719	0.00245749
Vcl	Hal_Chron_D2	Veh_Chron_D2	10.1938	1.13594	3.16573	0.00245749
Plxnb1	Hal_Chron_D2	Veh_Chron_D2	4.78546	0.590307	3.01912	0.00245749
5930403L14Rik	Hal_Chron_D2	Veh_Chron_D2	21.8046	2.84608	2.93758	0.00245749
Aars2	Hal_Chron_D2	Veh_Chron_D2	8.63602	1.37815	2.64764	0.00245749
Gpr45	Hal_Chron_D2	Veh_Chron_D2	7.92217	1.35705	2.54543	0.00245749
Dusp22	Hal_Chron_D2	Veh_Chron_D2	58.5961	13.2078	2.14941	0.00245749
Polr2f	Hal_Chron_D2	Veh_Chron_D2	109.398	29.1877	1.90615	0.00245749
Gca	Hal_Chron_D2	Veh_Chron_D2	26.3984	7.18261	1.87787	0.00245749
Asrgl1	Hal_Chron_D2	Veh_Chron_D2	35.2173	9.68361	1.86267	0.00245749
Bahcc1	Hal_Chron_D2	Veh_Chron_D2	117.634	32.3928	1.86056	0.00245749
Tnrc18	Hal_Chron_D2	Veh_Chron_D2	178.854	51.2109	1.80426	0.00245749
Syp	Hal_Chron_D2	Veh_Chron_D2	397.237	113.922	1.80196	0.00245749
Tbc1d16	Hal_Chron_D2	Veh_Chron_D2	16.3085	4.79884	1.76487	0.00245749
Mir6236	Hal_Chron_D2	Veh_Chron_D2	9506.12	2813.65	1.75641	0.00245749
Arhgap23	Hal_Chron_D2	Veh_Chron_D2	44.537	13.3989	1.73289	0.00245749
Grik5	Hal_Chron_D2	Veh_Chron_D2	41.9107	12.7381	1.71817	0.00245749
Pde1c	Hal_Chron_D2	Veh_Chron_D2	26.3543	8.02937	1.71468	0.00245749
Rcc2	Hal_Chron_D2	Veh_Chron_D2	24.3299	7.41785	1.71366	0.00245749
Hdac5	Hal_Chron_D2	Veh_Chron_D2	34.8841	10.7288	1.70108	0.00245749
Erf	Hal_Chron_D2	Veh_Chron_D2	37.362	11.6143	1.68567	0.00245749
Ptms	Hal_Chron_D2	Veh_Chron_D2	916.185	291.018	1.65453	0.00245749
Dagla	Hal_Chron_D2	Veh_Chron_D2	43.7193	13.9289	1.65019	0.00245749
Taok2	Hal_Chron_D2	Veh_Chron_D2	26.4419	8.43357	1.64861	0.00245749
Inhba	Hal_Chron_D2	Veh_Chron_D2	72.0943	23.2871	1.63036	0.00245749
Mpp2	Hal_Chron_D2	Veh_Chron_D2	94.5191	30.6631	1.6241	0.00245749
Psd	Hal_Chron_D2	Veh_Chron_D2	122.418	40.0558	1.61173	0.00245749
Shank3	Hal_Chron_D2	Veh_Chron_D2	42.1124	13.9044	1.59871	0.00245749
Prr12	Hal_Chron_D2	Veh_Chron_D2	435.184	145.354	1.58205	0.00245749
Nrxn2	Hal_Chron_D2	Veh_Chron_D2	26.2383	8.88435	1.56233	0.00245749
Sv2c	Hal_Chron_D2	Veh_Chron_D2	35.8625	12.1475	1.56182	0.00245749
Gab1	Hal_Chron_D2	Veh_Chron_D2	17.7586	6.05623	1.55202	0.00245749
Slc1a2	Hal_Chron_D2	Veh_Chron_D2	97.4879	34.6893	1.49073	0.00245749
Rasgrp2	Hal_Chron_D2	Veh_Chron_D2	49.5461	17.7528	1.48073	0.00245749
Rasl10b	Hal_Chron_D2	Veh_Chron_D2	55.1656	19.7823	1.47956	0.00245749
Klf7	Hal_Chron_D2	Veh_Chron_D2	90.9127	32.6882	1.47571	0.00245749
Zbtb7a	Hal_Chron_D2	Veh_Chron_D2	59.3655	21.5566	1.4615	0.00245749
Wnk2	Hal_Chron_D2	Veh_Chron_D2	23.1567	8.47926	1.44942	0.00245749
Sbk1	Hal_Chron_D2	Veh_Chron_D2	28.1993	10.3491	1.44616	0.00245749

Table 2.17: Top 40 upregulated genes in iSPNs following haloperidol administration. Genes are sorted by q-value and then $\log_2$fold change.

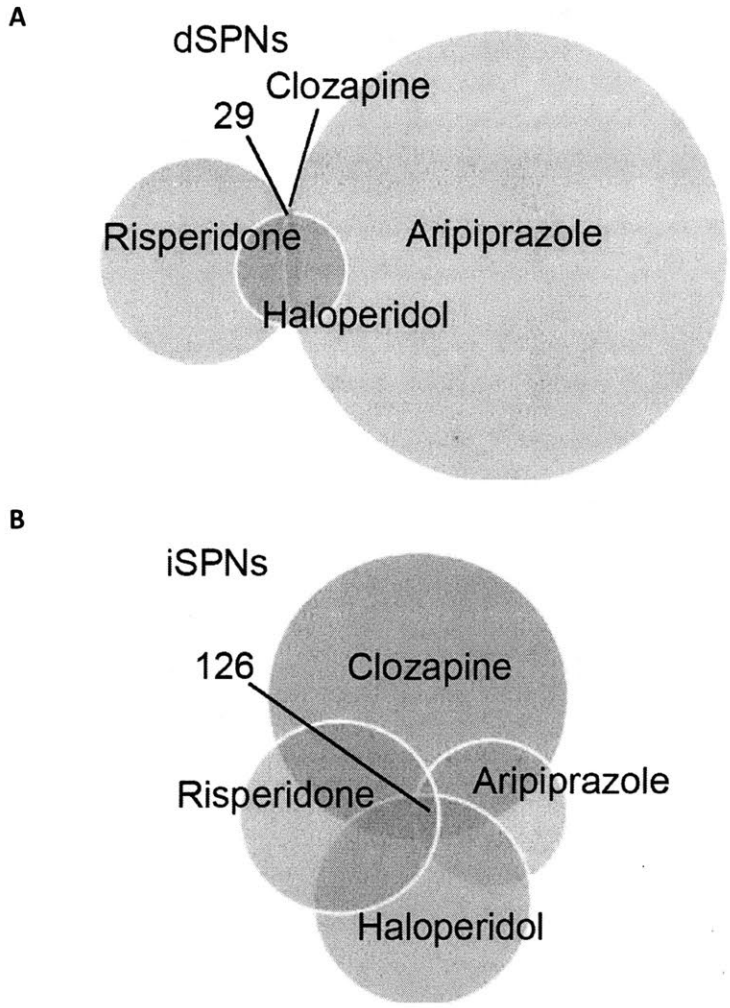

Figure 2.8: Common identities of differentially translated genes across antipsychotics. Venn overlaps of genes changing following each treatment in dSPNs (A) and iSPNs (B). Significant genes (adjusted p-value <0.05) are included.

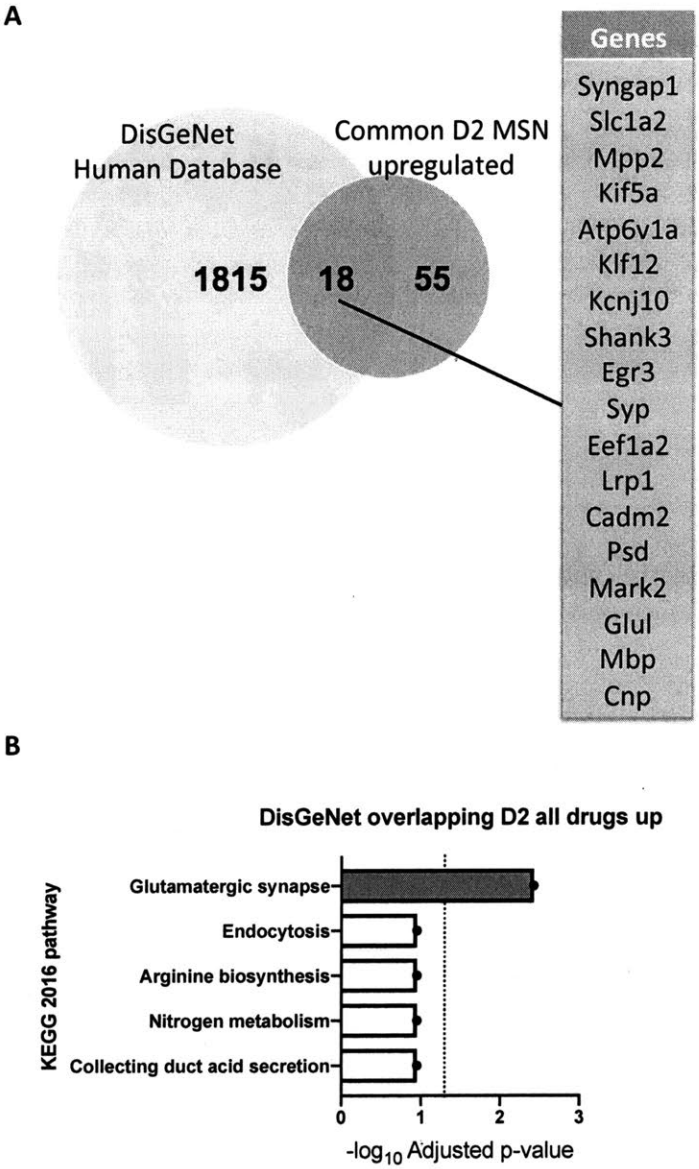

Figure 2.9: A subset of genes differentially translated following antipsychotic administration have been implicated in studies of schizophrenia pathophysiology. Overlap between genes upregulated across iSPN treatment conditions and genes previously implicated in schizophrenia pathophysiology (A). Names of genes in common between common iSPN upregulated and DisGeNet database (B). KEGG pathway analysis of overlapping genes (C).

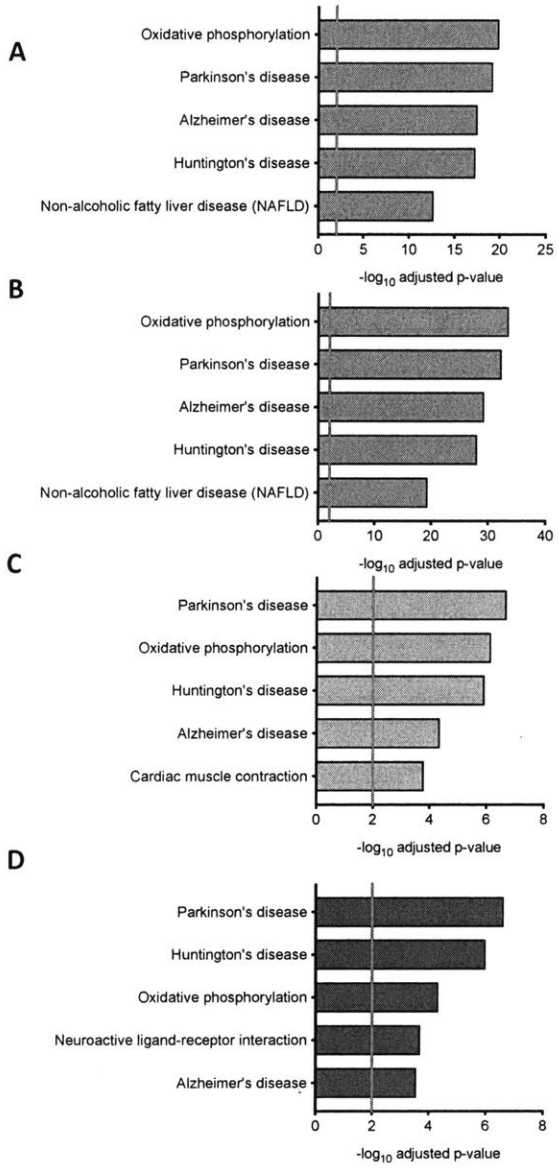

Figure 2.10: Antipsychotic administration decreases transcripts of genes associated with metabolism in iSPNs. Pathway analysis of decreased genes in iSPNs following aripiprazole (A), clozapine (B), risperidone (C), and haloperidol (D) administration.

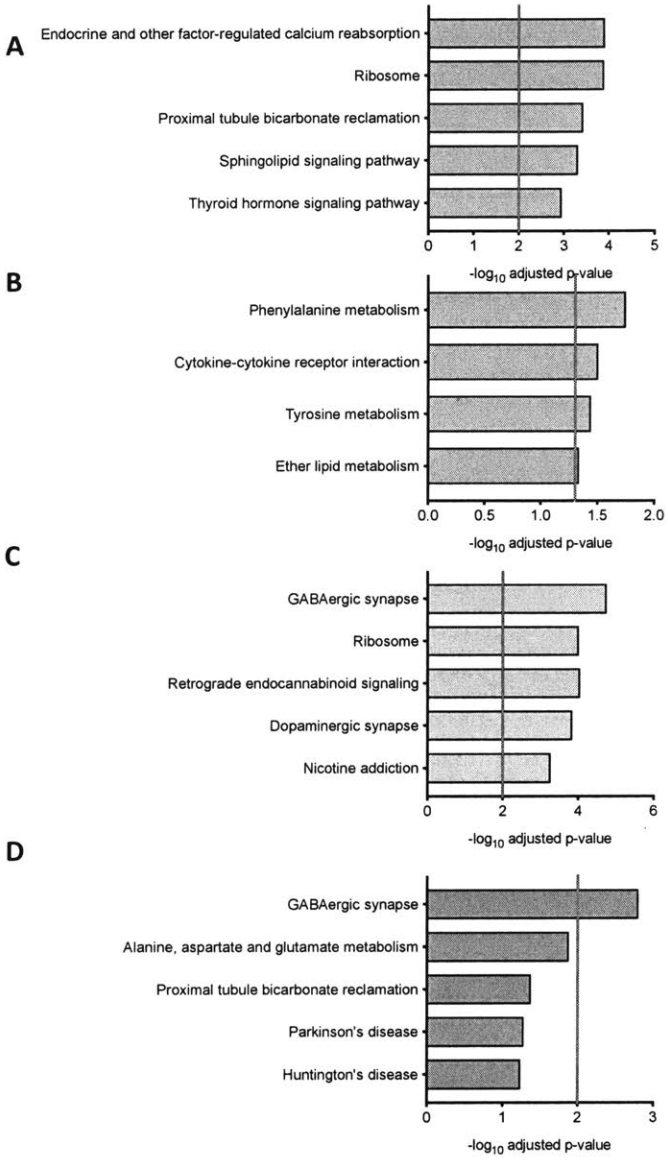

Figure 2.11: Antipsychotic administration decreases transcripts of genes associated with metabolism in dSPNs. Pathway analysis of decreased genes in dSPNs following aripiprazole (A), clozapine (B), risperidone (C), and haloperidol (D) administration.

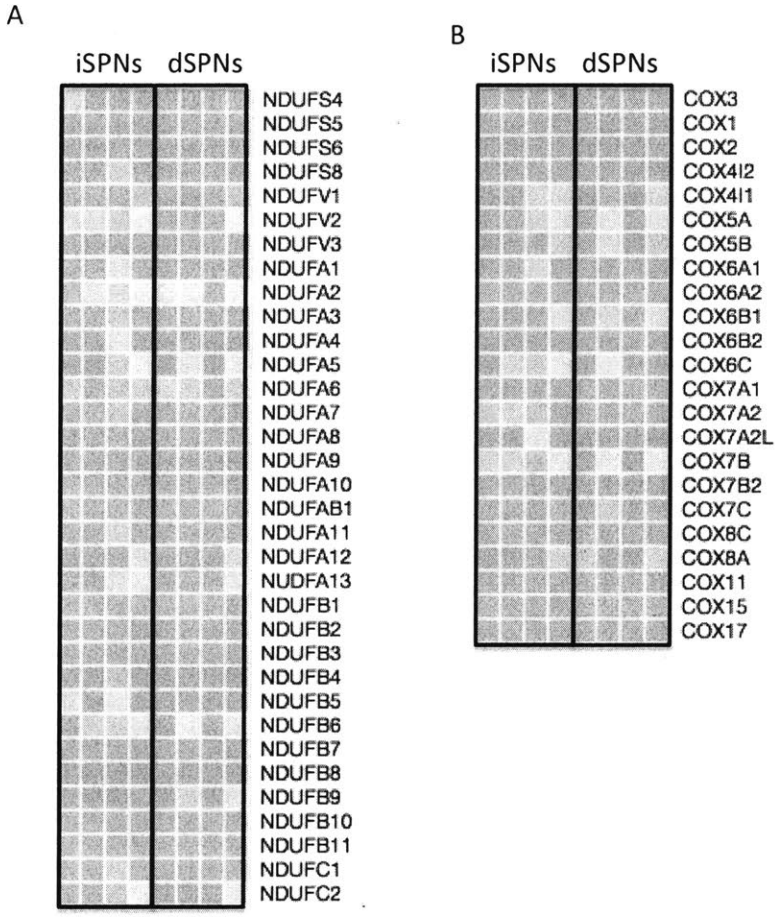

Figure 2.12: Translational alterations in Complex 1 and Complex IV genes following antipsychotic administration. Genes associted with either Complex I (A) or Complex IV (B) are shown. Blue indicates decreased translation, while red indicates increased translation. For each cell type, each column represents one drug treatment. These proceed L-R as haloperidol, risperidone, clozapine, aripiprazole for both cell types.

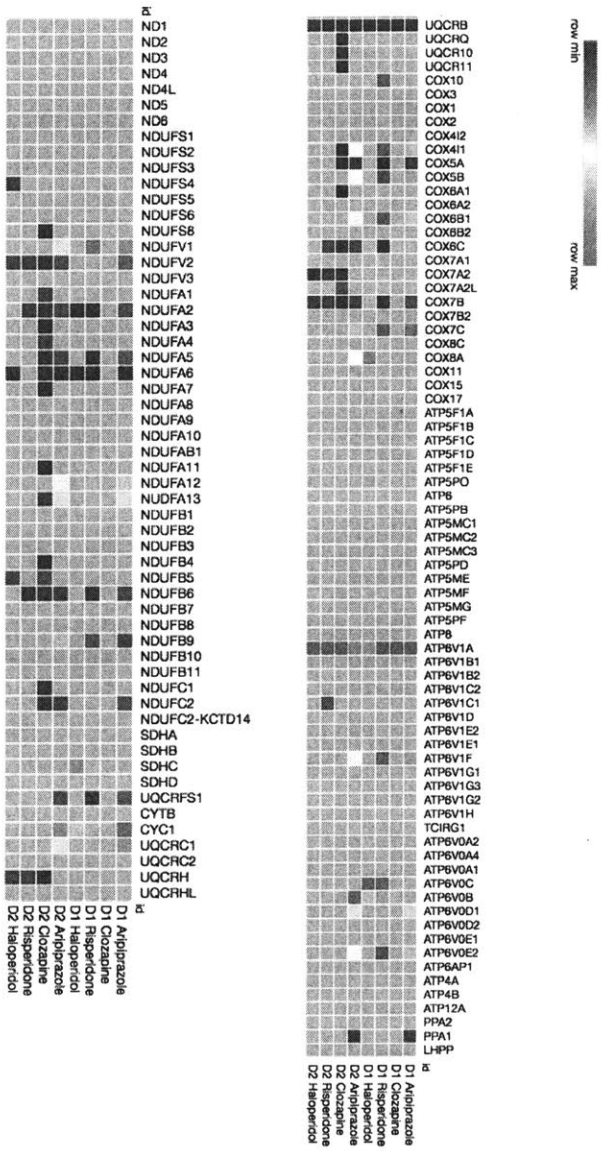

Figure 2.13: Decrease in genes associated with oxidative phosphorylation across cell types and antipsychotic treatments. Genes associated with oxidative phosphorylation are shown. Genes changing after antipsychotic administration in either cell type are highlighted in blue (downregulated) or red (upregulated).

Term	Overlap	P-value	Adjusted P-value	Z-score	Combined Score	Genes
Oxidative phosphorylation_Homo sapiens_hsa00190	23/133	1.19E-20	1.12E-18	-1.83	83.85	COX7B;NDUFA6;UQCRB;NDUFB6;NDUFA5;NDUFB4;COX4I1;NDUFA1;NDUFC2;UQCR11;COX7A2;ATP5H;ATP5G3;COX6A1;COX6C;COX7A1;COX5A;ATP5G1;UQCRH;ATP5J2;ATP5E;NDUFS4;NDUFV2
Parkinson's disease_Homo sapiens_hsa05012	23/142	5.60E-20	2.63E-18	-1.74	77.32	COX7B;NDUFA6;UQCRB;NDUFB6;NDUFA5;NDUFB4;COX4I1;NDUFA1;NDUFC2;UQCR11;COX7A2;ATP5H;ATP5G3;COX6A1;COX6C;COX7A1;COX5A;ATP5G1;UQCRH;ATP5E;NDUFS4;NDUFV2;DRD2
Huntington's disease_Homo sapiens_hsa05016	24/193	4.91E-18	1.15E-16	-1.83	72.80	COX7B;NDUFA6;UQCRB;NDUFB6;NDUFA5;NDUFB4;COX4I1;NDUFA1;NDUFC2;UQCR11;AP2A1;COX7A2;ATP5H;ATP5G3;COX6C;COX6A1;COX5A;COX7A1;ATP5G1;UQCRH;ATP5E;NDUFS4;POLR2E;NDUFV2
Alzheimer's disease_Homo sapiens_hsa05010	23/168	2.80E-18	8.76E-17	-1.79	72.42	COX7B;NDUFA6;UQCRB;NDUFB6;NDUFA5;NDUFB4;COX4I1;NDUFA1;NDUFC2;UQCR11;COX7A2;ATP5H;ATP5G3;COX6A1;COX6C;COX7A1;COX5A;ATP5G1;UQCRH;ATP5E;NDUFS4;NDUFV2;CDK5R1
Non-alcoholic fatty liver disease (NAFLD)_Homo sapiens_hsa04932	18/151	1.73E-13	3.25E-12	-1.86	54.66	COX7B;NDUFA6;UQCRB;NDUFB6;NDUFA5;NDUFB4;COX4I1;NDUFA1;NDUFC2;UQCR11;COX7A2;COX6A1;COX6C;COX7A1;COX5A;UQCRH;NDUFS4;NDUFV2
Ribosome_Homo sapiens_hsa03010	13/137	7.39E-09	1.16E-07	-1.62	30.42	RPL41;RPL12;RPLP1;RPL23A;RPS4X;RPL7A;RPS29;RPS20;RPS27A;RPL39;RPS13;RPS23;RPS12
Cardiac muscle contraction_Homo sapiens_hsa04260	10/78	2.29E-08	3.08E-07	-1.60	28.22	COX7B;UQCRB;COX4I1;UQCR11;COX7A2;COX6C;COX6A1;COX5A;COX7A1;UQCRH
Metabolic pathways_Homo sapiens_hsa01100	33/1239	6.87E-06	8.07E-05	-1.84	21.85	COX7B;GALNT13;UQCRB;NDUFB6;NDUFB4;COX4I1;MRI1;UQCR11;ATP5H;ATP5G3;COX6A1;COX5A;ATP5G1;UQCRH;FUT9;FLAD1;ATP5E;RFK;POLR2E;RIMKLA;NDUFV2;PLA2G12A;NDUFA6;NDUFA5;BHMT2;NDUFA1;GATC;NDUFC2;COX6C;COQ7;ATP5J2;DPM1;NDUFS4
Systemic lupus erythematosus_Homo sapiens_hsa05322	5/135	2.07E-02	2.16E-01	-1.55	6.00	H3F3B;SNRPD1;HIST1H3H;ELANE;HIST1H2BC
Alcoholism_Homo sapiens_hsa05034	5/179	5.79E-02	5.04E-01	-1.68	4.78	GNG10;H3F3B;HIST1H3H;DRD2;HIST1H2BC

Table 2.18: Top 10 KEGG pathways from downregulated transcripts in iSPNs following aripiprazole.

Term	Overlap	P-value	Adjusted P-value	Z-score	Combined Score	Genes
Oxidative phosphorylation_Homo sapiens_hsa00190	39/133	2.52E-34	4.25E-32	-1.83	141.39	COX7B;NDUFA13;UQCRB;NDUFB6;NDUFA11;NDUFB5;NDUFB4;COX4I1;ATP5C1;ATP5J;UQCR11;COX7A2;UQCR10;ATP5H;ATP5G3;COX6A1;ATP5O;COX5A;ATP5G1;UQCRH;ATP5L;ATP5E;NDUFV2;NDUFA7;NDUFA6;NDUFA5;NDUFA4;NDUFA3;NDUFA2;NDUFA1;NDUFC2;NDUFC1;ATP5F1;COX6C;COX7B2;ATP5J2;COX7A2L;NDUFS8;UQCRQ
Parkinson's disease_Homo sapiens_hsa05012	39/142	4.25E-33	3.59E-31	-1.74	130.01	COX7B;NDUFA13;UQCRB;NDUFB6;NDUFA11;NDUFB5;NDUFB4;COX4I1;ATP5C1;ATP5J;UQCR11;COX7A2;UQCR10;ATP5H;ATP5G3;COX6A1;ATP5O;COX5A;ATP5G1;UQCRH;ATP5E;NDUFV2;DRD2;NDUFA7;NDUFA6;NDUFA5;NDUFA4;NDUFA3;NDUFA2;NDUFA1;NDUFC2;NDUFC1;ATP5F1;COX6C;COX7B2;COX7A2L;NDUFS8;UQCRQ;SLC25A5
Alzheimer's disease_Homo sapiens_hsa05010	39/168	4.92E-30	2.77E-28	-1.79	120.92	COX7B;NDUFA13;UQCRB;NDUFB6;NDUFA11;NDUFB5;NDUFB4;COX4I1;LPL;ATP5C1;ATP5J;UQCR11;COX7A2;UQCR10;ATP5H;ATP5G3;COX6A1;ATP5O;COX5A;ATP5G1;UQCRH;ATP5E;NDUFV2;NDUFA7;NDUFA6;NDUFA5;NDUFA4;NDUFA3;NDUFA2;NDUFA1;NDUFC2;NDUFC1;ATP5F1;COX6C;COX7B2;COX7A2L;NDUFS8;UQCRQ;PLCB2
Huntington's disease_Homo sapiens_hsa05016	40/193	9.94E-29	4.20E-27	-1.83	117.78	COX7B;NDUFA13;NDUFA11;UQCRB;NDUFB6;NDUFB5;NDUFB4;COX4I1;ATP5C1;ATP5J;UQCR11;COX7A2;UQCR10;ATP5H;ATP5G3;COX6A1;ATP5O;COX5A;ATP5G1;UQCRH;ATP5E;POLR2E;NDUFV2;NDUFA7;NDUFA6;NDUFA5;NDUFA4;NDUFA3;NDUFA2;NDUFA1;NDUFC2;NDUFC1;COX6C;ATP5F1;COX7B2;COX7A2L;NDUFS8;UQCRQ;SLC25A5;PLCB2
Non-alcoholic fatty liver disease (NAFLD)_Homo sapiens_hsa04932	29/151	3.86E-20	1.31E-18	-1.86	83.14	COX7B;NDUFA13;UQCRB;NDUFB6;NDUFA11;NDUFB5;NDUFB4;COX4I1;UQCR11;COX7A2;UQCR10;COX6A1;COX5A;UQCRH;NDUFV2;NDUFA7;NDUFA6;NDUFA5;NDUFA4;NDUFA3;NDUFA2;NDUFA1;NDUFC2;NDUFC1;COX6C;COX7B2;COX7A2L;NDUFS8;UQCRQ
Ribosome_Homo sapiens_hsa03010	27/137	3.86E-19	1.09E-17	-1.62	68.89	RPL12;RPL36A;RPL9;MRPL32;RPL7;MRPL20;RPL7A;RPS17;MRPL2;RPL13;RPL38;RPS2;RPL37;RPS27A;RPL39;RPS13;RPS12;RPL41;RPL23;RPS5;RPL23A;RPS26;RPS25;RPS29;RPL22L1;RPS20;RPS23
Metabolic pathways_Homo sapiens_hsa01100	57/1239	7.58E-09	1.60E-07	-1.84	34.36	PIGU;COX7B;NDUFA13;GALNT13;NDUFA11;COX4I1;ATP5C1;ATP5G3;COX6A1;ATP5G1;UROD;FLAD1;RFK;XYLB;PLA2G12A;BHMT2;NDUFC2;NDUFC1;ATP5F1;ATP5J2;DPM1;NDUFS8;B3GNT2;PLCB2;IDO1;UQCRB;NDUFB6;NDUFB5;NDUFB4;ATP5J;UQCR11;ATP5H;UQCR10;ATP5O;COX5A;UQCRH;ATP5L;NT5E;FUT9;ATP5E;POLR2E;NDUFV2;KL;NDUFA7;NDUFA6;NDUFA5;NDUFA4;NDUFA3;NDUFA2;NDUFA1;GATC;COX6C;COX7B2;COQ7;POLE4;SUCLA2;UQCRQ
Cardiac muscle contraction_Homo sapiens_hsa04260	13/78	5.99E-09	1.45E-07	-1.60	30.38	COX7B;UQCRB;COX4I1;UQCR11;COX7A2;UQCR10;COX6C;COX6A1;COX7B2;COX5A;UQCRH;COX7A2L;UQCRQ
Retrograde endocannabinoid signaling_Homo sapiens_hsa04723	8/101	1.10E-03	2.07E-02	-1.71	11.65	GABRA2;GABRB3;GNG10;GABRA5;CNR1;GABRA4;GABRG3;PLCB2
GABAergic synapse_Homo sapiens_hsa04727	7/88	2.18E-03	3.34E-02	-1.55	9.53	GABRA2;GABRB3;GABARAPL2;GNG10;GABRA5;GABRA4;GABRG3

Table 2.19: Top 10 KEGG pathways from downregulated transcripts in iSPNs following clozapine.

Term	Overlap	P-value	Adjusted P-value	Z-score	Combined Score	Genes
Parkinson's disease_Homo sapiens_hsa05012	13/142	1.99E-07	2.94E-05	-1.77	27.28	COX7B;UQCRB;NDUFB6;NDUFA2;ATP5J;COX7A2;ATP5G3;COX6C;COX7A1;UQCRH;NDUFV2;SLC25A5;SLC25A4
Oxidative phosphorylation_Homo sapiens_hsa00190	12/133	6.89E-07	5.10E-05	-1.80	25.56	COX7B;UQCRB;NDUFB6;NDUFA2;ATP5J;COX7A2;ATP5G3;NDUFV2;COX6C;COX7A1;UQCRH;ATP6V1C1
Huntington's disease_Homo sapiens_hsa05016	14/193	1.17E-06	5.78E-05	-1.85	25.28	COX7B;UQCRB;NDUFB6;NDUFA2;ATP5J;COX7A2;ATP5G3;COX6C;COX7A1;UQCRH;POLR2E;NDUFV2;SLC25A5;SLC25A4
Alzheimer's disease_Homo sapiens_hsa05010	11/168	4.28E-05	1.58E-03	-1.77	17.77	COX7B;UQCRB;NDUFB6;NDUFA2;ATP5J;COX7A2;ATP5G3;NDUFV2;COX6C;COX7A1;UQCRH
Cardiac muscle contraction_Homo sapiens_hsa04260	7/78	1.56E-04	4.62E-03	-1.67	14.63	MYL4;COX7B;UQCRB;COX7A2;COX6C;COX7A1;UQCRH
Non-alcoholic fatty liver disease (NAFLD)_Homo sapiens_hsa04932	9/151	4.26E-04	9.00E-03	-1.81	14.04	COX7B;UQCRB;NDUFB6;NDUFA2;COX7A2;NDUFV2;COX6C;COX7A1;UQCRH
Nicotine addiction_Homo sapiens_hsa05033	5/40	2.95E-04	7.29E-03	-1.62	13.20	GABRA2;GABRB3;GABRA4;SLC17A6;SLC17A7
Ribosome_Homo sapiens_hsa03010	8/137	1.01E-03	1.86E-02	-1.58	10.88	RPL41;RPL23;RPL12;RPL23A;RPS27A;RPL39;RPS13;RPL7
GABAergic synapse_Homo sapiens_hsa04727	5/88	9.91E-03	1.13E-01	-1.49	6.89	GABRA2;GABRB3;GABARAPL2;GABRA4;GLS
Pathogenic Escherichia coli infection_Homo sapiens_hsa05130	4/55	8.87E-03	1.12E-01	-1.45	6.83	TUBB2A;YWHAQ;ARPC5L;TUBB4B

Table 2.20: Top 10 KEGG pathways from downregulated transcripts in iSPNs following risperidone.

Term	Overlap	P-value	Adjusted P-value	Z-score	Combined Score	Genes
Parkinson's disease_Homo sapiens_hsa05012	12/142	2.31E-07	2.89E-05	-1.77	27.01	COX7B;NDUFA6;UQCRB;NDUFB5;NDUFS4;COX7A2;ATP5G3;NDUFV2;DRD2;SLC25A5;SLC25A4;UQCRH
Huntington's disease_Homo sapiens_hsa05016	13/193	9.95E-07	6.22E-05	-1.88	25.93	COX7B;NDUFA6;UQCRB;NDUFB5;AP2A1;COX7A2;ATP5G3;UQCRH;NDUFS4;POLR2E;NDUFV2;SLC25A5;SLC25A4
Oxidative phosphorylation_Homo sapiens_hsa00190	9/133	4.57E-05	1.90E-03	-1.78	17.75	COX7B;NDUFA6;UQCRB;NDUFB5;NDUFS4;COX7A2;ATP5G3;NDUFV2;UQCRH
Neuroactive ligand-receptor interaction_Homo sapiens_hsa04080	12/277	2.02E-04	6.31E-03	-1.82	15.49	UTS2R;OXTR;CHRNA5;CNR2;GRM7;CHRNA9;TSPO;HTR2C;GPR50;S1PR3;AVPR1A;DRD2
Alzheimer's disease_Homo sapiens_hsa05010	9/168	2.72E-04	6.80E-03	-1.74	14.30	COX7B;NDUFA6;UQCRB;NDUFB5;NDUFS4;COX7A2;ATP5G3;NDUFV2;UQCRH
Non-alcoholic fatty liver disease (NAFLD)_Homo sapiens_hsa04932	8/151	6.37E-04	1.33E-02	-1.83	13.50	COX7B;NDUFA6;UQCRB;NDUFB5;NDUFS4;COX7A2;NDUFV2;UQCRH
Cardiac muscle contraction_Homo sapiens_hsa04260	5/78	2.95E-03	5.26E-02	-1.60	9.35	COX7B;UQCRB;TNNC1;COX7A2;UQCRH
Calcium signaling pathway_Homo sapiens_hsa04020	6/180	2.59E-02	3.59E-01	-1.76	6.42	OXTR;TNNC1;HTR2C;AVPR1A;SLC25A5;SLC25A4
Proteasome_Homo sapiens_hsa03050	3/44	1.75E-02	2.74E-01	-1.38	5.57	PSMB1;PSMB8;PSMB9
Ribosome_Homo sapiens_hsa03010	4/137	9.32E-02	8.68E-01	-1.48	3.51	RPL23;RPL12;RPL39;RPL7

Table 2.21: Top 10 KEGG pathways from downregulated transcripts in iSPNs following haloperidol.

Term	Overlap	P-value	Adjusted P-value	Z-score	Combined Score	Genes
Endocrine and other factor-regulated calcium reabsorption_Homo sapiens_hsa04961	11/47	1.23E-04	1.63E-02	-2.01	18.09	DNM3;KL;CALB1;PRKCB;GNAS;ATP1B3;ATP1A2;ATP1B2;PLCB1;RAB11A;SLC8A1
Ribosome_Homo sapiens_hsa03010	21/137	1.28E-04	1.63E-02	-1.72	15.44	RPS7;RPL23;RPL12;MRPL27;RPL23A;RPL9;MRPL32;RPL7;RPS4X;MRPL20;RPS28;RPS29;RPL22L1;RPS20;RPL15;RPS2;RPL37;RPS27A;RPL39;RPS13;RPS12
Sphingolipid signaling pathway_Homo sapiens_hsa04071	18/120	4.94E-04	3.15E-02	-1.70	12.93	OPRD1;ASAH1;ASAH2;CERS6;ROCK1;SGMS1;ROCK2;PRKCB;PTEN;PIK3R1;PPP2R3A;GNA13;MAPK11;PPP2CB;MAPK8;DEGS1;KRAS;PLCB1
Proximal tubule bicarbonate reclamation_Homo sapiens_hsa04964	7/23	3.81E-04	3.15E-02	-1.51	11.91	MDH1;ATP1A2;ATP1B3;ATP1B2;SLC4A4;GLS;AQP1
Thyroid hormone signaling pathway_Homo sapiens_hsa04919	17/118	1.11E-03	3.75E-02	-1.73	11.75	NOTCH2;NCOA2;PRKCB;ATP2A2;ATP1B3;ATP1A2;ATP1B2;PIK3R1;KAT2B;MED30;TBC1D4;RHEB;EP300;KRAS;ITGAV;SLC16A2;PLCB1
Dopaminergic synapse_Homo sapiens_hsa04728	18/129	1.18E-03	3.75E-02	-1.71	11.52	KCNJ6;PRKCB;PPP2R3A;GNG12;MAPK11;PPP2CB;MAPK8;GNG2;KIF5C;KIF5B;KIF5A;CREB3L2;GNAS;DRD2;PLCB1;GRIA3;CREB5;SCN1A
Cardiac muscle contraction_Homo sapiens_hsa04260	13/78	1.07E-03	3.75E-02	-1.67	11.41	COX7B;TPM4;UQCRB;CACNA2D1;ATP2A2;ATP1B3;ATP1A2;ATP1B2;COX6C;COX5A;SLC8A1;SLC9A6;UQCRFS1
GABAergic synapse_Homo sapiens_hsa04727	14/88	1.12E-03	3.75E-02	-1.68	11.38	GABRA2;GABRB3;GABRA1;GABRB2;GABARAPL2;KCNJ6;PRKCB;PLCL1;GABRA4;GAD1;GNG12;GABRG3;GLS;GNG2
Retrograde endocannabinoid signaling_Homo sapiens_hsa04723	15/101	1.56E-03	3.98E-02	-1.68	10.87	GABRA2;GABRB3;GABRA1;GABRB2;KCNJ6;PRKCB;GABRA4;GNG12;GABRG3;MAPK11;MAPK8;GNG2;CNR1;PLCB1;GRIA3
Vasopressin-regulated water reabsorption_Homo sapiens_hsa04962	9/44	1.42E-03	3.98E-02	-1.59	10.40	DYNC1I2;DCTN2;DCTN4;CREB3L2;GNAS;AQP4;RAB11A;DYNC1I1;CREB5

Table 2.22: Top 10 KEGG pathways from downregulated transcripts in dSPNs following aripiprazole.

Term	Overlap	P-value	Adjusted P-value	Z-score	Combined Score	Genes
Phenylalanine metabolism_Homo sapiens_hsa00360	1/17	1.77E-02	2.04E-01	-1.61	6.50	HPD
Cytokine-cytokine receptor interaction_Homo sapiens_hsa04060	2/265	3.11E-02	2.08E-01	-1.83	6.35	CCL4;PRLR
Tyrosine metabolism_Homo sapiens_hsa00350	1/35	3.61E-02	2.08E-01	-1.81	6.00	HPD
Ether lipid metabolism_Homo sapiens_hsa00565	1/45	4.62E-02	2.13E-01	-1.61	4.94	ENPP2
Ubiquinone and other terpenoid-quinone biosynthesis_Homo sapiens_hsa00130	1/11	1.15E-02	2.04E-01	-1.08	4.84	HPD
Prolactin signaling pathway_Homo sapiens_hsa04917	1/72	7.30E-02	2.15E-01	-1.77	4.64	PRLR
Cytosolic DNA-sensing pathway_Homo sapiens_hsa04623	1/64	6.51E-02	2.15E-01	-1.55	4.24	CCL4
Cardiac muscle contraction_Homo sapiens_hsa04260	1/78	7.88E-02	2.15E-01	-1.57	3.99	UQCRB
Toll-like receptor signaling pathway_Homo sapiens_hsa04620	1/106	1.06E-01	2.21E-01	-1.63	3.67	CCL4
Salmonella infection_Homo sapiens_hsa05132	1/86	8.66E-02	2.15E-01	-1.49	3.64	CCL4

Table 2.23: Top 10 KEGG pathways from downregulated transcripts in dSPNs following clozapine.

Term	Overlap	P-value	Adjusted P-value	Z-score	Combined Score	Genes
Circadian entrainment_Homo sapiens_hsa04713	9/95	3.82E-02	3.52E-01	-1.15	3.77	GUCY1A3;GUCY1A2;KCNJ6;GNG2;PLCB4;GNAS;ADCY2;GNG12;GRIA3
TGF-beta signaling pathway_Homo sapiens_hsa04350	9/84	1.90E-02	2.13E-01	-1.21	4.79	PPP2CB;LEFTY1;BMPR2;ROCK1;ID2;ID3;SMAD9;AMH;DCN
Gastric acid secretion_Homo sapiens_hsa04971	9/74	8.66E-03	1.18E-01	-1.40	6.66	KCNJ10;PLCB4;KCNE2;SST;GNAS;ATP1B3;ADCY2;ATP1A2;ATP1B2
Chemokine signaling pathway_Homo sapiens_hsa04062	9/187	5.42E-01	9.33E-01	1.94	-1.18	RAP1B;GNG2;PLCB4;ROCK1;ROCK2;CCL4;ADCY2;KRAS;GNG12
Calcium signaling pathway_Homo sapiens_hsa04020	9/180	4.96E-01	9.03E-01	1.52	-1.07	PLCB4;PLCZ1;GNAS;ATP2B3;ADCY2;PHKA1;PHKB;SLC25A4;SLC8A1
Phagosome_Homo sapiens_hsa04145	9/154	3.19E-01	8.35E-01	0.60	-0.68	DYNC1I2;TUBB2B;LAMP2;CANX;ITGAV;SEC61B;TUBB4B;TUBB4A;DYNC1I1
Hippo signaling pathway_Homo sapiens_hsa04390	9/153	3.12E-01	8.35E-01	0.55	-0.64	FZD1;PPP2CB;BMPR2;APC;YWHAQ;ID2;FGF1;AMH;TEAD1
Phospholipase D signaling pathway_Homo sapiens_hsa04072	9/144	2.54E-01	7.52E-01	0.30	-0.40	DGKG;GNA13;PLCB4;PPAP2B;KIT;GNAS;LPAR1;ADCY2;KRAS
Wnt signaling pathway_Homo sapiens_hsa04310	9/142	2.41E-01	7.41E-01	0.20	-0.29	FZD1;SFRP1;MAPK8;PLCB4;APC;ROCK2;CSNK1A1;PRICKLE2;CACYBP
Cell adhesion molecules (CAMs)_Homo sapiens_hsa04514	9/142	2.41E-01	7.41E-01	0.22	-0.32	CLDN11;NLGN1;SDC2;NRXN1;ITGB8;ITGAV;CLDN2;JAM2;ITGA9

Table 2.24: Top 10 KEGG pathways from downregulated transcripts in dSPNs following risperidone.

Term	Overlap	P-value	Adjusted P-value	Z-score	Combined Score	Genes
GABAergic synapse_Homo sapiens_hsa04727	6/88	1.56E-03	2.33E-01	-1.86	11.99	GABARAPL2;GNG2;GABRA4;GAD1;GABRG3;GLS
Alanine, aspartate and glutamate metabolism_Homo sapiens_hsa00250	3/35	1.31E-02	9.32E-01	-1.74	7.55	GAD1;RIMKLA;GLS
Huntington's disease_Homo sapiens_hsa05016	6/193	5.70E-02	9.32E-01	-1.80	5.16	NDUFA6;UQCRB;NDUFA2;HTT;ATP5G3;SLC25A5
Parkinson's disease_Homo sapiens_hsa05012	5/142	5.16E-02	9.32E-01	-1.70	5.03	NDUFA6;UQCRB;NDUFA2;ATP5G3;SLC25A5
Proximal tubule bicarbonate reclamation_Homo sapiens_hsa04964	2/23	4.15E-02	9.32E-01	-1.51	4.81	MDH1;GLS
Thyroid cancer_Homo sapiens_hsa05216	2/29	6.31E-02	9.32E-01	-1.48	4.09	TFG;TPR
Glyoxylate and dicarboxylate metabolism_Homo sapiens_hsa00630	2/28	5.93E-02	9.32E-01	-1.25	3.54	MDH1;CAT
Oxidative phosphorylation_Homo sapiens_hsa00190	4/133	1.20E-01	9.32E-01	-1.57	3.32	NDUFA6;UQCRB;NDUFA2;ATP5G3
Pyruvate metabolism_Homo sapiens_hsa00620	2/40	1.10E-01	9.32E-01	-1.48	3.27	MDH1;ACYP2
Primary immunodeficiency_Homo sapiens_hsa05340	2/37	9.62E-02	9.32E-01	-1.37	3.21	IL2RG;CD3E

Table 2.25: Top 10 KEGG pathways from downregulated transcripts in dSPNs following haloperidol.

Term	Overlap	P-value	Adjusted P-value	Z-score	Combined Score	Genes
Ether lipid metabolism_Homo sapiens_hsa00565	1/45	1.79E-02	8.82E-02	-1.81	7.27	ENPP2
Cardiac muscle contraction_Homo sapiens_hsa04260	1/78	3.08E-02	8.82E-02	-1.77	6.15	UQCRB
Non-alcoholic fatty liver disease (NAFLD)_Homo sapiens_hsa04932	1/151	5.88E-02	8.82E-02	-1.86	5.27	UQCRB
Oxidative phosphorylation_Homo sapiens_hsa00190	1/133	5.20E-02	8.82E-02	-1.78	5.25	UQCRB
Parkinson's disease_Homo sapiens_hsa05012	1/142	5.54E-02	8.82E-02	-1.70	4.91	UQCRB
Alzheimer's disease_Homo sapiens_hsa05010	1/168	6.53E-02	8.82E-02	-1.72	4.69	UQCRB
Proteoglycans in cancer_Homo sapiens_hsa05205	1/203	7.84E-02	8.82E-02	-1.83	4.66	IGF2
Huntington's disease_Homo sapiens_hsa05016	1/193	7.47E-02	8.82E-02	-1.75	4.55	UQCRB
Metabolic pathways_Homo sapiens_hsa01100	1/1239	4.01E-01	4.01E-01	-1.81	1.66	UQCRB

Table 2.26: Top 10 KEGG pathways from downregulated transcripts in dSPNs common across treatments.

Term	Overlap	P-value	Adjusted P-value	Z-score	Combined Score	Genes
Huntington's disease_Homo sapiens_hsa05016	8/193	3.98E-08	1.11E-06	-1.90	32.39	COX7B;UQCRB;POLR2E;COX7A2;ATP5G3;NDUFV2;SLC25A5;UQCRH
Parkinson's disease_Homo sapiens_hsa05012	7/142	9.20E-08	1.29E-06	-1.74	28.26	COX7B;UQCRB;COX7A2;ATP5G3;NDUFV2;SLC25A5;UQCRH
Oxidative phosphorylation_Homo sapiens_hsa00190	6/133	1.37E-06	1.28E-05	-1.78	23.97	COX7B;UQCRB;COX7A2;ATP5G3;NDUFV2;UQCRH
Alzheimer's disease_Homo sapiens_hsa05010	6/168	5.32E-06	3.72E-05	-1.77	21.46	COX7B;UQCRB;COX7A2;ATP5G3;NDUFV2;UQCRH
Non-alcoholic fatty liver disease (NAFLD)_Homo sapiens_hsa04932	5/151	4.92E-05	2.53E-04	-1.86	18.45	COX7B;UQCRB;COX7A2;NDUFV2;UQCRH
Cardiac muscle contraction_Homo sapiens_hsa04260	4/78	5.42E-05	2.53E-04	-1.64	16.08	COX7B;UQCRB;COX7A2;UQCRH
Ribosome_Homo sapiens_hsa03010	4/137	4.76E-04	1.90E-03	-1.60	12.25	RPL23;RPL12;RPL39;RPL7
Metabolic pathways_Homo sapiens_hsa01100	9/1239	4.89E-03	1.71E-02	-1.84	9.78	COX7B;GALNT13;UQCRB;FLAD1;GATC;POLR2E;ATP5G3;NDUFV2;UQCRH
Calcium signaling pathway_Homo sapiens_hsa04020	2/180	8.24E-02	2.01E-01	-1.71	4.26	AVPR1A;SLC25A5
RNA polymerase_Homo sapiens_hsa03020	1/32	8.15E-02	2.01E-01	-1.31	3.28	POLR2E

Table 2.27: Top 10 KEGG pathways from downregulated transcripts in iSPNs common across treatments.

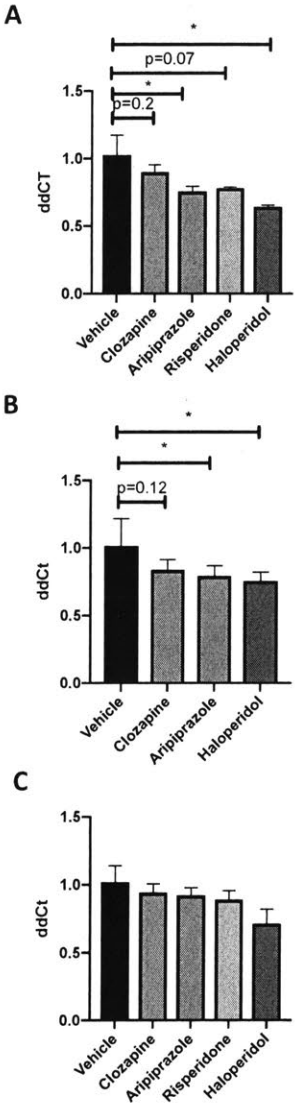

Figure 2.14: Antipsychotic administration decreases transcripts of genes associated with oxidative phosphorylation in total striatal RNA. RT-PCR analysis of antipsychotic-treated total RNA samples (n=4 mice/group) probing for Cox7b (A), Ndufa6 (B), and Uqcrb (C). Bars represent mean +/- SEM. * $p<0.05$.

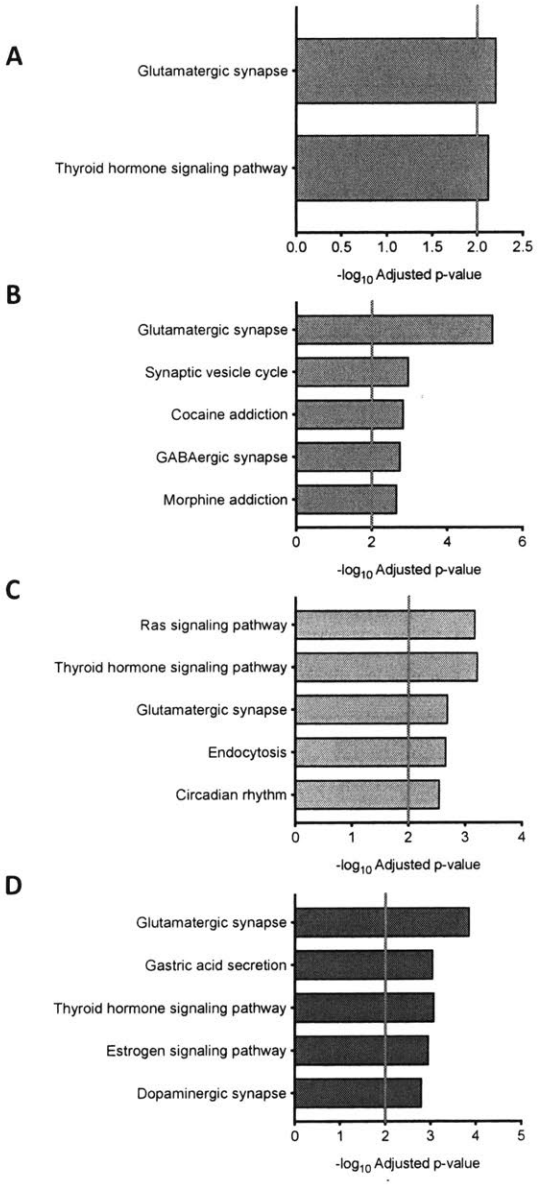

Figure 2.15: Antipsychotic administration increases transcripts of genes associated with glutamatergic synapse in iSPNs. Pathway analysis of decreased genes in iSPNs following aripiprazole (A), clozapine (B), risperidone (C), and haloperidol (D) administration.

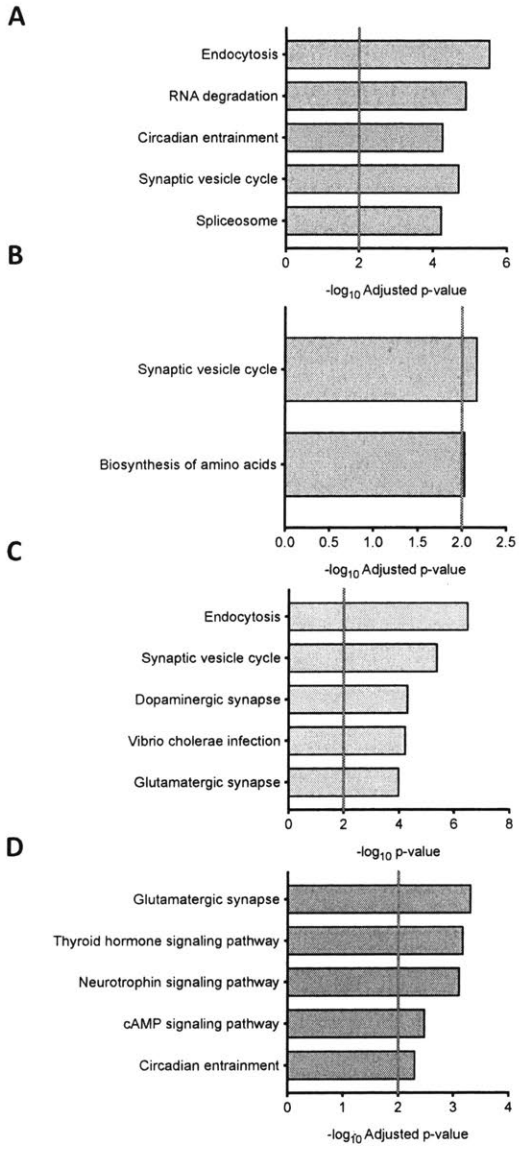

Figure 2.16: Risperidone and haloperidol administration increases transcripts of genes associated with the glutamatergic synapse in dSPNs. Pathway analysis of decreased genes in dSPNs following aripiprazole (A), clozapine (B), risperidone (C), and haloperidol (D) administration.

Figure 2.17: Increase in glutamatergic synapse pathway is most consistent alteration across treatments and cell types. Significantly altered pathways (p-value <0.01) were sorted according to their commonality.

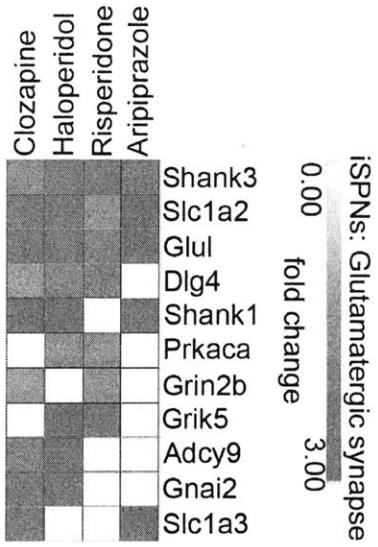

Figure 2.18: Increase in genes associated with glutamatergic synapse in iSPNs across antipsychotic treatments. Increased genes in common across at least two drug treatments in iSPNs, plotted by degree of fold change and sorted by commonality across treatments.

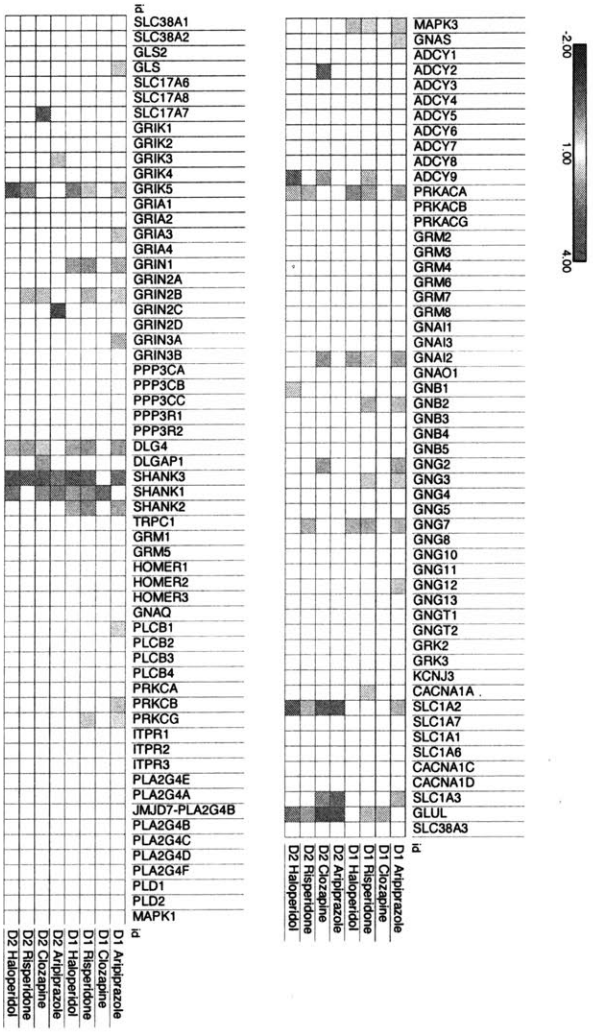

Figure 2.19: Increase in genes associated with glutamatergic function across cell types and antipsychotic treatments. Genes associated with glutamatergic function are shown. Genes changing after antipsychotic administration in either cell type are highlighted in blue (downregulated) or red (upregulated).

Term	Overlap	P-value	Adjusted P-value	Z-score	Combined Score	Genes
Glutamatergic synapse_Homo sapiens_hsa04724	7/114	6.13E-03	6.70E-01	-1.94	9.88	SLC1A2;GRIK3;SLC1A3;GRIN2C;GLUL;SHANK3;SHANK1
Thyroid hormone signaling pathway_Homo sapiens_hsa04919	7/118	7.37E-03	6.70E-01	-1.83	9.01	MED1;NOTCH1;MED13;ATP1A2;FOXO1;MED13L;SLC9A1
Longevity regulating pathway - multiple species_Homo sapiens_hsa04213	4/64	3.34E-02	9.42E-01	-1.87	6.34	RPTOR;EIF4EBP2;FOXO1;IGF1R
AMPK signaling pathway_Homo sapiens_hsa04152	6/124	3.12E-02	9.42E-01	-1.74	6.04	RPTOR;PPP2R2C;FASN;EEF2;FOXO1;IGF1R
Synaptic vesicle cycle_Homo sapiens_hsa04721	4/63	3.18E-02	9.42E-01	-1.59	5.49	ATP6V1A;STX1B;UNC13A;SLC32A1
Biosynthesis of amino acids_Homo sapiens_hsa01230	4/74	5.23E-02	9.42E-01	-1.61	4.75	CS;PSAT1;ALDOC;GLUL
Notch signaling pathway_Homo sapiens_hsa04330	3/48	6.29E-02	9.42E-01	-1.50	4.15	NCOR2;ADAM17;NOTCH1
Insulin secretion_Homo sapiens_hsa04911	4/85	7.86E-02	9.42E-01	-1.63	4.13	RYR2;PCLO;ATP1A2;KCNN3
Proteoglycans in cancer_Homo sapiens_hsa05205	7/203	9.33E-02	9.42E-01	-1.73	4.10	FZD5;SDC4;GAB1;ANK2;ANK3;SLC9A1;IGF1R
Lysine degradation_Homo sapiens_hsa00310	3/52	7.61E-02	9.42E-01	-1.59	4.10	KMT2D;SETD1B;KMT2B

Table 2.28: Top 10 KEGG pathways from upregulated transcripts in iSPNs following aripiprazole.

Term	Overlap	P-value	Adjusted P-value	Z-score	Combined Score	Genes
Glutamatergic synapse_Homo sapiens_hsa04724	13/114	5.91E-06	1.19E-03	-1.94	23.34	SLC1A2;SLC1A3;ADCY2;GRIN2B;GNAI2;ADCY9;GNG2;DLG4;DLGAP1;SLC17A7;GLUL;SHANK3;SHANK1
Synaptic vesicle cycle_Homo sapiens_hsa04721	7/63	1.00E-03	8.33E-02	-1.67	11.53	ATP6V1A;STX1B;UNC13A;SLC32A1;STXBP1;SLC17A7;DNM1
Cocaine addiction_Homo sapiens_hsa05030	6/49	1.37E-03	8.33E-02	-1.80	11.87	JUN;DLG4;FOSB;PDYN;GRIN2B;GNAI2
GABAergic synapse_Homo sapiens_hsa04727	8/88	1.67E-03	8.33E-02	-1.77	11.29	SLC12A5;ADCY9;GNG2;SLC32A1;ADCY2;ABAT;GLUL;GNAI2
Morphine addiction_Homo sapiens_hsa05032	8/91	2.07E-03	8.33E-02	-1.75	10.78	ADCY9;GNG2;SLC32A1;PDE1C;PDE1A;ADORA1;ADCY2;GNAI2
Gastric acid secretion_Homo sapiens_hsa04971	7/74	2.57E-03	8.61E-02	-1.85	11.04	KCNJ10;ADCY9;ADCY2;ATP1A2;CAMK2G;SLC9A1;GNAI2
cAMP signaling pathway_Homo sapiens_hsa04024	12/199	4.66E-03	1.34E-01	-1.79	9.61	JUN;ADCY9;ADORA1;ATP2B4;ADCY2;ATP1A2;SOX9;GRIN2B;CAMK2G;RAPGEF4;GNAI2;SLC9A1
Insulin secretion_Homo sapiens_hsa04911	7/85	5.57E-03	1.40E-01	-1.69	8.76	ADCY9;PCLO;SLC2A1;ADCY2;ATP1A2;CAMK2G;RAPGEF4
cGMP-PKG signaling pathway_Homo sapiens_hsa04022	10/167	9.81E-03	2.19E-01	-1.73	8.02	MEF2C;ADCY9;GNA12;ADORA1;ATP2B4;ADCY2;ATP1A2;SLC8A1;GNAI2;SLC8A2
Adrenergic signaling in cardiomyocytes_Homo sapiens_hsa04261	9/148	1.27E-02	2.20E-01	-1.63	7.14	ADCY9;ATP2B4;ADCY2;ATP1A2;CAMK2G;SLC8A1;SLC9A1;RAPGEF4;GNAI2

Table 2.29: Top 10 KEGG pathways from upregulated transcripts in iSPNs following clozapine.

Term	Overlap	P-value	Adjusted P-value	Z-score	Combined Score	Genes
Ras signaling pathway_Homo sapiens_hsa04014	13/227	6.56E-04	6.66E-02	-1.98	14.53	GAB1;KSR2;ELK1;GRIN2B;SYNGAP1;GNG7;AKT2;PAK6;CALM3;RGL1;PRKACA;FGF22;BCL2L1
Thyroid hormone signaling pathway_Homo sapiens_hsa04919	9/118	5.93E-04	6.66E-02	-1.86	13.83	MED1;GSK3B;NOTCH1;MED13;AKT2;PRKACA;FOXO1;SLC9A1;ACTG1
Glutamatergic synapse_Homo sapiens_hsa04724	8/114	2.02E-03	1.10E-01	-1.88	11.69	DLG4;GNG7;GRIK5;SLC1A2;PRKACA;GRIN2B;GLUL;SHANK3
Endocytosis_Homo sapiens_hsa04144	13/259	2.16E-03	1.10E-01	-1.89	11.59	ARF3;PSD;IQSEC2;WIPF2;AGAP2;AGAP1;ARPC4;VPS37B;ARFGAP2;PARD6B;KIF5A;RAB11FIP2;GIT1
Circadian rhythm_Homo sapiens_hsa04710	4/30	2.81E-03	1.14E-01	-1.66	9.74	PER1;PER3;FBXW11;BHLHE40
Dopaminergic synapse_Homo sapiens_hsa04728	8/129	4.32E-03	1.25E-01	-1.73	9.44	GSK3B;GNG7;AKT2;KIF5A;PPP1R1B;CALM3;PRKACA;GRIN2B
Hippo signaling pathway_Homo sapiens_hsa04390	9/153	3.61E-03	1.22E-01	-1.62	9.09	GSK3B;PARD6B;CCND2;FBXW11;DLG4;FZD9;AXIN1;NF2;ACTG1
Circadian entrainment_Homo sapiens_hsa04713	6/95	1.18E-02	2.66E-01	-1.71	7.61	PER1;PER3;GNG7;CALM3;PRKACA;GRIN2B
Glucagon signaling pathway_Homo sapiens_hsa04922	6/101	1.56E-02	2.86E-01	-1.66	6.93	PFKL;PRMT1;AKT2;CALM3;PRKACA;FOXO1
Cocaine addiction_Homo sapiens_hsa05030	4/49	1.62E-02	2.86E-01	-1.43	5.89	DLG4;PPP1R1B;PRKACA;GRIN2B

Table 2.30: Top 10 KEGG pathways from upregulated transcripts in iSPNs following risperidone.

Term	Overlap	P-value	Adjusted P-value	Z-score	Combined Score	Genes
Glutamatergic synapse_Homo sapiens_hsa04724	10/114	1.38E-04	2.94E-02	-1.94	17.24	ADCY9;DLG4;GRIK5;GNB1;SLC1A2;PRKACA;GLUL;SHANK3;SHANK1;GNAI2
Gastric acid secretion_Homo sapiens_hsa04971	7/74	8.81E-04	5.83E-02	-1.95	13.74	KCNJ10;ADCY9;CALM3;ATP1A2;PRKACA;SLC9A1;GNAI2
Thyroid hormone signaling pathway_Homo sapiens_hsa04919	9/118	8.25E-04	5.83E-02	-1.83	13.03	MED1;GSK3B;MED13;THRA;AKT2;ATP1A2;PRKACA;MED13L;SLC9A1
Estrogen signaling pathway_Homo sapiens_hsa04915	8/99	1.09E-03	5.83E-02	-1.84	12.54	JUN;ADCY9;SP1;AKT2;CALM3;FKBP4;PRKACA;GNAI2
Dopaminergic synapse_Homo sapiens_hsa04728	9/129	1.55E-03	6.60E-02	-1.79	11.57	GSK3B;PPP2R2C;AKT2;KIF5A;GNB1;PPP1R1B;CALM3;PRKACA;GNAI2
cAMP signaling pathway_Homo sapiens_hsa04024	11/199	3.16E-03	9.19E-02	-1.82	10.45	JUN;ADCY9;NPR1;AKT2;PPP1R1B;CALM3;ATP1A2;PRKACA;GLI3;GNAI2;SLC9A1
Adrenergic signaling in cardiomyocytes_Homo sapiens_hsa04261	9/148	3.93E-03	9.30E-02	-1.66	9.19	ADCY9;PPP2R2C;AKT2;BCL2;CALM3;ATP1A2;PRKACA;SLC9A1;GNAI2
Cocaine addiction_Homo sapiens_hsa05030	5/49	3.45E-03	9.19E-02	-1.57	8.89	JUN;DLG4;PPP1R1B;PRKACA;GNAI2
Circadian rhythm_Homo sapiens_hsa04710	4/30	3.32E-03	9.19E-02	-1.50	8.56	PER2;FBXW11;BHLHE40;NR1D1
Lysine degradation_Homo sapiens_hsa00310	5/52	4.47E-03	9.53E-02	-1.55	8.37	KMT2D;SETD1B;NSD1;KMT2C;ALDH9A1

Table 2.31: Top 10 KEGG pathways from upregulated transcripts in iSPNs following haloperidol.

Term	Overlap	P-value	Adjusted P-value	Z-score	Combined Score	Genes
Endocytosis_Homo sapiens_hsa04144	36/259	2.89E-06	7.43E-04	-1.96	25.02	ARF3;ARF1;RAB5C;SRC;AGAP2;AGAP1;ADRB1;AP2A1;VPS26B;AGAP3;PARD6B;PARD6A;ADRBK1;PIP5K1A;RAB11FIP2;HRAS;RAB11FIP4;GIT1;PSD;IQSEC2;GBF1;VPS37C;ARPC4;VPS37B;SNF8;AP2B1;ARPC5;DNM1;ARFGAP2;ACAP3;BIN1;ARPC3;SMAP2;VPS25;CHMP7;ARF5
RNA degradation_Homo sapiens_hsa03018	16/77	1.25E-05	1.61E-03	-1.84	20.76	BTG2;TOB2;ENO2;TOB1;LSM4;PATL1;LSM2;EXOSC7;LSM7;PFKL;CNOT7;CNOT3;RQCD1;SKIV2L;NUDT16;DCP1A
Circadian entrainment_Homo sapiens_hsa04713	17/95	5.22E-05	2.93E-03	-1.86	18.34	PRKCG;KCNJ9;CAMK2A;FOS;GRIN2B;CACNA1H;GRIN1;GNAI2;PER1;CACNA1I;GNG3;GNG7;GNB2;NOS1AP;CALM3;PRKACA;MAPK3
Synaptic vesicle cycle_Homo sapiens_hsa04721	14/63	1.94E-05	1.66E-03	-1.63	17.70	ATP6V1A;ATP6V0B;UNC13A;RAB3A;SLC32A1;STXBP1;AP2A1;AP2B1;DNM1;STX1B;ATP6V0D1;ATP6V0E2;STX1A;ATP6V1F
Spliceosome_Homo sapiens_hsa03040	21/134	5.70E-05	2.93E-03	-1.70	16.59	SF3B4;PPIL1;DDX23;PRPF40B;THOC3;WBP11;PRPF19;LSM4;PRPF8;CHERP;LSM2;U2AF1L4;LSM7;SNRNP40;PHF5A;SNRPD2;U2AF2;DHX38;ACIN1;SNRPD3;SNRPA
Dopaminergic synapse_Homo sapiens_hsa04728	20/129	9.89E-05	4.24E-03	-1.76	16.24	PRKCG;GSK3A;KCNJ9;CAMK2A;PPP2R5B;FOS;COMT;GRIN2B;PPP1CA;GNAI2;GNG3;CALY;PPP2R2C;GNG7;AKT2;GNB2;PPP1R1B;AKT1;CALM3;PRKACA
Amphetamine addiction_Homo sapiens_hsa05031	13/67	1.67E-04	5.82E-03	-1.80	15.62	PRKCG;CAMK2A;FOS;PDYN;GRIN2B;PPP1CA;GRIN1;ARC;PPP1R1B;FOSB;CALM3;PRKACA;STX1A
Alcoholism_Homo sapiens_hsa05034	24/179	2.18E-04	5.82E-03	-1.70	14.35	HDAC4;HDAC5;SHC1;H2AFZ;HDAC11;H3F3A;H2AFX;PDYN;GRIN2B;PPP1CA;GRIN1;GNAI2;GNG3;H2AFY2;GNG7;GNB2;PPP1R1B;FOSB;CALM3;HIST1H4C;PRKACA;HIST1H4D;HRAS;MAPK3
Alzheimer's disease_Homo sapiens_hsa05010	23/168	2.14E-04	5.82E-03	-1.67	14.08	COX8A;PSENEN;NDUFB9;NDUFA13;LRP1;NDUFA12;COX4I1;PSEN1;COX5B;GRIN2B;COX7C;HSD17B10;GRIN1;COX6B1;CDK5;ATP5D;UQCRC1;CALM3;CYC1;NDUFV1;GAPDH;SNCA;MAPK3
Huntington's disease_Homo sapiens_hsa05016	25/193	2.80E-04	5.99E-03	-1.63	13.32	NDUFB9;NDUFA13;NDUFA12;DCTN1;COX4I1;AP2A1;NRF1;COX5B;COX7C;BBC3;ATP5D;POLR2F;CYC1;NDUFV1;COX8A;GPX1;AP2B1;GRIN2B;COX6B1;GRIN1;SOD1;DLG4;UQCRC1;VDAC1;DNAL4

Table 2.32: Top 10 KEGG pathways from upregulated transcripts in dSPNs following aripiprazole.

Term	Overlap	P-value	Adjusted P-value	Z-score	Combined Score	Genes
Synaptic vesicle cycle_Homo sapiens_hsa04721	2/63	6.71E-03	1.37E-01	-1.71	8.54	ATP6V1A;UNC13A
Biosynthesis of amino acids_Homo sapiens_hsa01230	2/74	9.16E-03	1.37E-01	-1.74	8.16	ENO2;GLUL
Glutamatergic synapse_Homo sapiens_hsa04724	2/114	2.08E-02	1.90E-01	-1.88	7.30	GLUL;SHANK1
Axon guidance_Homo sapiens_hsa04360	2/127	2.54E-02	1.90E-01	-1.70	6.24	EFNB1;DPYSL2
Arginine biosynthesis_Homo sapiens_hsa00220	1/20	3.83E-02	1.90E-01	-1.37	4.46	GLUL
Collecting duct acid secretion_Homo sapiens_hsa04966	1/27	5.14E-02	1.90E-01	-1.35	4.00	ATP6V1A
Circadian rhythm_Homo sapiens_hsa04710	1/30	5.69E-02	1.90E-01	-1.34	3.85	BHLHE40
Nitrogen metabolism_Homo sapiens_hsa00910	1/17	3.27E-02	1.90E-01	-1.09	3.73	GLUL
Vibrio cholerae infection_Homo sapiens_hsa05110	1/51	9.49E-02	2.55E-01	-1.52	3.58	ATP6V1A
Alanine, aspartate and glutamate metabolism_Homo sapiens_hsa00250	1/35	6.61E-02	1.98E-01	-1.24	3.37	GLUL

Table 2.33: Top 10 KEGG pathways from upregulated transcripts in dSPNs following clozapine.

Term	Overlap	P-value	Adjusted P-value	Z-score	Combined Score	Genes
Endocytosis_Homo sapiens_hsa04144	35/259	3.12E-07	7.68E-05	-1.96	29.38	ARF3;ARF1;RAB5C;WIPF2;CLTB;SNX12;AGAP2;AGAP1;AP2A1;VPS26B;AGAP3;PARD6B;ADRBK1;PIP5K1A;PIP5K1C;RAB11FIP2;HRAS;RAB11FIP4;GIT1;PSD;IQSEC2;GBF1;VPS37C;ARPC4;SNF8;AP2B1;ARPC5;EPN1;DNM1;ARFGAP2;ACAP3;ARPC3;SMAP2;VPS25;ARF5
Synaptic vesicle cycle_Homo sapiens_hsa04721	14/63	3.92E-06	4.82E-04	-1.67	20.78	ATP6V1A;ATP6V0B;UNC13A;RAB3A;STXBP1;CLTB;CACNA1A;AP2A1;AP2B1;DNM1;STX1B;ATP6V0E2;ATP6V0C;ATP6V1F
Dopaminergic synapse_Homo sapiens_hsa04728	19/129	4.65E-05	3.49E-03	-1.84	18.37	PRKCG;GSK3A;ATF6B;CAMK2A;PPP2R5B;CACNA1A;GRIN2B;PPP1CA;GNAI2;GNG3;CALY;PPP2R2C;GNG7;AKT2;GNB2;PPP1R1B;AKT1;CALM3;PRKACA
Vibrio cholerae infection_Homo sapiens_hsa05110	11/51	5.68E-05	3.49E-03	-1.84	17.97	ATP6V1A;ARF1;ATP6V0B;ADCY9;KDELR1;ATP6V0E2;PRKACA;ATP6V0C;ACTB;ACTG1;ATP6V1F
Glutamatergic synapse_Homo sapiens_hsa04724	17/114	9.81E-05	4.82E-03	-1.83	16.89	PRKCG;GRIK5;CACNA1A;GRIN2B;GRIN1;GNAI2;GNG3;ADCY9;DLG4;GNG7;GNB2;ADRBK1;PRKACA;SHANK3;SHANK2;SHANK1;MAPK3
Circadian entrainment_Homo sapiens_hsa04713	15/95	1.29E-04	5.29E-03	-1.80	16.14	PRKCG;CAMK2A;GRIN2B;GRIN1;GNAI2;PER2;PER1;CACNA1I;GNG3;ADCY9;GNG7;GNB2;CALM3;PRKACA;MAPK3
Thyroid hormone signaling pathway_Homo sapiens_hsa04919	17/118	1.51E-04	5.31E-03	-1.70	14.96	PRKCG;THRA;ATP1A3;ACTB;MED13L;SLC9A1;ACTG1;RXRA;MED24;PLCZ1;AKT2;RCAN2;AKT1;PRKACA;RXRG;HRAS;MAPK3
Cholinergic synapse_Homo sapiens_hsa04725	15/111	7.25E-04	1.98E-02	-1.83	13.25	PRKCG;CHRM1;CAMK2A;CACNA1A;GNAI2;GNG3;ADCY9;GNG7;AKT2;GNB2;BCL2;AKT1;PRKACA;HRAS;MAPK3
Neurotrophin signaling pathway_Homo sapiens_hsa04722	16/120	5.69E-04	1.75E-02	-1.70	12.70	YWHAE;MAP3K3;CAMK2A;MATK;AKT2;ARHGDIA;ARHGDIB;BCL2;RAPGEF1;AKT1;CALM3;MAP2K7;HRAS;SH2B1;NFKBIB;MAPK3
Alcoholism_Homo sapiens_hsa05034	20/179	1.25E-03	3.01E-02	-1.68	11.21	HDAC5;ATF6B;H2AFZ;HIST1H2AK;H3F3A;H2AFX;GRIN2B;PPP1CA;GRIN1;GNAI2;GNG3;GNG7;GNB2;PPP1R1B;CALM3;HIST1H4C;PRKACA;HIST1H4D;HRAS;MAPK3

Table 2.34: Top 10 KEGG pathways from upregulated transcripts in dSPNs following risperidone.

Term	Overlap	P-value	Adjusted P-value	Z-score	Combined Score	Genes
Glutamatergic synapse_Homo sapiens_hsa04724	12/114	4.79E-04	5.69E-02	-1.94	14.82	DLG4;GNG7;GRIK5;ADRBK1;PRKACA;GLUL;SHANK3;SHANK2;GRIN1;SHANK1;GNAI2;MAPK3
Cytokine-cytokine receptor interaction_Homo sapiens_hsa04060	3/265	9.94E-01	9.94E-01	3.49	-0.02	INHBA;ACVR1B;CX3CL1
Measles_Homo sapiens_hsa05162	1/136	9.91E-01	9.94E-01	3.74	-0.03	AKT2
Systemic lupus erythematosus_Homo sapiens_hsa05322	1/135	9.91E-01	9.94E-01	3.77	-0.04	H2AFY2
Olfactory transduction_Homo sapiens_hsa04740	7/415	9.88E-01	9.94E-01	3.24	-0.04	SLC8A3;PDE1C;GNG7;ADRBK1;CALM3;PRKACA;SLC8A2
Herpes simplex infection_Homo sapiens_hsa05168	2/185	9.87E-01	9.94E-01	3.44	-0.04	TRAF3;GTF2IRD1
Pyrimidine metabolism_Homo sapiens_hsa00240	1/105	9.73E-01	9.94E-01	4.16	-0.11	POLR2F
Ubiquitin mediated proteolysis_Homo sapiens_hsa04120	2/137	9.48E-01	9.75E-01	3.52	-0.19	ANAPC13;FBXW11
Chemical carcinogenesis_Homo sapiens_hsa05204	1/82	9.41E-01	9.71E-01	4.80	-0.29	ARNT
MicroRNAs in cancer_Homo sapiens_hsa05206	6/297	9.39E-01	9.71E-01	3.29	-0.21	APC2;SHC1;DNMT3A;DDIT4;FSCN1;HRAS

Table 2.35: Top 10 KEGG pathways from upregulated transcripts in dSPNs following haloperidol.

Term	Overlap	P-value	Adjusted P-value	Z-score	Combined Score	Genes
Glutamatergic synapse_Homo sapiens_hsa04724	3/114	8.40E-03	4.03E-01	-1.94	9.27	SLC1A2;GLUL;SHANK3
Lysine degradation_Homo sapiens_hsa00310	2/52	1.55E-02	4.03E-01	-1.90	7.93	KMT2D;SETD1B
Gastric acid secretion_Homo sapiens_hsa04971	2/74	3.00E-02	4.34E-01	-1.95	6.85	KCNJ10;SLC9A1
Thyroid hormone signaling pathway_Homo sapiens_hsa04919	2/118	6.92E-02	4.34E-01	-1.75	4.69	MED1;SLC9A1
Arginine biosynthesis_Homo sapiens_hsa00220	1/20	7.06E-02	4.34E-01	-1.37	3.62	GLUL
Nitrogen metabolism_Homo sapiens_hsa00910	1/17	6.03E-02	4.34E-01	-1.20	3.37	GLUL
RNA transport_Homo sapiens_hsa03013	2/172	1.30E-01	4.34E-01	-1.65	3.36	EEF1A2;ACIN1
Collecting duct acid secretion_Homo sapiens_hsa04966	1/27	9.41E-02	4.34E-01	-1.35	3.19	ATP6V1A
Proteoglycans in cancer_Homo sapiens_hsa05205	2/203	1.70E-01	4.34E-01	-1.68	2.98	GAB1;SLC9A1
Epstein-Barr virus infection_Homo sapiens_hsa05169	2/202	1.68E-01	4.34E-01	-1.65	2.94	NCOR2;HDAC5

Table 2.36: Top 10 KEGG pathways from upregulated transcripts in iSPNs common across treatments.

Term	Overlap	P-value	Adjusted P-value	Z-score	Combined Score	Genes
Synaptic vesicle cycle_Homo sapiens_hsa04721	2/63	1.97E-03	4.54E-02	-1.71	10.63	ATP6V1A;UNC 13A
Circadian rhythm_Homo sapiens_hsa04710	1/30	3.10E-02	1.86E-01	-1.82	6.30	BHLHE40
Collecting duct acid secretion_Homo sapiens_hsa04966	1/27	2.80E-02	1.86E-01	-1.76	6.30	ATP6V1A
Vibrio cholerae infection_Homo sapiens_hsa05110	1/51	5.22E-02	1.86E-01	-1.84	5.43	ATP6V1A
Legionellosis_Homo sapiens_hsa05134	1/55	5.62E-02	1.86E-01	-1.75	5.04	EEF1A2
Glycolysis / Gluconeogenesis_Homo sapiens_hsa00010	1/67	6.81E-02	1.86E-01	-1.84	4.96	ENO2
Epithelial cell signaling in Helicobacter pylori infection_Homo sapiens_hsa05120	1/68	6.91E-02	1.86E-01	-1.74	4.64	ATP6V1A
RNA degradation_Homo sapiens_hsa03018	1/77	7.78E-02	1.86E-01	-1.61	4.12	ENO2
Biosynthesis of amino acids_Homo sapiens_hsa01230	1/74	7.49E-02	1.86E-01	-1.55	4.01	ENO2
Rheumatoid arthritis_Homo sapiens_hsa05323	1/90	9.04E-02	1.86E-01	-1.49	3.58	ATP6V1A

Table 2.37: Top 10 KEGG pathways from upregulated transcripts in dSPNs common across treatments.

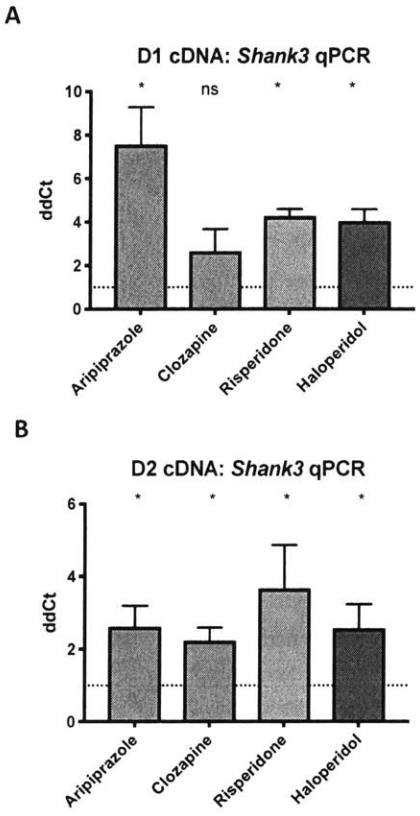

Figure 2.20: Antipsychotic administration increases transcripts of Shank3 in dSPNs and iSPNs. RT-PCR of cDNA from dSPNs (A) and iSPNs (B) of mice treated with aripiprazole, clozapine, risperidone, and haloperidol. Chronic antipsychotic administration increased Shank3 levels in all samples except for dSPNs following clozapine administration. Bars represent mean +/- SEM. * $p<0.05$.

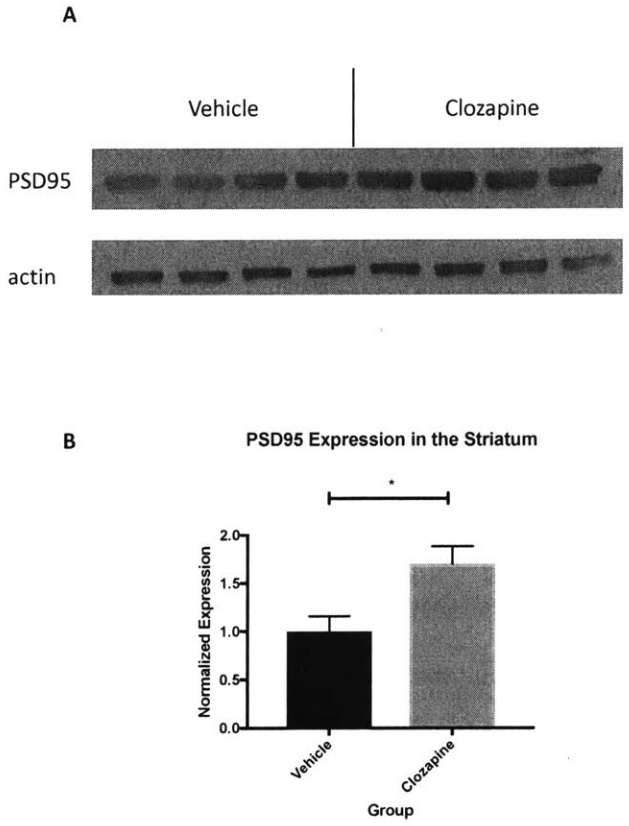

Figure 2.21: Clozapine administration increases PSD95 expression in the striatum. Western blot for PSD95 and actin from total striatum following 6 weeks of clozapine administration (A) and quantitation normalized to actin (B). Bars represent mean +/- SEM. * $p<0.05$.

Materials & Methods

Animal Usage

Animal experiments were approved by the MIT Committee on Animal Care (CAC). Mice were group housed with 2-5 mice per cage on a standard 12h light/12h dark cycle with food and water provided ab libitum. Same sex littermates were randomly assigned to experimental groups. No procedures were performed on any animal prior to experiments described. Male mice 8-16 weeks of age were used for all experiments. C57BL/6J male were used for all non-TRAP experiments. For TRAP experiments, Tg(Drd1a-EGFP/Rpl10a)CP73Htz mice (for dSPN TRAP experiments) and Tg(Drd2-EGFP/Rpl10a)CP101Htz mice (for iSPN TRAP experiments) were used. TRAP lines were bred as previously described (Doyle et al., 2008; Heiman et al., 2008), with the exception that the mice used in this study were backcrossed for at least 10 generations to the C57BL/6J background.

Open Field Test & Thigmotaxis Analysis

Open field test was performed using an IR photobeam open field with 16 IR beams along x, y, and z axes (#MED-OFAS-RSU, Med Associates, St. Albans VT). Experiments were performed in one 60-minute session per mouse.

Prepulse Inhibition Test & Startle Habituation

Prepulse inhibition was performed as previously described (Henderschott et al, 2016). Briefly, mice were placed in sound attenuating chambers and each test session consisted of 72 test trials. Each test trial consisted of equal numbers of the following

types of 40-msec trials in psudorandom order: a test stimulus of 120db; a test stimulus preceded by a 76dB stimulus; a test stimulus preceded by a 86dB stimulus; no stimulus. From these trials, percent of pre-pulse inhibition was calculated as (average response to test stimulus = average response to test stimulus + preceding stimulus) / (average response to test stimulus). Experiments were performed in the SR-Lab Startle Reponse System (San Diego Instruments, Inc, San Diego, California, USA). Startle habituation was calculating using the test stimulus trials alone.

Forced Swim Test

Cylindrical water tanks (30cm high, 20cm diameter) were filled with room-temperature water and a video camera for scoring was set up to view each water tank. The water was filled to 15cm above the bottom of the tanks and a white noise generator kept noise levels equal across tests. Each animal was dosed with either vehicle or clozapine and after either 30 minutes or 24 hours was slowly placed into the water, held by its tail and with the head never being submerged. The test was then run for 6 minutes/mouse, with the mouse removed from the test if any diving occurred. Scoring of immobility was performed with the scorer blinded to the identity of the injection.

Measurement of Clozapine Levels

30g of mouse striatum was added to 4 volumes of acetonitrile buffer (80:20(v:v) water:acetonitrile) followed by homogenization with a handheld probe. Research Grade Assay-1 liquid chromatography-mass spectrometry was performed on these samples by Agilux Labs (Charles River Laboratories, Wilmington, MA).

Immunofluorescence & Confocal Imaging

Mice were transcardially perfused and their tissue was processed and stained for immunofluorescence as described in Heiman et al, 2008. The following primary antibodies were used for experiments: Necab1 (PA5-54849, 5ug/mL, Thermo Fisher Scientific, Waltham, MA); GFP (ab13970, 1:1000, Abcam, Cambridge, MA). A Zeiss 700 confocal microscope was used to image slides using z-stacks.

Drug Administration

For chronic experiments, mice were injected with APD intraperitoneally from the ages of 8-14 weeks once per morning, seven days per week, for a total of 6 weeks of dosing. Aripiprazole dosing started at 0.074 mg/kg for 2 weeks and was then regularly increased for 7 days to a final dose of 0.294 mg/kg. Clozapine dosing started at 0.184 mg/kg and was then regularly increased for 16 days to a final dose of 2.0 mg/kg. Haloperidol dosing started at 0.074 mg/kg and was then regularly increased for 6 days to a final dose of 0.221 mg/kg. Risperidone dosing started at 0.015 mg/kg and was then regularly increased for 6 days to a final dose of 0.074 mg/kg. Drugs were highest purity non-pharmaceutical-grade available (Sigma-Aldrich, St. Louis MO), dissolved in cell-culture-grade dimethyl sulfoxide (Sigma-Aldrich, St. Louis MO), and stored in single-use aliquots at -20 °C. Drugs were diluted on the morning of use to final concentration in 0.1M sodium phosphate buffer [pH 6.2]. Mice were injected intraperitoneally (10 μL volume drug per gram of mouse). For acute experiments, mice were injected with the final dose for each individual antipsychotic for either 1 day or as noted in individual experiments.

mRNA Isolation

TRAP

Tissue harvest occurred 24H post final drug injection and dissections were performed on ice after cooling the head in liquid nitrogen for 4 seconds. Following dissection, cell type-specific mRNAs were purified (Heiman et al., 2014). Briefly, striata were homogenized in an ice-cold lysis buffer (150 mM KCl, 10 mM HEPES [pH 7.4], 5 mM $MgCl_2$, 0. 5mM dithiothreitol, 100 μg/mL cycloheximide, RNAse inhibitors, and protease inhibitors). Samples were then centrifuged at 2,000 x g at 4°C for 10 minutes and the supernatant was removed to a new tube. NP-40 (final concentration 1%) and 1,2-Diheptanoyl-sn-glycero-3-phosphocholine (DHPC, final concentration 30mM) were added and samples were incubated on ice for 5 minutes, followed by centrifugation at 13,000 x g at 4°C for 10 minutes and supernatant removal to a new tube. Streptavidin Dynabeads (Thermo Fisher Scientific, Waltham MA) coated with biotin-linked mouse anti-GFP antibodies were then added; the samples were incubated overnight at 4°C with end-over-end rotation (anti-GFP 19C8 antibody: RRID:AB_2716737; anti-GFP 19F7 antibody: RRID:AB2716736). Beads were collected on a magnetic rack and washed three times with wash buffer (350 mM KCl, 10 mM HEPES [pH 7.4], 5 mM $MgCl_2$, 0.5 mM dithiothreitol, 100 μg/mL cycloheximide, 1% NP-40). RNA was purified using the Absolutely RNA Isolation Nanoprep kit (Agilent Technologies, Satan Clara CA), and to ensure quality and accurate quantitation, purified RNA was run on a Bioanalyzer using the RNA 6000 Pico Kit (Agilent Technologies, Satan Clara CA).

RNA Sequencing and Analysis

Ovation RNA-Seq System v2 kit (NuGEN Technologies, San Carlos CA) was used to prepare samples for RNA-seq. Library quality was assessed using an Advanced Analytical-fragment Analyzer (Advanced Analytical, Ankeny IA) before mixing for sequencing on Illumina HiSeq 2000 (Illumina, San Diego CA) platform at the MIT BioMicro Center. Paired-end Illumina HiSeq 2000 75-bp reads were collected and Fastq data were aligned to the mouse reference genome assembly (mm9) using the STAR 2.4.0 RNA-Seq aligner (Dobin et al., 2013). The aligned bam files (sorted by the coordinates) were subsequently processed by Cuffquant module of Cufflinks 2.0.0 to quantify gene expression using UCSC mm9 for gene annotation. Differential analysis between two individual groups was performed using Cuffdiff module of Cufflinks with the geometric method for library normalization, with differentially expressed genes defined as genes with FDR adjusted p-value < 0.05. Enrichr was used to process differentially expressed genes for GO and pathway analyses (Chen et al., 2013; Kuleshov et al., 2016). The Morpheus software (The Broad Institute, https://software.broadinstitute.org/morpheus) was used to generate heat maps of changes in pathways and genes.

Chapter 3: Chronic Clozapine Induces Synaptic Changes Associated With Increased Glutamatergic Function

Background

The glutamate hypothesis of schizophrenia points to glutamatergic signaling as a major alteration in schizophrenia pathophysiology. This hypothesis originated from the findings that NMDA receptor antagonists, such as PCP and ketamine, can induce schizophrenia-like symptoms in people without schizophrenia, and that these drugs given to schizophrenia patients make their symptoms worse (Javitt & Zukin, 1991; Lahti et al, 1995; Malhotra et al, 1997). Functional glutamatergic synaptic alterations have been previously described in schizophrenia pathophysiology. It is known that patients with schizophrenia exhibit reduced spine size in the caudate and putamen as well as in the cortex (Roberts et al, 1996; Glausier & Lewis, 2013). More recently, genetic studies have consistently pinpointed glutamatergic signaling genes as associated with risk of schizophrenia (Harrison & Weinberger, 2005; Fromer et al, 2014; Schizophrenia Working Group of the Psychiatric Genomics Consortium, 2014). Glutamatergic function abnormalities have also been reported in mutant mice in schizophrenia-associated genes. For example, a Shank3-mutant mouse which has schizophrenia behavioral endophenotypes also displays cortical synaptic defects (Zhou et al, 2016) Neuregulin 1 and ErbB4 knock-out mice have reduced hippocampal spine density and decreased forebrain NMDA receptors (Harrison and Law, 2006a; Mei and Xiong, 2008). Together, these studies point to impaired glutamatergic synaptic function as a hallmark of schizophrenia pathophysiology.

Glutamatergic functional alterations have also been described in studies of antipsychotic effects on mouse neurons *in vitro* and in mouse models of schizophrenia. However, the findings of these studies appear to depend significantly upon the conditions of the experiment and the cell type studied. For example, length of treatment seems to matter. Acute haloperidol administration, unlike chronic treatment, does not induce new synapses following IP administration (Meshul & Casey, 1989). The experimental system used also shapes response to antipsychotics; haloperidol has been shown to increase synapse numbers in rats following IP administration, but decrease synapse numbers in rat neurons *in vitro* (Kerns et al, 1992; Park et al, 2013). When looking across brain regions, results vary further: haloperidol induces LTP in rats at corticostriatal synapses, but blocks spike timing-dependent LTP in the prefrontal cortex (Meshul & Casey, 1989; Centonze et al, 2004; Delotterie et al, 2010; Xu & Yao, 2010). Even within the SPN cell type in the striatum, 2 weeks of haloperidol administration can increase or decrease synaptic strength of corticostriatal synapses depending on whether those synapses are on dSPNs or iSPNs (Sebel et al, 2017).

These mixed results suggest that cellular responses to antipsychotics depend significantly on length of drug treatment, whether drugs are given in an *in vivo* context, and specific cellular identity in relation to broader circuitry connectivity. Taken together, they do tell us that antipsychotic administration can dramatically affect synaptic functioning. We therefore chose a specific context for our experiments investigating glutamatergic function following clozapine treatment. We chose to study glutamatergic synaptic function following chronic administration, due to its greater clinical relevance as patients continue to take antipsychotics for months to years of their lives. We chose to

study the effects of clozapine due to its remarkably high clinical efficacy. We performed whole-cell recordings specifically from SPNs of the nucleus accumbens because these cells have high expression of dopamine receptors and the nucleus accumbens is key for motivational behaviors linked to schizophrenia pathophysiology. We further peformed cell type specific recordings to test differences between dSPNs and iSPNs because our molecular profiling suggested that clozapine may have a biased effect towards iSPN changes translationally.

To better understand glutamatergic signaling following chronic clozapine administration, we systematically examined the basic properties of glutamatergic synaptic function in SPNs. To pinpoint the specific cell types and circuits altered, we studied both the dorsal and ventral striatum because these regions play different functional roles, with the dorsal striatum responsible for motor behaviors and the ventral striatum involved in motivation and reward (Cardinal et al, 2002; Balleine et al, 2007; Kreitzer & Malenka, 2008).

To better understand differences between acute and chronic clozapine administration, we studied SPN glutamatergic function following 1 week and 6 weeks of treatment. Additionally, to understand whether the chronic effects of clozapine administration were long-lasting, we looked at glutamatergic function following 6 weeks of treatment and 1 week of withdrawal from clozapine.

Results

1. Chronic clozapine administration does not alter paired pulse ratio or AMPA/NMDA ratio

We first looked at the paired pulse ratio in SPNs, which depends on presynaptic release probability. We did not observe any change to paired pulse ratio following chronic clozapine treatment, which suggests that antipsychotics did not significantly influence the presynaptic release probability of glutamatergic synaptic input to SPNs (Figure 3.1 A).

We then characterized the ratio of AMPAR- and NMDAR-mediated synaptic current (AMPA/NMDA ratio). We did not observe changes in AMPA/NMDA ratio, suggesting that following 6 weeks of clozapine treatment, relative contribution of AMPAR and NMDAR to synaptic transmission are not altered (Figure 3.1 B).

2. Chronic clozapine treatment leads to the presence of calcium-permeable AMPA receptors (CP-AMPARs)

AMPARs are calcium permeable during development and periods of extensive pruning and are associated with increased synaptic plasticity (Isaac et al, 2007; Wiltgen et al, 2010; Man, 2011). In general, AMPARs in adult mice are not calcium permeable as this period of development passes and the AMPAR subunit Gria2 is edited to make the receptor impermeable to calcium (Sommer et al, 1991; Pachernegg et al, 2015). However, under some pathological conditions, including withdrawal from cocaine, CP-AMPARs are inserted into synaptic membranes and render synapses calcium permeable (Ferrario et al., 2011; Lee et al., 2013; McCutcheon et al., 2011). Calcium-permeable AMPARs

display rectification at depolarizing voltages because intracellular polyamines such as spermine can enter calcium-permeable AMPARs and block the channel pore at depolarizing voltages (Bowie & Mayer, 1995; Donevan & Rogawski, 1995).

AMPAR mediated synaptic current from chronically clozapine-treated mice (6 weeks) displayed significant rectification (Figure 3.2 A) which was quantified an increase in rectification index (Figure 3.2 B), suggesting prevalence of CP-AMPAR after chronic clozapine treatment. Recordings from acutely clozapine-treated mice (1 week) did not display rectification, suggesting that chronic treatment is necessary for the synaptic incorporation of CP-AMPARs (Figure 3.2 C). Importantly, we did not see any change to rectification in the dorsal striatum, a region associated with motor side effects rather than reward and motivation (Figure 3.2 D). This suggests that the changes we are observing are likely to be region-specific.

The presence of CP-AMPARs could be explained by the presence of AMPARs lacking GluA2 subunits entirely or by AMPARs containing GluA2 subunits with an absence of RNA editing at the Q/R site, which renders them calcium permeable. Our TRAP data did not indicate altered levels of Gria2 transcripts in dSPNs (Figure 3.3 A) or iSPNs (Figure 3.3 B) across all four treatments. Aside from absolute levels of Gria2, it is also possible to explain CP-AMPARs through changes in editing status (Mishina et al, 1991; Swanson et al, 1997). We therefore quantified the amount of editing presence in Gria2 and found no difference between vehicle- and clozapine-treated samples in either dSPNs (Figure 3.3 C) or iSPNs (Figure 3.3 D).

3. Increased glutamatergic function in SPNs following chronic clozapine administration

The appearance of CP-AMPARs suggested alteration of glutamatergic synaptic function, potentially through incorporation at existing synapses or new synapses. We therefore recorded miniature EPSCs (mEPSCs) from the nucleus accumbens, which allowed us to quantify the frequency and amplitude of quantal release at the synapse, indicating changes in synapse number and synapse size respectively. Given the lack of significant change in paired pulse ratio, indicating unaltered presynaptic function of the glutamatergic synaptic inputs on SPNs (Figure 3.1 A), comparisons of mEPSC frequency can be used to estimate the relative numbers of AMPAR-transmitting synapses in different conditions. Following chronic clozapine treatment, we recorded an increased mEPSC frequency (Figure 3.4 A) but no change in mEPSC amplitude (Figure 3.4 B), suggesting that chronic clozapine administration leads to the generation of additional AMPAR-transmitting synapses but not the increased quantal size of existing synapses. Because we had observed the presence of rectification, we recorded mEPSCs in the presence of NASPM, a CP-AMPAR selective blocker (Koike et al, 1997). We found that the increase in mEPSC frequency induced by chronic clozapine administration is reversed in the presence of NASPM (Figure 3.4 A). This finding, in combination with the presence of rectification in SPNs, suggests that clozapine drives the creation of new, CP-AMPAR-containing, synapses.

Because our functional analysis predicts increased numbers of AMPAR transmitting synapses, we performed synaptic puncta staining for postsynaptic protein PSD-95 and counted puncta. We found a trend towards an increase in synaptic puncta in the nucleus

accumbens following clozapine treatment, in line with the functional predictions (Figure 3.4 C)

4. Clozapine preferentially increases mEPSC frequency in iSPNs

Our molecular profiling data indicated a cell type specific bias in clozapine's translational effects, with increased glutamatergic synapse components biased towards changes in iSPNs. We therefore recorded mEPSCs in a cell type-specific way to investigate whether the increased mEPSC frequency was biased towards iSPNs. We recorded mEPSCs from ventral striatum (nucleus accumbens) of Tg(Drd2-EGFP)S118Gsat mice, which allowed us to perform cell type-specific analysis by categorizing GFP-positive cells as iSPNs and GFP-negative cells as likely dSPNs. We found that chronic clozapine treatment increased mEPSC frequency significantly in iSPNs and not in dSPNs (Figure 3.5 A). Consistent with our non-cell-type-specific recordings, we found no change in mEPSC amplitude following chronic clozapine treatment in either dSPNs or iSPNs (Figure 3.5 B). These findings are consistent with our molecular profiling experiments and demonstrate an iSPN-biased glutamatergic synaptic inputs caused by chronic clozapine treatment.

5. Following withdrawal, clozapine-treated mice do not continue to display altered mEPSCs or prepulse inhibition

Many patients are able to cease their antipsychotic treatment without relapse (Lehman et al, 2010; Hasan et al, 2013). Furthermore, decreases in asymmetric synaptic density in the striatum of rats on long-term haloperidol treatment partially remain up to 4

weeks following withdrawal from drugs (Roberts et al, 1995) There are also long-lasting effects of drugs that act at dopamine receptors following withdrawal (Ferrario et al, 2011; Graziane et al, 2016). We saw increases in CP-AMPAR containing synapses only after chronic treatment, and it is not known whether chronic antipsychotic treatment may lead to long-lasting cellular effects. We hypothesized that our observed changes may be long-lasting and persist past treatment cessation. We tested this hypothesis by recording miniEPSCs after withdrawal from clozapine.

We recorded from the nucleus accumbens following 6 weeks of clozapine administration and 1 week of withdrawal. These data did not show a significant increase in mEPSC frequency following clozapine treatment and withdrawal, but they did show a significant decrease in mEPSC frequency following NASPM treatment, which suggests the continued presence of some CP-AMPARs following 6 weeks of clozapine treatment and 1 week of withdrawal (Figure 3.6 C). Altogether, these data provide some evidence that there is a lasting cellular effect of chronic clozapine treatment after 1 week of withdrawal, but that this effect is smaller than that seen immediately following 6 weeks of clozapine chronic administration.

Chapter 3 Summary & Discussion

Summary

Clozapine administration leads to an increase of CP-AMPAR containing synapses specifically in the ventral striatum, not the dorsal striatum, and following chronic, not acute, administration. This increase in CP-AMPAR containing synapses is biased towards iSPNs over dSPNs.

Chronic clozapine administration does not significantly change paired pulse ratio in the nucleus accumbens, suggesting unchanged presynaptic release probability at the glutamatergic synaptic inputs to the nucleus accumbens. In the same conditions, AMPA/NMDA ratio remains unchanged, suggesting relative contribution of AMPAR and NMDAR to synaptic transmission remains unaffected. The increase in CP-AMPAR containing synapses preferentially in iSPNs may shift the direct (dSPN) vs. indirect (iSPN) pathway balance, which through broader basal ganglia circuitry controls excitatory innervation into the striatum.

Mechanisms of CP-AMPAR Incorporation at the Synapse

Our TRAP profiling data from dSPNs and iSPNs did not find that Gria2 was present in its unedited, calcium-permeable form, or that Gria2 transcript levels were decreased. Beyond these mechanisms, it is possible that alterations in post-translational regulation of GluA2, such as phosphorylation alterations that lead to altered trafficking to the synaptic membrane, may explain the presence of CP-AMPARs (Ju et al, 2004; Grooms et al, 2006; Ferrario et al, 2011). Expression of AMPARs on synaptic surfaces is carefully

controlled by posttranslational mechanisms, including dendritic transport, receptor recycling, and exocytosis and endocytosis of AMPARs (Widagdo et al, 2017). GluA2 itself contains residues that can be palmitoylated and phosphorylated to alter rates of AMPAR trafficking (Lu & Roche, 2012). Future studies could perform quantitative immunofluorescence or Western blot for phosphorylation of GluA2 residues to assess whether GluA2 is alternatively phosphorylated following chronic clozapine administration.

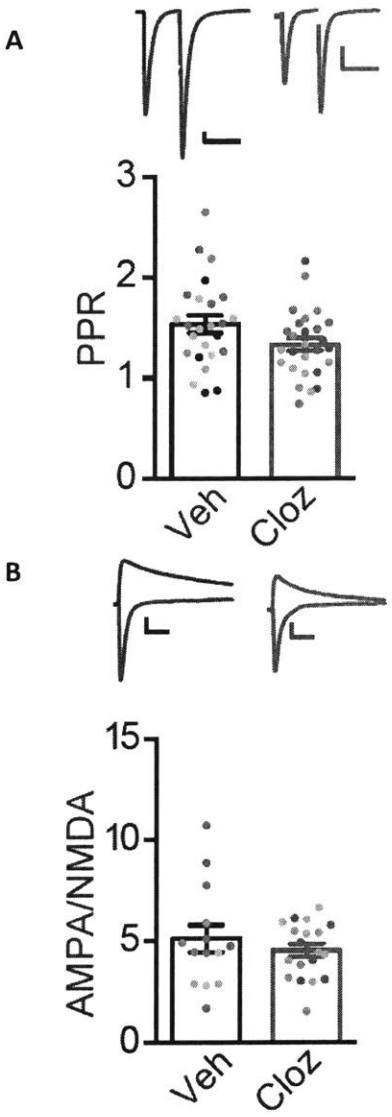

Figure 3.1: Chronic clozapine administration does not change paired pulse ratio or rectification index in the dorsal striatum. Whole cell recordings of ventrial striatum SPNs following vehicle and clozapine treatment. Paired pulse ratios (A) and current voltage relationships of AMPAR EPSCs in presence of AP5 (B). Bars represent mean +/- SEM.

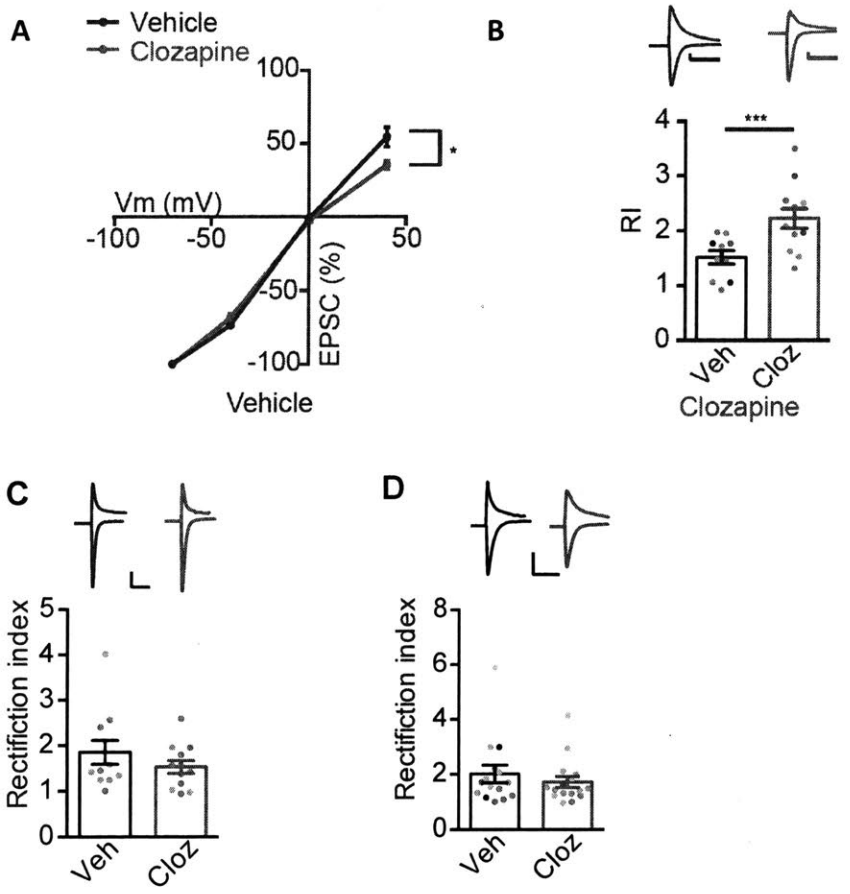

Figure 3.2 Clozapine induces rectification in nucleus accumbens core following chronic treatment. Whole cell recordings of ventral striatum SPNs following 6 weeks of vehicle and clozapine treatment, recording the current voltage relationships of AMPAR EPSCs in presence of AP5 (A) and quantification of rectification index, peak current at -40mV/peak current at +40mV (B). Rectification index was also calculated following chronic clozapine treatment in the dorsal striatum (C) and 1 week of clozapine treatment in the ventral striatum (D). Bars represent mean +/- SEM. * $p<0.05$, *** $p<0.001$.

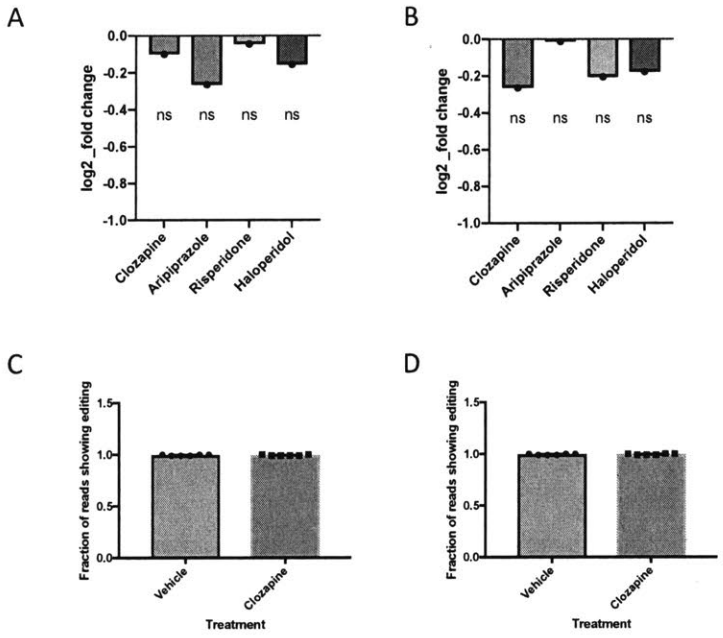

Figure 3.3: No evidence of decreased Gria2 translation or absence of Gria2 editing in SPN transcripts following chronic clozapine administration. Translation of Gria2 in dSPNs (A) and iSPNs (B) in each treatment condition compared to vehicle treatment. Fraction of RNA-seq reads indicating Gria2 Q/R site editing in dSPNs (C) and iSPNs (D) in the vehicle and clozapine conditions.

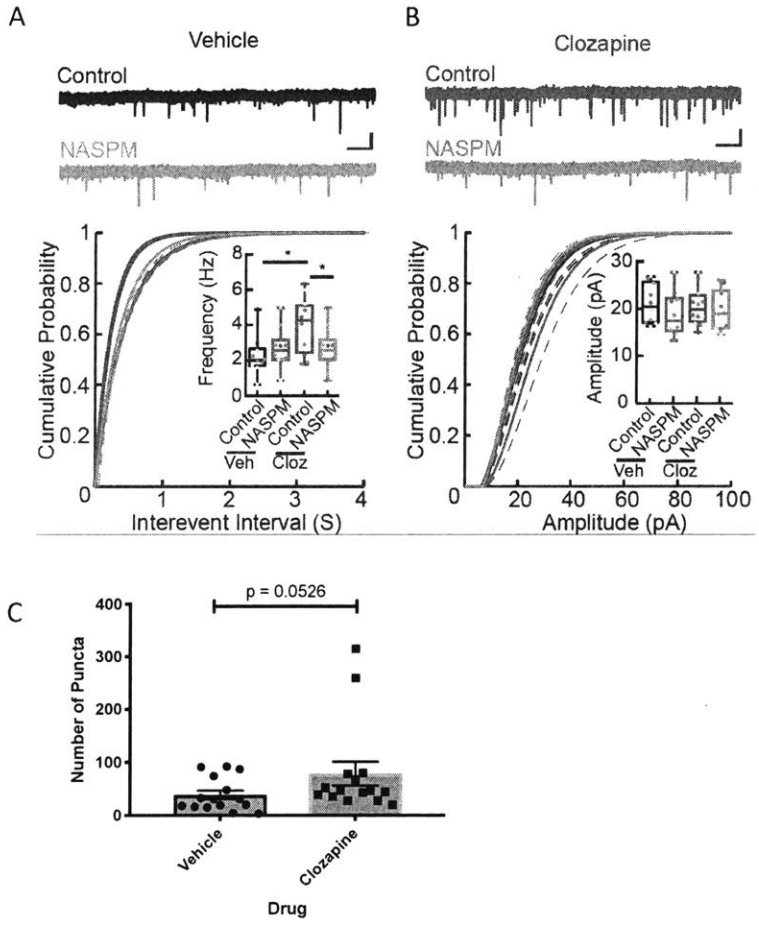

Figure 3.4: Clozapine administration increases mEPSC frequency and synaptic puncta. Whole cell recordings of ventrial striatum SPNs following vehicle and clozapine treatment. Cumulative probability plots for AMPAR mEPSC recordings and quantification of interevent intervals and mEPSC amplitudes (A). Synaptic puncta counts from ventral striatum (B). Bars represent mean +/- SEM. * $p<0.05$

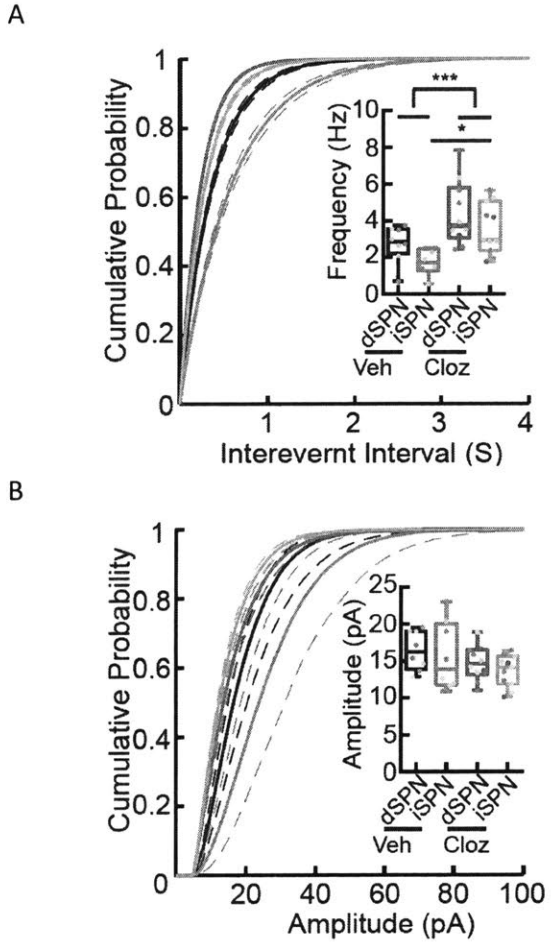

Figure 3.5: Clozapine administration leads to an increase in mEPSC frequency in iSPNs. Whole cell recordings of ventrial striatum SPNs following vehicle and clozapine treatment. Cumulative probability plots for AMPAR mEPSC recordings and quantification of interevent intervals and mEPSC amplitudes. Bars represent mean +/- SEM. * $p<0.05$ *** $p<0.001$

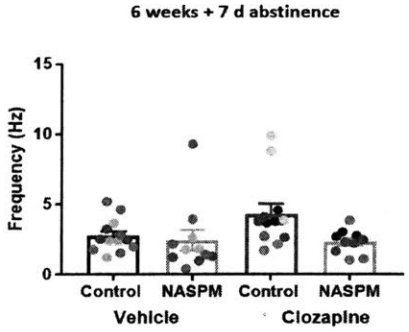

Figure 3.6: Increase in mEPSC frequency does not persist following 1 week of withdrawal. Whole cell recordings of ventrial striatum SPNs following vehicle and clozapine treatment and quantification of interevent intervals. Bars represent mean +/- SEM. * $p<0.05$ mEPSC amplitudes. Bars represent mean +/- SEM. * $p<0.05$ *** $p<0.001$

Materials & Methods

Animal Usage

Animal experiments were approved by the MIT Committee on Animal Care (CAC). Mice were group housed with 2-5 mice per cage on a standard 12h light/12h dark cycle with food and water provided ab libitum. Same sex littermates were randomly assigned to experimental groups. No procedures were performed on any animal prior to experiments described. Male mice 8-16 weeks of age were used for all experiments. C57BL/6J male were used for all non-TRAP and non-cell-type-specific experiments. For TRAP experiments, Tg(Drd1a-EGFP/Rpl10a)CP73Htz mice (for dSPN TRAP experiments) and Tg(Drd2-EGFP/Rpl10a)CP101Htz mice (for iSPN TRAP experiments) were used. TRAP lines were bred as previously described (Doyle et al., 2008; Heiman et al., 2008), with the exception that the mice used in this study were backcrossed for at least 10 generations to the C57BL/6J background. For cell-type-specific physiology studies, Tg(Drd2-EGFP)S118Gsat mice were used.

Drug Administration

For chronic experiments, mice were injected with APD intraperitoneally from the ages of 8-14 weeks once per morning, seven days per week, for a total of 6 weeks of dosing. Aripiprazole dosing started at 0.074 mg/kg for 2 weeks and was then regularly increased for 7 days to a final dose of 0.294 mg/kg. Clozapine dosing started at 0.184 mg/kg and was then regularly increased for 16 days to a final dose of 2.0 mg/kg. Haloperidol dosing started at 0.074 mg/kg and was then regularly increased for 6 days to a final dose of 0.221 mg/kg. Risperidone dosing started at 0.015 mg/kg and was then regularly increased

for 6 days to a final dose of 0.074 mg/kg. Drugs were highest purity non-pharmaceutical-grade available (Sigma-Aldrich, St. Louis MO), dissolved in cell-culture-grade dimethyl sulfoxide (Sigma-Aldrich, St. Louis MO), and stored in single-use aliquots at -20 °C. Drugs were diluted on the morning of use to final concentration in 0.1M sodium phosphate buffer [pH 6.2]. Mice were injected intraperitoneally (10 μL volume drug per gram of mouse). For acute experiments, mice were injected with the final dose for each individual antipsychotic for either 1 day or as noted in individual experiments.

Indirect Immunofluorescence

Mice were transcardially perfused and their tissue was processed and stained for immunofluorescence as described in Heiman et al, 2008. The following primary antibodies were used for experiments: PSD95 (ab18258, 1ug/mL, Abcam, Cambridge, MA); Vglut1 (AB5905, 1:5000, Millipore, Burlington, MA). A Zeiss 700 confocal microscope was used to image slides using z-stacks.

Prepulse Inhibition test

Prepulse inhibition was performed as previously described (Henderschott et al, 2016). Briefly, mice were placed in sound attenuating chambers and each test session consisted of 72 test trials. Each test trial consisted of equal numbers of the following types of 40-msec trials in psudorandom order: a test stimulus of 120db; a test stimulus preceded by a 76dB stimulus; a test stimulus preceded by a 86dB stimulus; no stimulus. From these trials, percent of pre-pulse inhibition was calculated as (average response to test stimulus = average response to test stimulus + preceding stimulus) / (average

response to test stimulus). Experiments wer performed in the SR-Lab Startle Reponse System (San Diego Instruments, Inc, San Diego, California, USA).

Electrophysiology

16 week old male mice were used for recording experiments. Ventral striatum/nucleus accumbens core parasagittal slices (250 um) were prepared, and recordings were performed 24H after the final IP injection, except in cases of withdrawal recordings, which were performed 1 week after the final IP injection. Recordings were set up according to previous protocols (Grueter et al, 2010; Han et al, 2017); in brief: mice were euthanized with isofluorane and their brains were placed in ice cold dissecting solution (2.5mM KCl, 1.0mM NaH_2PO_4, 26mM $NaHCO_3$, 30mM D-glucose, 119mM Choline chloride, 1mM $CaCl_2$, 7mM $MgCl_2$). Slices were cut with a vibratome and transferred to a 30-32°C recovery solution for 10-15 minutes (2.5mM KCl, 20mM HEPES, 1.2mM NaH_2PO_4, 25mM glucose, 93mM N-methyl-D-glutamine, 30mM $NaHCO_3$, 5mM sodium ascorbate, 3mM sodium pyruvate, 10mM $MgCl_2$, 0.5 $CaCl_2$). Slices were then transferred to a holding chamber with artificial cerebrospinal fluid for 60 minutes to recover (119mM NaCl, 2.5mM KCl, 1.3mM $MgCl_2$, 1.0mM NaH_2PO_4, 2.5mM $CaCl_2$, 26.2mM $NaHCO_3$, 11mM D-glucose). Slices were then placed in the recording chamber and perfused with oxygenated artificial cerebrospinal fluid (2mL/minute) at 30 ± 2 °C.

Recordings were performed in the presence of 50uM picrotoxin to block $GABA_A$ receptor mediated inhibitory synaptic currents. Recordings were performed from SPNs in either the nucleus accumbens core or the dorsal striatum. Electrodes were filled with

120mM $CsMeSO_3$, 15mM CsCl, 8mM NaCl, 10mM HEPES, 0.2mM EGTA, 10mM TEACl, 4mM Mg_2ATP, 0.3mM Na_2GTP, 0.1mM Spermine, 5mM QX-314 Bromide. A bipolar theta glass electrode was used to stimulate excitatory afferents at the border of the nucleus accumbens core and the cortex positioned above the anterior commssure. The Multiclamp 700B (Axon Instruments Molecular Devices, San Jose CA) was used to perform recordings and was filtered at 4kHz digitized at 20kHz using an ITC-18 computer interface (Heka Instruments, Pfalz Germany). Data analysis was performed using the Igor Pro Software (Wavemetrics, Lake Oswego OR).

EPSCs: cells were clamped at -70mV and EPSCs were evoked at a frequency of 0.1Hz. Cells with >25% change in input resistance and/or access resistance were excluded from EPSC analysis.

PPR: two stimuli, 50ms apart, of 0.1Hz were applied. PPR was calculated as EPSC2/EPSC1, and PPR across 20 consecutive responses was averaged. The PPR of 20

AMPA/NMDA ratios: ratios were calculated as the ratio of the peak amplitude of AMPAR EPSCs (EPSCs at -70mV in the presence of 50uM APV) to the peak amplitude of NMDAR EPSCs (EPSCs at +40 mV, 50 ms following afferent stimulation). Rectification index is plotted as the ratio of peak current at -40mV/ peak current at +40mV in presence of 50 μM APV.

mEPSCs: data were collected at a holding potential of -70mV in presence of 0.5 μM TTX. To block rectifying AMPA receptors, 150 μM NASPM trihydrochloride was added. mEPSC data were fitted with a model-based analysis method (Liu et al., 2014; Phillips et al., 2011).

For all electrophysiology experiments, data acquisition and analysis were performed blinded to the *in vivo* treatment.

Chapter 4: Non-neuronal Cell Types Exhibit Translational Alterations Following Chronic Clozapine Treatment

Background

Multiple groups have reported dopamine receptor expression in diverse cell types including interneurons, astrocytes and cells of the choroid plexus (Zanassi et al, 1999; Mignini et al, 2000; Alcantara et al, 2003). Therefore, we can identify mRNAs likely originating from other cell types in SPN TRAP datasets. We analyzed our molecular profiling dataset to identify potential cellular effects that antipsychotics were having on non-neuronal cell types. This was of particular interest to us because recent work has demonstrated important roles for non-neuronal cell types in the development of schizophrenia, most recently in the case of aberrant microglia-mediated synaptic pruning (Sekar et al, 2016). Astrocytes have been specifically implicated in schizophrenia as well; their numbers and morphology have been shown to be altered in schizophrenia, and it is thought that hypoactive astrocytes may in part underlie NMDA hypofunction that gives rise to schizophrenia pathophysiology (Seifert et al, 2006; Halassa et al, 2007).

Because astrocytes express dopamine receptors and are important for glutamatergic synapse function, we were particularly interested in profiling astrocytes following clozapine administration. Due to evidence that astrocytes display differing transcriptional profiles across brain regions, we were interested in performing this profiling in both the striatum and the cortex to determine whether astrocytes responded differentially to antipsychotic administration depending on their brain region of residence. We predicted that, following chronic clozapine administration, striatal

astrocytes would display a translational profile reflective of increased glutamatergic drive.

Results

1. Non-neuronal genes are present in iSPN TRAP database

Genes associated with non-neuronal cell types were detected in our TRAP dataset. Two choroid plexus-associated genes, *Enpp2* and *Ttr*, were detected. *Enpp2* translation was decreased in both dSPNs (Figure 4.1 A) and iSPNs (Figure 4.1 B) following all treatments, and *Ttr* was decreased to an even greater degree following all four antipsychotic treatments in both dSPNs (Figure 4.1 C) and iSPNs (Figure 4.1 D). This was interesting to us because the choroid plexus, and *Ttr* in particular, is involved in secretion of compounds crucial for neuronal function and synaptic plasticity, such as retinoic acid (Das et al, 2013; Lun et al, 2015). Preliminary staining confirmed both Enpp2 (Figure 4.1 E) and Ttr (Figure 4.1 F) protein expression changes in the choroid plexus. These data provide an interesting additional route by which antipsychotics may be exerting their effects.

Additionally, we noticed several genes associated with astroglial function coming through our dataset as significantly altered (Figure 4.2). These included a gene involved in glutamatergic function, *Slc1a2*. Because astrocytes play a key role at glutamatergic synapses, alterations in astrocytic function could have major implications for neuronal function in the striatum following antipsychotic treatment (Araque et al, 1999). We were therefore interested in following up on these results more directly by using a mouse line targeting astrocytes, the JD130-L10a BAC transgenic line (Heintz, 2004; Cahoy et al, 2008; Clarke et al, 2018).

2. Profiling astroglial mRNAs following clozapine administration

To more fully characterize astrocyte responses to clozapine administration, we harvested mRNAs following chronic drug administration and performed RNA-seq. We sequenced both cortical and striatal samples to investigate whether responses to clozapine were region-specific. We were particularly interested in this comparison because recent studies have suggested that astrocytes have varying gene expression programs depending on brain region (Clarke et al, 2018).

We found that striatal astrocytes did indeed express a dramatically different pattern of expression, especially when considering the expression of dopamine receptors, where striatal astrocytes express dopamine at a significantly higher level than cortical astrocytes do (Figure 4.3 A). In line with this observation, upon administration of clozapine, we found many more genes changing in the striatal astrocytes compared to the cortical astrocytes (Figure 4.3 B, Tables 4.1-4.2). Within the striatal astrocyte population, we found that previously-identified markers characteristic of activated astrocytes, such as H2-D1, Psmb8, and Srgn (Clarke et al, 2018) were expressed at lower levels following clozapine treatment (Figure 4.3 C, Tables 4.3-4.4). This was of particular interest given the evidence that reactive astrocytes are associated with removal of synapses; decreased levels of activated astrocytes could promote synaptogenesis and partially explain our molecular changes in SPNs and our physiological data pointing to increased glutamatergic function following clozapine treatment (Liddelow & Barres, 2017; Clarke et al, 2018).

Pathway analysis of these changing genes revealed significant differences between cortical and striatal astrocytes. Genes important for calcium signaling emerged

as the most significantly altered pathway in striatal astrocytes compared to cortical astrocytes (Figure 4.4 A). Genes important for immune activation in the "T cell receptor signaling pathway" were most significantly changed in both striatal (Figure 4.4 B) and cortical (Figure 4.4 C, Tables 4.5-4.6) astrocytes following clozapine, with both magnitude and number of gene expression alterations higher in striatal astrocytes.

Additional analyses of alterations in striatal astrocytes revealed that *Disc1* was significantly upregulated following clozapine treatment (Figure 4.6 A). Analysis of cDNA by qRT-PCR showed a confirmatory trend towards an increase in *Disc1* in clozapine-treated samples (Figure 4.6 B). These findings are particularly interesting because *Disc1* expression in astrocytes has been shown to affect dendrite growth in the hippocampus (Terrillion et al, 2017).

Chapter Summary & Discussion

Summary

Genes expressed the in the choroid plexus are altered following chronic antipsychotic administration, and astrocyte-associated genes are altered following chronic clozapine administration. Astrocytes in particular express high levels of dopamine receptors selectively in the striatum and respond dramatically to antipsychotic administration, while cortical astrocytes do not express dopamine receptor levels to the same degree or respond as broadly as striatal astrocytes do. Altered gene expression profiles in striatal astrocytes following clozapine administration display a profile associated with a reduction in activated astrocytes, which would concord with an astrocytic cell population more permissive of synaptogenesis. Furthermore, clozapine increases expression of *Disc1* in striatal astrocytes, which may also enable these astrocytes to play a pro-synaptogenesis role in the context of antipsychotic treatment.

The Role of Astrocytes in Psychiatric Disorders

Previous studies have implicated microglia in schizophrenia pathophysiology through abnormal C4 mediated synapse elimination (Sekar et al, 2016). Astrocytes have also been implicated in schizophrenia, as their morphology and numbers are altered in patients with schizophrenia and their hypoactivity is thought to potentially partially underlie NMDA hypofunction in schizophrenia (Seifert et al, 2006; Halassa et al, 2007). Furthermore, astrocytes have been shown to express functional dopamine receptors that modulate neuroinflammation (Shao et al, 2013).

Our study also points to astroglia in the striatum as an important glial consideration in antipsychotic mechanisms. We have found that striatal astrocytes express higher levels of dopamine receptors than cortical astrocytes do, which may explain our finding that striatal astrocytes display more translational alterations following chronic clozapine administration than cortical astrocytes do. Furthermore, we find that striatal astrocytes downregulate markers of activated astrocyte and upregulate Disc1; each of these molecular alterations is correlated with synaptogenesis.

One interesting question these data raise is whether the translational alterations we observed in astrocytes following chronic clozapine treatment is due to long-term adaptations in response to synaptic alterations in SPNs or due to direct astrocytic response to D2 antagonism. *In vitro* experiments of signaling cascades in astrocytes following administration of D2 antagonists could help to elucidate whether and how astrocytes respond to D2 receptor binding. It would also be interesting to study astrocytic abnormalities in mouse models of schizophrenia, examining their transcriptional profiles to see if they are associated with reduced glutamatergic synapse function in the striatum.

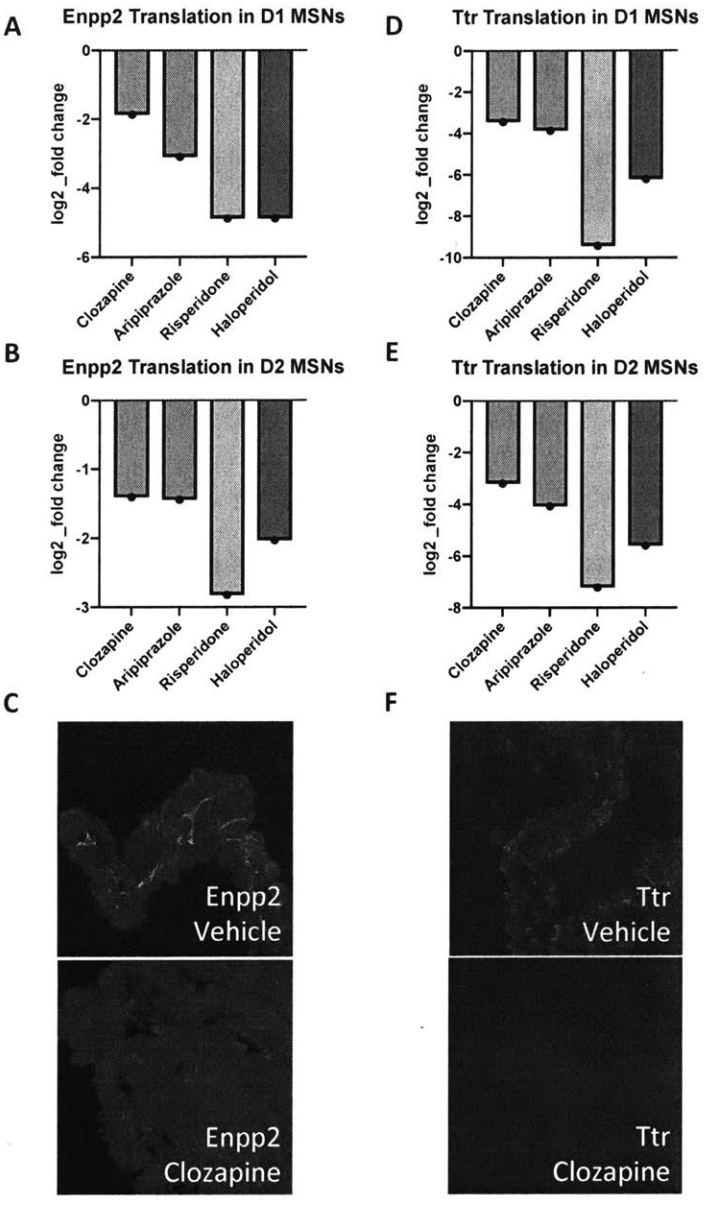

Figure 4.1: Decreased expression of choroid plexus genes *Enpp2* and *Ttr* following antipsychotic administration. Decreases in translation of *Enpp2* (A) and *Ttr* (B). Decreased expression of *Enpp2* (C) and *Ttr* (D). N=6 mice for translational alterations and N=1 mouse for expression alterations.

A

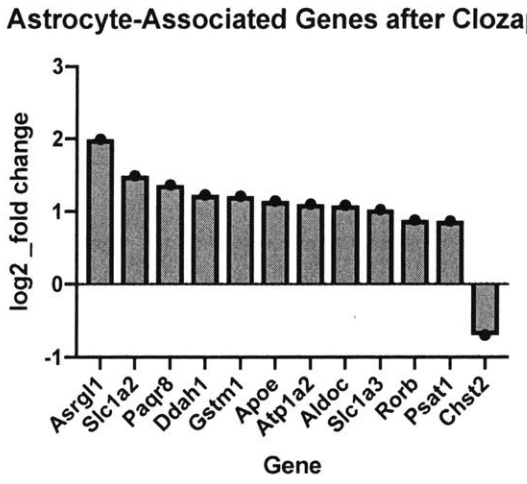

Figure 4.2: Altered expression of astrocyte-associated genes following clozapine administration. Fold change of genes associated with astrocyte expression in D2-TRAP list of genes changing after clozapine administration (A).

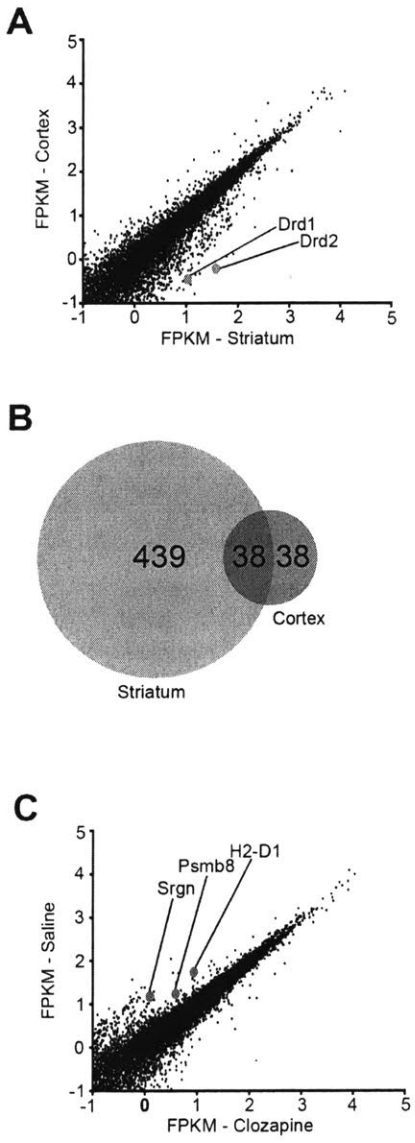

Figure 4.3: Altered translational profiles in astrocytes following clozapine administration. Higher *Drd1a* and *Drd2* expression in striatal astrocytes compared to cortical astrocytes (A) and increased translational alterations of striatal astrocytes compared to cortical astrocytes (B) and downregulation of activated astrocyte-associated genes following clozapine administration (C).

gene	sample_1	sample_2	value_1 (cortex)	value_2 (striatum)	log2 (fold_change) Striatum vs. Cortex	q_value
Slc22a6	Ctx_Veh	Str_Veh	3.77796	0.194517	-4.27964	0.00204632
Spp1	Ctx_Veh	Str_Veh	8.51647	0.816362	-3.38298	0.00204632
Ptgds	Ctx_Veh	Str_Veh	3579.32	388.976	-3.20193	0.00204632
Fmod	Ctx_Veh	Str_Veh	16.0115	2.07289	-2.94939	0.00204632
Slc25a18	Ctx_Veh	Str_Veh	289.017	42.2274	-2.7749	0.00204632
Myoc	Ctx_Veh	Str_Veh	27.3751	4.01026	-2.7711	0.00204632
Slc6a13	Ctx_Veh	Str_Veh	6.32365	0.989526	-2.67595	0.00204632
Kalrn	Ctx_Veh	Str_Veh	1422.34	228.212	-2.63982	0.00204632
Gm11549	Ctx_Veh	Str_Veh	4.38961	0.716409	-2.61524	0.00204632
Aldh1a2	Ctx_Veh	Str_Veh	21.2528	4.19414	-2.3412	0.00204632
Gfra2	Ctx_Veh	Str_Veh	8.81366	1.74433	-2.33707	0.00204632
Rasgrf2	Ctx_Veh	Str_Veh	4.03198	0.814676	-2.30719	0.00204632
Trp53i11	Ctx_Veh	Str_Veh	35.4547	7.38949	-2.26243	0.00204632
Slc17a7	Ctx_Veh	Str_Veh	19.6012	4.32833	-2.17906	0.00204632
Stac2	Ctx_Veh	Str_Veh	10.2665	2.31624	-2.14809	0.00204632
Nrn1	Ctx_Veh	Str_Veh	50.5269	11.4894	-2.13675	0.00204632
Sncb	Ctx_Veh	Str_Veh	12.6551	3.06056	-2.04785	0.00204632
Cck	Ctx_Veh	Str_Veh	100.931	24.7936	-2.02533	0.00204632
Gpd1	Ctx_Veh	Str_Veh	61.4045	15.1956	-2.01469	0.00204632
Iqsec3	Ctx_Veh	Str_Veh	5.79283	1.43778	-2.01042	0.00204632
Olig2	Ctx_Veh	Str_Veh	24.277	6.02917	-2.00956	0.00204632
Pygm	Ctx_Veh	Str_Veh	40.1679	10.5157	-1.9335	0.00204632
Satb2	Ctx_Veh	Str_Veh	6.70731	1.78951	-1.90617	0.00204632
Exph5	Ctx_Veh	Str_Veh	3.27687	0.887348	-1.88475	0.00204632
Shank1	Ctx_Veh	Str_Veh	29.5686	8.1809	-1.85374	0.00204632
Kcng4	Ctx_Veh	Str_Veh	9.26747	2.59275	-1.83769	0.00204632
Ubr3	Ctx_Veh	Str_Veh	503.547	142.393	-1.82225	0.00204632
Pde1a	Ctx_Veh	Str_Veh	23.7964	6.80859	-1.80532	0.00204632
Adcy1	Ctx_Veh	Str_Veh	19.4904	5.62033	-1.79404	0.00204632
Plcxd2	Ctx_Veh	Str_Veh	4.92581	1.44466	-1.76963	0.00204632
Vsnl1	Ctx_Veh	Str_Veh	376.054	111.701	-1.75129	0.00204632
Snhg4	Ctx_Veh	Str_Veh	18.5186	5.54811	-1.7389	0.00204632
Nptx1	Ctx_Veh	Str_Veh	4.62229	1.39102	-1.73246	0.00204632
2610100L16Rik	Ctx_Veh	Str_Veh	58.2517	17.6354	-1.72383	0.00204632
Hcn1	Ctx_Veh	Str_Veh	3.35701	1.03084	-1.70336	0.00204632
Slc22a8	Ctx_Veh	Str_Veh	12.1022	3.72468	-1.70008	0.00204632
Eya1	Ctx_Veh	Str_Veh	48.2465	14.9086	-1.69428	0.00204632
Ranbp3l	Ctx_Veh	Str_Veh	12.7264	3.94191	-1.69085	0.00204632
Ptgs1	Ctx_Veh	Str_Veh	10.5694	3.28561	-1.68566	0.00204632
Elavl4	Ctx_Veh	Str_Veh	7.18637	2.29077	-1.64943	0.00204632

Table 4.1: Top 40 decreased genes in striatal vs. cortical astrocytes.

gene	sample_1	sample_2	value_1 (cortex)	value_2 (striatum)	log2 (fold_change) Striatum vs. Cortex	q_value
Six3os1	Ctx_Veh	Str_Veh	0.162836	14.6892	6.4952	0.00204632
Drd2	Ctx_Veh	Str_Veh	0.606526	37.9249	5.96643	0.00204632
Lrrc10b	Ctx_Veh	Str_Veh	1.16314	60.3392	5.697	0.00204632
Crym	Ctx_Veh	Str_Veh	5.41431	218.375	5.33388	0.00204632
Six3	Ctx_Veh	Str_Veh	0.476327	18.5535	5.2836	0.00204632
Drd1a	Ctx_Veh	Str_Veh	0.349337	10.8497	4.95689	0.00204632
Aqp1	Ctx_Veh	Str_Veh	0.569027	12.2472	4.42781	0.0036931
Gpr88	Ctx_Veh	Str_Veh	0.823927	17.5122	4.4097	0.00204632
Tac1	Ctx_Veh	Str_Veh	0.645219	13.0736	4.34072	0.00204632
Ocln	Ctx_Veh	Str_Veh	0.113935	2.01525	4.14467	0.0036931
Ak7	Ctx_Veh	Str_Veh	0.200107	3.49017	4.12445	0.00204632
Car12	Ctx_Veh	Str_Veh	2.05145	35.6578	4.11951	0.00204632
Slc29a4	Ctx_Veh	Str_Veh	1.21776	20.9472	4.10446	0.00204632
Scube3	Ctx_Veh	Str_Veh	0.199876	3.43606	4.10358	0.0036931
Mrap2	Ctx_Veh	Str_Veh	0.31477	5.23797	4.05664	0.00204632
Rsph4a	Ctx_Veh	Str_Veh	0.772563	12.683	4.0371	0.00204632
Tmem72	Ctx_Veh	Str_Veh	1.28628	19.868	3.94916	0.00204632
Dynlrb2	Ctx_Veh	Str_Veh	1.75411	27.0663	3.94768	0.00204632
Cldn2	Ctx_Veh	Str_Veh	1.53642	23.12	3.9115	0.00204632
Slc4a5	Ctx_Veh	Str_Veh	1.70505	25.3219	3.8925	0.00204632
Nexn	Ctx_Veh	Str_Veh	0.219804	2.97027	3.7563	0.0036931
Scn4b	Ctx_Veh	Str_Veh	1.32457	17.5782	3.73019	0.00204632
Sostdc1	Ctx_Veh	Str_Veh	4.80999	63.5584	3.72397	0.00204632
Lbp	Ctx_Veh	Str_Veh	1.28626	16.9871	3.72319	0.00204632
Sult1c2	Ctx_Veh	Str_Veh	0.565511	7.36392	3.70285	0.00204632
Cdr2	Ctx_Veh	Str_Veh	2.77188	36.0634	3.7016	0.00204632
Abca4	Ctx_Veh	Str_Veh	0.377532	4.70207	3.63862	0.00204632
Ttr	Ctx_Veh	Str_Veh	804.654	9966.65	3.63067	0.00204632
Pde10a	Ctx_Veh	Str_Veh	5.8597	71.5333	3.60972	0.00204632
Paqr5	Ctx_Veh	Str_Veh	0.152095	1.8488	3.60354	0.0036931
Abca8a	Ctx_Veh	Str_Veh	0.263523	3.19391	3.59932	0.00204632
Penk	Ctx_Veh	Str_Veh	6.23683	74.359	3.57562	0.00204632
Kl	Ctx_Veh	Str_Veh	5.62952	65.6124	3.54288	0.00204632
F5	Ctx_Veh	Str_Veh	1.17025	13.6157	3.54039	0.00204632
Arsg	Ctx_Veh	Str_Veh	3.99222	45.5023	3.51068	0.00204632
Kcne2	Ctx_Veh	Str_Veh	2.78622	31.6488	3.50577	0.00204632
Dmrt3	Ctx_Veh	Str_Veh	0.291814	3.28584	3.49314	0.00204632
Sulf1	Ctx_Veh	Str_Veh	1.96684	22.1193	3.49136	0.00204632
Cd59a	Ctx_Veh	Str_Veh	1.82786	20.3019	3.47338	0.00204632
Enpp2	Ctx_Veh	Str_Veh	102.69	1121.27	3.44877	0.00204632

Table 4.2: Top 40 increased genes in striatal vs. cortical astrocytes.

gene	locus	sample_1	sample_2	value_1 (clozapine)	value_2 (vehicle)	log2 (fold_change) Clozapine vs. Vehicle	q_value
Hist1h4d	chr13:23673470-23673838	Str_Clz	Str_Veh	876.059	1611.75	-0.879526	0.00204632
Ubr3	chr2:69735302-69862070	Str_Clz	Str_Veh	68.4532	142.393	-1.05668	0.00204632
H2-K1	chr17:34132956-34137278	Str_Clz	Str_Veh	23.6635	64.1352	-1.43845	0.00204632
Mir6236	chr9:110183790-110183913	Str_Clz	Str_Veh	99537.6	287318	-1.52934	0.00204632
Tmsb4x	chrX:163645025-163647150	Str_Clz	Str_Veh	117.493	357.006	-1.60337	0.00204632
Limd2	chr11:106017569-106021456	Str_Clz	Str_Veh	3.13076	10.3701	-1.72784	0.00204632
Psme2	chr14:56206276-56209938	Str_Clz	Str_Veh	16.9566	75.5024	-2.15467	0.00204632
Psmb8	chr17:34335139-34338399	Str_Clz	Str_Veh	3.84175	17.191	-2.16182	0.00204632
H2-D1	chr17:35400038-35462354	Str_Clz	Str_Veh	8.65955	54.8914	-2.66422	0.00204632
Lcp1	chr14:75530929-75630649	Str_Clz	Str_Veh	1.07772	8.84087	-3.03621	0.00204632
Coro1a	chr7:133843287-133848268	Str_Clz	Str_Veh	3.92517	32.4193	-3.04602	0.00204632
Ms4a6b	chr19:11593048-11604893	Str_Clz	Str_Veh	1.11341	10.3372	-3.21478	0.00204632
Ets1	chr9:32503626-32565405	Str_Clz	Str_Veh	0.525528	6.10511	-3.53818	0.00204632
Laptm5	chr4:130469248-130492063	Str_Clz	Str_Veh	0.943861	11.6663	-3.62763	0.00204632
Il2rg	chrX:98459725-98463545	Str_Clz	Str_Veh	1.24021	19.5325	-3.97722	0.00204632
Ly6a	chr15:74825306-74828461	Str_Clz	Str_Veh	0.377497	6.01561	-3.99417	0.00204632
Il2rb	chr15:78310978-78325496	Str_Clz	Str_Veh	0.70268	11.491	-4.03149	0.00204632
Lck	chr4:129225587-129250885	Str_Clz	Str_Veh	0.716653	12.3748	-4.10998	0.00204632
Ptprc	chr1:139959435-140071882	Str_Clz	Str_Veh	0.381736	6.8884	-4.17352	0.00204632
Rac2	chr15:78389598-78403213	Str_Clz	Str_Veh	0.438187	9.31197	-4.40947	0.00204632
Sell	chr1:165992206-166010916	Str_Clz	Str_Veh	0.617412	13.5364	-4.45446	0.00204632
Rhoh	chr5:66254807-66287939	Str_Clz	Str_Veh	0.0730995	1.62457	-4.47405	0.00204632
Tnfrsf4	chr4:155387803-155390698	Str_Clz	Str_Veh	0.561121	12.7049	-4.50093	0.00204632
Tnfrsf9	chr4:150294263-150320211	Str_Clz	Str_Veh	0.15916	4.21046	-4.72543	0.00204632
Srsf12	chr4:33295965-33320315	Str_Clz	Str_Veh	1.86194	7.91559	-2.08789	0.0036931
Ctla4	chr1:60965868-60972676	Str_Clz	Str_Veh	0.166244	3.62208	-4.44544	0.0036931
Arhgap30	chr1:173319090-173340370	Str_Clz	Str_Veh	0.0658788	1.47084	-4.48068	0.0036931
Il2ra	chr2:11564418-11614821	Str_Clz	Str_Veh	0.132754	3.54635	-4.73951	0.0036931
Ltb	chr17:35331451-35333250	Str_Clz	Str_Veh	0.857776	24.2689	-4.82236	0.0036931
Itgb2	chr10:76993092-77028419	Str_Clz	Str_Veh	0.638521	4.72947	-2.88887	0.00514589
Skap1	chr11:96325904-96620936	Str_Clz	Str_Veh	0.226032	3.0353	-3.74724	0.00514589
Cd6	chr19:10863828-10904548	Str_Clz	Str_Veh	0.258456	4.95028	-4.25952	0.00514589
Selplg	chr5:114267806-114280510	Str_Clz	Str_Veh	0.258393	6.27631	-4.60228	0.00514589
Cd2	chr3:101079830-101091862	Str_Clz	Str_Veh	0.689065	18.9948	-4.78482	0.00514589
Vav1	chr17:57418522-57468659	Str_Clz	Str_Veh	0.159008	1.47352	-3.2121	0.00645759
Cd3d	chr9:44789868-44795135	Str_Clz	Str_Veh	0.469558	8.77115	-4.22339	0.00645759
Pfn1	chr11:70465348-70468152	Str_Clz	Str_Veh	235.573	412.167	-0.807057	0.00775018
Lrrc10b	chr19:10529860-10531937	Str_Clz	Str_Veh	33.1149	60.3392	-0.865616	0.00775018
Ky	chr9:102408467-102448569	Str_Clz	Str_Veh	1.48684	4.46186	-1.58539	0.00775018
Myo1g	chr11:6406550-6420961	Str_Clz	Str_Veh	0.105429	1.94931	-4.20861	0.00775018

Table 4.3: Top 40 decreased genes in striatal astrocytes following clozapine administration.

gene	locus	sample_1	sample_2	value_1 (clozapine)	value_2 (vehicle)	log2 (fold_change) Clozapine vs. Vehicle	q_value
Kcnj10	chr1:174271340-174304216	Str_Clz	Str_Veh	228.736	131.691	0.796527	0.00204632
1700003M07Rik	chr4:129637617-129642382	Str_Clz	Str_Veh	121.024	66.4665	0.864596	0.00204632
Ptms	chr6:124863692-124867964	Str_Clz	Str_Veh	443.223	239.013	0.890945	0.00204632
Rgs8	chr1:155500166-155544795	Str_Clz	Str_Veh	27.7306	14.7978	0.906099	0.00204632
Atf6	chr1:172634587-172797902	Str_Clz	Str_Veh	14.7612	7.86831	0.907686	0.00204632
Cdc42ep4	chr11:113588163-113613129	Str_Clz	Str_Veh	250.97	133.71	0.90841	0.00204632
Fasn	chr11:120667271-120685861	Str_Clz	Str_Veh	39.4546	20.8504	0.920118	0.00204632
Slmo1	chr18:67624502-67640235	Str_Clz	Str_Veh	151.028	79.3585	0.928356	0.00204632
Pdzd8	chr19:59370573-59420270	Str_Clz	Str_Veh	26.3146	13.7314	0.938383	0.00204632
Itpr2	chr6:146056820-146450745	Str_Clz	Str_Veh	6.72226	3.45542	0.960088	0.00204632
Slc25a18	chr6:120723785-120744000	Str_Clz	Str_Veh	83.6082	42.2274	0.985466	0.00204632
Fto	chr8:93837423-94192332	Str_Clz	Str_Veh	63.1004	31.8293	0.987295	0.00204632
Abcb8	chr5:23899973-23915765	Str_Clz	Str_Veh	20.1988	9.93432	1.02378	0.00204632
Clasp1	chr1:120285634-120506039	Str_Clz	Str_Veh	39.4607	19.3959	1.02466	0.00204632
Fmn2	chr1:176431955-176752860	Str_Clz	Str_Veh	42.7607	20.9193	1.03145	0.00204632
Taok2	chr7:134009190-134028481	Str_Clz	Str_Veh	22.4347	10.96	1.03349	0.00204632
Ncan	chr8:72616983-72644743	Str_Clz	Str_Veh	354.842	172.871	1.03748	0.00204632
Cdh20	chr1:106665395-106892058	Str_Clz	Str_Veh	48.6164	23.4421	1.05234	0.00204632
Mllt6	chr11:97524725-97546772	Str_Clz	Str_Veh	27.2389	13.0632	1.06016	0.00204632
Gucy2e	chr11:69031618-69050524	Str_Clz	Str_Veh	38.8095	18.3133	1.08352	0.00204632
Fgfrl1	chr5:109123247-109135969	Str_Clz	Str_Veh	70.5559	33.1775	1.08856	0.00204632
Spock2	chr10:59569004-59596661	Str_Clz	Str_Veh	45.3072	21.1893	1.0964	0.00204632
Abcd1	chrX:70961935-70983626	Str_Clz	Str_Veh	32.5117	14.8165	1.13375	0.00204632
Kazn	chr4:141658304-141795316	Str_Clz	Str_Veh	43.35	19.6527	1.1413	0.00204632
Prr12	chr7:52283076-52308251	Str_Clz	Str_Veh	42.4442	19.0671	1.15449	0.00204632
Slc35f1	chr10:52410306-52831428	Str_Clz	Str_Veh	22.6564	10.1474	1.15882	0.00204632
Adamts1	chr16:85794072-85803360	Str_Clz	Str_Veh	13.6441	5.9882	1.18809	0.00204632
Plec	chr15:76001403-76061808	Str_Clz	Str_Veh	26.7667	11.5666	1.21047	0.00204632
Slc9a1	chr4:132925686-132979613	Str_Clz	Str_Veh	25.4128	10.9721	1.21172	0.00204632
Paqr7	chr4:134052675-134066152	Str_Clz	Str_Veh	37.5581	16.1559	1.21706	0.00204632
Smdt1	chr15:82176475-82179492	Str_Clz	Str_Veh	592.525	254.774	1.21766	0.00204632
Eif4ebp2	chr10:60895244-60915417	Str_Clz	Str_Veh	116.586	49.0979	1.24766	0.00204632
4632415L05Rik	chr3:19794870-19798984	Str_Clz	Str_Veh	23.7116	9.90409	1.25949	0.00204632
Srcin1	chr11:97370653-97436440	Str_Clz	Str_Veh	6.71008	2.77407	1.27433	0.00204632
Gm13375	chr2:20890500-20891975	Str_Clz	Str_Veh	33.3617	13.6268	1.29174	0.00204632
Zfp329	chr7:13389126-13404209	Str_Clz	Str_Veh	18.6869	7.62648	1.29294	0.00204632
Cenpb	chr2:131003024-131005748	Str_Clz	Str_Veh	21.0916	8.49593	1.31183	0.00204632
Tox2	chr2:163051189-163148838	Str_Clz	Str_Veh	24.2412	9.75746	1.31288	0.00204632
Unc13a	chr8:74150611-74195656	Str_Clz	Str_Veh	9.80293	3.87719	1.3382	0.00204632
Taf5l	chr8:126520215-126545209	Str_Clz	Str_Veh	16.0644	6.10968	1.3947	0.00204632

Table 4.4: Top 40 increased genes in striatal astrocytes following clozapine administration.

gene	sample_1	sample_2	value_1 (clozapine)	value_2 (vehicle)	log2 (fold_change) Clozapine vs. Vehicle	q_value
Tmsb4x	Ctx_Clz	Ctx_Veh	150.991	309.061	-1.03343	0.00204632
H2-D1	Ctx_Clz	Ctx_Veh	16.9223	43.2069	-1.35234	0.00204632
Lcp1	Ctx_Clz	Ctx_Veh	1.60813	5.5608	-1.78991	0.00204632
Enpp2	Ctx_Clz	Ctx_Veh	29.2386	102.69	-1.81235	0.00204632
Elovl7	Ctx_Clz	Ctx_Veh	1.03852	3.83727	-1.88556	0.00204632
Il2rg	Ctx_Clz	Ctx_Veh	3.12269	13.8262	-2.14654	0.00204632
Rac2	Ctx_Clz	Ctx_Veh	1.55897	7.06838	-2.18079	0.00204632
Ptprc	Ctx_Clz	Ctx_Veh	1.12812	5.39959	-2.25893	0.00204632
Ttr	Ctx_Clz	Ctx_Veh	92.186	804.654	-3.12575	0.00204632
Arhgdib	Ctx_Clz	Ctx_Veh	10.0794	29.5909	-1.55374	0.0036931
Lck	Ctx_Clz	Ctx_Veh	2.18472	9.06388	-2.05268	0.0036931
Cd2	Ctx_Clz	Ctx_Veh	2.94231	13.4144	-2.18876	0.0036931
Slc4a5	Ctx_Clz	Ctx_Veh	0.262943	1.70505	-2.69699	0.00514589
Sell	Ctx_Clz	Ctx_Veh	2.25871	9.97219	-2.14241	0.00645759
Laptm5	Ctx_Clz	Ctx_Veh	2.5316	7.87542	-1.63731	0.00775018
Coro1a	Ctx_Clz	Ctx_Veh	9.22632	24.026	-1.38077	0.00893732
Ptpn6	Ctx_Clz	Ctx_Veh	0.601982	2.82213	-2.22899	0.0100524
Folr1	Ctx_Clz	Ctx_Veh	0.370746	4.0168	-3.43754	0.0100524
Ms4a4b	Ctx_Clz	Ctx_Veh	4.02299	17.2697	-2.10191	0.0111566
Il2rb	Ctx_Clz	Ctx_Veh	1.70149	7.73881	-2.18531	0.0111566
Gimap3	Ctx_Clz	Ctx_Veh	1.65852	7.59528	-2.19521	0.0111566
Ltb	Ctx_Clz	Ctx_Veh	3.94806	17.9431	-2.18422	0.0122302
Lcp2	Ctx_Clz	Ctx_Veh	0.460292	2.43593	-2.40385	0.0122302
Kl	Ctx_Clz	Ctx_Veh	2.0659	5.62952	-1.44624	0.0132337
Clic6	Ctx_Clz	Ctx_Veh	1.60326	5.44166	-1.76304	0.0169219
Cd52	Ctx_Clz	Ctx_Veh	9.84804	38.0394	-1.94959	0.0169219
Itgb7	Ctx_Clz	Ctx_Veh	1.35597	5.90496	-2.12261	0.0169219
Ets1	Ctx_Clz	Ctx_Veh	1.84593	4.75637	-1.36551	0.0186624
Ms4a6b	Ctx_Clz	Ctx_Veh	1.86488	7.238	-1.9565	0.0186624
Prr32	Ctx_Clz	Ctx_Veh	0.792425	7.78469	-3.29629	0.0210174
Vat1l	Ctx_Clz	Ctx_Veh	3.6757	8.40244	-1.19279	0.0218416
Dsp	Ctx_Clz	Ctx_Veh	0.359914	1.3492	-1.90638	0.0226742
Cd3g	Ctx_Clz	Ctx_Veh	2.17485	10.8445	-2.31797	0.0226742
Cd48	Ctx_Clz	Ctx_Veh	1.44256	5.97218	-2.04963	0.0258562
Ctss	Ctx_Clz	Ctx_Veh	1.59788	6.96552	-2.12407	0.0258562
F5	Ctx_Clz	Ctx_Veh	0.193669	1.17025	-2.59515	0.0287878
Bin2	Ctx_Clz	Ctx_Veh	1.73828	6.11484	-1.81465	0.0294532
Tbc1d10c	Ctx_Clz	Ctx_Veh	0.966009	4.32162	-2.16146	0.0330188
H2-K1	Ctx_Clz	Ctx_Veh	26.5655	45.7603	-0.784544	0.0336223
Prkch	Ctx_Clz	Ctx_Veh	0.546642	2.48267	-2.18322	0.0336223

Table 4.5: Top 40 decreased genes in cortical astrocytes following clozapine administration.

gene	sample_1	sample_2	value_1 (clozapine)	value_2 (vehicle)	log2 (fold_change) Clozapine vs. Vehicle	q_value
Map3k2	Ctx_Clz	Ctx_Veh	7.79669	4.79548	0.701187	0.0493818
Gucy1a2	Ctx_Clz	Ctx_Veh	6.6408	4.086	0.700667	0.0471073
Zfp111	Ctx_Clz	Ctx_Veh	9.0368	5.42994	0.734877	0.0465653
Adarb2	Ctx_Clz	Ctx_Veh	2.79213	1.08671	1.36141	0.0407843
Nr4a2	Ctx_Clz	Ctx_Veh	8.03017	3.56635	1.17098	0.0382865
Gsel	Ctx_Clz	Ctx_Veh	21.1587	13.1273	0.688685	0.0330188
Bcor	Ctx_Clz	Ctx_Veh	15.021	9.14935	0.715239	0.030167
Ubr4	Ctx_Clz	Ctx_Veh	10.1225	6.38658	0.664451	0.030167
Sikl	Ctx_Clz	Ctx_Veh	5.26449	2.25493	1.22321	0.0287878
Limk2	Ctx_Clz	Ctx_Veh	18.7839	10.4173	0.850513	0.0280873
Prr12	Ctx_Clz	Ctx_Veh	13.3495	8.02137	0.73487	0.0280873
Hesl	Ctx_Clz	Ctx_Veh	42.3617	23.8923	0.826215	0.0273191
Prpf8	Ctx_Clz	Ctx_Veh	125.612	80.8434	0.635776	0.0258562
Hook3	Ctx_Clz	Ctx_Veh	26.4674	17.0061	0.638163	0.025188
Fnl	Ctx_Clz	Ctx_Veh	3.41133	1.40493	1.27984	0.0218416
Zfp871	Ctx_Clz	Ctx_Veh	62.54	39.5047	0.662754	0.0177876
Btg2	Ctx_Clz	Ctx_Veh	18.9643	10.3013	0.880468	0.0140822
Rgs2	Ctx_Clz	Ctx_Veh	13.3276	6.11737	1.12343	0.0111566
Synel	Ctx_Clz	Ctx_Veh	15.7861	8.78426	0.845661	0.00893732
Rail	Ctx_Clz	Ctx_Veh	23.9875	11.9897	1.00049	0.00775018
Fos	Ctx_Clz	Ctx_Veh	63.0867	11.6305	2.43942	0.00204632
Nr4al	Ctx_Clz	Ctx_Veh	26.0803	11.4199	1.19141	0.00204632
Duspl	Ctx_Clz	Ctx_Veh	207.088	93.7931	1.14269	0.00204632
Bahccl	Ctx_Clz	Ctx_Veh	13.2763	7.11282	0.900355	0.00204632
Sh3gl2	Ctx_Clz	Ctx_Veh	47.4375	25.4186	0.900144	0.00204632

Table 4.6: Increased genes in cortical astrocytes following clozapine administration.

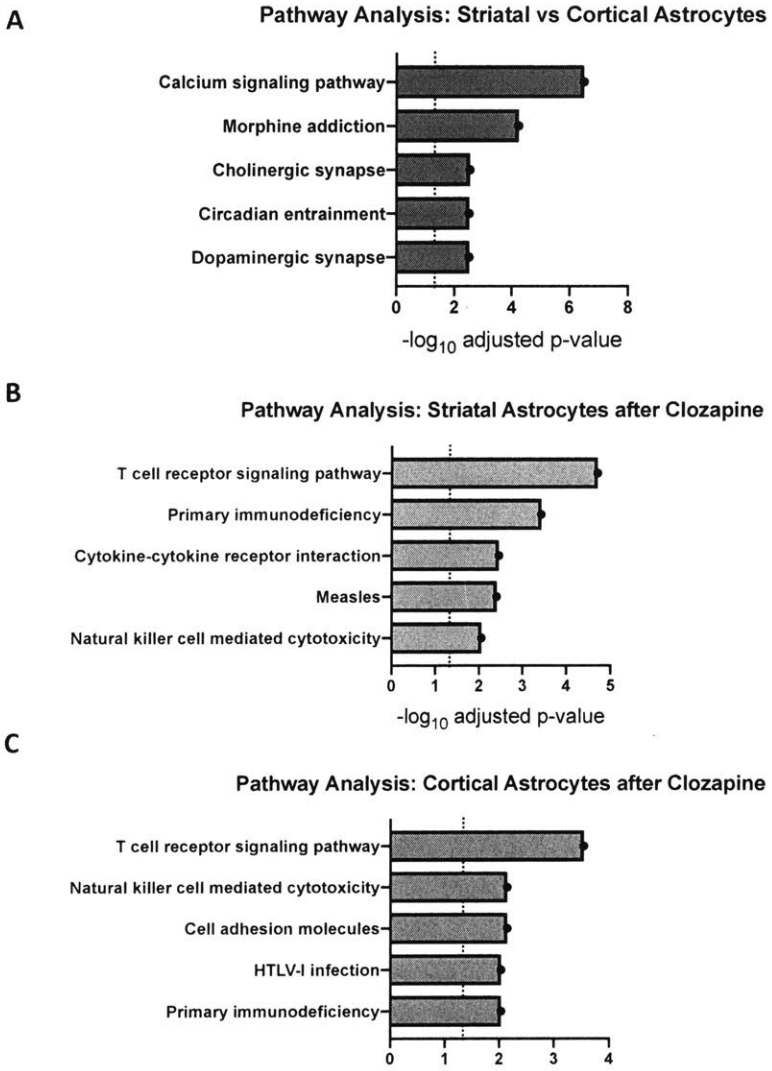

Figure 4.4: Altered pathways between striatal and cortical astrocytes and altered pathways following clozapine administration. KEGG Pathway alterations in striatal astrocytes compared to cortical astrocytes (A), striatal astrocytes following clozapine administration (B), and cortical astrocytes following clozapine administration (C).

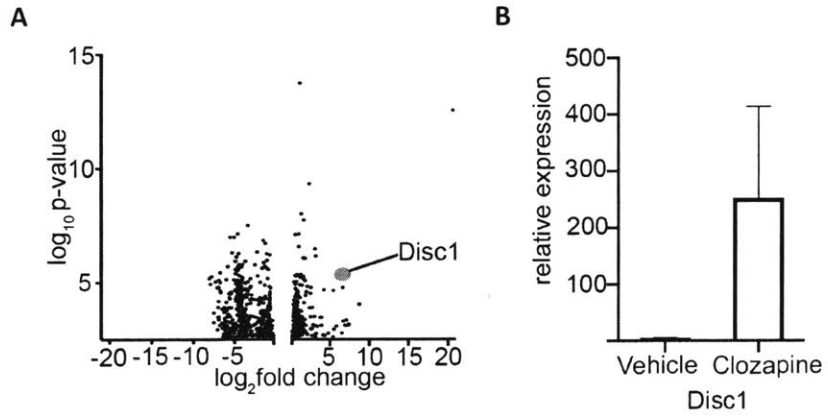

Figure 4.5: Increase in *Disc1* expression in astrocytes following clozapine administration. Volcano plot of gene expression changes in striatal astrocytes (A) and qRT-PCR for *Disc1* (B).

Materials & Methods

Animal Usage

Animal experiments were approved by the MIT Committee on Animal Care (CAC). Mice were group housed with 2-5 mice per cage on a standard 12h light/12h dark cycle with food and water provided ab libitum. Same sex littermates were randomly assigned to experimental groups. No procedures were performed on any animal prior to experiments described. Male mice 8-16 weeks of age were used for all experiments. For TRAP experiments, Tg(Drd1a-EGFP/Rpl10a)CP73Htz mice (for dSPN TRAP experiments), Tg(Drd2-EGFP/Rpl10a)CP101Htz mice (for iSPN TRAP experiments), and Tg(Aldh1l1-EGFP/Rpl10a)JD130Htz/J (for astrocyte TRAP experiments) were used. TRAP lines were bred as previously described (Doyle et al., 2008; Heiman et al., 2008), with the exception that the mice used in this study were backcrossed for at least 10 generations to the C57BL/6J background.

Drug Administration

For chronic experiments, mice were injected with APD intraperitoneally from the ages of 8-14 weeks once per morning, seven days per week, for a total of 6 weeks of dosing. Aripiprazole dosing started at 0.074 mg/kg for 2 weeks and was then regularly increased for 7 days to a final dose of 0.294 mg/kg. Clozapine dosing started at 0.184 mg/kg and was then regularly increased for 16 days to a final dose of 2.0 mg/kg. Haloperidol dosing started at 0.074 mg/kg and was then regularly increased for 6 days to a final dose of 0.221 mg/kg. Risperidone dosing started at 0.015 mg/kg and was then regularly increased

for 6 days to a final dose of 0.074 mg/kg. Drugs were highest purity non-pharmaceutical-grade available (Sigma-Aldrich, St. Louis MO), dissolved in cell-culture-grade dimethyl sulfoxide (Sigma-Aldrich, St. Louis MO), and stored in single-use aliquots at -20 °C. Drugs were diluted on the morning of use to final concentration in 0.1M sodium phosphate buffer [pH 6.2]. Mice were injected intraperitoneally (10 μL volume drug per gram of mouse).

mRNA Isolation

TRAP

Tissue harvest occurred 24H post final drug injection and dissections were performed on ice after cooling the head in liquid nitrogen for 4 seconds. Following dissection, cell type-specific mRNAs were purified (Heiman et al., 2014). Briefly, striata were homogenized in an ice-cold lysis buffer (150 mM KCl, 10 mM HEPES [pH 7.4], 5 mM $MgCl_2$, 0. 5mM dithiothreitol, 100 μg/mL cycloheximide, RNAse inhibitors, and protease inhibitors). Samples were then centrifuged at 2,000 x g at 4°C for 10 minutes and the supernatant was removed to a new tube. NP-40 (final concentration 1%) and 1,2-Diheptanoyl-sn-glycero-3-phosphocholine (DHPC, final concentration 30mM) were added and samples were incubated on ice for 5 minutes, followed by centrifugation at 13,000 x g at 4°C for 10 minutes and supernatant removal to a new tube. Streptavidin Dynabeads (Thermo Fisher Scientific, Waltham MA) coated with biotin-linked mouse anti-GFP antibodies were then added; the samples were incubated overnight at 4°C with end-over-end rotation (anti-GFP 19C8 antibody: RRID:AB_2716737; anti-GFP 19F7 antibody: RRID:AB2716736). Beads were collected on a magnetic rack and washed three times with wash buffer (350

mM KCl, 10 mM HEPES [pH 7.4], 5 mM $MgCl_2$, 0.5 mM dithiothreitol, 100 μg/mL cycloheximide, 1% NP-40). RNA was purified using the Absolutely RNA Isolation Nanoprep kit (Agilent Technologies, Satan Clara CA), and to ensure quality and accurate quantitation, purified RNA was run on a Bioanalyzer using the RNA 6000 Pico Kit (Agilent Technologies, Satan Clara CA).

RNA Sequencing and Analysis

Ovation RNA-Seq System v2 kit (NuGEN Technologies, San Carlos CA) was used to prepare samples for RNA-seq. Library quality was assessed using an Advanced Analytical-fragment Analyzer (Advanced Analytical, Ankeny IA) before mixing for sequencing on Illumina HiSeq 4000 (Illumina, San Diego CA) platform at the University of California, San Francisco Functional Genomics Core. Single-end Illumina HiSeq 4000 50-bp reads were collected and Fastq data were aligned to the mouse reference genome assembly (mm9) using the STAR 2.4.0 RNA-Seq aligner (Dobin et al., 2013). The aligned bam files (sorted by the coordinates) were subsequently processed by Cuffquant module of Cufflinks 2.0.0 to quantify gene expression using UCSC mm9 for gene annotation. Differential analysis between two individual groups was performed using Cuffdiff module of Cufflinks with the geometric method for library normalization and Deseq2, with differentially expressed genes defined as genes with FDR adjusted p-value < 0.05. Enrichr was used to process differentially expressed genes for GO and pathway analyses (Chen et al., 2013; Kuleshov et al., 2016). The Morpheus software (The Broad Institute, https://software.broadinstitute.org/morpheus) was used to generate heat maps of changes in pathways and genes.

qRT-PCR

qRT-PCR experiments used amplified cDNA generated for the RNA-seq experiments using the Ovation RNA-Seq System v2 kit (NuGEN Technologies, San Carlos, CA). Taqman Universal Master Mix and Taqman probes for Disc1 (Mm00533313_m1) and Atp5a1 (Mm00431960_m1) were used (ThermoScientific, Rockford, IL). Reactions were run on the StepOnePlus system (ThermoScientific, Rockford, IL).

Indirect Immunofluorescence

Mice were transcardially perfused and their tissue was processed and stained for immunofluorescence as described in Heiman et al, 2008. The following primary antibodies were used for experiments: Ttr (ab106558, 3ug/mL, Abcam, Cambridge, MA); Enpp2 (ab77104, 1ug/mL, Abcam, Cambridge, MA). A Zeiss 700 confocal microscope was used to image slides using z-stacks.

Discussion

Interpreting Results from Wild-Type Mice

We conducted our studies entirely in wild-type models instead of mouse models of schizophrenia. There are similarities in behavioral effects of antipsychotics in wild-type and schizophrenia model mice, specifically in reductions in startle amplitude and increases in prepulse inhibition (Duncan et al, 2006). Furthermore, NMDA antagonists such as PCP and ketamine, and dopamine reuptake inhibitors such as amphetamine, are both used as pharmacological animal models of schizophrenia and induce schizophrenia-like symptoms in people without schizophrenia, and make symptoms worse in people with schizophrenia (Griffith et al, 1968; Angrist & Gershon, 1970; Bell, 1973; Javitt & Zukin, 1991; Lahti et al, 1995; Malhotra et al, 1997). These effects of antipsychotics and schizophrenia-mimetic drugs in mice and people suggest that some of the cellular and behavioral effects of antipsychotics may be similar in both a wild-type and a schizophrenia or schizophrenia model context.

Furthermore, choosing a single mouse model of schizophrenia is difficult and unlikely to represent the global deficits of schizophrenia. Many of the positive symptoms of schizophrenia are dependent upon functions unique to humans, such as delusions, hallucinations, and speech deficits (O'Tuathaigh et al, 2012). This has led to the use of specific endophenotypes including prepulse inhibition, hyperactivity, social withdrawal, and memory impairments (Powell & Miyakawa, 2006).

Due to these significant limitations in mouse models of schizophrenia and the evidence that antipsychotics have similar behavioral effects in wild-type and genetic mouse models of schizophrenia, we chose to conduct our initial study in wild-type mice

with the hypothesis that the cellular mechanisms we uncovered would likely represent relevant alterations. However, it will be important to confirm the relevance of our findings to the disease context, as we cannot conclude that the precise alterations we see in the wild type context would be present if antipsychotics were administered in a schizophrenia context. To better understand the relevance of our studies in wild-type mice to schizophrenia, future work could study transcriptional profiles of SPNs in schizophrenia mouse models and perform mEPSC recordings from iSPNs in the nucleus accumbens of these mice. Our hypothesis would be strengthened if we found that glutamatergic transcripts and mEPSCs are in fact decreased in mouse model SPNs, and that these levels are brought up to the wild-type baseline after antipsychotic administration.

Altogether, we are working to better understand schizophrenia in a context in which the underlying pathophysiology and the mechanism of action of antipsychotics is not fully understood. Because of significant limitations in schizophrenia mouse models, it is not clear that better understanding these models will lead to a better understanding of the human disorder. Furthermore, we know that antipsychotics appear to have similar effects in schizophrenia-associated behaviors in people with and without schizophrenia and wild-type and mouse models of schizophrenia. We hypothesize that downstream cellular effects following antipsychotic administration are therefore similar in both therapeutic contexts and in wild-type conditions and have conducted our studies accordingly. However, future work remains to demonstrate that the effects we see following antipsychotic administration at the translational and functional level are indeed compensating for underlying cellular alterations in a schizophrenia context.

Broader Circuitry Effects of Antipsychotic Administration

However, questions remain regarding whether this effect is specific to the nucleus accumbens, given that D2 receptors are also expressed in other cell types and brain regions. Many brain regions apart from the striatum have been implicated in schizophrenia, especially the hippocampus, the prefrontal cortex, and, more recently, the thalamic reticular nucleus (Knable & Weinberger, 1997; Farrarelli & Tononi, 2011; Lieberman et al, 2018). Each of these brain regions is associated with varied functions implicated in schizophrenia, and furthermore, each of them functions as part of a broader circuitry with connections throughout the brain, including to and from SPNs of the striatum. Our own profiling of astrocytes following chronic clozapine administration demonstrate that non-SPN cells in the striatum are also altering their transcriptional profiles in response to chronic antipsychotic administration.

Due to the importance of dopamine in schizophrenia pathophysiology and the high expression of dopamine receptors in the striatum, we chose the striatum as a starting point in understanding the transcriptional and synaptic functional effects of antipsychotics. However, other brain regions are also likely altered following antipsychotic treatment; in fact, our transcriptional data from SPNs point to increased GABAergic release from SPNs, which may lead to functional alterations in neurons receiving input from SPNs, implicating numerous brain regions in the basal ganglia.

Furthermore, chronic administration could incur circuit-wide rewiring that manifests in various brain regions.

To further test our model that chronic antipsychotic action promotes glutamatergic drive into the striatum, we would want to (1) examine brain regions and cell types beyond nucleus accumbens SPNs; (2) distinguish between acute and chronic transcriptional effects of antipsychotics; and (3) characterize functional similarities or differences between clozapine and other antipsychotics we profiled transcriptionally.

To look beyond striatal SPNs, future work could continue to dissect circuit-wide alterations following antipsychotic treatment to gain a better understanding of the global effects of these drugs. Given our findings, two initial places to start would be the neurons directly upstream and downstream from SPNs, namely, thalamo-striatal neurons and cortico-striatal neurons (upstream from SPNs); and neurons of the globus pallidus and substantia nigra (downstream from SPNs). We would predict functional alterations in thalamo-striatal and/or cortico-striatal neurons reflective of increased glutamatergic transmission, and functional alterations in the globus pallidus reflective of increased presynaptic iSPN GABAergic release.

To dissociate acute versus chronic effects of antipsychotic administration, it would also be informative to profile SPNs following a single, acute dose of antipsychotics, as this could help to elucidate the initial signaling cascades leading towards chronic transcriptional alterations. It is possible that the immediate effects of antipsychotics are to increase translation of glutamatergic PSD scaffolding molecules such as; alternatively, it is possible that immediate translational effects are dramatically different from chronic translational profiles and that long-term cellular responses are required to lead to increased translation of glutamatergic PSD components.

Finally, in this study, we performed functional studies following clozapine administration, but it would also be important to understand whether mEPSCs increase and CP-AMPARs are present following aripiprazole, risperidone, or haloperidol administration. If they are, this would add further evidence to the idea that increased glutamatergic drive through the striatum is indeed a core mechanism explaining the efficacy of antipsychotic drugs.

Linking the Dopamine and Glutamate Hypotheses of Schizophrenia

Studies of risk factors for schizophrenia, including human GWAS, have consistently pointed to alterations to glutamatergic neurotransmission and/or dopaminergic neuromodulation of glutamateric neurotransmission. Rodent models of schizophrenia have been developed using both NMDA antagonists and dopamine receptor agonists as means to generating behaviors reminiscent of psychosis. Furthermore, structural and functional abnormalities have been observed in dopaminergic and glutamatergic cells across the brain, from the striatum to the hippocampus to the cortex. The field is currently lacking a framework towards integrating these observations into a consistent, single model for schizophrenia pathophysiology.

To work towards elucidating this pathophysiology, we took the approach of studying the mechanism of action of antipsychotic drugs. Although not sufficient to treat schizophrenia in all patients, these drugs do have demonstrated benefits for many patients, and we hypothesized that better understanding their effects could elucidate molecular mechanisms underlying schizophrenia. Because of consistent studies pointing towards the dopamine D2 receptor as a risk gene for schizophrenia and the fact that all

effective antipsychotics display dopamine D2 receptor antagonism, we initially targeted the striatum, the site of highest dopamine D2 receptor expression. We treated mice chronically with a panel of antipsychotics and harvested mRNAs from SPNs and astrocytes in a cell type-specific fashion. We also performed recordings from SPNs in the nucleus accumbens core following clozapine treatment to study changes in synaptic function. Our molecular and cellular findings demonstrate that treatment with antipsychotics alters translational profiles in dSPNs, iSPNs, and astrocytes, and that it in particular increases transcript levels of genes associated with glutamatergic synaptic development in iSPNs and astrocytes. In line with this translational profiling, we further found that clozapine increases the frequency of mEPSCs specifically in iSPNs of the nucleus accumbens core through the incorporation of calcium-permeable AMPARs. These data demonstrate a link between dopamine receptor antagonism and alterations in glutamatergic signaling in the striatum, a key region for broader basal ganglia circuitry. The fact that we see translational alterations in dSPNs following aripiprazole, haloperidol, and risperidone suggests that dopamine D2 receptor antagonism can have circuit-wide effects that alter glutamatergic function in multiple cell types.

Human genetics studies have implicated the Drd2 receptor and genes important for the glutamatergic postsynaptic density in schizophrenia pathophysiology. In the context of this previous research, our data provide evidence that a key part of schizophrenia pathophysiology may arise from aberrant signaling through D2 receptors that results in decreased glutamatergic drive in the striatum.

Integrating Molecular Profiling and Physiological Recording Data to Understand Glutamatergic Alterations

As described earlier, previous studies of schizophrenia pathophysiology and antipsychotic mechanisms of action have implicated glutamatergic signaling and pointed to the striatum as a brain region of interest. We built upon these studies and followed two approaches to better understand alterations following chronic antipsychotic administration: first, we performed cell type-specific molecular profiling to gain an unbiased appreciation for alterations at a high resolution. Second, we performed whole-cell recordings from the ventral and dorsal striatum to characterize synaptic function following chronic and acute clozapine administration. Each of these approaches revealed increased glutamatergic signaling into the striatum following antipsychotic administration, and these approaches together form a more complete depiction of the functional effects of antipsychotics.

In particular, the presence of increased levels of PSD proteins, such as Shank3, alongside increased mEPSCs, in the absence of increased transcript levels of AMPAR or NMDAR subunits, suggests the possibility that increasing transcription of PSD proteins could be a key mechanism of antipsychotic drugs. Previous work has shown that reducing levels of Shank3 is sufficient to reduce spine density, while overexpression of Shank3 alone increases numbers of functional spines by recruiting glutamate receptors (Roussignol et al, 2005). It is possible that a similar response occurs in striatal SPNs following antipsychotic treatment and leads to signaling alterations that produce therapeutic effects for patients.

To test whether increased expression of Shank3 is sufficient to explain antipsychotic action, future work could drive expression of Shank3 protein in iSPNs of schizophrenia model mice. We would predict that this would induce additional functional synapses in this cell type. If this change is indeed underlying therapeutic benefits of antipsychotics, we would further predict that endophenotypes of schizophrenia in these mouse models would be reduced following overexpression of Shank3. To test whether increased expression of Shank3 is necessary to explain antipsychotic action, we could knock down Shank3 expression in iSPNs and subsequently administer clozapine to schizophrenia model mice. If Shank3 is necessary for clozapine's effects, we would predict that spine numbers on iSPNs would be lower in this condition compared to clozapine alone or Shank3 overexpression alone, and we would predict that the endophenotypes normally improved by clozapine administration would be the same as in the untreated mouse models or, potentially, worsened compared to untreated mice.

A Model of Antipsychotic Therapeutic Benefit

Our molecular profiling data found consistent genetic signatures across all four drugs in iSPNs and consistent genetic signatures across aripiprazole, risperidone, and haloperidol in dSPNs. For all drugs except clozapine, these signatures pointed towards an increase in glutamatergic components across cell types, but to a greater degree in iSPNs; in clozapine, this effect was nearly exclusively present in iSPNs. Altogether, our data support a model for antipsychotics that long-term D2 receptor antagonism leads to synaptic alterations in SPN glutamatergic synapses reflective of increased glutamatergic signaling. Previous postmortem studies have suggested that chronic antipsychotic

administration of schizophrenia patients leads to increased excitatory input in ventral striatum, consistent with our findings (McCollum et al, 2015). However, it is also possible that the data we collected are a side effect of antipsychotic administration, or perhaps an artifact of administration in the wild-type context, that is not relevant to the therapeutic benefits of these drugs.

One way to test this hypothesis directly would be to increase glutamatergic drive into the striatum and then test prepulse inhibition in mouse models of schizophrenia. First, we could directly drive activity in iSPNs using Cre-dependent channelrhodopsin viruses and light. Second, we could drive iSPN-specific input from the cortex using Cre-dependent helper viruses to enable retrograde channelrhodopsin virus travel from D2-Cre expressing iSPNs to the cortex (Wall et al, 2010). These two experimental cohorts would allow us to test whether driving activity in iSPNs directly ameliorates endophenotypes in schizophrenia mouse models and increases PPI in wild-type mice and further to test specifically the role of the cortico-striatal iSPN synapse. We would predict that directly activating iSPNs or driving iSPN-specific cortical input would increase PPI in wild-type controls and mouse models of schizophrenia and would improve additional social and memory endophenotypes associated with schizophrenia mouse models.

Schizophrenia models that we could test this modification in could include genetic mouse models, including DISC1 and NRG1 models (Cash-Padgett & Jaaro-Peled, 2013; Stefansson et al, 2002), or drug-induced models of schizophrenia, including PCP and amphetamine models (Marcotte et al, 2001; Castane et al, 2015); or developmental models, such as the maternal activation model (MAM) (Jones et al, 2011; Lodge, 2014). Our data would predict that increasing glutamatergic drive in these mouse models of

schizophrenia should improve PPI ratio and, potentially, ameliorate other endophenotypes associated with these mouse models.

Parallels with Drugs of Abuse

A great deal of work has been conducted in the study of addiction in the mesolimbic dopamine system using drugs of abuse, like cocaine, which act as dopamine agonists. Sensitization to these drugs in particular, which the ventral tegmental area and nucleus accumbens are crucially involved in, is frequently used as a model of experience-dependent plasticity (Thomas et al, 2001).

It is interesting to contextualize our findings in the case of withdrawal from cocaine. Self- administration of cocaine followed by withdrawal leads to incorporation of CP-AMPARs in the nucleus accumbens core and shell of adult rats, but experimenter-administered injections followed by withdrawal do not lead to CP-AMPAR incorporation despite the presence of sensitized behavior (McCutcheon et al, 2011). This implicates motivated behaviors in formation of CP-AMPARs following withdrawal, not cocaine administration alone. Additionally, cocaine induces silent synapses in dSPNs that subsequently become unsilenced during withdrawal as they recruit AMPARs to the excitatory synapses (Pascoli et al, 2014; Graziane et al, 2016). Cocaine withdrawal induces calcium-permeable AMPARs in the nucleus accumbens of rats starting at day 30 and persisting through day 69 (Ferrario et al, 2011; Pascoli et al, 2014). It is interesting that, in both cocaine withdrawal and antipsychotic administration, we see evidence for incorporation of CP-AMPARs. In these studies, the effect of removing cocaine effectively reduces dopamine signaling, as does antipsychotic administration. Perhaps

there is a similar mechanism underlying withdrawal from drugs of abuse and administration of antipsychotic drugs.

Explaining Clozapine's Superiority in the Clinic

It has long been known that clozapine displays dramatically improved therapeutic benefit over all other antipsychotics. It does have a unique receptor binding profile, in that it has a comparatively lower affinity for dopamine D2 receptors. However, its use is limited by its accompanying serious side effect of agranulocytosis, which can lead to death. An improved understanding of the mechanisms by which clozapine exerts its improved therapeutic benefit and the ways in which clozapine differs from other drugs could be of immense value for treatment of schizophrenia if similar drugs without major side effects could be developed.

Our data demonstrate that clozapine alone displays a greater effect on iSPN gene expression rather than dSPN gene expression, with very few genes changing in dSPNs following clozapine treatment. It is possible that this cell type specificity confers the benefits of clozapine. Further work could drive activity specifically into iSPNs and test the resulting effect upon behaviors such as prepulse inhibition in mice and test whether this iSPN-specific alteration is sufficient to explain clozapine's improvement of prepulse inhibition. It would also be interesting to examine animal models of schizophrenia and test whether selective drive of iSPNs rescued behavioral or anatomical phenotypes in these models. If rescue were observed, it would be interesting to compare this rescue to clozapine administration alone. To test whether this alteration is necessary to explain clozapine's efficacy, it would also be interesting to administer clozapine while also

reducing activity specifically into iSPNs. If this drive is necessary, we would expect to see no change in PPI despite the co-administration of clozapine.

It is interesting to consider the mechanisms by which clozapine may be exerting this cell type-specific effect. In particular, which form of dopamine D2 receptors are being targeted by antipsychotics has long been an open question. There are two isoforms of D2, D2L and D2S, which are long- and short-forms of the receptor. The D2S isoform is expressed presynaptically and acts as an autoreceptor; antagonism of this receptor would increase dopamine release generally into the striatum. The D2L isoform is expressed postsynaptically; antagonism of this receptor would specifically make iSPNs more receptive to glutamatergic inputs via downstream dopamine system signaling. It is possible that the differing dopamine D2 affinities between clozapine and the other antipsychotics means that their ratio of binding pre- and post-synaptically also differs and leads to divergent cellular effects. Greater presynaptic binding could lead to alterations in dopamine generally, which would affect signaling in both D1 and D2 postsynaptic receptors. On the other hand, if clozapine skews towards more postsynaptic binding of the D2 receptor, this could explain its more cell type-specific effects.

An additional hypothesis is that clozapine is exerting comparatively more effects on D4 receptors, which clozapine has a comparatively higher affinity for than other antipsychotics (Van Tol et al, 1991; Coward, 1992). These receptors are D2-class receptors and primarily expressed on iSPNs. Action at these receptors would therefore tend to have a cell type-specific effect as well. To test this hypothesis, it would be interesting to test pure antagonists of the D4 receptor to see if the transcriptional profile mimics that of clozapine and if this results in increased glutamatergic signaling into

iSPNs. Although pure D4 antagonists have been disappointing in clinical trials (Kulkarni & Ninan, 2000), it is possible that a different ratio of D4/D2 antagonism may still be beneficial in schizophrenia therapeutics.

Summary

We have shown enhanced glutamatergic function in the ventral striatum following chronic antipsychotic administration. We have demonstrated this through translational profiling of dSPNs, iSPNs, and astrocytes following a panel of treatments, which revealed cell type-specific alterations in components of the glutamatergic postsynaptic density in SPNs and a translational profile associated with synaptogenesis in astrocytes. Functional experiments following chronic clozapine administration futher pinpointed this increased glutamatergic function in the form of increased mEPSC frequency via an increase in CP-AMPARs in iSPNs of the ventral striatum. Together, these data have identified a core molecular signature of increased glutamatergic transmission in the striatum induced by chronic antipsychotic treatment. This work provides evidence that effective antipsychotics address a lack of glutamatergic drive into the striatum in cases of schizophrenia. Additionally, it identifies a cell type-specific effect of clozapine administration that distinguishes it from other drugs and could help to explain its greater efficacy in the clinic. Finally, it suggests that drug development efforts seeking improved antipsychotics may benefit by finding compounds that feature an increased glutamatergic drive into the striatum as a core function.

Appendix 1: Improving RNA Purification Protocols

Background

Translating Ribosome Affinity Purification (TRAP) is a powerful technology that allows for the cell type-specific profiling of mRNAs (Heiman et al, 2008). TRAP-Seq uniquely provides the ability to profile a population of a genetically defined cell type in a whole-genome, unbiased fashion from actively translated mRNAs purified *in situ*. Because of these features, TRAP-Seq allows us to identify small magnitude changes and also to gain a snapshot specifically of the mRNAs being actively translated into proteins, a powerful reflection of the function of a population of cells. This technology has led to studies discovering biological differences across cell types as well as novel mechanisms in diseases including Fragile X Syndrome and narcolepsy, among others (Doyle et al, 2008; Dalal et al, 2013; Thomson et al, 2017). Our ability to conduct these studies is limited by two major experimental constraints: our ability to detect and read the mRNAs that belong to a given cell population, and our ability to avoid unspecific binding, with increased background binding lowering our signal: noise ratio. The TRAP protocol as published has some degree of unspecific binding and there are many applications of TRAP which require adjustment and experimentation to determine how much starting material is necessary to accumulate a detectable amount of mRNA (Heiman et al, 2014). We continue to appreciate the major differences between cell populations in a variety of contexts, and it becomes increasingly important to detect smaller and smaller populations of cells.

We therefore first sought to improve the signal: noise ratio of TRAP IPs by adjusting bead/GFP antibody resin conditions. There is some degree of background RNA binding to the resin, especially in myelin-rich tissues, and this background rate of binding is increased with higher volumes of resin and with poorly performed bead wash steps (Heiman et al, 2014). Previous work had shown high rates of GFP-bead binding and low background binding in a protocol using M-270 epoxy Dynabeads and short incubation periods (Cristea et al, 2005). We undertook a comparison of this protocol with the published TRAP protocol *in vitro* and *in vivo* to determine which approach allowed for maximal binding of GFP-tagged polysomes with minimal background RNA binding.

Additionally, in collboration with Dr. Kay Tye's laboratory, we sought to purify mRNAs from a small subset of cells in the mouse PFC defined by their projections to other brain regions. Successfully purifying mRNAs from these populations could allow us to find markers that define particular projections in the brain but is a technical challenge due to the small numbers of cells.

Results

1. *In vitro* testing shows no difference in binding or background with m270 beads

We sought to improve the published TRAP protocol by simultaneously reducing background binding and increasing mRNA yields compared to the protocol published by Heiman et al, 2008. The major change we attempted was to use a different bead and GFP antibody matrix preparation (Figure 1.1 A). In brief, instead of using Streptavidin Dynabeads coated with protein L and BSA and subsequently binding antibody to the beads in buffer, we used M-270 Epoxy Dynabeads, which were reported to potentially have lower amounts of background protein binding than Streptavidin Dynabeads (Cristea et al, 2005). We used these beads to directly attempt antibody conjugation in buffer.

We first tried this in HEK 293 cell purifications *in vitro* because HEK 293 cells are capable of robustly expressing the GFP-TRAP L10a transgene. Initial experiments showed no difference in RNA concentration between protein-L and m270 conjugated beads in either HEK 293 cells transfected with a GFP-L10a tag (Figure 1.1 B) or in untransfected cells (Figure 1.1 C). We therefore proceeded to test *in vivo*.

2. *In vivo* testing shows increased binding and increased background with m270 beads

We tested these two resins in the context of striata from the Aldh1l1 TRAP line, which directly targets astrocytes (Heintz, 2004; Cahoy et al, 2008; Clarke et al, 2018). We found that the m270 conjugation did indeed increase yield dramatically (Figure 1.2 A), but that it also increased background binding from wild-type striata (Figure 1.2 B).

We hypothesized that using a different incubation time might to help reduce background while retaining yields, and so we compared a 3H vs. 16H bead and RNA incubation time. We found that decreasing incubation time decreased mRNA yields in both transgenic (Figure 1.2 C) and wild-type animals (Figure 1.2 D) and maintained the same ratio of background to yield, therefore not improving our signal: noise ratio (Figure 1.2 E).

3. Pooling samples allows for purification of mRNAs from specific projections with low cell numbers

In addition to changing the conditions of GFP antibody-bead conjugation, there are additional experimental changes that can be made to allow for the purification of low-abundance RNAs. In earlier work, Dr. Myriam Heiman had demonstrated that decreased resin volumes and increased wash times could reduce background binding as compared to earlier protocols (data not shown). An additional possible adjustment is to pool biological samples, thus increasing the total amount of mRNAs and permitting the detection of these mRNAs above background RNA binding. We pursued these experimental modifications in collaboration with Professor Kay Tye's laboratory.

There are numerous projections from the medial prefrontal cortex (mPFC) to other brain regions, including the thalamus, amygdala, nucleus accumbens, hippocampus, and periaqueductal grey (PAG) (Vertes et al, 2001; Franklin et al, 2017). A study in Professor Kay Tye's laboratory revealed behavioral implications of these three distinct circuits, and we wanted to try to identify the mRNAs specific to these projection cells in the cortex. To do so, in collaboration with Dr. Cody Siciliano in Professor Tye's

laboratory, we genetically identified the cells projecting from the mouse PFC to the dPAG, nucleus accumbens (NAC), and lateral hypothalamus (LH).

Identification of projection-specific cells in the mouse PFC was achieved using a retroviral approach, namely with an HSV-L10a-GFP virus. The HSV-L10a-GFP virus was injected into the dPAG, NAC, and LH, and then allowed to retrograde into PFC neurons directly projecting to each of these three injection sites. Successful surgical approach was confirmed by performing immunofluorescence to the GFP tag and confocal imaging of the PFC (Figure 1.3 A). Based on the limited immunofluorescent signal we observed, we decided to pool mouse replicates in an effort to collect sufficient yields of mRNAs. TRAP was subsequently performed on 3 pooled mouse replicates per sample. We confirmed presence of RNA above background level in these samples (Figure 1.3 B) and also confirmed enrichment of GFP in purified TRAP RNA compared to supernatant RNA from GFP-positive samples, which confirmed the enrichment of ribosome-associated mRNAs in our TRAP samples compared to the unbound fraction (Figure 1.3 C).

Appendix I Summary

We undertook a series of experiments in an attempt to improve the signal: noise ratio of the TRAP protocol using a different GFP-bead system. Although this new protocol did increase yields *in vivo,* it also increased background binding by the same proportion. We therefore did not see an experimental improvement using m270 beads. When we decreased incubation time periods, we found that both yields and background decreased, keeping the ratio of signal: noise the same. In future experiments we therefore continued to use Streptavidin Dynabeads incubated with protein L.

In the case of low starting material from mPFC projection neurons, we found that decreasing resin volumes, increasing wash times, pooling samples, and using high-fidelity quantitation methods allowed us to detect low amounts of RNA and proceed with RNA-seq studies. We were able to detect an enrichment of EGFP signal following TRAP of retro-TRAP injected samples and the presence of RNA above background signal. This allowed us to proceed to RNA sequencing of these samples and identification of region-specific markers.

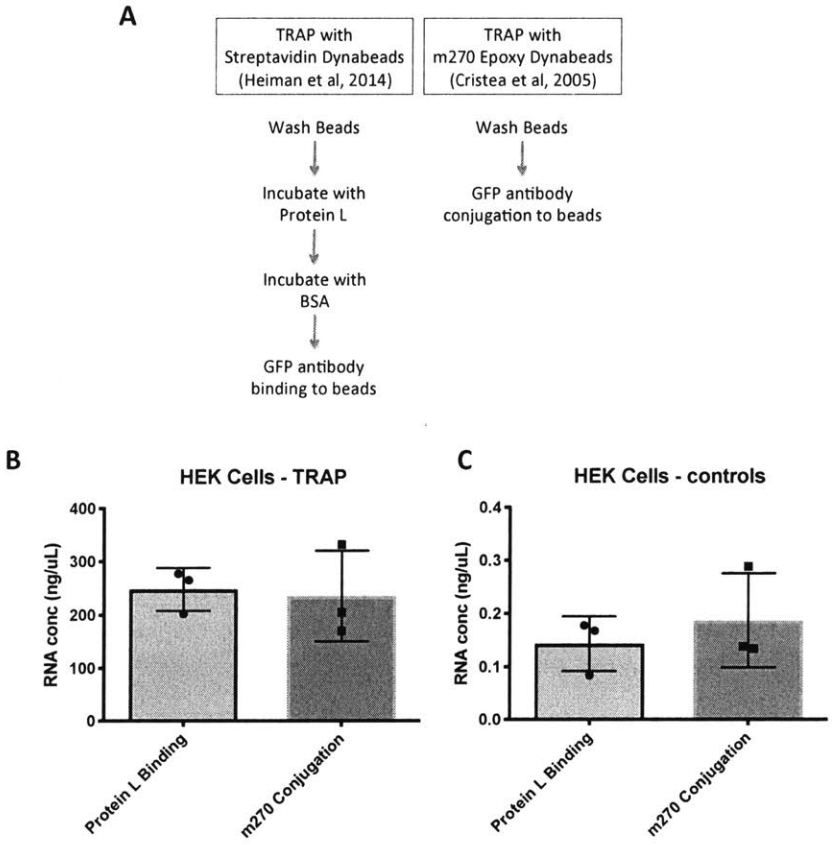

Figure A-1.1: Streptavidin Dynabeads and m270 Epoxy Dynabeads demonstrate similar yields and background *in vitro*. Major differences between Streptavidin and m270 Epoxy protocols (A). RNA yields following each protocol as detected by Bioanalyzer in both TRAP-transfected HEK cells (B) and GFP-transfected control HEK cells (C). N=3 dishes of cells per group. All error bars: mean +/- SEM.

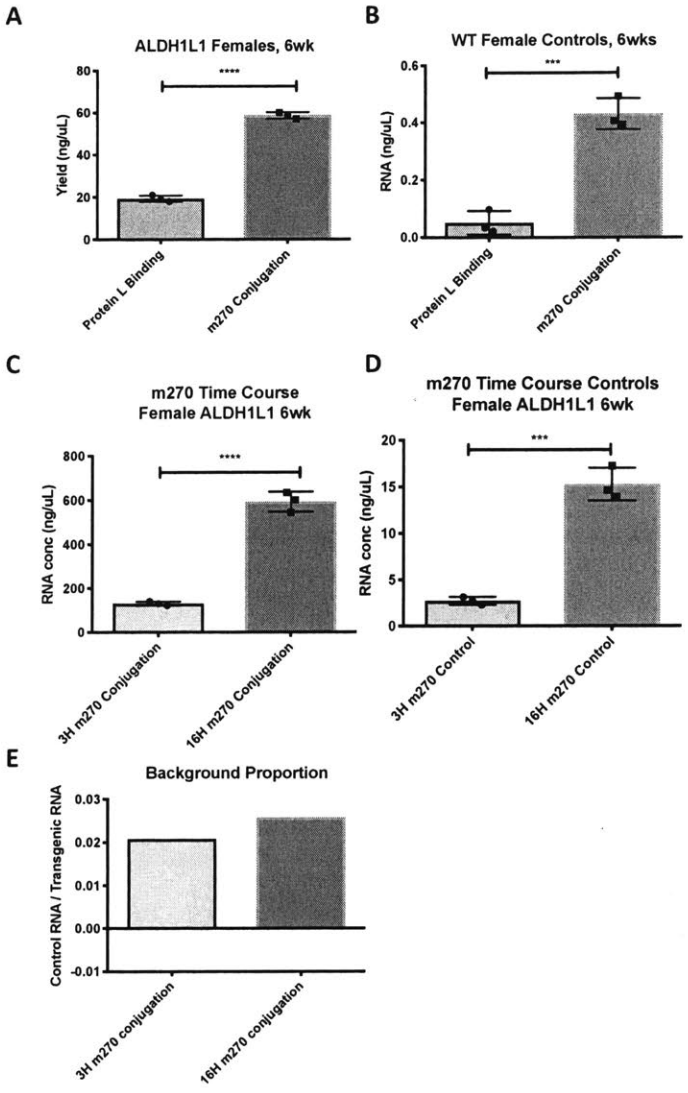

Figure A-1.2: Streptavidin Dynabeads and m270 Epoxy Dynabeads demonstrate similar yields and backgrounds *in vivo*. Increase in RNA yield following m270 Epoxy protocol *in vivo* in both Aldh1l1-TRAP mice and wild-type control mice (A). Increase in RNA yield following 16H bead incubation compared to 3H bead incubation in both Aldh1l1-TRAP mice and wild-type control mice (B). Consistent background proportion in both 3H and 16H incubation with m270 Epoxy protocol (C). N=3 animals per group. All error bars: mean +/- SEM. *** $p<0.001$, **** $p<0.0001$.

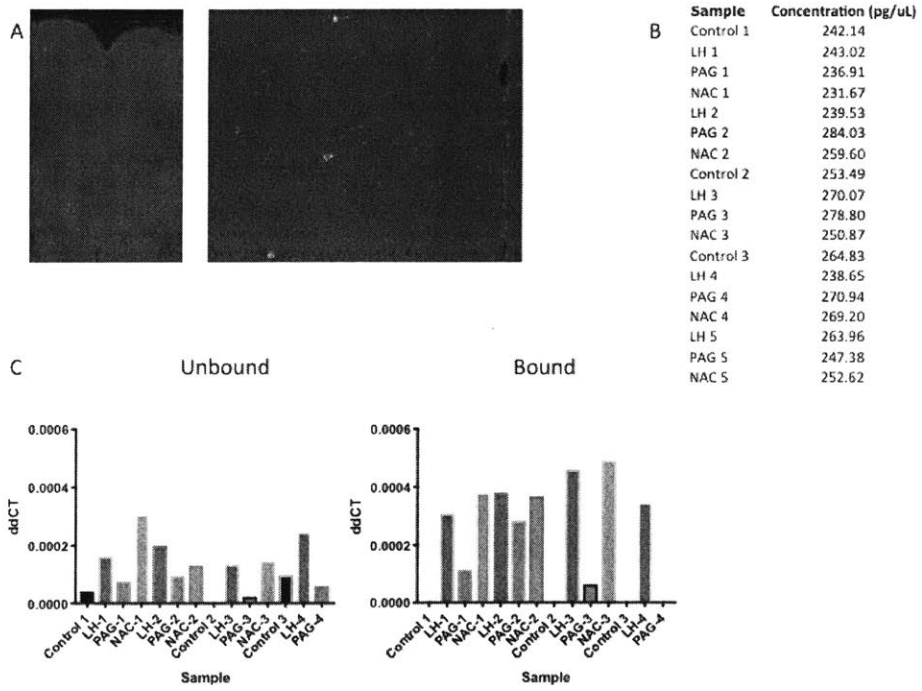

Figure A-1.3: TRAP enables projection-specific profiling in the cases of the mPFC-dPAG, mPFC-PAG, and mPFC-NAC. HSV virus with TRAP transgene injections into the dPAG (A). Quantitation of mRNAs purified from mPFC-dPAG neurons (B). EGFP expression in the unbound and bound fractions (C).

Materials & Methods

Animal Usage

Animal experiments were approved by the MIT Committee on Animal Care (CAC). Mice were group housed with 2-5 mice per cage on a standard 12h light/12h dark cycle with food and water provided ad libitum. Same sex littermates were randomly assigned to experimental groups. No procedures were performed on any animal prior to experiments described. 16-week-old female mice were used for experiments. C57BL/6J male were used for all non-TRAP experiments. For TRAP experiments, Tg(Aldh1l1-EGFP/Rpl10a)JD130Htz/J were used. TRAP lines were bred as previously described (Doyle et al., 2008; Heiman et al., 2008), with the exception that the mice used in this study were backcrossed for at least 10 generations to the C57BL/6J background.

HEK/293 Cell Culture

HEK/293 cells (ATCC, Manassas, VA) were grown in Dulbelcco's Modified Eagle's medium (DMEM, ThermoScientific, Rockford, IL) with 10% bovine serum albumin (BSA, Gemini, West Sacramento, CA). Transfection with either TRAP or GFP plasmid DNA (Heiman et al, 2008) was performed using the FuGENE HD reagent (Promega, Madison WI). Briefly, room temperature FuGENE HD was incubated at 3:1 ratio with plasmid DNA for 15 minutes, then added to HEK/293 cells and incubated for 48 hours.

mRNA Isolation

TRAP

Dissections were performed on ice after cooling the head in liquid nitrogen for 4 seconds. Following dissection, cell type-specific mRNAs were purified (Heiman et al., 2014). Briefly, striata were homogenized in an ice-cold lysis buffer (150 mM KCl, 10 mM HEPES [pH 7.4], 5 mM $MgCl_2$, 0. 5mM dithiothreitol, 100 μg/mL cycloheximide, RNAse inhibitors, and protease inhibitors). Samples were then centrifuged at 2,000 x g at 4°C for 10 minutes and the supernatant was removed to a new tube. NP-40 (final concentration 1%) and 1,2-Diheptanoyl-sn-glycero-3-phosphocholine (DHPC, final concentration 30mM) were added and samples were incubated on ice for 5 minutes, followed by centrifugation at 13,000 x g at 4°C for 10 minutes and supernatant removal to a new tube. Streptavidin Dynabeads (Thermo Fisher Scientific, Waltham MA) coated with biotin-linked mouse anti-GFP antibodies were then added; the samples were incubated overnight at 4°C with end-over-end rotation (anti-GFP 19C8 antibody: RRID:AB_2716737; anti-GFP 19F7 antibody: RRID:AB2716736). Beads were collected on a magnetic rack and washed three times with wash buffer (350 mM KCl, 10 mM HEPES [pH 7.4], 5 mM $MgCl_2$, 0.5 mM dithiothreitol, 100 μg/mL cycloheximide, 1% NP-40). RNA was purified using the Absolutely RNA Isolation Nanoprep kit (Agilent Technologies, Satan Clara CA), and to ensure quality and accurate quantitation, purified RNA was run on a Bioanalyzer using the RNA 6000 Pico Kit (Agilent Technologies, Satan Clara CA).

M270 Epoxy Dynabead Purification

Instead of biotin-linked mouse anti-GFP antibodies, samples were incubated with GFP-conjugated m270 Epoxy Dynabeads. Briefly, 3mg beads per IP (Dynal, NY, USA) were

resuspended with 10ug IgG anti-GFP antibodies/1mg beads. GFP-bead conjugation took place at RT overnight on a rotor. The following day, beads were washed sequentially with sodium phosphate buffer, 100mM Glycine HCl, 10mM Tris, 100mM Triethylamine solution, 3% BSA in PBS, 0.5% TritonX-100 in PBS, and PBS. Conjugated beads were then used for IP as outlined above.

qRT-PCR

qRT-PCR experiments used RNA from TRAP experiments (Heiman et al, 2008). Taqman One-Step RT-PCR and Taqman probes for EGFP (Mm01219987_m1) and Atp5a1 (Mm00431960_m1) were used (ThermoScientific, Rockford, IL). Reactions were run on the StepOnePlus system (ThermoScientific, Rockford, IL).

Retro-TRAP

Injections of an HSV-L10a-GFP virus were made into the PAG, NAC, and LH in separate cohorts of BL6/C57 adult male mice. Viral injections were given 4 weeks for full expression before TRAP harvest.

Immunofluorescence & Confocal Imaging

Mice were transcardially perfused and their tissue was processed and stained for immunofluorescence as described in Heiman et al, 2008. The following primary antibodies were used for experiments: GFP (ab13970, 1:1000, Abcam, Cambridge, MA). A Zeiss 700 confocal microscope was used to image slides using z-stacks.

References

Agid, O., Kapur, S., Arenovich, T., Zipursky, R.B. (2003) Delayed-onset hypothesis of antipsychotic action: a hypothesis tested and rejected. *Archives of General Psychiatry,* 60, 1228-1235. http://doi.org/10.1001/archpsyc.60.12.1228

Alcantara, A.A., Chen, V., Herring, B.E., Mendenhall, J.M., Berlanga, M.L. (2003). Localization of dopamine D2 receptors on cholinergic interneurons of the dorsal striatum and nucleus accumbens of the rat. *Brain Res,* 986(1-2), 22-9.

Alvir, J.M.J., Lieberman, J.A., Safferman, A.Z., Schwimmer, J.L., Schaaf, J.A. (1993). Clozapine-induced agranulocytosis – incidence and risk factors in the United States. *N Engl J Med,* 329, 162-167. http://doi.org/ 10.1056/NEJM199307153290303

Angrist, B.M., Gershon, S. (1970). The phenomenology of experimentall induced amphetamine psychosis – preliminary observations. *Biol Psychiatry*, 2(2), 95-107.

Aoto, J., Nam, C.I., Poon, M.M., Ting, P., and Chen, L. (2008). Synaptic signaling by all-trans retinoic acid in homeostatic synaptic plasticity. *Neuron,* 60, 308-320. http://doi.org/ 10.1016/j.neuron.2008.08.012

Araque, A., Parpura, V., Sanzgiri, R.P., Haydon, P.G. (1999). Tripartite synapses: glia, the unacknowledged partner. *Trends in Neurosciences*, 5(1), 208-215.

Bal, A., Bachelot, T., Savasta, M., Manier, M., Verna, J.M., Benabid, A.L., Feuerstein, C. (1994). Evidence for dopamine D2 receptor mRNA expression by striatal astrocytes in culture: in situ hybridization and polymerase chain reaction studies. *Brain Research Molecular Brain Research*, 23, 204-212.

Baldwin, K.T., Eroglu, C. (2017). Molecular mechanisms of astrocyte-induced synaptogensis. *Current Opinion in Neurobiology*, 45, 113-120. http://doi.org/ 10.1016/j.conb.2017.05.006

Balleine, B.W., Delgado, M.R., Hikosaka, O. (2007). The role of the dorsal striatum in reward and decision-making. *J Neurosci*, 27(31), 8161-8165.

Bardin, L., Kleven, M.S., Barret-Grevoz, C., Depoortere, R., Newman-Tancredi, A. (2006). Antipsychotic-like vs cataleptogenic actions in mice of novel antipsychotics having D2 antagonist and 5-HT1A agonist properties. *Neuropsychopharmacology,* 31, 1869-1879. http://doi.org/ 10.1038/sj.npp.1300940

Barr, M.S., Farzan, F., Tran, L.C., Chen, R., Fitzgerald, P.B., Daskalakis, Z.J. (2010). Evidence for excessive frontal evoked gamma oscillatory activity in schizophrenia during working memory. *Schizophrenia Research*, 121, 146-152. http://doi.org/10.1016/j.schres.2010.05.023

Bartzokis, G., Nuechterlein, K.H., Lu, P.H., Gitlin, M., Rogers, S., Mintz, J. (2003). Dysregulated brain development in adult men with schizophrenia: a magnetic resonance imaging study. *Biol Psychiatry*, 53(5), 412-421.

Basar-Eroglu, C., Brand, A., Hildebrant, H., Kedzior, K.K., Mathes, B., Schmiedt, C. (2007). Working memory related gamma oscillations in schizophrenia patients. *International Journal of Psychophysiology*, 64(1), 39-45. http://doi.org/10.1016/j.ijpsycho.2006.07.007

Bell, D.S. (1973). The experimental reproduction of amphetamine psychosis. *Arch Gen Psychiatry*, 29, 35-40.

Belzung, C., Lemoine, M. (2011). Criteria of validity for animal models of psychiatric disorders: focus on anxiety disorders and depression. *Biol Mood Anxiety Disord*, 1, 9.

Benes, F.M., Kwok, E.W., Vincent, S.L., Todtenkopf, M.S. (1998). A reduction of nonpyramidal cells in sector CA2 of schizophrenics and manic depressives. *Biol Psychiatry*, 44(2), 88-97.

Blackwood, D.H.R., Fordyce, A., Walker, M.T., St Clair, D.M., Porteous, D.J., Muir, W.J. (2001). Schizophrenia and affective disorders—cosegregation with a translocation at chromosome 1q42 that directly disrupts brain-expressed genes: clinical and P300 findings in a family. *Am J Hum Genet*, 69(2), 428-433.

Bliss, T.V.P., Collingridge, G.L., Morris, R.G.M. (2014). Synaptic plasticity in health and disease: introduction and overview. *Philos Trans R Soc Lond B Biol Sci*, 369(1633), 20130129. http://doi.org/10.1098/rstb.2013.0129

Bowie, D., Mayer, M.L. (1995). Inward rectification of both AMPA and kainate subtype glutamate receptors generated by polyamine-mediated ion channel block. *Neuron*, 15(2), 453-462.

Boyson, S.J., McGonigle, P., Molinoff, P.B. (1986). Quantitative autoradiographic localization of the D1 and D2 subtypes of dopamine receptors in rat brain. *The Journal of Neuroscience,* 6, 3177-3188.

Bramham, C.R., Wells, D.G. (2007). Dendritic mRNA: transport, translation and function. *Nature Reviews Neuroscience*, 8, 776-789. http://doi.org/ 10.1038/nrn2150

Brown, A.S., Derkits, E.J. (2010). Prenatal infection and schizophrenia: a review of epidemiologic and translational studies. *American Journal of Psychiatry,* 167(3), 261-280. http://doi.org/ 10.1176/appi.ajp.2009.09030361

Buenrostro, J., Wu, B., Chang, H., Greenleaf, W. (2015). ATAC-seq: a method for assaying chromatin accessibility genome-wide. *Curr Protoc Mol Biol*, 109, 21.29.1-21.29.9. http://doi.org/10.1002/0471142727.mb2129s109

Burke, R.E., Fahn, S., Jankovic, J., Marsden, C.D., Lang, A.e., Gollomp, S., Ilson, J. (1982). Tardive dystonia: late-onset and persistent dystonia caused by antipsychotic drugs. *Neurology*, 32(12), 1335-1346.

Buzsaki, G., Draguhn, A. (2004). Neuronal oscillations in cortical networks. *Science*, 304(5679), 1926-1929.

Byrne, P. (2007). Managing the acute psychotic episode. *BMJ*, 334(7595), 686-692. http://doi.org/10.1136/bmj.39148.668160.80

Cahoy, J.D., Emery, B., Kaushal, A., Foo, L.C., Zamanian, J.L, Christopherson, K.S., ... Barres, B.A. (2008). A transcriptome database for astrocytes, neurons, and oligodendrocytes: a new resource for understanding brain development and function. *J Neurosci,* 28(1), 264-78. http://doi.org/ 10.1523/JNEUROSCI.4178-07.2008

Calabresi, P., Picconi, B., Tozzi, A., Ghiglieri, V., Di Filippo, M. (2014). Direct and indirect pathways of basal ganglia: a critical reappraisal. *Nat Neurosci*, 17(8), 1022-1030. http://doi.org/10.1038/nn.3743

Cannon, M., Jones, P.B., Murray, R.M. (2002). Obstetric complications and schizophrenia: historical and meta-analytic review. *Am J Psychiatry,* 159(7), 1080-1092. http://doi.org/10.1176/appi.ajp.159.7.1080

Cannon, T.D., Chung, Y., He, G., Sun, D., Jacobson, A., van Erp, T.G., ... North American Prodrome Longitudinal Study Consortium. (2015). Progressive reduction in cortical thickness as psychosis develops: a multisite longitudinal neuroimaging study of youth at elevated clinical risk. *Biol Psychiatry*, 77(2), 147-157. http://10.1016/j.biopsych.2014.05.023

Cardinal, R.N., Parkinson, J.A., Hall, J., Everitt, B.J. (2002). Emotion and motivation: the role of the amygdala, ventral striatum, and prefrontal cortex. *Neuroscience and Biobehavioral Reviews,* 26(3), 321-352.

Casademont, J., Garrabou, G., Miro, O., Lopez, S., Pons, A., Bernardo, M., Cardellach, F. (2007). Neuroleptic treatment effect on mitochondrial electron transport chain: peripheral blood mononuclear cells analysis in psychotic patients. *Journal of clinical psychopharmacology*, 27, 284-288. http://doi.org/ 10.1097/JCP.0b013e318054753e

Cash-Padgett, T., Jaaro-Peled, H. (2013). DISC1 mouse models as a tool to decipher gene-environment interactions in psychiatric disorders. *Front Behav Neurosci*, 7, 113. http://doi.org/10.3389/fnbeh.2013.00113

Castane, A., Santana, N., Artigas, F. (2015). PCP-based mice models of schizophrenia: differential behavioral neurochemical, and cellular effects of acute and subchronic

treatments. *Psychopharmacology (Berl)*, 232(21-22), 4085-4097. http://doi.org/10.1007/s00213-015-3946-6

Centonze, D., Usiello, A., Costa, C., Picconi, B., Erbs, E., Bernardi, G., ... Calabresi, P. (2004). Chronic haloperidol promotes corticostriatal long-term potentiation by targeting dopamine D2L receptors. *The Journal of Neuroscience*, 24, 8214-8222. http://doi.org/10.1523/JNEUROSCI.1274-04.2004

Cepeda, C., Buchwald, N.A., Levine, M.S. (1993). Neuromodulatory actions of dopamine in the neostriatam are dependent upon the excitatory amino acid receptor subtypes activated. *Proc Natl Acad Sci,* 90, 9576-80.

Cervetto, C., Venturini, A., Passalacqua, M., Guidolin, D., Genedani, S., Fuxe, K., ... Agnati, L.F. (2017). A2A-D2 receptor-receptor interaction modulates gliotransmitter release from striatal astrocyte processes. *Journal of Neurochemistry*, 140, 268-279. http://doi.org/10.1111/jnc.13885

Chan, C.S., Peterson, J.D., Gertler, T.S., Glajch, K.E., Quintana, R.E., Cui, Q., ... Surmeier, D.J. (2012). Strain-specific regulation of striatal phenotype in Drd2-eGFP BAC transgenic mice. *The Journal of Neuroscience,* 32, 9124-9132. http://doi.org/10.1523/JNEUROSCI.0229-12.2012

Chen, E.Y., Tan, C.M., Kou, Y., Duan, Q., Wang, Z., Meirelles, G.V., ... Ma'ayan, A. (2013) Enrichr: interactive and collaborative HTML5 gene list enrichment analysis tool. *BMC Bioinformatics,* 14, 128. https://doi.org/10.1186/1471-2105-14-128

Cho, R.Y., Konecky, O., Carter, C.S. (2006). Impairments in frontal cortical y synchrony and cognitive control in schizophrenia. *Proc Natl Acad Sci U S A*, 103(52), 19878-19883. http://doi.org/10.1073/pnas.0609440103

Choi, J.S., Chon, M.W., Kang, D.H., Jung, M.H., Kwon, J.S. (2009). Gender difference in the prodromal symptoms of first-episode schizophrenia. *J Korean Med Sci*, 24(6), 1083-1088.

Clarke, L.E., Liddelow, S.A., Chakraborty, C., Munch A.E., Heiman, M., Barres, B.A. (2018). Normal aging induces A1-like astrocyte reactivity. *Proc Natl Acad Sci U S A,* 115(8), E1896-E1905. https://doi.org/10.1073/pnas.1800165115

Cornett, E.M., Novitch, M., Kaye, A.D., Kata, V., Kaye, A.M. (2017) Medication-induced tardive dyskinesia: a review and update. *Ochsner J*, 17(2), 162-174.

Coward, D.M. (1992). General pharmacology of clozapine. *Br J Psychiatry Suppl*, 17, 5-11.

Coyle J.T., Tsai G. (2004). The NMDA receptor glycine modulatory site: a therapeutic target for improving cognition and reducing negative symptoms in schizophrenia. *Psychopharmacology,* 174:1, 32-38. http://doi.org/10.1007/s00213-003-1709-2

Crow, T.J. (1980a) Molecular pathology of schizophrenia: more than one disease process? *British Medical Journal*, 280, 66-68.

Cryan, J.F., Mombereau, C. (2004). In search of a depressed mouse: utility of models for studying depression-related behavior in genetically modified mice. *Mol Psychiatry*, 9(4), 326-357. http://doi.org/10.1038/sj.mp.4001457

Curley, A.A., Lewis, D.A. (2012) Cortical basket cell dysfunction in schizophrenia. *Journal of Physiology,* 590(4), 715-724. http://doi.org/10.1113/jphysiol.2011.224659

Dalal, J., Roh, J.H., Maloney, S.E., Akuffo, A., Shah, S., Yuan, H., ... Dougherty, J.D. (2013). Translational profiling of hypocretin neurons identifies candidate molecules for sleep regulation. *Genes Dev*, 27, 565-578. http://doi.org/10.1101/gad.207654.112

Das, B.C., Thapa, P., Karki, R., Das, S., Mahapatra, S. Liu, T.C., ... Evans, T. (2014). Retinoic acid signaling pathways in devleopment and diseases. *Bioorg Med Chem,* 22(2), 673-83. http://doi.org/ 10.1016/j.bmc.2013.11.025

Dazzan, P., Morgan, K.D., Orr, K., Hutchinson, G., Chitnis, X., Suckling, J., ... Murray. R.M. (2005). Different effects of typical and atypical antipsychotics on grey matter in first episode psychosis: the AESOP study. *Neuropsychopharmacology*, 30(4), 765-774. http://doi.org/10.1038/sj.npp.1300603

De la Fuente Revenga, M., Ibi, D., Cuddy, T., Toneatti, R., Kurita, M., Gonzalez-Maeso, J. (2019). Chronic clozapine treatment restrains via HDAC2 the performance of mGlu2 receptor agonism in a rodent model of antipsychotic activity. *Neuropsychopharmacology,* 44, 443-454. https://doi.org/10.1038/s41386-018-0143-4

De Sena, C.A., Degenhardt, F., Strohmaier, J., Lang, M., Weiss, B., Roeth, R., ... Berkel, S. (2017). Investigation of SHANK3 in schizophrenia. *Am J Med Genet B Neuropsychiatr Genet*, 174(4), 390-398. http://doi.org/10.1002/ajmg.b.32528

Deloitterie, D., Ruiz, G., Brocard, J., Schweitzer, A., Roucard, C., Roche, Y., ... Andrieux, A. (2010). Chronic administration of atypical antipsychotics improves behavioral and synaptic defects of STOP null mice. *Psychopharmacology (Berl)*, 208(1), 131-141. http://doi.org/10.1007/s00213-009-1712-3.

Dobin, A., Davis, C.A., Schlesinger, F., Drenkow, J., Zaleski, C., Jha, S., ... Gingeras, T.R. (2013). STAR: ultrafast universal RNA-seq aligner. *Bioinformatics*, 29, 15-21. http://doi.org/10.1093/bioinformatics/bts635

Donevan, S.D., Rogawski, MA. (1995). Intracellular polyamines mediate inward rectification of Ca^{2+}-permeable a-amino-3-hydroxy-5-methyl-4-isoxazolepropionic acid receptors. *Proc Natl Acad Sci U S A*, 92(20), 9298-9302.

Doyle, J.P., Dougherty, J.D., Heiman, M., Schmidt, E.F., Stevens, T.R., Ma, G., ... Heintz, N. (2008). Application of a translational profiling approach for the comparative analysis of CNS cell types. *Cell,* 135(4), 749-762. http://doi.org/10.1016/j.cell.2008.10.029

Duncan, G.E., Moy, S.S., Lieberman, J.A., Koller, B.H. (2006). Typical and atypical antipsychotic drug effects on locomotor hyperactivity and deficits in sensorimotor gating in a genetic model of NMDA receptor hypofunction. *Pharmacol Biochem Behav*, 85(3), 481-491.

Erlenmeyer-Kimling, L., Rock, D., Roberts, S.A., Janal, M., Kestenbaum, C., Cornblatt, B., ... Gottesman, I.I. (2000). Attention, memory, and motor skills as childhood predictors of schizophrenia-related psychoses: the New York High-Risk Project. *American Journal of Psychiatry,* 157(9), 16-22. http://doi.org/10.1176/appi.ajp.157.9.1416

Fatemi, S.H., Folsom, T.D., Reutiman, T.J., Novak, J., Engel, R.H. (2011). Comparative gene expression study of the chronic exposure to clozapine and haloperidol in rat frontal cortex. *Schizophrenia Research*, 134(2-3), 211-218. https://doi.org/10.1016/j.schres.2011.11.013

Feifel, D., Shilling, P.D. (2010). Promise and pitfalls of animal models of schizophrenia. *Curr Psychiatry Rep*, 12(4), 327-334. http://doi.org/10.1007/s11920-010-0122-x

Ferrarelli, F., Tononi, G. (2011). The thalamic reticular nucleus and schizophrenia. *Schizophr Bull*, 37(2), 306-315. http://doi.org/10.1093/schbul/sbq142

Ferrario, C.R., Loweth, J.A., Milovanovic, M., Ford, K.A., Galinanes, G.L., Heng, L.J., ... Wolf, M.E. (2011). Alterations in AMPA receptor subunits and TARPs in the rat nucleus accumbens related to the formation of Ca2+-permeable AMPA receptors during the incubation of cocaine craving. *Neuropharmacology,* 61, 1141-1151. http://doi.org/10.1016/j.neuropharm.2011.01.021

Fornito, A., Harrison, B.J., Goodby, E., Dean, A., Ooi, C., Nathan, P.J., ... Bullmore, E.T. (2013). Functional dysconnectivity of corticostriatal circuitry as a risk phenotype for psychosis. *JAMA Psychiatry,* 70(11), 1143-1151. http://doi.org/10.1001/jamapsychiatry.2013.1976

Franklin, T.B., Silva, B.A., Perova, Z., Marrone, L., Masferrer, M.E., Zhan, Y., ... Gross, T.C. (2017). Prefrontal cortical control of a brainstem social behavior circuit. *Nat Neurosci*, 20(2), 260-270. http://doi.org/10.1038/nn.4470

Fromer, M., Pocklington, A.J., Kavanagh, D.H., Williams, H.J., Dwyer, S., Gormley, P., ... O'Donovan, M.C. (2014). De novo mutations in schizophrenia implicate synaptic networks. *Nature,* 506, 179-184. http://doi.org/10.1038/nature12929

Gauthier, J., Champagne, N., Lafreniere, R.G., Xiong, L., Spiegelman, D., Brustein, E., ... S2D Team. (2010). De novo mutations in the gene encoding the synaptic scaffolding protein SHANK3 in patients ascertained for schizophrenia. *Proc Natl Acad Sci U S A,* 107(17), 7863-7868. http://doi.org/10.1073/pnas.0906232107

Girgenti, M.J., Nisenbaum, L.K., Bymaster, F., Terwilliger, R., Duman, R.S., Newton, S.S. (2010). Antipsychotic-induced gene regulation in multiple brainr egions. *J Neurochem,* 113(1), 175-187. http://doi.org/10.1111/j.1471-4159.2010.06585.x

Glantz, L.A., Lewis, D.A. (2000). Decreased dendritic spine density on prefrontal cortical pyramidal neurons in schizophrenia. *Arch Gen Psychiatry,* 57(1), 65-73.

Glausier, J.R., Lewis, D.A. (2013). Dendritic spine pathology in schizophrenia. *Neuroscience,* 251, 90-107. http://doi.org/10.1016/j.neuroscience.2012.04.044

Gokce, O., Stanley, G.M., Treutlein, B., Neff, N.F., Camp, J.G., Malenka, R.C., ... Quake, S.R. (2016). Cellular taxonomy of the mouse striatum as revealed by single-cell RNA-seq. *Cell Rep,* 16(4), 1126-1137. http://doi.org/10.1016/j.celrep.2016.06.059

Gonzalez-Burgos, G., Fish, K.N., Lewis, D. (2011). GABA neuron alterations, cortical circuit dysfunction and cognitive deficits in schizophrenia. *Neural Plasticity,* 2011, http://doi.org/10.1155/2011/723184

Graziane, N.M., Sun, S., Wright, W.J., Jang, D., Liu, Z., Huang, Y.H., ... Dong, Y. (2016) Opposing mechanisms mediate morphine- and cocaine-induced generation of silent synapses. *Nature Neuroscience,* 19(7), 915-925. http://doi.org/10.1038/nn.4313

Greif G.J., Lin Y.J., Liu J.C., Freedman J.E. (1995). Doapmine-modulated potassium channels on rat striatal neurons: specific activation and cellular expression. *J Neurosci,* 15(6), 4533-44.

Griffith, J.D., Oates, J.A., Cavanaugh, J. (1968). Paranoid episodes induced by drugs. *J Am Med Assoc,* 205(39).

Grooms, S.Y., Noh, K.M., Regis, R., Bassell, G.J., Bryan, M.K., Carroll, R.C., Zukin, R.S. (2006). Activity bidirectionally regulates AMPA receptor mRNA abundance in dendrites of hippocampal neurons. *J Neurosci,* 26(32), 8339-8351. http://doi.org/10.1523/JNEUROSCI.0472-06.2006

Grueter, B.A., Brasnjo, G., Malenka, R.C. (2010). Postsynaptic TRPV1 triggers cell type-specific long-term depression in the nucleus accumbens. Nature Neuroscience, 13(12), 1519-1525. http://doi.org/10.1038/nn.2685

Hakansson K., Galdi S., Hendrick J., Synder G., Greengard P., Fisone G. (2006). Regulation of phosphorylation of the GluR1 AMPA receptor by dopamine D2 receptors. *J Neurochem,* 96(2), 482-8. http://doi.org/10.1111/j.1471-4159.2005.03558.x

Halassa, M.M., Fellin, T., Haydon, P.G. (2007) The tripartite synapse: roles for gliotransmission in health and disease. *Trends Mol Med*, 13(2), 54-63. http://doi.org/10.1016/j.molmed.2006.12.005

Hallett, P.J., Spoelgen, R., Hyman, B.T., Standaert, D.G., Dunah, A.W. (2006). Dopamine D1 activation potentiates striatal NMDA receptors by tyrosine phosphorylation-dependent subunit trafficking. *J Neurosci,* 26(17), 4690-4700. http://doi.org/10.1523/JNEUROSCI.0792-06.2006

Han, K.S., Cooke, S.F., Xu, W. (2017). Experience-dependent equilibration of AMPAR-mediated synaptic transmission during the critical period. *Cell Rep,* 18, 892-904. http://doi.org/10.1016/j.celrep.2016.12.084

Harrison, P.J., Weinberger, D.R. (2005). Schizophrenia genes, gene expression, and neuropathology: on the matter of their convergence. *Mol Psychiatry*, 10(1), 40-68. http://doi.org/10.1038/sj.mp.4001558

Harrison, P.J., Law, A.J. (2006). Neuregulin 1 and schizophrenia: genetics, gene expression, and neurobiology. *Biol Psychiatry*, 60(2), 132-140. http://doi.org/10.1016/j.biopsych.2005.11.002

Hasan, A., Falkai, P., Wobrock, T., Lieberman, J., Glenthoj, B., Gattaz, W.F., ... World Federation of Societies of Biological Psychiatry Task force on Treatment Guidelines For Schizophrenia. (2013). World federation of societies of biological psychiatry (WFSbp) guidelines for biological treatment of schizophrenia, part 2: update 2012 on the long-term treatment of schizophrenia and management of antipsychotic induced side effects. *World J Biol Psychiatry,* 14(1), 2-44. http://doi.org/10.3109/15622975.2012.739708

Hasan, A., Falkai, P., Wobrock, T., Lieberman, J., Glenthoj, B., Gattaz, W.F., ... World Federation of Societies of Biological Psychiatry Task force on Treatment Guidelines For Schizophrenia. (2012) World federation of societies of biological psychiatry (WFSbp) guidelines for biological treatment of schizophrenia, part 1: update 2012 on the acute treatment of schizophrenia and the management of treatment resistance. *World J Biol Psychiatry,* 13(5), 318-378. http://doi.org/10.3109/15622975.2012.696143

Hayashi-Takagi, A., Takaki, M., Graziane, N., Seshadri, S., Murdoch, H., Dunlop, A.J., ... Sawa, A. (2010). Disrupted-in-Schizophrenia 1 (DISC1) regulates spines of the glutamate synapse via Rac1. *Nat Neurosci*, 13(3), 327-32. http://doi.org/10.1038/nn.2487

Hearing, M.C., Jedynak, J., Ebner, S.R., Ingebretson, A., Asp, A.J., Fischer, R.A., ... Thomas, M.J. (2016) Reversal of morphine-induced cell-type-specific synaptic plasticity

in the nucleus accumbens shell blocks reinstatement. *Proc Natl Acad Sci U S A*, 113(3), 757-762. http://doi.org/10.1073/pnas.1519248113

Henderson, D.C., Cagliero, E., Copeland, P.M., Borba, C.P., Evins, A.E., Hayden, D., ... Goff, D.C. (2005). Glucose metabolism in patients with schizophrenia treated with antipsychotic agents: a frequently sampled intravenous glucose tolerance test and minimal model analysis. *Arch Gen Psychiatry,* 62(1), 19-28. http://doi.org/10.1001/archpsyc.62.1.19

Hensch, T.K. (2005). Critical period plasticity in local cortical circuits. *Nat Rev Neurosci*, 6(11), 877-888. http://doi.org/10.1038/nrn1787

Heiman, M., Kulicke, R., Fenster, R.J., Greengard, P., and Heintz, N. (2014) Cell type-specific mRNA purification by translating ribosome affinity purification (TRAP). *Nat Protoc*, 9(6), 1282-1291. http://doi.org/10.1038/nprot.2014.085

Heiman, M., Schaefer, A., Gong, S., Peterson, J.D., Day, M., Ramsey, K.E., ... Heintz, N. A translational profiling approach for the molecular characterization of CNS cell types. *Cell,* 135(4), (2008) 738-748. http://doi.org/10.1016/j.cell.2008.10.028

Heinrichs, R.W., and Zakzanis, K.K. (1998) Neurocognitive deficit in schizophrenia: A quantitative review of the evidence. *Neuropsychology,* 12(3), 426-445.

Hershenberg, R., Gros, D.F., Brawman-Mintzer, O. (2014). Role of atypical antipsychotics in the treatment of generalized anxiety disorder. *CNS Drugs*, 28(6), 519-533. http://doi.org/10.1007/s40263-014-0162-6

Ho, N.F., Iglesias, J.E., Sum, M.Y., Kuswanto, C.N., Sitoh, Y.Y., De Souza, J., ... Holt, D.J. (2017). Progression from selective to general involvement of hippocampal subfields in schizophrenia. *Mol Psychiatry*, 22(1), 142-152. http://doi.org/10.1038/mp.2016.4

Ho, V.M., Lee, J.A., Martin, K.C. (2011). The Cell Biology of Synaptic Plasticity. *Science*, 334(6056), 623-628. http://doi.org/10.1126/science.1209236

Hollmann, M., Hartley, M., Heinemann, S. (1991). Ca2+ permeability of KA-AMPA—gated glutamate receptor channels depends on subunit composition. *Science,* 252(5007), 851-853.

Horton, L.E., Tarbox, S.I., Olino, T.M., Haas, G.L. (2015). Trajectories of premorbid childhood and adolescent functioning in schizophrenia-spectrum psychoses: a first-episode study. *Psychiatry Res*, 227(0), 339-346. http://doi.org/10.1016/j.psychres.2015.02.013

Howes, O.D., Kapur, S. (2009). The dopamine hypothesis of schizophrenia: version III – the final common pathway. *Schiozphr Bull,* 35(3), 549-562. https://doi.org/10.1093/schbul/sbp006

Huckins, L.M., Dobbyn, A., Ruderfer, D.M., Hoffman, G., Wang, W., Pardinas, A.F., ... Stahl, E.A. (2019) Gene expression imputation across multiple brain regions provides insights into schizophrenia risk. *Nature Genetics*. https://doi.org/10.1038/s41588-019-0364-4

Isaac, J.T.R., Nicoll, R.A., Malenka, R.C. (1995). Evidence for silent synapses: implications for the expression of LTP. *Neuron*, 15(2), 427-434.

Isaac, J.T., Ashby, M.C., McBain, C.J. (2007). The role of the GluR2 subunit in AMPA receptor function and synaptic plasticity. *Neuron*, 54(6), 859-71. http://doi.org/10.1016/j.neuron.2007.06.001

Ito, R., Robbins, T.W., Pennartz, C.M., Everitt, B.J. (2008). Functional interaction between the hippocampus and nucleus accumbens shell is necessary for the acquisition of appetitive spatial context conditioning. *J Neurosci,* 28(27), 6950-6959. http://doi.org/10.1523/JNEUROSCI.1615-08.2008

Javitt D.C., Zukin, S.R. (1991). Recent advances in the phencyclidine model of schizophrenia. *Am J Psychiatry*, 148(10), 1301-1308. http://doi.org/10.1176/ajp.148.10.1301

Jones, C.A., Watson, D.J.G., Fone, K.C.F. (2011). Animal models of schizophrenia. *Br J Pharmacol*, 164(4), 1162-1194. http://doi.org/10.1111/j.1476-5381.2011.01386.x

Jones, P.B., Barnes, T.R.E., Davies, L., Dunn, G., Lloyd, H., Hayhurst, K.P., ... Lewis, S.W. (2006). Randomized controlled trial of the effect on quality of life of second- vs first-generation antipsychotic drugs in schizophrenia. *Arch Gen Psychiatry,* 63(10), 1079-1087. http://doi.org/10.1001/archpsyc.63.10.1079

Ju, W., Morishita, W., Tsui, J., Gaietta, G., Derrinck, T.J., Adams, S.R., ... Malenka, R.C. (2004). Activity-dependent regulation of dendritic synthesis and trafficking of AMPA receptors. *Nat Neurosci,* 7(3), 244-253. http://doi.org/10.1038/nn1189

Kanehisa, M., Goto, S. (2000). KEGG: Kyoto Encyclopedia of Genes and Genomes. *Nucleic Acids Res*, 28(1), 27-30.

Kay, S.R., Fiszbein, A., Opler, L.A. (1987). The positive and negative syndrome scale (PANSS) for schizophrenia. *Schizophr Bull* 13(2), 261-276.

Kerchner, G.A., Nicoll, R.A. (2008). Silent synapses and the emergence of a postsynaptic mechanism for LTP. *Nat Rev Neurosci*, 9(11), 813-825. http://doi.org/10.1038/nrn2501

Kerns J.M., Sierens D.K., Kao L.C., Klawans H.L., Carvey P.M. (1992). Synaptic plasticity in the rat striatum following chronic haloperidol treatment. *Clin Neuropharmacol,* 15(6), 488-500.

Keshavan, M.S., Diwadkar, V.A., Montrose, D.M., Stanley, J.A., Pettegrew, J.W. (2004). Premorbid characterization in schizophrenia: the Pittsburgh High Risk Study. *World Psychiatry,* 3(3) 163-168.

Kestler, L.P., Walker, E., Vega, E.M. (2001). Dopamine receptors in the brains of schizophrenia patients: a meta-analysis of the findings. *Behav Pharmacol*, 12(5), 355-371.

King, B.H., Lord, C. (2011). Is schizophrenia on the autism spectrum? *Brain Res*, 1380, 34-41. http://doi.org/10.1016/j.brainres.2010.11.031

Knable, M.B., Weinberger, D.R. (1997). Dopamine, the prefrontal cortex and schizophrenia. *J Psychopharmacol*, 11(2), 123-131. http://doi.org/10.1177/026988119701100205

Koike, M., Iino, M., Ozawa, S. (1997). Blocking effect of 1-naphthyl acetyl spermine on Ca(2+)-permeable AMPA receptors in cultured rat hippocampal neurons. *Neurosci Res,* 29(1), 27-36.

Konradi, C., Yang, C.K., Zimmerman, E.I., Lohmann, K.M., Gresch, P., Pantazopoulos, H., ... Heckers, S. (2011). Hippocampal interneurons are abnormal in schizophrenia. *Schizophr Res*, 131(1-3), 165-173. http://doi.org/10.1016/j.schres.2011.06.007

Koro, C.E., Fedder, D.O., L'Italien G.J., Weiss S., Magder L.S., Kreyenbuhl J., ... Buchanan R.W. (2002). An assessment of the independent effects of olanzapine and risperidone exposure on the risk of hyperlipidemia in schizophrenic patients. *Arch Gen Psychiatry,* 59(11), 1021-6.

Kozorovitskiy, Y., Saunders, A., Johnson, C.A., Lowell, B.B., Sabatini, B.L. (2012). Recurrent network activity drives striatal synaptogenesis. *Nature,* 485(7400), 646-650. http://doi.org/10.1038/nature11052

Kravitz, A.V., Freeze, B.S., Parker, P.R.L., Kay, K., Thwin, M.T., Deisseroth, K., Kreitzer, A.C. (2019). Regulation of parkinsonian motor behaviours by optogenetic control of basal ganglia circuitry. *Nature,* 466(7306), 622-626. http://doi.org/10.1038/nature09159

Kreitzer, A.C., Malenka, R.C. (2008). Striatal plasticity and basal ganglia circuit function. *Neuron*, 60(4), 543-554.

Krishnna, G., Hetrick, W., Brenner, C., Shekhar, A., Steffen, A., O'Donnell, B. (2009). Steady state and induced auditory gamma deficits in schizophrenia. *Neuroimage*, 47(1), 1711-1719.

Kubicki, M., McCarley, R.W., Shenton, M.E. (2005). Evidence for white matter abnormalities in schizophrenia. *Curr Opin Psychiatry*, 18(2), 121-134.

Kuhn, S., Musso, F., Mobascher, A., Warbrick, T., Winterer, G., Gallinat, J. (2012). Hippocampal subfields predict positive symptoms in schizophrenia: first evidence from brain morphometry. *Transl Psychiatry*, 2(6), e127. http://doi.org/10.1038/tp.2012.51.

Kuleshov, M.V., Jones, M.R., Rouillard, A.D., Fernandez, N.F., Duan, Q., Wang, Z., ... Ma'ayan, A. (2016). Enrichr: a comprehensive gene set enrichment analysis web server 2016 update. *Nucleic Acids Res,* 44(W1), W90-W97. http://doi.org/10.1093/nar/gkw377

Kulkarni, S.C., Ninan, I. (2000). Dopamine D4 receptors and development of newer antipsychotic drugs. *Fundam Clin Pharmacol*, 14(6), 529-539.

Kurita, M., Holloway, T., Aintzane, G.B., Kozlenkov, A., Friedman, A.K., Moreno, J.L. ... Gonzalez-Maeso, J. (2012). HDAC2 regualtes atypical antipsychotic responses through the modulation of mGlu2 promoter activity. *Nature Neuroscience*, 15(9), 1245-1254. http://doi.org/10.1038/nn.3181

Kwon, J., O'Donnell B., Wallenstein, G., Green, R., Hirayasu, Y., Nestor, P., ... McCarley, R. (1999). Gamma frequency-range abnormalities to auditory stimulation in schizophrenia. *Arch Gen Psychiatry*, 56(11), 1011-1005.

Lahti, A.C., Koffel, B., LaPorte, D., Tamminga, C.A. (1995). Subanesthetic doses of ketamine stimulate psychosis in schizophrenia. *Neuropsychopharmacology*, 13(1), 9-19. http://doi.org/10.1016/0893-133X(94)00131-I

Lederbogen, F., Kirsch, P., Haddad, L., Streit, F., Tost, H., Schuch, P., ... Meyer-Lindenberg, A. (2011). City living and urban upbringing affect neural social stress processing in humans. *Nature,* 474(7352), 498-501. http://doi.org/10.1038/nature10190

Lee B.R., Ma, Y.Y., Huang, Y.H., Wang, X., Otaka, M., Ishikawa, M., ... Dong, Y. (2013). Maturation of silent synapses in amygdala-accumbens projection contributes to incubation of cocaine craving. *Nat Neurosci,* 16(11), 1644-1651. http://doi.org/10.1038/nn.3533

Lehman, A.F., Lieberman, J.A., Dixon, L.B., McGlashan, T.H., Miller, A.L., Perkins, D.O, Kreyenbuhl, J. (2004). Practice guideline for the treatment of patients with schizophrenia. *Am J Psychiatry,* 161(2 Suppl), 1-56.

Lein, E.S., Hawrylycz, M.J., Ao, N., Ayres, M., Bensinger, A., Bernard, A., ... Jones, A.R. (2007). Genome-wide atlas of gene expression in the adult mouse brain. *Nature*, 445, 168-176. http://doi.org/10.1038/nature05453

Lennertz, L., Wagner, M., Wolwer, W., Schuhmacher, A., Frommann, I., Berning, J., ... Mossner, R. (2012). A promoter variant of SHANK1 affects auditory working memory in

schizophrenia patients and in subjects clinically at risk for psychosis. *Eur Arch Psychiatry Clin Neurosci*, 262(2), 117-124. http://doi.org/10.1007/s00406-011-0233-3

Lerer, B., Segman, R.H., Fangerau, H., Daly, A.K., Basile, V.S., Cavallaro, R., ... Macciardi, F. (2002). Pharmacogenetics of tardive dyskinesia: combined analysis of 780 patients supports association with dopamine D3 receptor gene Ser9Gly polymorphism. *Neuropsychopharmacology*, 27(1), 105-119.

Levey, A.I., Hersch, S.M., Rye, D.B., Sunahara, R.K., Niznik, H.B., Kitt, C.A., ... Ciliax, B.J. (1993). Localization of D1 and D2 dopamine receptors in brain with subtype-specific antibodies. *Proc Natl Acad Sci U S A*, 90(19), 8861-8865.

Liao, D., Hessler, N.A., Maliow, R. (1995). Activation of postsynaptically silent synapses during pairing-induced LTP in CA1 region of hippocampal slice. *Nature*, 375(6530), 400-404. http://doi.org/10.1038/375400a0

Lichtenstein, P., Yip, B.H., Bjork, C., Pawitan, Y., Cannon T.D., Sullivan P.F., Hultman C.M. (2009). Common genetic determinants of schizophrenia and bipolar disorder in Swedish families: a population-based study. *Lancet,* 272(9659), 234-9. http://doi.org/10.1016/S0140-6736(09)60072-6

Liddelow, S.A., Guttenplan, K.A., Clarke, L.E., Bennett, F.C., Bohlen, C.J., Schirmer, L., ... Barres, B.A. (2017). Neurotoxic reactive astrocytes are induced by activated microglia. *Nature,* 541(7638), (2017) 481-487. http://doi.org/10.1038/nature21029

Liddelow, S.A., Barres, B.A. (2017) Reactive astrocytes: production, function, and therapeutic potential. *Immunity,* 46(6), 957-967. http://doi.org/10.1016/j.immuni.2017.06.006

Lieberman, J.A., Stroup, T.S., McEvoy, J.P., Swartz, M.S., Rosenheck, R.A., Perkins, D.O., ... Hsiao, J.K. (2005). Effectiveness of antipsychotic drugs in patients with chronic schizophrenia. *N Engl J Med,* 353(12), 1209-1223. http://doi.org/10.1056/NEJMoa051688

Lieberman, J.A., Girgis, R.R., Brucato, G., Moore, H., Provenzano, F., Kegeles, L., ... Small, S.A. (2018). Hippocampal dysfunction in the pathophysiology of schizophrenia: a selective review and hypothesis for early detection and intervention. *Mol Psychiatry*, 23(8), 1764-1772. http://doi.org/10.1038/mp.2017.249

Lisman, J.E., Coyle, J.T., Green, R.W., Javitt, D.C., Benes, F.M., Heckers, S., Grace, A.A. (2008). Circuit-based framekwork for understanding neurotransmitter and risk gene interactions in schizophrenia. *Trends Neurosci,* 31(5), 234-242. http://doi.org/10.1016/j.tins.2008.02.005

Liu, M., Lewis, L.D., Shi, R., Brown, E.N., Xu, W. (2014). Differential requirement for NMDAR activity in SAP97beta-mediated regulation of the number and strength of

glutamatergic AMPAR-containing synapses. *J Neurophysiol,* 111(3), 648-658. http://doi.org/10.1152/jn.00262.2013

Lodge, D.J. (2014). The MAM rodent model of schizophrenia. *Curr Protoc Neurosci,* 63(1), 9.43.1-9.43.7. http://doi.org/10.1002/0471142301.ns0943s63

Lun, M.P., Monuki, E.S., Lehtinen, M.K. (2015). Development and functions of the choroid plexus-cerebrospinal fluid system. *Nat Rev Neurosci,* 16(8), 445-57. http://doi.org/10.1038/nrn3921

Maas, J.W., Bowden, C.L., Miller, A.L., Javors, M.A., Funderburg, L.G., Berman, N., Weintraub, S.T. (1997). Schizophrenia, psychosis, and cerebral spinal fluid homovanillic acid concentrations. *Schizophr Bull,* 23(1), 147-154.

Malenka, R.C., Bear, M.F. (2004). LTP and LTD: an embarrassment of riches. *Neuron,* 44(1), 5-21.

Malhotra, A.K., Pinals, D.A., Adler, C.M., Elman, I., Clifton, A., Pckar, D., Breier, A. (1997). Ketamine-induced exacerbation of psychotic symptoms and cognitive impairment in neuroleptic-free schizophrenics. *Neuropsychopharmacology,* 17(3), 141-150.

Man, H.Y. (2011). GluA2-lacking, calcium-permeable AMPA receptors – inducers of plasticity? *Curr Opin Neurobiol,* 21(2), 291-298. http://doi.org/10.1016/j.conb.2011.01.001

Marcotte, E.R., Pearson, D.M., Srivastava, L.K. (2001). Animal models of schizophrenia: a critical review. *J Psychiatry Neurosci,* 26(5), 395-410.

Marshall, C.R., Howrigan, D.P., Merico, D., Thiruvahindrapuram, B., Wu, W., Greer, D.S., ... CNV & Schizophrenia Working Groups of the Psychiatric Genomics Consortium. (2017). Contribution of copy number variants to schizophrenia from a genome-wide study of 41,321 subjects. *Nat Genet,* 49(1), 27-35. http://doi.org/10.1038/ng.3725

McCollum, L.A., Walker, C.K., Roche, J.K., Roberts, R.C. (2015). Elevated excitatory input to the nucleus accumbens in schizophrenia: a postmortem ultrastructural study. *Schizophrenia Bulletin,* 41(5) (2015) 1123-1132. http://doi.org/10.1093/schbul/sbv030

McCutcheon, J.E., Wang, X., Tseng, K.Y., Wolf, M.E., Marinelli, M. (2011). Calcium-permeable AMPA receptors are present in nucleus accumbens synapses after prolonged withdrawal from cocaine self-administration but not experimenter-administered cocaine. *J Neurosci,* 31(15), 5737-5743. http://doi.org/10.1523/JNEUROSCI.0350-11.2011

McEvoy, J.P. (2007). The costs of schizophrenia. *J Clin Psychiatry,* 68 (Suppl 14), 4-7.

Meader-Woodruff, J.H., Mansour, A., Bunzow, J.R., Van Tol, H.H.M., Watson Jr, S.J., Civelli, O. (1989). Distribution of D2 dopamine receptor mRNA in rat brain. *Proc Natl Acad Sci U S A,* 86(19), 7625-7628.

Mednick, S.A., Machon, R.A., Huttunen, M.O., Bonett, D. (1988). Adult schizophrenia following prenatal exposure to an influenza epidemic. *Arch Gen Psychiatry*, 45(2), 189-192.

Mei, L., Xiong, W.C. (2008). Neuregulin 1 in neural development, synaptic plasticity and schizophrenia. *Nat Rev Neurosci,* 9(6), 437-452. http://doi.org/10.1038/nrn2392

Meltzer, H.Y. (1992). Treatment of the neuroleptic-nonresponsive schizophrenic patient. *Schizophr Bull,* 18(3), 515-542.

Meshul, C.K., Casey, D.E. (1989). Regional, reversible ultrastructural changes in rat brain with chronic neuroleptic treatment. *Brain Res,* 489(2), 338-346.

Miayamoto, S., Duncan, G.E., Marx, C.E., Lieberman, J.A. (2005). Treatments for schizophrenia: a critical review of pharmacology and mechanisms of action of antipsychotic drugs. *Mol Psychiatry,* 10(1), 79-104. http://doi.org/10.1038/sj.mp.4001556

Middleton, F.A., Mirnics, K., Pierri, J.N., Lewis, D.A., Levitt, P. (2002). Gene expression profiling reveals alterations of specific metabolic pathways in schizophrenia. *J Neurosci*, 22(7), 2718-2729. http://doi.org/20026209

Mignini, F., Bronzetti, E., Felici, L., Ricci, A., Sabbatini, M., Tayebati, S.K., Amenta, F. (2008). Dopamine receptor immunohistochemistry in the rat choroid plexus. *Autonomic & Autacoid Pharmacology,* 20(5-6), 325-332. https://doi.org/10.1046/j.1365-2680.2000.00198.x

Mirnics, K., Middleton, F.A., Marquez, A., Lewis, D.A., Levitt, P. (2000). Molecular characterization of schizophrenia viewed by microarray analysis of gene expression in prefrontal cortex. *Neuron*, 28(1), 53-67.

Mishina, M., Sakimura, K., Mori, H., Kushiya, E., Harabayashi, M., Uchino, S., Nagahari, K. (1991). A single amino acid residue determines the Ca2+ permeability of AMPA-selective glutamate receptor channels. *Biochem Biophys Res Commun,* 180(2), 813-821.

Moine, C.L., Normand, E., Guitteny, A.F., Fouque, B., Teoule, R., Bloch, B. (1990). Dopamine receptor gene expression by enkephalin neurons in rat forebrain. *Proc Natl Acad Sci,* 87(1), 230-234.

Moreno, J.L., Holloway, T., Umali, A., Rayannavar, V., Sealfon, S.C., Gonzalez-Maeso, J. (2013). Persistent effects of chronic clozapine on the cellular and behavioral responses

to LSD in mice. *Psychopharmacology(Berl),* 225(1), 217-26. http://doi.org/10.1007/s00213-012-2809-7

Morris, R.W., Vercammen, A., Lenroot, R., Moore, L, Langton, J.M., Short, B., ... Weikert, T.W. (2012). Disambiguating ventral striatum fMRI-related BOLD signal during reward prediction in schizophrenia. *Mol Psychiatry,* 17(3), 280-289. http://doi.org/10.1038/mp.2011.75

Nguyen, T.V., Kosofsky, B.E., Birnbaum, R., Cohen, B.M., Hyman, S.E. (1992). Differential expression of c-Fos and Zif268 in rat striatum after haloperidol, clozapine, and amphetamine. *Proc. Natl. Acad. Sci.*, 89, 4270-4274.

Nieto-Sampredo, M., Hoff, S.F., Cotman, C.W. (1982). Perforated postsynaptic densities: probable intermediates in synapse turnover. *Proc Natl Acad Sci U S A*, 79(18), 5718-5722.

Nimchinsky, E.A., Sabatini, B.L., Svoboda, K. (2002). Structure and function of dendritic spines. *Annual Review of Physiology*, 64, 313-353. https://doi.org/10.1146/annurev.physiol.64.081501.160008

O'Connell, K.S., McGregor, N.W., Lochner, C., Emsley, R., Warnich, L. (2018). The genetic architecture of schizophrenia, bipolar disorder, obsessive-compulsive disorder and autism spectrum disorder. *Mol Cell Neurosci*, 88, 300-307. http://doi.org/10.1016/j.mcn.2018.02.010

O'Tuathaigh, C.M., Desbonnet, L., Waddington, J.L. (2012). Mutant mouse odels in evaluating novel approaches to antipsychotic treatment. *Hand Exp Pharmacol*, 2012(213), 113-145. http://doi.org/10.1007/978-3-642-25758-2_5

Ouagazzal, A.M., Jenck, F., Moreau, J.L. (2001). Drug-induced potentiation of prepulse inhibition of acoustic startle reflex in mice: a model for detecting antipsychotic activity? *Psychopharmacology (Berl)*, 156(2-3), 273-283.

Pachernegg, S., Munster, Y., Muth-Kohne, E., Fuhrmann, G., Hollmann, M. (2015). GluA2 is rapidly edited at the Q/R site during neural differentiation in vitro. *Front Cell Neurosci,* 9(69). doi: http://doi.org/10.3389/fncel.2015.00069

Park, S.W., Lee, C.H., Cho, H.Y., Seo, M.K., Lee, J.G., Seol, W., ... Kim, Y.H. (2013). Effects of antipsychotic drugs on the expression of synaptic proteins and dendritic outgrowth in hippocampal neuronal cultures. *Synapse,* 65(5), 224-34. http://doi.org/10.1002/syn.21634

Pascoli, V., Terrier, J., Espallergues, J., Valjent, E., O'Connor, E.C., Luscher, C. (2014). Contrasting forms of cocaine-evoked plasticity control components of relapse. *Nature,* 509(7501), 459-463. http://10.1038/nature13257

PDR Network LLC. (2016). PDR drug information handbook (Montvale, NJ: PDR, LLC).

Perry, T.L., Kish, S.J., Buchanan, J., Hansen, S. (1979). Gamma-aminobutyric-acid deficiency in brain of schizophrenic patients. *Lancet,* 1(8110), 237-239.

Phillips, M.A., Colonnese, M.T., Goldberg, J., Lewis, L.D., Brown, E.N., Constantine-Paton, M. (2011). A synaptic strategy for consolidation of convergent visuotopic maps. *Neuron,* 71(4), 710-724. http://doi.org/10.1016/j.neuron.2011.06.023

Pinero, J., Queralt-Rosinach, N., Bravo, A., Deu-Pons, J., Bauer-Mehren, A., Baron, M., ... Furlong, L.I. (2015). DisGeNET: a discovery platform for the dynamical exploration of human diseases and their genes. *Database(Oxford),* bav024. http://doi.org/10.1093/database/bav028

Piwecka, M. Glazar, P., Hernandez-Miranda L.R., Memczak, S., Wolf, S.A., Rybak-Wolf, A., ... Rajewsky, N. (2017). Loss of a mammalian circular RNA locus causes miRNA deregulation and affects brain function. *Science,* 357(6357), pii: eaam8526. http://doi.org/10.1126/science.aam8526

Plotkin, J.L., Day, M., Surmeier, D.J. (2011). Synaptically driven state transitions in distal dendrites of striatal spiny neurons. *Nat Neurosci,* 14(7), 881-888. http://doi.org/10.1038/nn.2848

Porsolt, R.D., Anton, G., Blavet, N., Jalfre, M. (1978). Behavioural despair in rats: a new model sensitive to antidepressant treatments. *Eur J Pharmacology,* 47(4), 379-391.

Powell, C.M., Miyakawa, T. (2006). Schizophrenia-relevant behavioral testing in rodent models: a uniquely human disorder? *Biol Psychiatry*, 59(12), 1198-1207. http://doi.org/10.1016/j.biopsych.2006.05.008

Pratt, J., Winchester, C., Dawson, N., Morris, B. (2012). Advancing schizophrenia drug discover: optimizing rodent models to bridge the translational gap. *Nature Reviews Drug Discovery*, 11, 560-579.

Ray, M.T., Weickert, S., Webster, M.J. (2014). Decreased BDNF and TrkB mRNA expression in multiple cortical areas of patients with schizophrenia and mood disorders. *Transl Psychiatry*, 6(4), e389. http://doi.org/10.1038/tp.2014.26

Richtand, N.M., Welge, J.A., Logue, A.D., Keck, P.E. Jr., Strakowski, S.M., McNamara, R.K. (2008). Role of serotonin and dopamine receptor binding in antipsychotic efficacy. *Prog Brain Res*, 172, 155-175. http://doi.org/10.1016/S0079-6123(08)00908-4

Rigdon, G.C., Kaido, Viik. (1991). Prepulse inhibition as a screening test for potential antipsychotics. *Drug Development Research*, 23, 91-99.

Roberts, R.C., Gaither, L.A., Gao, X.M., Kashyap, S.M., Tamminga, C.A. (1995). Ultrastructural correlates of haloperidol-induced oral dyskinesias in rat striatum. *Synapse*, 20(3), 234-243. http://doi.org/10.1002/syn.890200307

Roberts, R.C., Conley, R., Kung, L., Peretti, F.J., Chute, D.J. (1996). Reduced striatal spine size in schizophrenia: a postmortem ultrastructural study. *Neuroreport*, 7(6), 1214-8.

Robinson, T.E., Kolb, B. (1999). Alterations in the morphology of dendrites and dendritic spines in the nucleus accumbens and prefrontal cortex following repeated treatment with amphetamine or cocaine. *Eur J Neurosci,* 11(5), 1598-1604.

Romero, I.G., Pai, A.A., Tung, J., Gilad, Y. (2014). RNA-seq: impact of RNA degredation on transcript quantification. *BMC Biol,* 12(42). http://doi.org/10.1186/1741-7007-12-42

Rossler, W., Salize, H.J., van Os, J., Riecher-Rossler, A. (2005). Size of burden of schizophrenia and psychotic disorders. *Eur Neuropsychopharmacol,* 15(4), 399-409. http://doi.org/10.1016/j.euroneuro.2005.04.009

Roussignol, G., Ango, F., Romorini, S., Tu, J.C., Sala, C., Worley, P.F., ... Fagni, L. (2005). Shank expression is sufficient to induce functional dendritic spine synapses in aspiny neurons. *J Neurosci*, 25(14), 3560-3570. http://doi.org/10.1523/JNEUROSCI.4354-04.2005

Sahoo P.K., Smith, D.S., Perrone-Bizzozero, N., Twiss, J.L. (2018). Axonal mRNA transport and translation at a glance. *J Cell Sci*, 131(8), jcs196808. http://doi.org/10.1242/jcs.196808

Sakuma, K., Komatsu, H., Maruyama, M., Imaichi, S., Habata, Y., Mori, M. (2015). Temporal and spatial transcriptional fingerprints by antipsychotic or propsychotic drugs in mouse brain. *PloS One,* 10(2), e0118510. http://doi.org/10.1371/journal.pone.0118510

Schizophrenia Working Group of the Psychiatric Genomics Consortium. (2014). Biological insights from 108 schizophrenia-associated genetic loci. *Nature,* 511(7510), 421-427. http://doi.org/10.1038/nature13595

Schobel, S.A., Chaudhury, N.H., Khan, U.A., Paniagua, B., Styner, M.A., Asllani, I., ... Small, S.A. (2013). Imaging patients with psychosis and a mouse model establishes a spreading pattern of hippocampal dysfunction and implicates glutamate as a driver. *Neuron*, 78(1), 81-93. http://doi.org/10.1016/j.neuron.2013.02.011

Sebel, L.E., Graves, S.M., Chan, C.S., Surmeier, D.J. (2017). Haloperidol selectively remodels striatal indirect pathway circuits. *Neuropsychopharmacology,* 42(4), 963-973. http://doi.org/10.1038/npp.2016.173

Seifert, G., Schilling, K., Steinhauser, C. (2006). Astrocyte dysfunction in neurological disorders: a molecular perspective. *Nat Rev Neurosci*, 7(3), 194-206. http://doi.org/10.1038/nrn1870

Sekar, A., Bialas, A.R., de Rivera, H., Davis, A., Hammond, T.R., Kamitaki, N., ... McCarroll, S.A. (2016). Schizophrenia risk from complex variation of complement component 4. *Nature,* 530(7589), 177-83. http://doi.org/10.1038/nature16549

Shao, W., Zhang, S.Z., Tang, M., Zhang, X.H., Zhou, Z., Yin, Y.Q., ... Zhou, J.W. (2013) Supression of neuroinflammation by astrocytic dopamine D2 receptors via aB-crystallin. *Nature*, 494(7435), 90-94. http://doi.org/10.1038/nature11748

Shen, W., Flajolet, M., Greengard, P., Surmeier, D.J. (2008). Dichotomous dopaminergic control of striatal synaptic plasticity. *Science,* 321(5890), 848-851. http://doi.org/10.1126/science.1160575

Simon, P., Dupuis, R., Costentin, J. (1994). Thigmotaxis as an index of anxiety in mice. Influence of dopaminergic transmissions. *Behav Brain Res*, 61(1), 59-64.

Skene, N.G., Bryois, J., Bakken, T.E., Breen, G., Crowley, J.J., Gaspar, H.A., ... Hjerling-Leffler, J. (2018). "Genetic identification of brain cell types underlying schizophrenia." *Nat Genet,* 50(6), 825-833. http://doi.org/10.1038/s41588-018-0129-5

Smith, R.C., Leucht, S., Davis, J.M. (2018). Maximizing response to first-line antipsychotics in schizophrenia: a review focused on finding from meta-analysis. *Psychopharmacology (Berl)*. http://doi.org/10.1007/s00213-018-5133-z

Smith, S.E.P., Li, J., Garbett, K., Mimics, K., Patterson, P.H. (2007). Maternal immune activation alters fetal brain development through interleukin-6. *J Neurosci,* 27(40), 10695-10702. http://doi.org/10.1523/JNEUROSCI.2178-07.2007

Snyder, G.L., Allen, P.B., Fienberg, A.A., Valle, C.G., Huganir, R.L., Nairn, A.C., Greengard, P. (2000). Regulation of phosphorylation of the GluR1 AMPA receptor in the neostriatum by dopamine and psychostimulates in vivo. *J Neurosci,* 20(12), 4480-4488.

Sommer, B., Kohler, M., Sprengel, R., Seeburg, P.H. (1991). RNA editing in brain controls a determinant of ion flow in glutamate-gated channels. *Cell*, 67(1), 11-19.

Spellman, T.J., Gordon, J.A. (2015). Synchrony in schizophrenia: a window into circuit-level pathophysiology. *Curr Opin Neurobiol*, 0, 17-23. http://doi.org/10.1016/j.conb.2014.08.009

Spencer, K.M., Salisbury, D., Shenton, M., McCarley, R. (2008). Gamma-band auditory steady-state responses are impaired in first episode psychosis. *Biol Psychiatry*, 64 (1), 369-375.

Spencer, K., Niznikiewicz, M., Nestor, P., Shenton, M., McCarley, R. (2009). Left auditory cortex gamma synchronization and auditory hallucination symptoms in schizophrenia. *BMC Neurosci*, 10 (1), 85.

Stefansson, H., Sigurdsson, E., Steinthorsdottir, V., Bjornsdottir, S., Sigmundsson, T., Ghosh, S., ... Stefansson, K. (2002). Neuregulin 1 and susceptibility to schizophrenia. *Am J Hum Genet*, 71(4), 877-892. http://doi.org/10.1086/342734

Sudmant, P.H., Lee, H., Dominguez, D., Heiman, M., Burge, C.B. (2018). Widespread accumulation of ribosome-associated isolated 3'UTRs in neuronal cell populations of the aging brain. *Cell Rep*, 25(9), 2447-2454e. https://doi.org/10.1016/j.celrep.2018.10.094

Sullivan, P.F., Kendler, K.S., Neale, M.C. (2003). Schizophrenia as a complex trait: evidence from a meta-analysis of twin studies. *Arch Gen Psychiatry,* 60(12), 1187-1192. http://doi.org/10.1001/archpsyc.60.12.1187

Surmeier, D.J., Song, W.J., Yan, Z. (1996). Coordinated expression of dopamine receptors in neostriatal medium spiny neurons. *J Neurosci,* 16(20), 6579-91.

Surmeier, D.J., Ding, J., Day, M., Wang, Z., Shen, W. (2007). D1 and D2 dopamine-receptor modulation of striatal glutamatergic signaling in striatal medium spiny neurons. *Trends Neurosci,* 30(5), 228-235. http://doi.org/10.1016/j.tins.2007.03.008

Sutton, M.A., Ito, H.T., Cressy, P., Kempf, C., Woo, J.C., Schuman, E.M. (2006). Miniature neurotransmission stabilizes synaptic function via tonic suppression of local dendritic protein synthesis. *Cell,* 125(4), 785-99. http://doi.org/10.1016/j.cell.2006.03.040

Swanson, G.T., Kamboj, S.K., Cull-Candy, S.G. (1997). Single-channel properties of recombinant AMPA receptors depend on RNA editing, splice variation, and subunit composition. *J Neurosci,* 17(1), 58-69.

Swerdlow, N.R., Geyer, M.A. (1993). Clozapine and haloperidol in an animal model of sensorimotor gating deficits in schizophrenia. *Pharmacol Biochem Behav*, 44(3), 741-744.

Terrillion, C.E., Abazyan, B., Yang, Z., Crawford, J., Shevelkin, A.V., Jouroukhin, Y., ... Pletnikov, M.V. (2017). DISC1 in astrocytes influences adult neurogenesis and hippocampus-dependent behaviors in mice. *Neuropsychopharmacology,* 42(11), 2242-2251. http://doi.org/10.1038.npp.2017.129

The International Schizophrenia Consortium, Purcell, S.M., Wray, N.R., Stone, J.L., Visscher, P.M., O'Donovan, M.C., ... Sklar, P. (2009). Common polygenic variation contributes to risk of schiozphrenia and bipolar disorder. *Nature*, 460(7256), 748-752. http://doi.org/10.1038/nature08185

Thomas, E.A. (2006). Molecular profiling of antipsychotic drug function: convergent mechanisms in the pathology and treatment of psychiatric disorders. *Mol Neurobiol,* 34(2), 109-128. http://doi.org/10.1385/MN:34:2:109

Thomas, M.J., Beurrier, C., Bonci, A., Malenka, R.C. (2001). Long-term depression in the nucleus accumbens: a neural correlate of behavioral sensitization to cocaine. *Nat Neurosci,* 4(12), 1217-23. http://doi.org/10.1038/nn757

Thomson, S.R., Seo, S.S., Barnes, S.A., Louros, S.R., Muscas, M., Dando, O., ... Osterweil, E.K. (2017). Cell-type-specific translation profiling reveals a novel strategy for treating fragile X syndrome. *Neuron*, 95(3), 550-563. http://doi.org/10.1016/j.neuron.2017.07.013

Turrigiano G.G., Leslie K.R., Desai N.S., Rutherford L.C., Nelson S.B. (1998). Activity-dependent scaling of quantal amplitude in neocortical neurons. *Nature,* 26(391), 892-6. http://doi.org/10.1038/36103

Ullian, E.M., Sapperstein, S.K., Christopherson, K.S., Barres, B.A. (2001). Control of synapse number by glia. *Science,* 291(5504), 657-661. http://doi.org/10.1126/science.291.5504.657

Ursini, G., Punzi, G., Chen, Q., Marenco, S., Robinson, J.F., Porcelli, A., ... Weinberger, D.R. "Convergence of placenta biology and genetic risk for schizophrenia." *Nat Med,* 24(6), 792-801. http://doi.org/10.1038/s41591-018-0021-y

Van Os, J., Kenis, G., Rutten, B.P.F. (2010). The environment and schizophrenia. *Nature,* 468(7321), 203-212. http://doi.org/10.1038/nature09563

Van Tol, H.H., Bunzow, J.R., Guan, H.C., Sunahara, R.K., Seeman, P., Niznik, H.B., Civelli, O. (1991). Cloning of the gene for a human dopamine D4 receptor with high affinity for the antipsychotic clozapine. *Nature*, 350(6319), 610-614. http://doi.org/10.1038/350610a0

Vertes, R.P. (2001). Analysis of projections from the medial prefrontal cortex to the thalamus in the rat, with emphasis on nucleus reuniens. *Journal of Comparative Neurology*, 442(2), 163-187. https://doi.org/10.1002/cne.10083

Wall, N.R., Wickersham, I.R., Cetin, A., De La Parra, M., Callaway, E.M. (2010). Monosynaptic circuit tracing in vivo through Cre-dependent targeting and complementation of modified rabies virus. *Proc Natl Acad Sci U S A*, 107(5), 21848-21853. http://doi.org/10.1073/pnas.1011756107

Walsh, T., McClellan, J.M., McCarthy, S.E., Addington, A.M., Pierce, S.B., Cooper, G.M., ... Sebat, J. (2008). Rare structural variants disrupt multiple genes in neurodevelopmental pathways in schizophrenia. *Science*, 320(2875), 539-543. http://doi.org/10.1126/science.1155174

Wang, H.X,. Gao, W.J. (2010). Development of calcium-permeable AMPA receptors and their correlation with NMDA receptors in fast-spiking interneurons of rat prefrontal cortex. *J Physiol*, 588(pt 15), 2823-2838. http://doi.org/10.1113/jphysiol.2010.187591

Wei, J., and Hemmings, G.P. (2000). The NOTCH4 locus is associated with susceptibility to schizophrenia. *Nat Genet*, 25(4), 376-377. http://doi.org/10.1038/78044

Weickert, C.S., Hyde, T.M., Lipska, B.K., Herman, M.M., Weinberger, D.R., Kleinman, J.E. (2003). Reduced brain-derived neurotrophic factor in prefrontal cortex of patients with schizophrenia. *Mol Psychiatry*, 8(6), 592-610. http://doi.org/10.1038/sj.mp.4001308

Weinberger, D.R. (1987). Implications of normal brain development for the pathogenesis of schizophrenia. *Arch Gen Psychiatry*, 44(7), 660-669.

Wen, Z., Nguyen, H.N., Guo, Z., Lalli, M.A., Wang, X., Su, Y., ... Ming, G.L. (2014). Synaptic dysregulation in a human iPS cell model of mental disorders. *Nature*, 515(7527), 414-418. http://doi.org/10.1038/nature13716

Wiltgen, B.J., Royle, G.A., Gray, E.E., Abdipranoto, A., Thangthaeng, N., Jacobs, N., ... Vissel, B. (2010). A role for calcium-permeable AMPA receptors in synaptic plasticity and learning. *PLoS One*, 5(9), e12818. http://doi.org/10.1371/journal.pone.0012818

Woo, T.U., Whitehead, R.E., Melchitzky, D.S., Lewis, D.A. (1998). A subclass of prefrontal gamma-aminobutyric acid axon terminals are selectively altered in schizophrenia. *Proc Natl Acad Sci U S A,* 95(9), 5341-5346.

Woo, T.U., Walsh, J.P., Benes, F.M. (2004). Density of glutamic acid decarboxylase 67 messenger RNA-containing neurons that express the N-methyl-D-aspartate receptor subunit NR2A in the anterior cingulate cortex in schizophrenia and bipolar disorder. *Arch Gen Psychiatry*, 61(7), 649-657. http://doi.org/10.1001/archpsyc.61.7.649

Wu, E.Q., Birnbaum, H.G., Shi, L., Ball, D.E., Kessler, R.C., Moulis, M., Aggarwal, J. (2005). The economic burden of schizophrenia in the United States in 2002. *J Clin Psychiatry,* 66(9), 1122-1129.

Xu, T.X., Yao, W.D. (2010). D1 and D2 dopamine receptors in separate circuits cooperate to drive associative long-term potentiation in the prefrontal cortex. *Proc Natl Acad Sci National Acad Sciences*, 107(37), 16366-16371.

Yankelevitch-Yahav, R., Franko, M., Huly, A., Doron, R. (2015). The forced swim test as a model of depressive-like behavior. *J Vis Exp,* 97. http://doi.org/10.3791/52587

Yung, A.R., McGorry, P.D. (1996). The prodromal phase of first-episode psychosis: past and current conceptualizations. *Schizophr Bull,* 22(2), 353-370.

Yung, A.R., Phillips, L.J., Yuen, H.P., Francey, S.M., McFarlane, C.A., Hallgren, M., McGorry, P.D. (2003). Psychosis prediction: 12-month follow up of a high-risk ("prodromal") group. *Schizophr Res,* 60(1), 21-32.

Zanassi, P., Paolillo, M., Montecucco, A., Avvedimento, E.V., Schinelli, S. (1999) Pharmacological and molecular evidence for dopamine D1 receptor expression by striatal astrocytes in culture. *J Neurosci Res,* 58(4), 544-552.

Zhang, Z.J., Reynolds, G.P. (2002). A selective decrease in the relative density of parvalbumin-immunoreactive neurons in the hippocampus in schizophrenia. *Schizophrenia Res*, 55(1-2), 1-10.

Zhou, Y., Kaiser, T., Monteiro, P., Zhang, X., Van der Goes, M.S., Wang, D., ... Feng, G. (2016). Mice with Shank3 mutations associated with ASD and Schizophrenia display both shared and distinct defects. *Neuron*, 89(1), 14-162. http://doi.org/10.1016/j.neuron.2015.11.023